Investigations into the Effects of Transcatheter Valve Implantations on the Cardiac Conduction System and Cardiac Anatomy

A DISSERTATION
SUBMITTED TO THE FACULTY OF THE GRADUATE SCHOOL
OF THE UNIVERSITY OF MINNESOTA
BY

Michael G. Bateman

IN PARTIAL FULFILLMENT OF THE REQUIREMENTS
FOR THE DEGREE OF
DOCTOR OF PHILOSOPHY

Advisor: Paul A. Iaizzo, PhD

August 2012

Acknowledgements

The number of colleagues, friends and family members who deserve my thanks and acknowledgements for helping me complete my graduate studies at the University of Minnesota are too abundant to list in full. However, it would be amiss of me not to mention a few key payers who made the journey exciting, challenging and, most importantly, rewarding.

The continual encouragement and guidance of my principal investigator, Prof. Paul A. Iaizzo, has pushed me to strive for excellence in my studies and his contagious optimism has initiated more than its fair share of unexpected discoveries chasing seemingly lost causes. His commitment to exposing all of his students to phenomenal academic and industrial opportunities is unwavering and a significant reason for my successful transition to industry. I am truly honored to consider him and his family friends and look forward to staying in contact over the coming years. Bill Gallagher and Monica Mahre also deserve special thanks for keeping me on the straight and narrow, both in the lab and at home. Bill's commitment to my studies and Monica's unbelievable ability to make stuff happen have both been recurring reasons for my successes over the past 5 years. In addition, Gary Williams, Tinen Iles and Charles Soule have helped greatly in many different aspects of my work.

My fellow graduate students, in particular Chris Rolfes and Steve Howard, have shared many of the ups and downs of this journey with me and have always been ready with kind words, an unrepeatable joke or an ice cold beverage at the appropriate moment. I would also like to thank Jason Quill for his guidance when I was just finding my feet in the lab. His patience and support helped shape my decision to concentrate my studies on structural anatomy and initiated my fascination with cardiac valves. Additionally, I would not have completed this body of work without the help of countless medical students, undergraduates and masters students who have volunteered in the lab during my time here. My friends and family beyond the confines of the lab have provided a great support network through the years, providing reprieve from the rigors of work and forgiving my, now legendary, tardiness when work took just that little bit longer than expected. I was truly humbled by the number who made the distinct effort to attend my oral defense. I would also like to single out my loving parents whose unerring commitment to my cause has given me the opportunity to succeed.

Last but not least, I would like to thank all of the organ donors and their families for the generous gift to science. Without these individuals' dedication to helping further the fields of medical science and engineering much of my work would not have been possible. I hope that my work will educate and inspire future researchers to further the understanding of cardiac anatomy and develop the next generation of restorative therapies.

Many, many thanks to everyone!!

Table of Contents

List of Tables

List of Figures

Thesis Statement

In 2006 Stuge and Liddicoat reported that approximately 2.3 million people in the US alone had been diagnosed with mitral regurgitation, 220,000 of which were classified as severe and 749,000 individuals were diagnosed with aortic stenosis, with 125,000 being classified as severe[1]. Of these two populations only 48,000, or 2.1%, of the mitral patients and 79,000, or 10.5%, of the aortic patients had been treated[1]. The increased prevalence of cardiac diseases and chronic cardiomyopathies suggests that these values may be a gross underestimation of the current populations of patients suffering from valve disease. These numbers, particularly the low number of treated patients, indicate the need for improved valvular heart repair therapies and technologies that are available to a greater portion of the world patient population. One of the routes being pursued to achieve this goal is the development of transcathater delivered valve therapies. My research, as described in this thesis, is to better understand the importance of the cardiac electrical conduction system and valve anatomies in the design of novel trans-catheter delivered valve therapies. Additionally, I sought to develop bespoke in-vitro and in-situ models for the development and testing of current and next generation valve designs and delivery systems.

In order to achieve these goals I first have established a comprehensive understanding of the anatomy of the four cardiac valves and the cardiac conduction system. As such, Chapter 1 presents: 1) a comprehensive review of the atrioventricular and semi-lunar valves, embellished by anatomical studies concentrating on unique mitral anatomy; 2) a review the cardiac conduction system. It is a further aim of my thesis to apply such anatomical knowledge to develop a better understanding on the potential complications that transcatheter devices may impose on the cardiac anatomy. It is important to note that advances in computed tomography, magnetic resonance imaging and echocardiography have allowed for high spatial and temporal resolution imaging of the heart in-vivo. Real-time clinical imaging of the valve using these various imaging modalities has in turn driven an important evolutionary step in the nomenclature of cardiac anatomy and helps expand the in-vitro imaging capabilities of the Visible Heart® laboratory.

The accurate in-vivo analysis of the heart has provided extensive hemodynamic and structural information regarding various valve disease states. A large part of my thesis is based on the development of models of three such disease states: 1) aortic stenosis, 2) mitral prolapse and 3) pulmonary valve insufficiency, such as those which occur in patients recovering from the surgical correction of tetralogy of Fallot. Chapter 3 of this thesis, describes the creation and validation of an in-vitro beating heart model of calcific aortic stenosis, designed specifically to analyze the effect of large calcific deposition on the deployment of transcatheter delivered aortic valves. This chapter also describes collaborative work with Jason Quill, PhD and James St. Louis, MD using Visible Heart® methodologies to create mitral prolapse in a beating heart and then acutely assessing the function of the prolapsing valve before, during and after "edge-to-edge" repair: thus, providing control data for the development of percutaneous devices using the same repair technique. Finally, following the first human implant of a stented pulmonary valve in 2000, research into increasing the possible patient population has grown to include one of the patient populations initially excluded from transcatheter delivered valves; surgically corrected tetralogy of Fallot patients. Our laboratory collaboration with James St. Louis, MD has led to the development of an animal model for the testing of novel stented artificial pulmonary valves in patients with irregular pulmonary trunk anatomies.

Additionally, due to the increased awareness and importance of the effect of transcatheter delivered devices on the functioning of the conduction system, our laboratory initiated a collaboration with Drs. Boyett and Dobrzynski at the University of Manchester: specifically designed to document the electrical activity and the three dimensional anatomical detailing of the human cardiac conduction system, see Chapter 4. Such detailing of the atrioventricular node, the bundle of His and the left and right bundle branches will provide useful maps of the cardiac conduction system. These maps will provide information to designers addressing the recent concerns that the pressure on the ventricular septum from transcatheter delivered aortic valves can cause acute conduction complications (such as left bundle branch block).

Currently the most effective and accurate way of recording these conduction abnormalities is via the use of non-contact endocardial mapping systems. However, there is extensive research at the University of Minnesota into the development of an entirely non-invasive trans-thoracic cardiac mapping system. One of the many benefits of such a system will be the ability to map trans-mural electrical propagation patterns without introducing any devices into the body;

thereby enabling the detection of conduction abnormalities deep within the myocardium. Working collaboratively with Dr. He's team, our laboratory developed an invasive quadripolar electrode system used to electrically map the transmural propagation of electrical activity in the heart.

The understanding of the interactions of novel transcatheter devices and their delivery systems with the cardiac anatomy and conduction system is critical for the advancement of these medical devices. I believe that my research is truly translational and will help to bridge the gap between the surgeon or cardiologist and the device engineer. The capabilities afforded to me by the Visible Heart® lab and the collaborations I have cultivated will further my understanding of these topics and help me become an expert in the field.

1. Stuge, O. & Liddicoat, J. Emerging opportunities for cardiac surgeons within structural heart disease *J. Thorac. Cardiovasc. Surg.* **132**, 1258-1261 (2006).

Anatomical Analysis

Section Summary

The primary objective of this thesis is to investigate the potential interactions between the local cardiac anatomy and electrophysiology and various novel transcatheter delivered valve therapies. In order to appropriately address any anatomical or electrical changes that may occur, a thorough understanding of the four cardiac valves and the cardiac conduction system in a healthy heart is required. This chapter will present a review of the 'normal' anatomy of the four valves, submitted and edited as chapters for the textbook "Heart Valves: From Design to Clinical Implantation" (Iaizzo, 2012), and the healthy cardiac conduction system in order to lay a strong foundation for the rest of the thesis.

The advent of high resolution noninvasive imaging and high spatial and temporal mapping technologies allowing modern cardiac clinics to collect detailed images of myocardial contractions, blood movement, activation sequences and valve function has accelerated the understanding of functional human heart anatomy. This, in turn, has brought new nomenclature to define the anatomical features of the heart so to align with the overall anatomy of the body, a concept known as attitudinally correct anatomy. A detailed understanding of the anatomy, electrophysiology and function of the four cardiac valves and the conduction system is required before conducting investigations into the performance and design of novel transcatheter valvular repairs or replacements.

Specific anatomical studies that I have completed, including the discovery of a double orifice mitral valve and investigational studies into the papillary muscles of the left ventricle can be found in Appendix A.

Michael G. Bateman MEng[1], Jason L. Quill PhD[2], Alexander J. Hill PhD[2], Paul A. Iaizzo PhD[1]

[1]Departments of Surgery and Biomedical Engineering, University of Minnesota, Minneapolis, MN, USA
[2]Medtronic, Inc., Minneapolis, MN, USA

1. Anatomy of the Cardiac Valves and Conduction System

Introduction

Anatomy is documented as being one of the original branches of medicine. During the 2nd and 3rd century BC, early anatomists and physicians used post-mortem examinations to try to better understand the frailties of the human body. Many great anatomists over the centuries, including Galen, Vesalius, da Vinci, Hunter, Gray and Netter have recreated their knowledge gained from such dissections in elegant treatises: e.g., relevant for today's studies is the culmination presented in Netter's medical school mainstay, the Atlas of Human Anatomy[1]. More recently, with the advent of high resolution noninvasive imaging the understanding of the functional internal anatomy of the body has progressed rapidly. The circulatory system benefited dramatically from such imaging capabilities with modern cardiac centers of excellence routinely collecting detailed images of myocardial contractions, blood movements and valve functions. The advances in cardiac surgery and consequently the development and deployment of numerous cardiac devices over the late 20th century has reinforced the need to describe areas of the heart as functional complexes, consisting of various anatomical parts, rather than simplistically as individual anatomical features[2] Furthermore, the present field of cardiac anatomy has undergone a shift to correct the perceived orientation of the organ's anatomical features so to align with the overall anatomy of the body: this has been coined as *attitudinally correct anatomy*[3].

Attitudinally correct anatomy

Cardiac anatomy itself, although a relatively young branch of human anatomy, has not adhered to the same fundamental rules of anatomical orientation as more generalized gross anatomy. More specifically, the three planes of the body, sagittal, coronal and transverse (shown in figure (1.1)), are used to describe the position and nature of almost all other aspects of internal anatomy with respect to the patient's own orientation. This convention is designed to minimize confusion in determining which of the many structures and organs within the body a particular diagnosis may be referring to. On the other hand, the anatomical features of the heart have commonly been described as though the heart had been removed from the body and held in front of the observer, with the right chambers to the patients right and the apex to the ground. Only quite recently have cardiac anatomy specialists pushed to redefine the nomenclature as though the heart was situated within the body and describe the anatomical features relative to

the body's anatomical planes. Thus, structures closest to the spine are described as being posteriorly positioned and those nearest to the diaphragm, inferiorly positioned[3]. This change in convention is particularly important given the increase in high definition images of the heart functioning *in-vivo* aiding in the diagnosis of many cardiac pathologies.

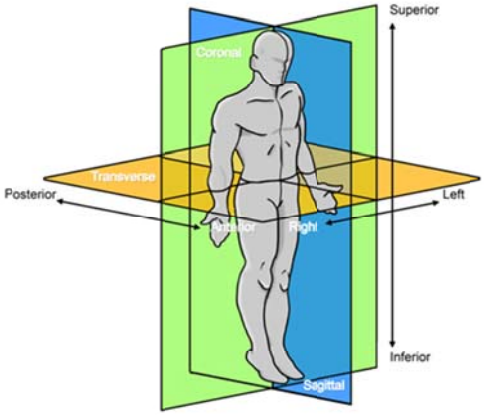

Figure 1.1 The defined anatomical planes of the human body. (www.vhlab.umn.edu/atlas)

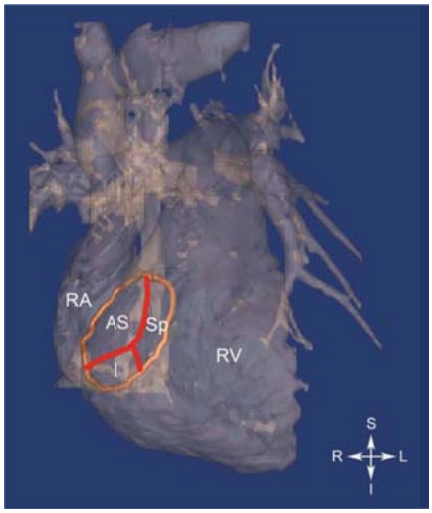

Figure 1.2 Shown here is a volumetric reconstruction of a human heart created from magnetic resonance imaging (MRI): one can observe the anterior surfaces of both the right ventricle and atrium. The tricuspid annulus is highlighted in orange, and was superimposed onto the MRI image. The theorized positions of the commissures between the leaflets are drawn in red, and the leaflets are labeled appropriately. AS, anterosuperior; I, inferior; L, left; R, right; RA, right atrium; RV, right ventricle; RV, right ventricle; S, superior; Sp, septal[4]. (Used with permission)

When considering the cardiac valves, the anatomical description of the atrio-ventricular valves has been particularly muddled by these inconsistent terminologies and as a result the nomenclatures commonly used to describe the leaflets of the atrioventricular valves are typically not attitudinally correct[4]. Note that the tricuspid valve is situated between the right atrium and right ventricle, and is so named because, in the majority of cases, there are three major leaflets or cusps. These are currently referred to as the anterior, posterior and septal leaflets, and were most likely termed in this manner during extra-corporal examinations of the heart. Figure (1.2) shows an anterior view of a human heart in an attitudinally correct orientation, with the tricuspid annulus shown in orange. The theorized locations of the commissures between the leaflets are in red. This positions the annulus in an oblique plane, as shown, and the leaflets in positions whereby they would be more correctly termed antero-superior, inferior, and septal.

An alternative nomenclature should also be defined for the mitral valve. The mitral valve has two leaflets, commonly referred to as the anterior and posterior. However, the leaflets are not strictly anterior or posterior, and would be better described as antero-superior and postero-inferior. Some anatomists have moved away from using relative anatomical planes to describe the features when other, distinct, anatomical features can be used. In the case of the mitral valve Wilcox, Cook and Anderson chose to describe the two leaflets as being aortic (previously anterior) and mural (previously posterior), described as such due to the relative proximity to both the aortic valve and the freewall of the left ventricle respectively[5].

The naming of the cardiac semi-lunar valves is not directly affected by attitudinally correct nomenclature due to the leaflets, or cusps, of each valve being described by their surrounding anatomies rather than their position within the heart. For example the three leaflets of the aortic valve are named after the coronary arteries (or lack thereof), that supply the left and the right sides of the heart with blood (that branch from the sinus of Valsalva): the left-, right- and non-coronary leaflets, see figure (2). Further, due to its oblique positioning in the body the pulmonary valve leaflets are not named according to the sagittal, coronal and axial planes, but have been rather described by their relationships to the aortic valve[5]. More specifically, in a normal anatomical orientation the right and the left coronary cusps of the aortic valve face the septum between the right and the left chambers. These leaflets are usually opposed by two leaflets of the pulmonary valve and hence these two leaflets of the pulmonary valve are labeled

the “right and left facing leaflets”. The third leaflet of the pulmonary valve is consequently labeled the “non-facing leaflet”, so to complete the trifecta. The specific anatomies of each semi-lunar valve will be described in more details, later in this chapter.

The nomenclature of the cardiac conduction system, like the semi-lunar valves, is not tied to the anatomical planes of the body. The features of the conduction system are predominantly named for the area of the heart they control or after the anatomists or physicians that first understood their importance and function. Any directional nomenclature, left or right bundle branches for example, are named with respect to the side of the heart that they innervate. The anatomy and position of the conduction system will also be described at length later in this chapter.

The Cardiac Valves

The Cardiac Skeleton

Before investigating the specific anatomies of the four cardiac valves, the anatomical framework that holds them in position must be described[5]. Figure (1.3) shows a 3D reconstruction of the valve annuli of a human heart highlighting the close proximity of all four cardiac valves to each other. Traditionally, the four valves of the heart have been described as being supported by a fibrous framework or cardiac skeleton made of dense connective tissue passing transversely through the base of the heart between the atria and the ventricles. This skeleton is considered to be a formation of four attached rings with the opening for the aortic semilunar valve in the central position with the other valve rings attached[6]. However, it has since been proposed by Anderson et al. that the fibrous skeleton does not uniformly support all four valves and rather should be considered as a series of fibrous structures that support the aortic valve and portions of the atrioventricular valve concentrated toward the center of the heart[5]. This structure includes three distinct fibrous regions: the right and left fibrous trigones and the membranous septum, graphically represented in figure (1.4).

The right fibrous trigone, considered to be the strongest portion of the cardiac skeleton, is defined by the triangular formation between the aortic semilunar valve and the medial parts of the tricuspid and mitral valve openings. The smaller left fibrous trigone is formed between the aortic semilunar valve and the anterior cusp of the mitral valve. Strong collagenous tissue passes anteriorly from the right and left fibrous trigones to encircle the aortic annulus and complete

the supporting structure of the valve[6]. The membranous interventricular septum is an inferior extension of the central fibrous body that attaches to the muscular interventricular septum. Continuations of fibroelastic tissue from the right and left fibrous trigone partially encircle the atrioventricular openings to form the tricuspid and mitral annuli[6]. The annular ring of the mitral valve extends from the two trigones as a complete collagenous structure and fades around the postero-inferior leaflet of the valve. The annular ring of the tricuspid valve usually emanates from the membranous septum, at the attachment of the septal leaflet, and fades quickly around the atrioventricular junction[5]. These annuli serve as attachment sites for the atrioventricular valves and also form a boundary between the atrial and ventricular myocardium which insulates the electrical signals of the atrium from the electrical signals of the ventricle. Finally, the pulmonary valve is considered to be exclusively supported by cardiac muscle, i.e., within the free standing infundibulum of the supraventricular crest of the right ventricle, otherwise known as the right ventricular outflow tract. It should be noted that this unique positioning, away from the other valve structures, greatly facilities the removal of this valve during surgical procedures such as the Ross procedure[5].

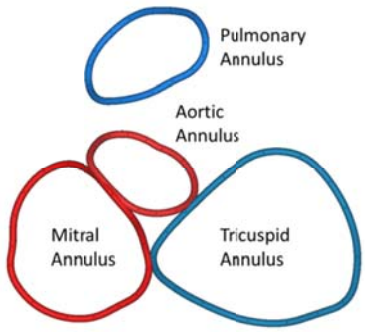

Figure 1.3. 3D reconstruction in Mimics® (Materialise, Belgium) of the valve annuli from a multi slice computed tomography scan of a human patient.

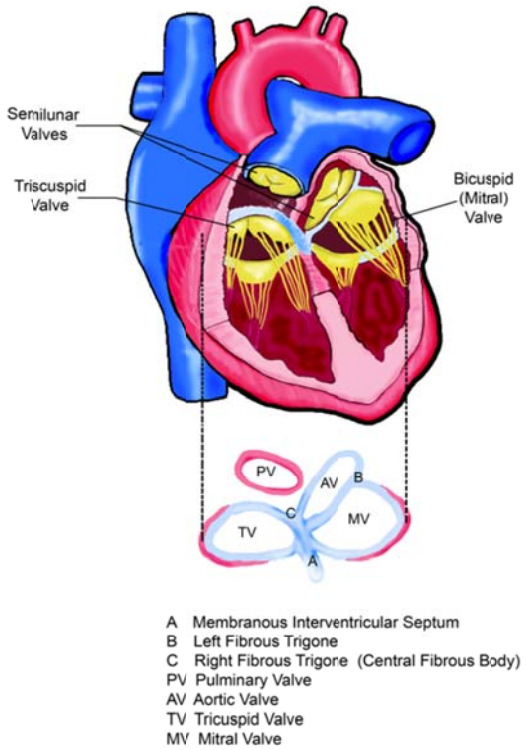

Figure 1.4. The cardiac skeleton. A dense connective tissue that functions to attach the atrial and ventricular myocardium, support and reinforce the valves of the heart, and electrically separate the ventricles from the atria.

The Atrio-ventricular Valves

In the most basic anatomical sense, the atrioventricular valves are made up of three main components:

- valve leaflets attached to the respective annuli within the cardiac skeleton;
- chordae tendinae attaching the leaflets themselves to the ventricular myocardium;
- papillary muscles providing the anchoring points for the chordae tendinae to the ventricular wall.

Anderson et al. elegantly describe the leaflets of the atrioventricular valves can be thought as forming a skirt that hangs from the annulus, and are divided into a series of sections that constitute the distinct leaflets of each valves. Due to the extent of variations between individuals with regard to leaflet morphologies, there has been much debate relative to nomenclature on the number of leaflets of both the mitral and tricuspid valves[7–9]. Traditionally,

the division of the leaflets has been determined by the presence of commisures which can be described as the peripheral attachment of a break in the skirt[5].

The leaflets themselves are attached to the ventricles via the subvalvular apparatus of each valve. In general, each apparatus consists of both the chordae tendinae and the papillary muscle complexes of each valve. The chordae tendinae are usually categorized by: 1) those that support the free edges of the valves; 2) those that support the rough zones (the region between the free edge and each annulus); and/or 3) those that attach to the leaflets near to the annulus. Typically, the chordae supporting the free edges of the leaflets are known as fan chordae due to the presence of multiple fenestrations of the chordae. Those that attach to the rough zone of the leaflets are distinguished by their size and are commonly defined as strut chordae. Finally, those that attach near the annulus are known as basal chordae. The strut chordae are relevant for two reasons: 1) in general, they bear the highest mechanical loads during systole[10]; and 2) they have been shown to contain the highest degrees of vascularization. Note that in such cases these blood vessels are likely to supply the leaflet tissue that is furthest from the annulus of the valve[11]. Furthermore, the number and distribution of the chordae tendinae across a given valve are critical to its function; it is well documented that dysfunction of these structures can lead to prolapse of the valves[2,12,13]. In general, the chordae attach to the heads of the papillary muscles which themselves play an important role in the function of each valve by contracting during systole to help prevent the valve from prolapsing into the atrium; additionally they aid in ventricular ejection by effectively drawing the apex of the ventricle toward the basal ring. Additionally, it has also been shown that the subvalvular apparatus plays a crucial role during diastole, while the ventricle is filling, by moderating wall tensions and improving the efficiencies of the ventricular myocardium[14,15].

Atrioventricular Valve Function

During systole, when the ventricles are contracting, the subvalvular apparatus of each valve prevents the leaflets from prolapsing into the atria. During systole in normal/healthy cardiac function, the valve leaflets, which bulge toward the atrium, can be considered to stay pressed together throughout the contraction. During diastole, when the ventricles are relaxing and the chambers are filling through the open atrioventricular valves, eddy currents that form behind the leaflets and tension in the subvalvular apparatus keep the leaflets close together. The sequence of valve function throughout the cardiac cycle can be seen in figures (1.5) and (1.6).

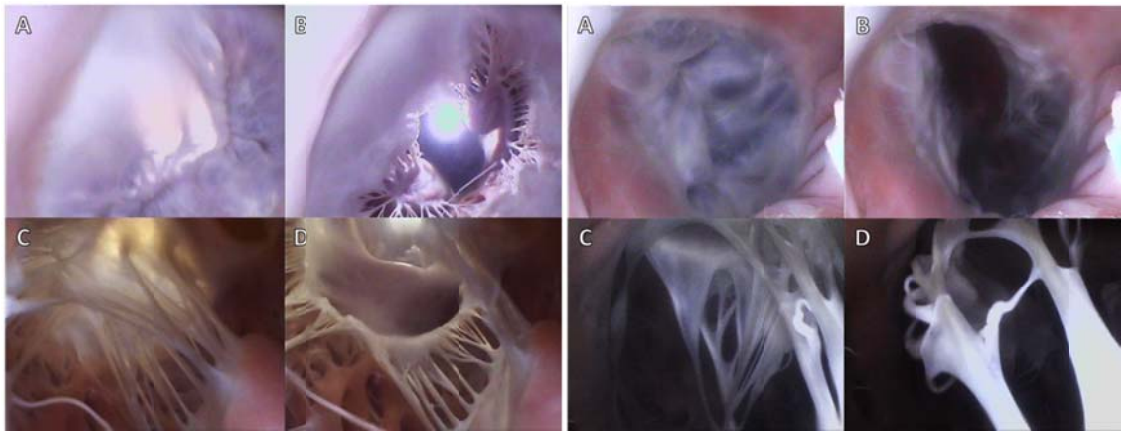

Figures 1.5 and 1.6 show image sequences of the mitral and tricuspid valves respectively[16,17] obtained employing Visible Heart® methodologies. These sequences were obtained from the atria (above the valve) and from the ventricular apexes (below the valve).

Dysfunction of the atrioventricular valves is usually characterized by one of two symptoms: 1) failure of a given valve to successfully close; or 2) failure of a valve to successfully open. Dysfunction of the valves during systole (i.e., failures of the valve to successfully close) results in the regurgitation of blood back in a retrograde direction though the atrioventricular junction, into the atria. Such dysfunction results in a decrease in cardiac output (ejection of blood through the semi lunar valves) and also increases the pressures within the atria (potentially causing atrial dilation and/or eventually atrial fibrillation). Dysfunction of the valves in diastole (failures of the valve to fully open and allow blood to fill the expanding ventricles) is termed stenosis. This decrease in effective orifice area of the open valve can often be attributed to stiffening or calcification of the valve leaflets.

Atrio-Ventricular Valve Histologies

Interestingly, the atrioventricular valves share very similar leaflet histologies. The atrial sides of the leaflets consist of spongy tissue (lamina spongiosa) comprised of fibrocytes, histiocytes, and collagen fibers[18]. It is these collagen fibers that are considered to supply the mechanical strength required of the atrioventricular valves. The ventricular sides consist of fibrous tissue (lamina fibrosa) and both these layers are surrounded by endothelial cells. This cellular construction can be seen in figure (1.7).

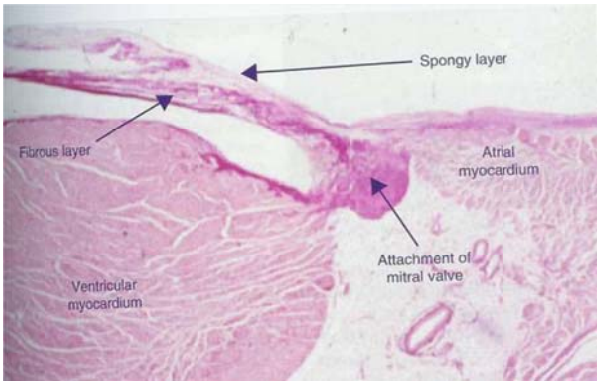

Figure 1.7. Histology of the mitral valve[5]. (Used with permission)

Additionally, valve leaflets have been shown to incorporate both primary sensory and autonomic innervation. In general, it is considered that the anterior leaflet of the mitral valve has twice the innervation of the posterior leaflet[19]. These nerves are typically situated in the lamina spongiosa and extend over the proximal and medial portions of the leaflet[18]. Fibroblasts[20], smooth muscle cells[21,22], and myocardial cells[23] are also commonly located within the leaflet tissue. Cells within the leaflets have shown to elicit two types of contractile activities: 1) a brief contraction or twitch at the beginning of each heart beat (reflecting contraction of myocytes in the leaflet in communication with and excited by atrial muscle) which has relaxed by midsystole and whose contractile activity is eliminated with β-receptor blockade; and 2) sustained tonic contractions (or tone) during isovolumic relaxation, which has been shown to be insensitive to β-blockade, but doubled by stimulation of the neurally rich region of aortic-mitral continuity[24]. These contractile activities within the leaflets are hypothesized to aid in the maintenance of anterior leaflet shape. This, in turn, could help prevent mechanical shock to the leaflets upon valve closure and also aid in optimizing the leaflet shape for funneling blood into the left ventricular outflow tract[24].

The chordae tendinae can be considered to be primarily composed of a collagen core, surrounded by elastin fibers interwoven in layers of loose collagen, and they also have an outer layer of endothelial cells. It is these collagen cores that support the greatest degree of mechanical load during systole and allow for the wavy configuration during diastole. The elastin fibers are normally arranged in parallel fashion relative to the collagen fibers. As the chordae are stretched during systole, the elastin fibers are also stretched and thus the wavy configuration of the collagen is straightened. It is hypothesized that it is this composite configuration of elastin and collagen that provides a smooth mechanism for the transmission of chordal forces from the

papillary muscles ultimately to the leaflets. Additionally, during diastole, the stretched elastin fibers likely help to restore the wavy configurations of the primary collagen cores. The relative amount of collagen and elastin within the given chordae varies according to their relative types, as does the relative amount of contained DNA and their degree of vascularization. Normally the vascularization of the chordae tendinae is located between their collagen cores and the elastin fibers, and is further considered to supply nutrients to the leaflets. It has been reported that a higher DNA content within both the anterior and posterior marginal chordae relates to inherently higher rates of collagen syntheses in order to prevent mechanical deterioration compared with other types of chordae[11].

The papillary muscles themselves can be considered part of the ventricular myocardium and, as such, the contained cells are histologically similar to ventricular wall myocytes. The cells exhibit complex junctions, called intercalated discs, allowing multiple cells to form long cellular networks. When grouped together these myocytes form cardiac muscle fibers. Within the papillary muscles, these muscle fibers run parallel to each other along the length of the muscle to increase contractile force and efficiency. The papillary muscles are extensively innervated and have complex vascular systems in order to maintain coordinated contractions with the continuum of the ventricular myocardium[25].

The Mitral Valve

The left atrioventricular valve, or mitral valve, named by Andreas Vesalius due to its structural resemblance to the cardinal's mitre, is situated in the left atrioventricular junction and modulates the flow of blood between the left atria and ventricle. Commonly, the valve consists of an annulus, two leaflets, two papillary muscle complexes, and two sets of chordae tendinae, as seen in figure (1.8).

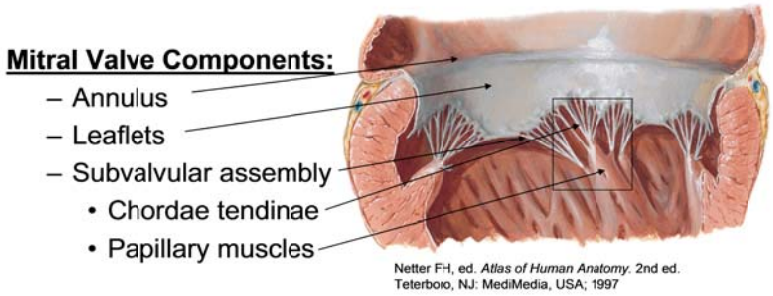

Figure 1.8. The main components of the mitral valve. (Used with permission)

In 1976 Carpentier described the mitral valve as consisting of two apposing leaflets— a posterior leaflet with three scallops, an anterior leaflet with one scallop, and regions of each leaflet described with alphanumerically assigned regions, figure (1.9). As previously noted, however, when one considers these structures relative to the landmarks of the body (i.e., in an attitudinally correct nomenclature[3]), the leaflets are located in postero-inferior or mural and antero-superior or aortic positions; in this chapter we will use such nomenclature. The junctions of the two leaflets are commonly referred to as the anterolateral and the posteromedial commissures, however these are more accurately described as superior and inferior. The line of apposition of the leaflets during valvular closure is known as the fibrous ridge. The simplicity and practicality of Carpentier's anatomic description of the mitral leaflets led to its widespread use after being introduced in 1976[26]; yet, while this description describes a majority of mitral valve anatomies, there can be wide variability in both the number of scallops within each leaflet and their relative positions[27]. An anatomical plate showing the dissected mitral valve can be seen in figure (1.10).

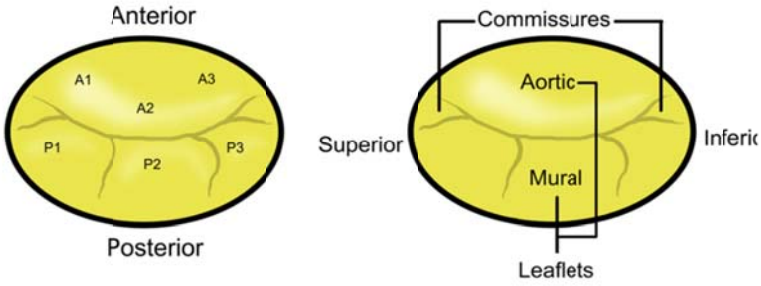

Figure 1.9. The naming of the mitral leaflets as describes by Carpentier on the left and the attitudinally correct nomenclature on the right

The mitral annulus, considered as part of the fibrous cardiac skeleton, and can elicit distinctly varying circumferential lengths[5]. In general, the aortic leaflet is found to be attached to approximately one third of the annulus circumference and is supported by the aorto-mitral fibrous continuity, which terminates in the left and right fibrous trigones. Importantly, the aorto-mitral continuity not only the highest point of the annulus, discussed later, but is essentially separate from the mitral annulus[29] and consequently plays an important role in the design of mitral repair and replacement devices. The mural leaflet is attached to the remaining two-thirds of the annulus and also to the fibrous extensions that continue from the trigones around the mitral valve. However, the lengths of these extensions can be highly variable.

Furthermore, a fibrous-fatty tissue surrounds the valve in areas where the cardiac skeleton is not present. The annulus is three dimensional, with the so-called saddle shape[28]. The highest point of the annulus occurs in the A2 region of the mitral annulus and is termed the saddlehorn. Both Delgado and Veronisi and their colleagues reported a series of annular dimensions that were recorded using echocardiography in healthy patients; these data are summarized in table 1.1[30-32]. It should be noted that the mitral annulus is a highly dynamic feature of the heart and changes dramatically in shape and size throughout the cardiac cycle from systole to diastole.

Table 1.1 Data on the mitral valve annulus measured via CT [32] and 3D echocardiography[30,31].

Measured Anatomical Feature	**Data**	**Sample Size**
Systolic annular area	9.12 ± 1.71 cm2 [30] 9.49 ± 1.25 cm2 [31]	N=84 N=13
Septal-lateral (A2-P2) diameter (Considered the short axis of the valve)	2.38 ± 0.40 cm [30] 3.00 ± 0.45 cm [31]	N=84 N=13
Commissure-commissure diameter (Considered the long axis of the valve)	4.10 ± 0.48 cm [30] 3.42 ± 0.40 cm [31]	N=84 N=13
Annulus height during systole	8.1 ± 1.7 mm [32]	N=24

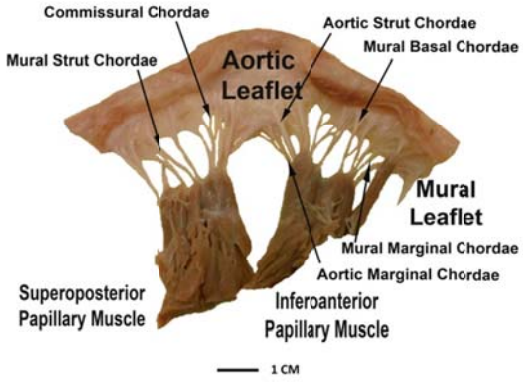

Figure 1.10. The human mitral valve dissected from a perfusion fixed heart showing the leaflets and the sub-valvular apparatus.

In general, the subvalvular apparatus of the mitral valve, as seen in figure (1.10), consists of two adjacent papillary muscle complexes—the superoposterior (anterior or APM) and the inferoanterior (posterior or PPM)—with their attached chordae tendinae which, in turn, insert onto the ventricular surfaces of each of the two valve leaflets[33]. In other words, the superoposterior papillary muscle complex is not solely associated with the aortic leaflet, but rather both the leaflets; likewise, the inferoanterior papillary muscle complex is not solely associated with the mural leaflet. It is important to note that the morphologies of the papillary

muscle are highly variable[31]. Typically, the papillary muscles are poorly characterized. Current assessment/nomenclature could be deemed as an oversimplification, as both papillary complexes can exhibit enormous variation in anatomies. For example, figures (1.11) and (1.12) show work by the author displaying the clocking of the two papillary complexes in the left ventricle and images of the subvalvular apparatus of the mitral valve taken from human hearts in the Visible Heart® library.

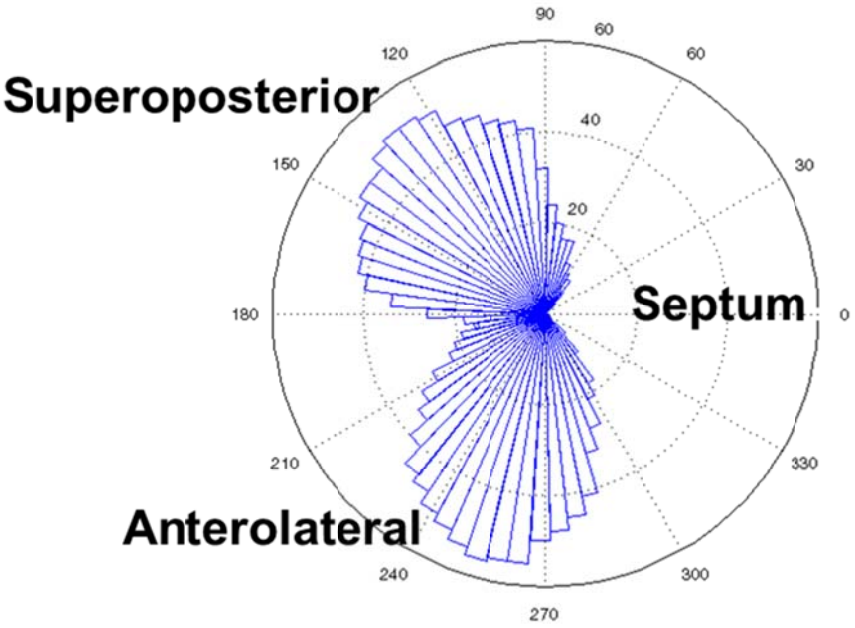

Figure 1.11. Analysis of the position of the superoposterior and anterolateral papillary muscle complexes.

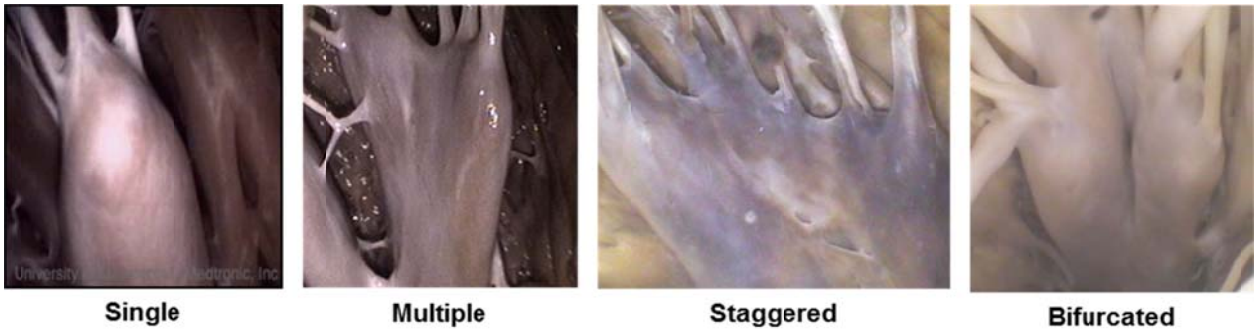

Figure 1.12. Images of the left ventricular papillary muscles taken from the Visible Heart® library.

Chordae tendinae are typically analyzed with respect to their number and length, and quantified by one of two measurement techniques—tethering length and insertion length. Tethering lengths are defined as the distances from the papillary heads to the saddle horn of the mitral

annulus. Insertion lengths are defined as the lengths from the chordae from their origins at the papillary head to their insertion into the leaflet tissue. Anatomical dimensions obtained from patients with no reported mitral regurgitation or other valvular pathologies as reported by Sonne et al. and Lam et al., and summarized in Table 2[34,35]. Yet, it should be emphasized that, as with other anatomical studies, these data do not account for all anatomical variations. For example, it has also been reported that for the mural leaflet, occasionally the chordae may extend simply from the ventricular myocardium to the leaflet, i.e., without a papillary muscle attachment. Furthermore, it is well known that the chordae tendinae themselves may elicit highly variably anatomies, and various subpopulations of chordae have been classified by both function[36] and type[11]. Figure (1.10) shows examples of these identified variations in the types of chordae, including: posterior marginal chordae, commissural chordae, anterior strut chordae, anterior marginal chordae, basal posterior chordae, and posterior intermediate chordae.

Table 1.2 Data on the chordal lengths of the mitral sub-valvular apparatus measured in vivo via 3D echocardiography[34] and post mortem[35,36].

Measured Anatomical Feature	**Data**	**Sample Size**
APM tethering length in systole	3.54 ± 0.82 cm [34]	N=120
PPM tethering length in systole	3.76 ± 0.78 cm [34]	N=120
Anterior leaflet insertion length	1.81 ± 0.49 cm [35]	N=50
Posterior leaflet insertion length	1.18 ± 0.26 cm [35]	N=50
Ratio of chordal origins to insertions	1:5 [36]	N=18

APM = Superoposterior (Anterior) papillary muscle
PPM = Inferoanterior (Posterior) papillary muscle

The Tricuspid Valve

The right atrioventricular valve, or tricuspid valve, is situated within the right atrioventricular junction and modulates the flow of blood between the right atria and right ventricle. This valve is typically defined by three leaflets suspended from the muscular atrioventricular junction. When considered relative to the landmarks of the body, or employing an attitudinally correct nomenclature, these leaflets are located in septal, antero-superior (traditionally anterior), and inferior (traditionally posterior) positions, figure (1.13)[37]. The antero-superior leaflet is commonly the largest of the three, and extends from the medial border of the ventricular septum to the anterior free wall. This, in effect, also forms a partial separation between the inflow and outflow tracts of the right ventricle. The inferior leaflet extends from the lateral free

wall to the inferior portion of the ventricular septum. Finally, the septal leaflet extends from the annulus of the orifice to the medial side of the interventricular septum (on the inflow side), and often includes the membranous part of the septum[6]. See figure (1.14) for an anatomical dissection of the tricuspid valve. When closed due to the high pressure in the ventricle during contraction (systole) the leaflets press together (coaptation) and their boundaries are defined by three commissures, or zones of apposition, named for the two adjoining leaflets (antero-septal, antero-inferior, and inferior-septal)[37].

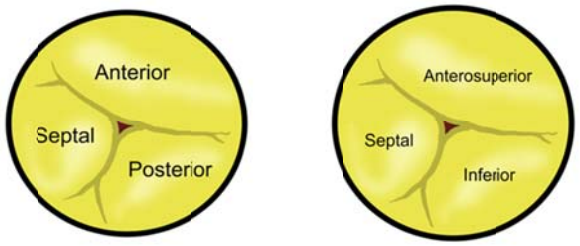

Figure 1.13. Nomenclature of the Tricuspid valve

To date, the morphology of the tricuspid valve has received less attention than the mitral valve, hence thorough anatomical studies are limited. The tricuspid annulus is known to have a non-planar three-dimensional shape, similar to the mitral valve annulus. Further, it has been described as changing its shape dramatically throughout the course of the cardiac cycle. These changes in annular geometries during systole, from a more circular shape to an elliptical shape, result in overall reductions of annular sizes by up to 40%[38]. As the heart contracts, the annulus reaches its minimum size during isovolumetric relaxation and its maximum during isovolumetric contraction[28]. Data relating to the tricuspid annulus from Kwan et al., Silver et al, Seccombe et al. and Wenink et al. can be seen in table 1.3.

Table 1.3 Data on the tricuspid valve annulus measured in vivo via 3D echocardiography[29] and post mortem[39–41].

Measured Anatomical Feature	Data	Sample Size
Systolic annular area	10.75 ± 1.81 cm2 [29]	N=13
Post mortem orifice area	10.60 ± 3.40 cm [39]	N=160
Systolic septo-medial dimension	3.31 ± 0.32 cm [29]	N=13
Systolic anterior-posterior dimension	3.79 ± 0.43 cm [29]	N=13
Post-mortem annular circumference	11.10 ± 1.10 cm [40] 11.30 ± 0.50 cm [42]	N=50 N=24

As with the mitral valve, the leaflets of the tricuspid valve are complimented by a subvalvular apparatus consisting of papillary muscle complexes that work to tether the valve leaflets via chordal tendons. The papillary muscle complexes that support the three composite leaflets of the tricuspid valve commonly elicit marked differences in structure. The septal papillary complex can consist of a collection of small muscles in close proximity and usually attaches to both the septal and antero-superior leaflets. In addition, chordae may extend from the septal wall itself without a distinguishable papillary muscle head[6]. See figures (1.14) and (1.15). The medial complex lies superior and distinct from the septal complex and, as with the septal complex, consists of a collection of muscles and chordal attachments to both the septal and antero-superior leaflets[42]. The much larger anterior papillary muscle complex supports the zone of apposition between the antero-superior and inferior leaflets in the majority of hearts. In general, it is considered that in half of all normal individuals, the large anterior papillary muscle supports only the leading edge of the antero-superior leaflet. It is then typical for a smaller inferior (or posterior) muscle (or in many observed human hearts, multiple muscles) to support the zones of apposition between the inferior and septal leaflets. Nonetheless, the most constant and characteristic feature of the normal tricuspid valve is the presence of multiple attachments of cords from the septal leaflet directly onto the ventricular septum[37]. Due to its somewhat remote location away the septum, coordinated contractions of the anterior papillary muscle complex are facilitated by special conduction fibers located within the moderator band, a continuation of trabeculations within the right ventricle[6].

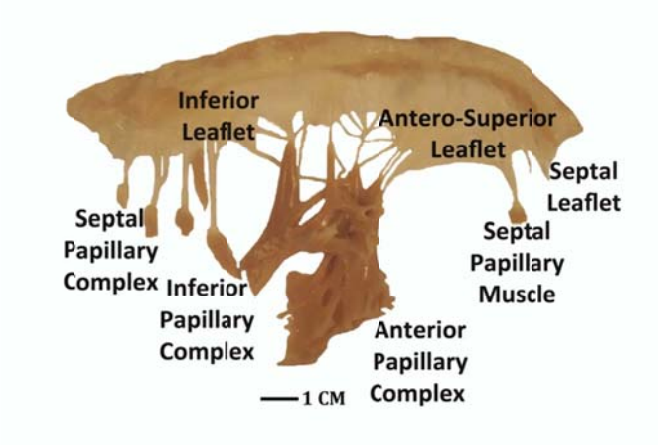

Figure 1.14. The subvalvular apparatus of the tricuspid valve dissected from a human heart.

Figure 1.15. displays videoscopic images of the subvalvular apparatus of the tricuspid valve taken from reanimated human hearts utilizing Visible Heart® methodologies, as described in Chapter 20. Such images emphasize the large anatomical variations that can exist from heart to heart (unpublished data).

Table 1.4 Data on the chordal lengths of the tricuspid sub-valvular apparatus measured post mortem[40]

Measured Anatomical Feature	Data	Sample Size
Septal leaflet insertion length	1.50 ± 0.87 cm [40]	N=50
Anterior leaflet insertion length	1.53 ± 0.69 cm [40]	N=50
Posterior leaflet insertion length	1.37 ± 0.64 cm [40]	N=50

Previously, Silver et al. reported the common insertion lengths of chordae tendinae for healthy human hearts, which were defined as the distances from the origins of the papillary muscles to their corresponding insertion points on the valve leaflets, i.e., emanating from the relative three papillary complexes (anterior, inferior, and septal; Table 1.4)[40]. These measurements were completed on 50 formalin fixed human hearts, thus it should be noted that these data may have specific limitations when compared to the tethering lengths measured using modern imaging techniques, e.g., those used to measure the tethering lengths of the mitral chordae mentioned earlier in the chapter. As such, we suggest that future detailed assessments of the tricuspid subvalvular apparatus employing modern imaging techniques could greatly benefit the field of cardiac anatomy.

The Semi-lunar Valves

A healthy semilunar valve is composed of three valve leaflets, each attached to its respective annuli, situated between the ventricular outflow tracts and the main arteries carrying blood away from the heart. This elegant structure is much simpler than that of the atrioventricular valves described above, in that the semilunar valve leaflets do not require an apparatus to prevent regurgitation. When closed, the three leaflets co-apt along zones of apposition, or commissures: fibrous areas that extend some distance from the free edge of the leaflets. At the

center of the valve where all three leaflets co-apt a distinct fibrous nodule can be found on each leaflet. The leaflet margins are attached to the arterial wall in the shape of a half-moon, hence the semilunar moniker. Normally, the regions of the valves where the commissures meet the arterial wall are considerably higher than the seats of the leaflets, thereby giving the valve a crown-like shape. These three points, particularly in the aortic valve, are used to define the sinotubular junctions, figure (1.16). Although we have discussed the positioning of the valves in the heart by referring to their respective annuli, many anatomists contest the idea that there are single defined annuli for both the pulmonary and aortic valves[43]. Interestingly, there is a defined annulus where the respective arteries are attached to the ventricular outflow tract; however, due to the crown-like structure of the valve, the true hemodynamic junction of the valves spans this annulus. Anderson et al. report that this structural shape results in part of the arterial wall being considered a ventricular structure (in a hemodynamic sense) and part of the ventricular wall (hemodynamically) an arterial structure. Just distal to the valves are the arterial sinuses that are represented by dilations of the artery positioned above each leaflet and additionally house the coronary artery ostium. The sinus also provides a recess for the valve leaflets to retract into, allowing for unrestricted flow from the ventricle to the artery. Finally, the virtual ring, upon which all annular measurements are based and which defines the basal plane of aortic valve, is defined by the three anatomical anchors at the nadir of each aortic leaflet[44]. These features are illustrated by the diagram in figure (1.16).

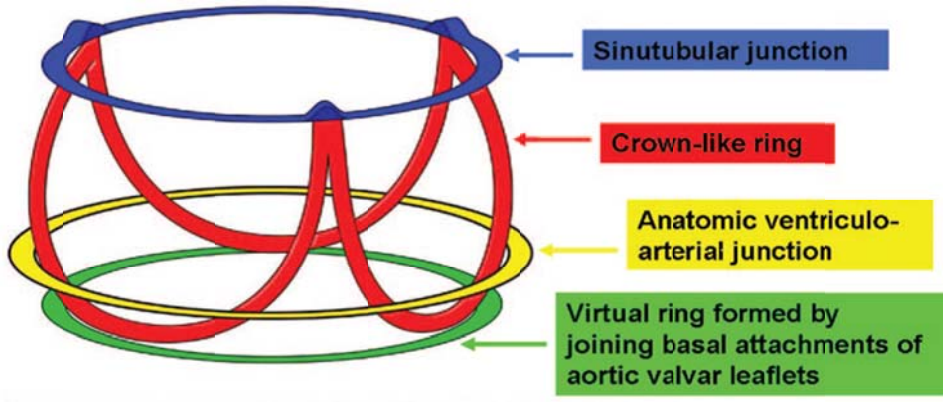

Figure 1.16. Three-dimensional arrangement of the aortic root, which contains 3 circular "rings," but with the leaflets suspended within the root in crown-like fashion[45]. (Used with permission)

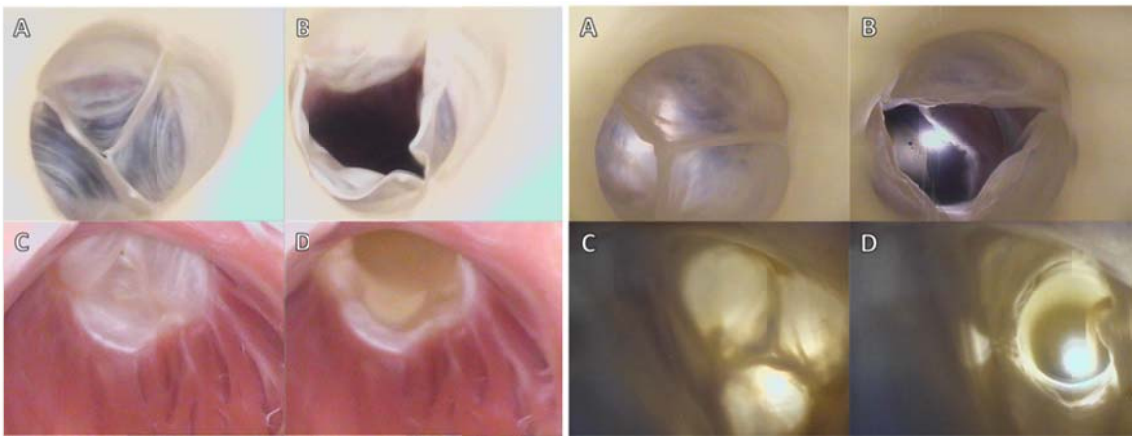

Figures 1.17 and 1.18 show image sequences of the functional movements of the pulmonary and aortic valves respectively; these images were obtained from reanimated human hearts employing Visible Heart® methodologies[16,17]. The images include views of semilunar valves from above (i.e., from videoscopes within the pulmonary artery and the aorta) and from below (with videoscopes within the right and left ventricular outflow tracts).

The Functioning of the Semilunar Valves

When a semilunar valve is functioning correctly, the leaflets are pushed into the sinus during myocardial contraction (systole) to allow blood to leave the ventricles. As the myocardium relaxes and the pressure within the ventricle drops below the pressure distal to the valve in the arterial system (the aorta or pulmonary artery), the valve snaps shut. This usually happens soon after ventricular systole but before the heart has completely relaxed, so that during diastole, when the chambers are filling through the atrioventricular valves, the leaflets of the semilunar valves remain tightly closed. A positive pressure difference between the aorta and the coronary sinus, which lies within the right atrium, allows for the flow of blood through the coronary vasculature. Thus, it should be noted that the heart muscle is perfused with blood when the semilunar valves are closed and the cardiac myocytes are relaxing. The sequence of valve function can be seen in figures (1.17) and (1.18).

In general, dysfunctions of the semilunar valves are usually characterized by one of two symptoms: failure of the valves to successfully close or failure of the valves to successfully open. Such dysfunctions of the valves during systole, i.e., failure of the valve to successfully open, are defined as stenosis of the valve. This pathology is characterized by reduction in the effective orifice area of the valve (the size of the opening that allows blood to pass), which in turn forces the ventricles to work harder to move blood to the body or lungs. Dysfunctions of the semilunar valves during diastole, when the ventricles are relaxing, result in regurgitation; this occurs when

blood is allowed back into the ventricle from the arterial system, overloading the ventricles and potentially causing ventricular arrhythmias or initiating chronic heart failure.

Histologic Features of the Semilunar Valves

Each leaflet of the semilunar valve has a fibrous core, or fibrosa, with an endothelial lining containing delicate sheets of elastin on its arterial and ventricular aspects. This so-called fibrous "backbone" is represented by a dense collagenous layer, which gives way to a much looser structure, or spongiosa, toward the ventricular aspects of the leaflet cusps. The zone of apposition of the leaflets consists of an abrupt thickening of the fibrous layer made up of closely packed vertically directed fibers and builds at the central portion of the free edge, creating a node termed the Nodulus Arantii[18,46]. Figure (1.19) displays a cross-section of an aortic valve leaflet displaying the varying tissue types[45].

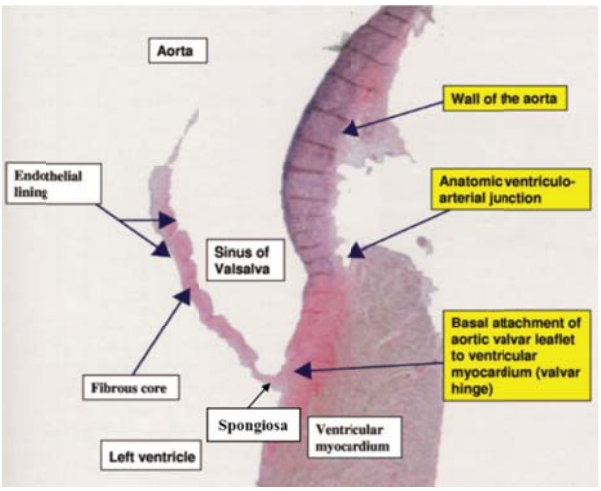

Figure 1.19. Histology of the aortic valve[45] (Used with permission)

The Aortic Valve

Located in the center of the fibrous skeleton between the mitral valve and the tricuspid valve, the aortic valve is considered as the "centerpiece" of the heart and is often considered the most important cardiac valve with respect to normal cardiac function[45].

The Aortic Root

The aortic root contains three circular rings and one crown-like ring, figure (1.16)[43]. The semi lunar connection of the three leaflets to the arterial wall mimics the shape of a crown, whose base forms a virtual ring known as the basal plane of the valve. This plane represents the inlet from the left ventricular outflow tract into the aortic root. Distal to the valve a true ring joining

the top of each commissure, represented by the crown arches, is defined as the sinotubular junction (STJ)[45]. Hence the STJ dictates the transition from the aortic root into the ascending aorta. The semilunar hinges then cross another defined "ring" known as the anatomic ventriculoarterial junction. This overall anatomic arrangement is described previously in figure 1.16, but can be readily observed when the aortic root is opened linearly as seen in figure (1.20)[45].

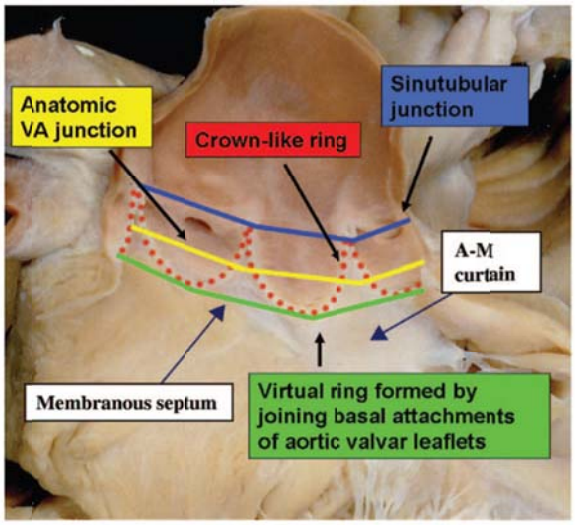

Figure 1.20. The leaflets have been removed from this specimen of the aortic root, showing the location of the 3 rings relative to the crown-like hinges of the leaflets. VA indicates ventriculoarterial; A-M, aortic-mitral.[45] (Used with permission)

The normal aortic root elicits a relatively consistent shape between patients, but can vary dramatically in size. Kunzelman et al. demonstrated a definable mathematical relationship between root diameter and clinically measurable leaflet dimensions (Table 1.5)[47]. Note that the aortic annulus exhibits a max and min dimension similar to an ellipse, whereas the STJ is considered to be circular in shape. In general, the diameter at the level of the sinotubular junction typically exceeds that at the level of the basal plane by a factor of 1:1.6[47,48]. The valvular complex is a dynamic structure with its geometric parameters changing continuously throughout the phases of the cardiac cycle and in relation to the associated changes in pressure that will occur within the aortic root[49]. For example, from diastole to systole, the relative changes in diameter at the level of the outlets and at the base of the aortic valve has been noted to increase by ~12% and decrease by ~16%, respectively[50,51]. Additionally, the orientation of the left ventricular outflow tract and the aortic root (i.e., the angle between the two) is known to

vary from patient to patient. It is also understood that this angle becomes more acute with age. Middelhof et al. reported that hearts from individuals aged >60 years exhibited angles between 90 and 120 degrees, whereas individuals aged <20 years presented with angles between 135 and 180 degrees[52].

Table 1.5 Data on the aortic valve annulus, sinus of valsalva and sinotubular junction measured using multislice computed tomography[44,53].

Measured Anatomical Feature	Data	Sample Size
Maximum aortic annular diameter	26.9 ± 2.8 mm [44] 26.4 ± 2.8 mm [53]	N=25 N=150
Minimum aortic annular diameter	21.4 ± 2.8 mm [44] 24.0 ± 2.6 mm [53]	N=25 N=150
Sinus of Valsalva mean diameter	32.3 ± 3.9 mm [53]	N=150
Sinus of Valsalva height above the basal plane	17.2 ± 2.7 mm [53]	N=150
Sinotubular junction mean diameter	28.1 ± 3.1 mm [53]	N=150
Sinotubular junction height above basal plane	20.3 ± 3.1 mm [53]	N=150

It is important to note that one of the most critical functions of the aortic root is to facilitate coronary artery perfusion during ventricular diastole. This is achieved by directing 3-5% of the circulating blood through both the left and right coronary arteries while the aortic valve itself is closed. In general, the orifices of the coronary arteries arise within the two anterior sinuses of Valsalva, usually positioned just below the sinotubular junctions[48,54,55]. However, it is not unusual to find these arteries positioned superior relative to the sinotubular junction. Cavalcanti et al. reports the mean distance measured from the orifice of the left coronary artery to the basal attachments of the corresponding leaflets were 12.6±2.61 mm, and for the right coronary artery they were 13.2±2.64 mm in 51 normal postmortem hearts[56]. It should also be recalled that it is the location of these coronary arteries that dictates the naming of the aortic valve leaflets/cusps—the left coronary, the right coronary, and the noncoronary.

The Aortic Leaflets

As noted above, the leaflets of the aortic valve are named for the branching coronary arteries that feed the left and right sides of the heart. More specifically, both the right and left leaflets attach to the aortic root in the predominantly muscular region of the left ventricular outflow tract, whereas the noncoronary cusp is chiefly attached to the fibrous region above the membranous septum. This fibrous continuity connects the aortic valve to the anterior (aortic)

leaflet of the mitral valve, forming the aortic-mitral curtain. It is the ends of this area of fibrous continuity that thicken and then form the fibrous trigones of the cardiac skeleton[5].

Piazza et al. state that variations exist in all aspects of the aforementioned dimensions of individual leaflets, including: 1) height; 2) width; 3) surface area; and 4) volume of each of their supporting sinuses of Valsalva[45]. Vollebergh et al. reported average widths (measured between the peripheral zones of attachment along the sinus ridge) for the right, the noncoronary, and the left coronary leaflets were 25.9, 25.5, and 25.0 mm respectively, in an investigation of 200 normal hearts[57]. It was also described that the average heights (measured from the base of the center of the leaflet to their free edges) for the right coronary, noncoronary, and left coronary cusps were 14.1, 14.1, and 14.2 mm respectively. Such variations in the leaflet dimensions of healthy valves highlight the need to focus on the anatomy and function of each leaflet when developing prosthesis for either the surgical or transcatheter treatment of aortic valve pathologies.

The Pulmonary Valve

Due to its relative location within the infundibular musculature (at the distal portion of the right ventricular outflow tract), the pulmonary valve is considered, in an anatomical sense, a more simple valvular structure than the aortic valve. Anderson et al. note that the left and the right leaflets of the aortic valve face lie adjacent to the pulmonary trunk, and this relative anatomic orientation has been used to name the pulmonary valve leaflets: the right and left facing leaflets and the nonfacing leaflet[5]. Anatomically, the commissure of both the right and left leaflets are supported by the supraventricular crest of the right ventricle, which separates the pulmonary valve from the tricuspid valve. The opposite edge of the valve is in general the most anterior part of the heart (i.e., the nonfacing leaflet is supported by the anterior wall of the infundibulum)[5].

The pulmonary valve is generally considered a less important anatomical feature with respect to cardiac disease. Valve replacement is considered less challenging due to the pressure gradient across the valve and the relative ease of access to the annulus. As previously mentioned, the ease of complete valve removal from the cardiac skeleton has led to the use of the pulmonary valve as an autograft replacement for the aortic valve in some congenital heart patients. Even so, information on the valve is less abundant and reports on variations in valve dimensions are

less comprehensive. Capps et al. report the mean diameter of the valve as 25.4 mm ± 3.2 mm in a study comparing the size of the aortic and pulmonary valve to the overall body surface area (Table 1.6). However, these measurements were taken on valves removed postmortem using a Hegar dilator without annular dilation. By the authors' admission, this sizing presents limitations regarding the material properties of the pulmonary annulus differing significantly from the aortic[58]. As such, these measurements should be used as a rough guideline and the alternate methodology explains the difference in the aortic measurements reported here from those measured at end systole in vivo by Schultz et al. and Tops et al. [44,53] shown in table 1.5.

Table 1.6 Post mortem mean pulmonary and aortic diameters[58].

Measured Anatomical Feature	Data	Sample Size
Mean annular diameter	25.4 ± 3.2 mm [58]	N=3997
Mean aortic annular diameter	22.4 ± 2.7 mm [58]	N=3370

Cardiac Valve Co-location with Other Cardiac Structures

It should be considered that when performing cardiac valve surgeries and/or contemplating novel percutaneous approaches to valvular repairs, it is vital to have a strong anatomical appreciation of the relevant associated structures, i.e., those cardiac structures that surround either the mitral and tricuspid valves.

Atrioventricular valves

It is important to understand the position and course of the coronary vasculature in relation to the mitral and tricuspid valves. The coronary sinus, although usually superior to the mitral annulus, circles the heart in the posterior atrioventricular groove[53,59]. The circumflex artery, after bifurcating with the left anterior descending, courses between the aorta and the pulmonary artery and continues around the left atrioventricular groove. This path results in the artery running very close to the posterior region of the mitral valve annulus. Barker et al. report that in 85% of reported cases, its course stops here, although it can extend into the posterior atrioventricular groove in left dominant hearts[28]. Additionally, in many cases the left circumflex coronary artery crosses underneath the coronary sinus at a variable distances[28,53,59], figure (1.21). Therefore, such structures are at risk when performing operations on the posterior mitral valve annulus; this may be particularly relevant when complex reconstructive techniques are employed [4]. In much the same way, the tricuspid valve can be bordered by the right coronary

artery within the anterior atrioventricular groove, i.e., as it courses from the aortic root to the inferior aspect of the heart[28].

The proximity of the aortic valve to the mitral valve and the fact that the inter-trigonal tissue within the anterior mitral valve annulus courses beneath the aortic valve leaflets should be considered if sutures are required in either the anterolateral and posteromedial portions of the mitral valve to prevent damage to the aortic leaflets[28], figure (1.21).

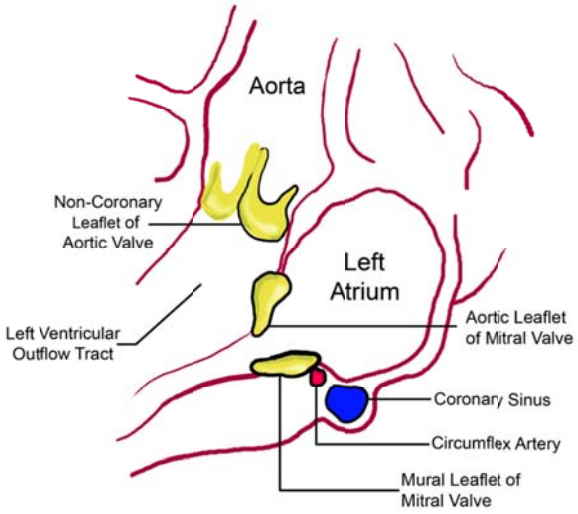

Figure 1.21. Diagram indicating the surrounding anatomy of the mitral valve

Finally, the atrioventricular bundles of conduction fibers from the atrioventricular node penetrate the heart's central fibrous body, which passes through the membranous septum and subsequently splits to form the left and right bundle branches. Additionally on the right side of the human heart, the atrioventricular node is seated within the superior aspect of the triangle of Koch, a series of anatomical landmarks within the right atrium that are used to define integral parts of the conduction system, figure (1.22). Barker et al. define the triangle of Koch as being bordered by the septal leaflet of the tricuspid valve on its left side, the coronary sinus inferiorly, and the Tendon of Todaro on its right side[28]. As with the coronary vasculature and the surrounding valves these anatomical features can play an important role in the planning of surgical and/or device-related repair of the atrioventricular valves, as damage to the conduction fibers running through it can have severely detrimental results on the overall cardiac health of the patient.

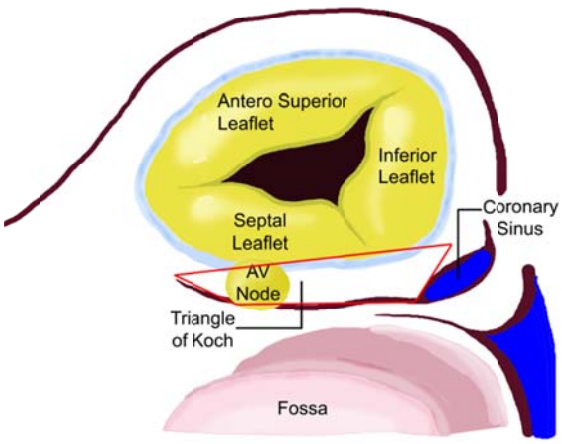

Figure 1.22. Diagram indicating the surrounding anatomy of the tricuspid valve.

Semilunar valves

The pulmonary valve's location above the base of the heart allows operation on or replacement of the valve to be completed with significantly less concern of damaging any other anatomical features. One needs to consider the cardiac vasculature as early branches from both the right and left coronary arteries that feed the right ventricular outflow tract. Additionally, being the most anterior portion of the heart, this valve lies close to the patient's sternum, thus sternal compression may alter its shape or affect the performance of any prosthesis placed in the pulmonary annulus.

The anatomical position of the aortic valve is considered to pose many more challenges, thus the remainder of this section will focus on this valve. One of the most important and complex structures in proximity to the aortic valve is the cardiac conduction system. Within the right atrium, the atrioventricular node is located within the triangle of Koch, situating the node in close proximity to the subaortic region of the left ventricular outflow tract and the membranous septum, part of the cardiac skeleton. This relationship allows one to understand why pathologies involving the aortic valve may lead to either a complete heart block or to an intraventricular conduction abnormality[45]. Further, the atrioventricular node continues as the bundle of His, piercing the membranous septum and then penetrating into the left ventricle through the central fibrous body. On the left side, this conduction bundle (left bundle branch) exits immediately beneath the membranous septum and runs superficially along the crest of the

ventricular septum, where it then subdivides into the fascicles of the Purkinje system[45]. This relationship is beautifully demonstrated in the anatomical model drawn by Tawara in 1906 and shown in figure (1.30)[60]. It is important to note that this anatomical relationship can have major implications with the potential to induce abnormalities of conduction after percutaneous or surgical valve implants and result in the patient requiring cardiac rhythm management[45].

In addition to the conduction system, an intimate knowledge of the aortic valve's proximity to both the coronary arteries and the mitral valve helps to minimize post procedural complications. In particular, the left coronary artery can bifurcate into the left anterior descending artery and the circumflex artery early in some patients, leaving portions of these critical vessels close to the aortic annulus and consequently demanding attention during the placement of supra-annular surgical valves. Additionally, knowledge of the locations of the coronary artery ostia is essential for an appropriate percutaneous replacement of the aortic valve. In the instance of transcatheter valve deployment, the prosthesis typically will crush the leaflets of the native valve against the aortic wall. This combination of a relatively low-lying coronary artery ostium and a large, heavily calcified native aortic leaflet can lead to obstruction of the flow into the coronary arteries[45].

The Cardiac Conduction System

Function of the Cardiac Conduction System

In its most fundamental form the cardiac conduction system, as seen in figure (1.23), consists of a series of specialized heart cells, or pacemaker cells, that control the sequence of excitation and rate of contraction of the remaining myocardium. There are three primary anatomical structures; the sinoatrial (SA) node, the atrioventricular (AV) node and the His-Purkinje system. The SA node, the natural pacemaker of the heart, was first described by Keith et al.[61] and is located in the upper right atrium near the junction of the superior vena cava. The electrical signal propagates from the SA node through the atrial tissue before reaching the AV node located at the base of the right atrium above the base of the heart. After a slight pause the AV node advances the electrical signal into the bundle of His, a group of electrically conductive cardiac cells that penetrate the fibrous skeleton and distribute the electrical signal to the ventricles. Upon entering the ventricles the His bundle bifurcates into a left and right branch which run down the septum and excite the left and right ventricles respectively. Finally the

electrical signal passes through the Purkinje fibers allowing for the coordinated contraction of the ventricles.

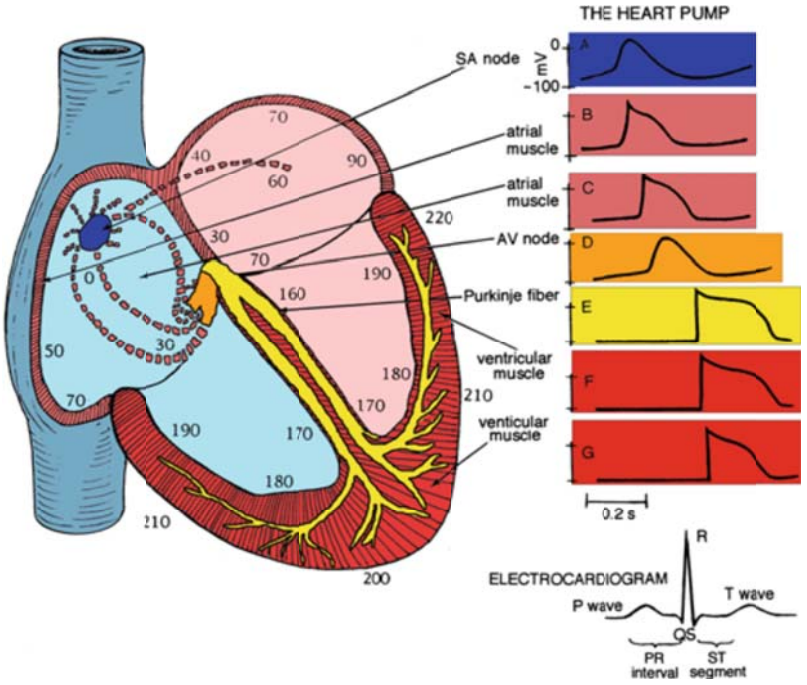

Figure 1.23. The conduction system of the heart defining the sequence of activation in a healthy heart from the sinoatrial node, through the atrioventricular node to the His-Purkinje system. AV=atrioventricular; SA=sinoatrial [25] (Used with permission)

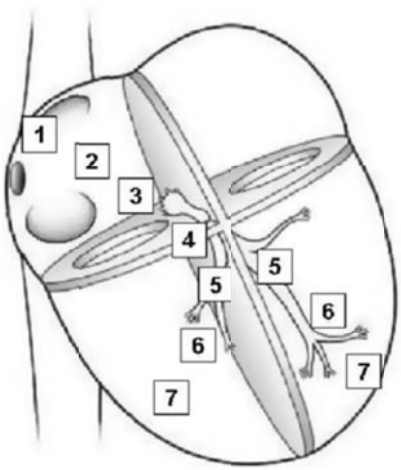

Normal Activation Sequence	Structure	Conduction velocity (m/sec)	Pacemaker rate (beats/min)
1	SA node	< 0.01	60 – 100
2	Atrial myocardium	1.0 – 1.2	None
3	AV node	0.02 – 0.05	40 – 55
4	Bundle of His	1.2 – 2.0	25 – 40
5	Bundle branches	2.0 – 4.0	25 – 40
6	Purkinje network	2.0 – 4.0	25 – 40
7	Ventricular myocardium	0.3 – 1.0	None

Figure 1.24 Conduction velocities and intrinsic pacemaker rates of various structures within the cardiac conduction pathway. Tabulation adapted from Katz AM, ed. Physiology of the heart. 3rd ed. 2001 [25] (Used with permission)

As this signal passes along the cardiac conduction system the depolarization of the pacemaker cells initiates a coordinated depolarization of myocardial cells throughout the remaining myocardium. This cell to cell conduction is achieved through gap junctions, ion channels formed by the connection of intercalated disks which hold the cells together. The speed at which the action potential propagates through the myocardium is known as the conduction velocity and can vary dramatically depending on the tissue type. For example, the conduction velocity in the AV node is considerably slower than the Purkinje fibers due to cell size and the tortuous orientation of the cells within the node[62]. This timed depolarization causes an efficient and effective contraction of the myocardium that moves blood through the heart, shown graphically in figure (1.24).[25]

Electrophysiology

In the healthy cardiac myocyte, the resting membrane potential lies at approximately -90mV, dominated by the K+ equilibrium potential. Laske et al. elegantly describe the depolarization and repolarization of the cardiac myocytes as follows. An action potential is initiated when this resting potential becomes shifted toward a more positive value of approximately –60 to –70 mV. When a myocyte is brought to the threshold potential, by a neighboring pacemaker cell for example, voltage-gated fast Na+ channels actively open (activation gates) allowing Na+ to rapidly crosses the cell membrane. Within a few milliseconds, these fast Na+ channels automatically inactivate. The membrane depolarization due to the activation of the Na+ induces the opening of the voltage-gated slow Ca2+ channels located within both the sarcolemma and sarcoplasmic reticulum (internal storage site for Ca2+) membranes. Thus, there is an increase in the permeability of Ca2+, which allows the concentration to dramatically increase intracellularly. At the same time, the membrane permeability to K+ ions decreases due to closing of K+ channels. For approximately 200–250 ms, the membrane potential stays close to 0 mV, as a small outflow of K+ just balances the inflow of Ca2+. After this fairly long delay, voltage-gated K+ channels open and active repolarization is initiated. The opening of these K+ channels (increased membrane permeability) allows for K+ to diffuse out of the cell due to its concentration gradient. At the same time, Ca2+ channels begin to close, and net charge movement is dominated by the outward flux of the positively charged K+, restoring the negative resting membrane potential to approximately –90 mV. This flow of ions can be seen graphically in figure (1.25)[25].

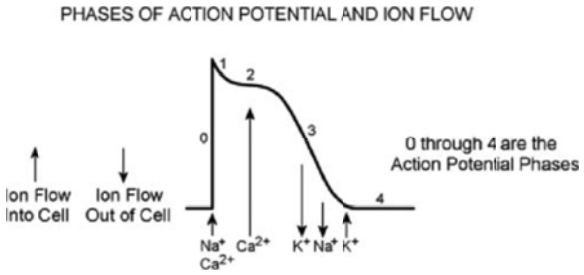

Figure 1.25. Ion flow during the phases of a cardiac action potential.[25] (Used with permission)

It is important to note that, once depolarized, a myocyte cannot contract again until its membrane potential has begun to return to the cell's resting membrane potential. This time period is known as the relative refractory period and varies depending on the cell type. This variation in temporal response to these changes in ion concentration; slow and fast response cells have differing shaped action potentials with different electrical properties in each phase.

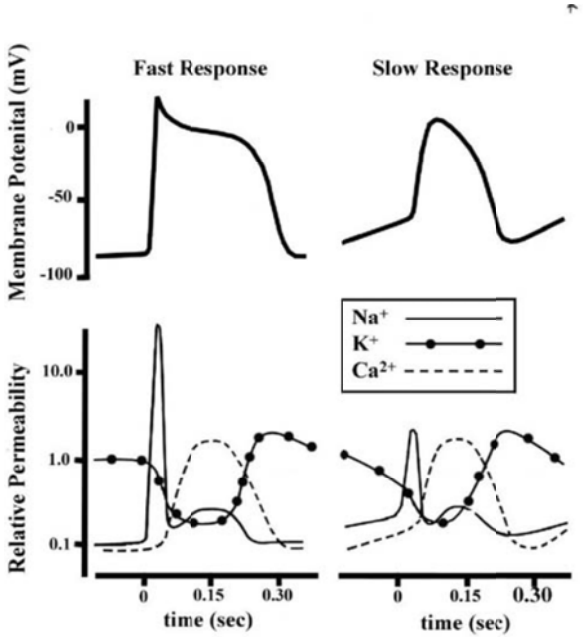

Figure 1.26. The comparative time courses of membrane potentials and ion permeabilities that would typically occur in a fast response (left, e.g., ventricular myocyte) and a slow response cell (right, e.g., a nodal myocyte). Modified from Mohrman DE, Heller LJ, eds. Cardiovascular physiology. 5th ed. 2003 [25] (Used with permission)

Critically, pacemaker cells (slow response type) have the ability to spontaneously depolarize until they reach threshold and thus elicit action potentials. This is achieved via a slow leak of Na+ ions when the cell is repolarized causing a spontaneous rise in the resting membrane potential, ultimately leading to instability and depolarization[63]. The fundamental differences

between the action potentials of fast and slow response cells can be seen in figure (1.26). The intrinsic pacemaker rate is slower in structures further along the activation pathway. For example, the AV nodal rate is slower than the SA nodal rate. This prevents the atrioventricular node from generating a spontaneous rhythm under normal conditions, since it remains refractory at rates <55 beats/min. Interestingly, if the SA node becomes inactive, the AV nodal rate will then determine the ventricular rate.

Location and Specific Function of the Primary Structures of the Conduction System

Although the location of the cardiac conduction system was reported by Tawara (1906), Aschoff (1910) and Monckeberg (1910) [60,64,65] the histological attributes used to designate the pacemakers cells did not utilize the now common immunohistochemical techniques available to researchers. However, the SA and AV node and the His-Purkinje system are highly complex and heterogeneous in terms of function and morphology, differing significantly from other myocardial cells. Extensive research has been done to better understand their form and function and to recreate a three dimensional (3D) anatomic model of the human conduction system. As such, the definition of the nodal regions of the heart is still being researched and reported on and will be surmised below. [66–68]

Sinoatrial Node

The SA node is located at the junction of the superior vena cava and the right atrium usually positioned slightly inferior to the crest of the right atrial appendage. In one tenth of individuals the node forms a horseshoe across the groove reaching into the interatrial groove[69]. From this central region an extensive area of nodal cells can be seen extending into the muscular structure of the terminal crest and interacting with atrial myocytes, see figure (1.27)[70]. In 2005 Dobrzynski et al. and Li et al. used magnetic resonance imaging (MRI) slices and multiple immune-histological techniques to create a detailed model of the rabbit SA node, see figure (1.28)[71,72]. The role of this paranodal area can only be speculated upon and my involve the distribution of the action potential to the atrial muscle[73] or it may have a function in normal pacemaking[68]. However, it has been documented in both canine models[74] and in clinical practice[75] that cessation of SA node electrical activity has required the ablation of the entire crista terminalis.

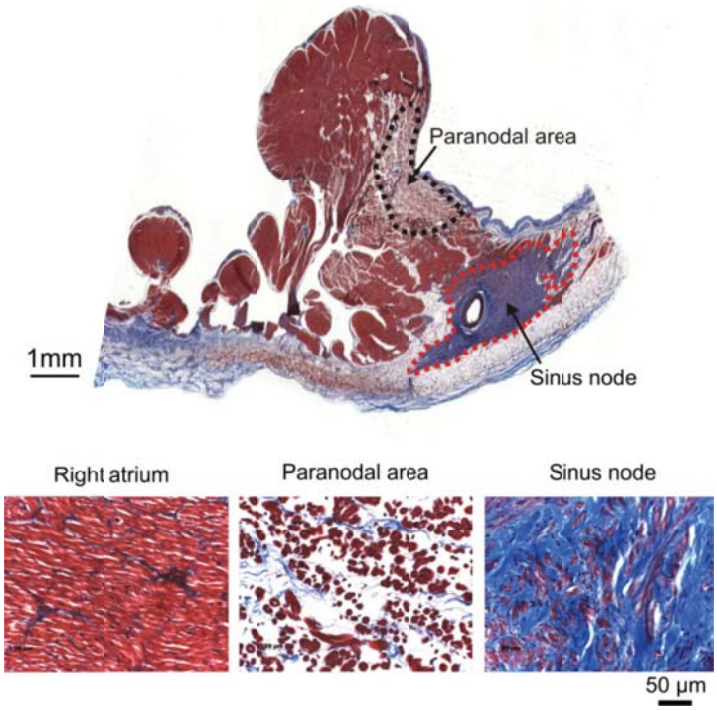

Figure 1.27. The upper panel shows the location of the sinus node in a normal human heart, along with the extensive paranodal area of cells within the terminal crest. The lower panels show the histological features of the working myocytes making up the terminal crest, the myocytes in the paranodal area, and the specialized myocytes making up the sinus node.[73] (Used with permission)

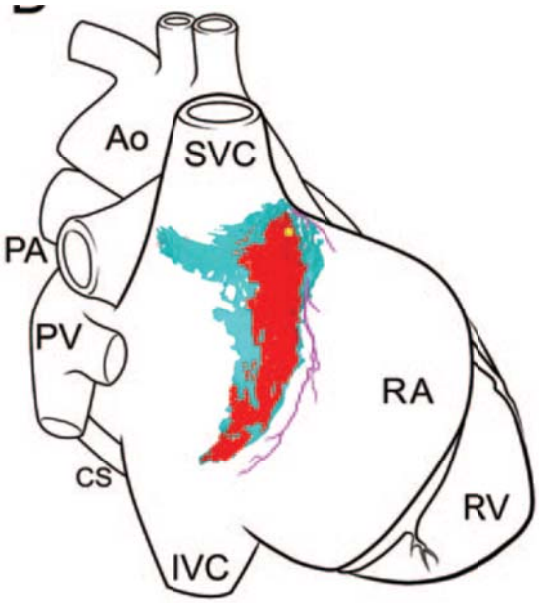

Figure 1.28. SA myocytes displayed on a schematic diagram of the heart. Ao indicates aorta; CS, coronary sinus; PA and PV, pulmonary artery and vein; RA and RV, right atrium and ventricle; SVC and IVC, superior and inferior vena cava[72]. (Used with permission)

Under normal physiologic conditions, the pacemaker cells of the SA node are responsible for generating the "normal sinus rhythm" of the heart usually between 60 – 100 beats per minute in a healthy human heart. The frequency of this rhythm is dictated by the autonomic nervous system and by local changes in the vascular pressures or chemical environment. For example, in an individual at rest, modulation by the parasympathetic nervous system dominates which slows the sinoatrial nodal rate.[25]

Connection to the AV node

After SA nodal activation the electrical signal propagates through the atria via preferentially ordered myofibril pathways including three microscopically identifiable pathways that connect the SA node to the AV node[76]. The most anterior of these pathways bifurcates into Bachman's bundle, delivering impulses to the left atrium, and a second pathway running along the interatrial septum and connecting to the anterior aspect of the AV node. Wenckbach's pathway extends superiorly from the SA node and tracks posteriorly to the superior vena cava before diving down the interatrial septum and connecting to the AV node. Finally Thorel's pathway extends inferiorly from the SA node and follows the crista terminalis before passing the coronary sinus and connecting to the posterior aspect of the AV node[25].

Atrioventricular Node

The atrial aspect of the AV node is considered to reside in the area defined by the superior point of the triangle of Koch, defined by the coronary sinus, the septal leaflet of the tricuspid vale and the tendon of Todaro. Anderson et al. describe the AV node is described as a half-oval of myocytes compacted against the insulating tissues of the central fibrous body by layers of transitional atrial myocytes. This fibrous body is formed via a fusion of the membranous septum and the fibrous continuity between the aortic and mitral valves. When traced inferiorly, the compact part of the AV node branches into rightward and leftward inferior extensions, also known as the left and right bundle branches or the start of the His-Purkinje system, see figure (1.29)[70].

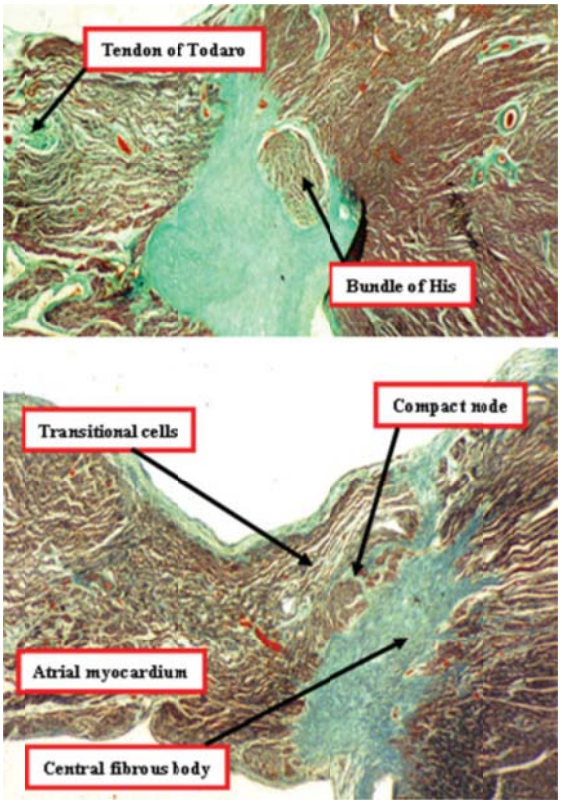

Figure 1.29. The histological sections through the triangle of Koch show the histological features of the atrioventricular node (lower panel) and the bundle of His (upper panel).[70] (Used with permission)

Although usually driven by the SA node, the AV node can autonomously generate rhythms in the range of 25 to 55 beats/min in the human heart. These lower rate rhythms are commonly referred to as ‘‘ventricular escape rhythms,’’ and are important for patient survival, since they maintain some degree of cardiac output in situations when the SA node becomes dysfunctional[25].

His-Purkinje System

As the conduction system courses into the ventricular septum the fibers enter the fibrous body known as the bundle of His. Anderson et al. explain that having entered the central fibrous body, the His bundle branches as it enters the ventricles at the crest of the muscular ventricular septum. These left and right bundle branches are enclosed within fibrous sheaths as they extend into the ventricles. As depicted by Tawara (1906), see figure (1.30), the left bundle in the human heart further branches into three interlinked fascicles as it passes down toward the ventricular. The right bundle continues as a thin cord of insulated cells, emerging on the right side of the septum immediately beneath the medial papillary muscle and then running through

smaller branches within trabeculation before crossing to the free wall of the ventricle in the moderator band[70]. The complex network of conducting fibers that extends from either the right or left bundle branches is composed of the rapid conduction cells known as ‘‘Purkinje fibers.’’ These fibers act as preferential conduction pathways to provide rapid activation and coordinate the excitation pattern within the various regions of the ventricular myocardium[25]. The right and left ventricles both exhibit extensive trabeculations on the endocardial surfaces that, along with the presence of fibrous conduction bands, help the Purkinje network propagate the activation sequence across the whole heart.

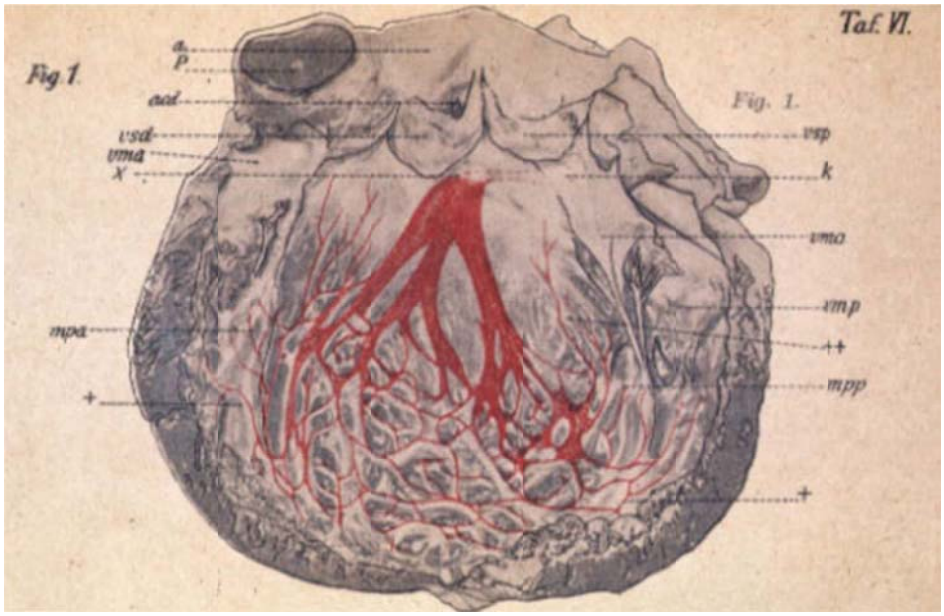

Figure 1.30. Tawara’s anatomical diagram of the left bundle branch showing the conduction system exiting from the fibrous cardiac skeleton in close proximity to the aortic valve. It then branches out and descends along the septal, endocardial surfaces of the left ventricular myocardium[60]. (Used with permission)

Cardiac Arrhythmias

Dysfunction of the cardiac conduction system results in the development of abnormal rhythms of heart rate and can result in a reduction in cardiac performance or death. Briefly, disturbances of cardiac impulse formation and/or transmission comprise the principal mechanisms causing abnormalities of heart rhythm. These can be classified as either brady- or tachy-arrhythmias:

Bradycardia may be physiologic in some individuals or it may be the result of either SA node dysfunction or AV conduction block, i.e. the intermittent or permanent block of impulse transmission from the atria to the ventricles. Either of these conditions can be caused by

intrinsic disease in the pacemaker cell or conduction system or by extrinsic factors such as medications or autonomic system disturbances.

Tachycardias can be classified as being due to either abnormally rapid impulse initiation, i.e. abnormal rates from any aspect of the conduction system or abnormal impulse conduction. The term "arrhythmia'' is typically used to refer to disturbances of the normal heart rhythm.

The clinical significance of these cardiac arrhythmias is predominantly related to their associated hemodynamic consequences in addition to the increased risks of life-threatening consequences (e.g., sudden cardiac death due to ventricular fibrillation) and is exquisitely described by Li et al.[77].

Cardiac Valve Co-location with Other Cardiac Structures

For the purposes of this thesis the co-location of the conduction system to the four cardiac valves holds the most relevance and has been described previously. However, it is worth mentioning that due to its pervasiveness throughout the whole heart the cardiac conduction system becomes a relevant anatomical feature during any cardiac surgical or catheterization procedure. Additionally, whilst knowledge of the location of the conduction fibers themselves is critical, care needs to be taken to locate and avoid the coronary arteries that supply blood to the SA and AV nodes. A fundamental knowledge of this anatomical feature greatly reduces the chance of conduction related pathologies occurring as a result of cardiac procedures or device implantations design for the treatment of other non-related pathologies.

Conclusion

The advent of high resolution noninvasive imaging and high spatial and temporal mapping technologies allowing modern cardiac clinics to collect detailed images of myocardial contractions, blood movement, activation sequences and valve function has accelerated the understanding of functional human heart anatomy. This, in turn, has brought new nomenclature to define the anatomical features of the heart so to align with the overall anatomy of the body, a concept known as attitudinally correct anatomy. A detailed understanding of the anatomy, electrophysiology and function of the four cardiac valves and the conduction system is required before conducting investigations into the performance and design of novel transcatheter valvular repairs or replacements.

References

1. Netter, F. *Atlas of human anatomy*. Saunders, Philadelphia PA, USA: (2006).

2. Perloff, J.K. & Roberts, W.C. The mitral apparatus. Functional anatomy of mitral regurgitation. *Circulation* **46**, 227-39 (1972).

3. Cook, a C. & Anderson, R.H. Attitudinally correct nomenclature. *Heart (British Cardiac Society)* **87**, 503-6 (2002).

4. Hill, A.J. *Attitudinally Correct Cardiac Anatomy.* In: Iaizzo PA (ed) The handbook of cardiac anatomy, physiology, and devices, 2nd edn. Humana Press, Totowa NJ, 15-22 (2009)

5. Wilcox, B., Cook, A. & Anderson, R.H. *Surgical anatomy of the valves of the heart*. In: Wilcox BR, Cook AC, Anderson RH (eds) Surgical anatomy of the heart. Cambridge University Press, Cambridge, UK 45-82 (2005)

6. Weinhaus, A.J. & Roberts, K.P. *Anatomy of the Human Heart.* In: Iaizzo PA (ed) The handbook of cardiac anatomy, physiology, and devices, 2nd edn. Humana Press, Totowa NJ, 59-86 (2009)

7. Kumar, N., Kumar, M. & Duran, C.M. A revised terminology for recording surgical findings of the mitral valve . *The Journal of heart valve disease* **4**, 70-77 (1995).

8. Yacoub, M. *Anatomy of the mitral valve chordae and cusps*. (1976).

9. Victor, S. & Nayak, V.M. The tricuspid valve is bicuspid. *The Journal of heart valve disease* **3**, 27-36 (1994).

10. Ritchie, J., Jimenez, J., He, Z., Sacks, M.S. & Yoganathan, A.P. The material properties of the native porcine mitral valve chordae tendineae: an in vitro investigation. *Journal of biomechanics* **39**, 1129-35 (2006).

11. Ritchie, J., Warnock, J.N. & Yoganathan, A.P. Structural characterization of the chordae tendineae in native porcine mitral valves. *The Annals of thoracic surgery* **80**, 189-97 (2005).

12. Becker, A.E. & De Wit, A.P. Mitral valve apparatus. A spectrum of normality relevant to mitral valve prolapse. *British heart journal* **42**, 680-9 (1979).

13. van der Bel-Kahn, J., Duren, D.R. & Becker, A.E. Isolated mitral valve prolapse: chordal architecture as an anatomic basis in older patients. *Journal of the American College of Cardiology* **5**, 1335-40 (1985).

14. Gams, E. *et al.* Importance of the mitral apparatus for left ventricular function: an experimental approach . *European journal of cardio-thoracic surgery : official journal of*

the European Association for Cardio-thoracic Surgery **6 Suppl 1**, S17-23; discussion S24 (1992).

15. Gams, E. *et al.* Importance of the left ventricular subvalvular apparatus for cardiac performance . *The Journal of heart valve disease* **2**, 642-645 (1993).

16. Hill, A.J. *et al.* In vitro studies of human hearts. *The Annals of Thoracic Surgery* **79**, 168-177 (2005).

17. Atlas of Human Cardiac Anatomy. **http://www.vhlab.umn.edu/atlas**

18. Misfeld, M. & Sievers, H.-H. Heart valve macro- and microstructure. *Philosophical transactions of the Royal Society of London. Series B, Biological sciences* **362**, 1421-36 (2007).

19. Marron, K. *et al.* Innervation of human atrioventricular and arterial valves. *Circulation* **94**, 368-75 (1996).

20. Filip, D.A., Radu, A. & Simionescu, M. Interstitial cells of the heart valves possess characteristics similar to smooth muscle cells. *Circulation research* **59**, 310-20 (1986).

21. Icardo, J.M. & Colvee, E. Atrioventricular valves of the mouse: II. Light and transmission electron microscopy. *The Anatomical record* **241**, 391-400 (1995).

22. Icardo, J.M. & Colvee, E. Atrioventricular valves of the mouse: III. Collagenous skeleton and myotendinous junction. *The Anatomical record* **243**, 367-75 (1995).

23. Fenoglio, J.J., Tuan-Duc-Pham, Wit, A.L., Bassett, A.L. & Wagner, B.M. Canine mitral complex. Ultrastructure and electromechanical properties. *Circulation research* **31**, 417-30 (1972).

24. Itoh, A. *et al.* Active stiffening of mitral valve leaflets in the beating heart. *American journal of physiology. Heart and circulatory physiology* **296**, H1766-73 (2009).

25. Laske, T.G., Shrivastav, M. & Iaizzo, P.A. *The Cardiac Conduction System*. In: Iaizzo PA (ed) The handbook of cardiac anatomy, physiology, and devices, 2nd edn. Humana Press, Totowa NJ, 159-176 (2009)

26. Carpentier, A. Cardiac valve surgery--the “French correction” . *The Journal of thoracic and cardiovascular surgery* **86**, 323-337 (1983).

27. Quill, J.L., Hill, A.J., Laske, T.G., Alfieri, O. & Iaizzo, P.A. Mitral leaflet anatomy revisited . *The Journal of thoracic and cardiovascular surgery* **137**, 1077-1081 (2009).

28. Barker, T.A. & Wilson, I.C. *Surgical anatomy of the mitral and tricuspid valve*. In: Bonser RS, Pagano D, Haverich A (eds) Mitral Valve Surgery. Springer-Verlag London Limited, 3-19 (2011)

29. Asante-Korang A, O'Leary PW, Anderson RH (2006) Anatomy and echocardiography of the normal and abnormal mitral valve. Cardiol Young 16(Suppl 3):27-34

30. Kwan, J. *et al.* 3D geometry of a normal tricuspid annulus during systole: a comparison study with the mitral annulus using real-time 3D echocardiography. *European journal of echocardiography : the journal of the Working Group on Echocardiography of the European Society of Cardiology* **8**, 375-83 (2007).

31. Veronesi, F. *et al.* A study of functional anatomy of aortic-mitral valve coupling using 3D matrix transesophageal echocardiography. *Circulation. Cardiovascular imaging* **2**, 24-31 (2009).

32. Delgado, V. *et al.* Assessment of mitral valve anatomy and geometry with multislice computed tomography. *JACC. Cardiovascular imaging* **2**, 556-65 (2009).

33. Anderson, R.H., Razavi, R. & Taylor, A.M. Cardiac anatomy revisited. *Journal of anatomy* **205**, 159-77 (2004).

34. Sonne, C. *et al.* Age and body surface area dependency of mitral valve and papillary apparatus parameters: assessment by real-time three-dimensional echocardiography. *European journal of echocardiography : the journal of the Working Group on Echocardiography of the European Society of Cardiology* **10**, 287-94 (2009).

35. Lam, J.H., Ranganathan, N., Wigle, E.D. & Silver, M.D. Morphology of the human mitral valve. I. Chordae tendineae: a new classification. *Circulation* **41**, 449-58 (1970).

36. Kunzelman, K.S., Cochran, R.P., Verrier, E.D. & Eberhart, R.C. Anatomic basis for mitral valve modelling. *The Journal of heart valve disease* **3**, 491-6 (1994).

37. Martinez, R.M., O'Leary, P.W. & Anderson, R.H. Anatomy and echocardiography of the normal and abnormal tricuspid valve. *Cardiology in the Young* **16**, 4 (2006).

38. Tsakiris, A.G., Mair, D.D., Seki, S., Titus, J.L. & Wood, E.H. Motion of the tricuspid valve annulus in anesthetized intact dogs. *Circulation research* **36**, 43-8 (1975).

39. Westaby, S., Karp, R.B., Blackstone, E.H. & Bishop, S.P. Adult human valve dimensions and their surgical significance. *The American journal of cardiology* **53**, 552-6 (1984).

40. Silver, M.D., Lam, J.H., Ranganathan, N. & Wigle, E.D. Morphology of the human tricuspid valve. *Circulation* **43**, 333-48 (1971).

41. Seccombe, J.F., Cahill, D.R. & Edwards, W.D. Quantitative MorpholoBy of the Normal Human Tricuspid Valve: Autopsy Study of 24 Cases. *In Situ* **212**, 203-212 (1993).

42. Wenink, A.C. The medial papillary complex. *British heart journal* **39**, 1012-8 (1977).

43. Anderson, R.H., Devine, W. a., Ho, S.Y., Smith, A. & McKay, R. The myth of the aortic annulus: The anatomy of the subaortic outflow tract☆. *The Annals of Thoracic Surgery* **52**, 640-646 (1991).

44. Schultz, C.J. *et al.* Three dimensional evaluation of the aortic annulus using multislice computer tomography: are manufacturer's guidelines for sizing for percutaneous aortic valve replacement helpful? *European heart journal* **31**, 849-56 (2010).

45. Piazza, N. *et al.* Anatomy of the aortic valvar complex and its implications for transcatheter implantation of the aortic valve. *Circulation. Cardiovascular interventions* **1**, 74-81 (2008).

46. Gross, L. & Kugel, M.A. Topographic Anatomy and Histology of the Valves in the Human Heart. *The American journal of pathology* **7**, 445-474.7 (1931).

47. Kunzelman, K.S., Grande, K.J., David, T.E., Cochran, R.P. & Verrier, E.D. Aortic root and valve relationships. Impact on surgical repair. *The Journal of thoracic and cardiovascular surgery* **107**, 162-70 (1994).

48. Reid, K. The anatomy of the sinus of Valsalva. *Thorax* **25**, 79-85 (1970).

49. Swanson, M. & Clark, R.E. Dimensions and geometric relationships of the human aortic valve as a function of pressure. *Circulation research* **35**, 871-82 (1974).

50. Brewer, R.J., Deck, J.D., Capati, B. & Nolan, S.P. The dynamic aortic root. Its role in aortic valve function. *The Journal of thoracic and cardiovascular surgery* **72**, 413-7 (1976).

51. Thubrikar, M., Piepgrass, W.C., Shaner, T.W. & Nolan, S.P. The design of the normal aortic valve. *The American journal of physiology* **241**, H795-801 (1981).

52. Middelhof, C.J.F.M. & Becker A.E. *Ventricular septal geometry: a spectrum with clinical relevance.* In: Wenink ACG et al. (eds) The ventricular septum of the heart. Martinus Nijhoff Publishers, The Hague, Netherlands (1981)

53. Tops, L.F. *et al.* Noninvasive evaluation of the aortic root with multislice computed tomography implications for transcatheter aortic valve replacement. *JACC. Cardiovascular imaging* **1**, 321-30 (2008).

54. Turner, K. & Navaratnam, V. The positions of coronary arterial ostia. *Clinical anatomy (New York, N.Y.)* **9**, 376-80 (1996).

55. Muriago, M., Sheppard, M.N., Ho, S.Y. & Anderson, R.H. Location of the coronary arterial orifices in the normal heart. *Clinical anatomy (New York, N.Y.)* **10**, 297-302 (1997).

56. Cavalcanti, J.S., de Melo, N.C.V. & de Vasconcelos, R.S. Morphometric and topographic study of coronary ostia. *Arquivos brasileiros de cardiologia* **81**, 359-62, 355-8 (2003).

57. Vollebergh, F.E. & Becker, A.E. Minor congenital variations of cusp size in tricuspid aortic valves. Possible link with isolated aortic stenosis. *British heart journal* **39**, 1006-11 (1977).

58. Capps, S.B., Elkins, R.C. & Fronk, D.M. Body surface area as a predictor of aortic and pulmonary valve diameter. *The Journal of thoracic and cardiovascular surgery* **119**, 975-82 (2000).

59. Choure, A.J. *et al.* In vivo analysis of the anatomical relationship of coronary sinus to mitral annulus and left circumflex coronary artery using cardiac multidetector computed tomography: implications for percutaneous coronary sinus mitral annuloplasty. *Journal of the American College of Cardiology* **48**, 1938-45 (2006).

60. Tawara, S. Das reizleitungssystem de saugetierherzens: eine anatomichhisologische studie uber das atrioventricularbundel und die Purkinjeschen faden. Verlag von Gustav Fischer, Jena, Germany. (1906)

61. Keith, A. & Flack, M. The form and nature of the muscular connections between the primary divisions of the vertebrate heart. *Journal of Anatomy and Physiology* **41**, 172 (1907).

62. Racker, D.K. & Kadish, A.H. Proximal atrioventricular bundle, atrioventricular node, and distal atrioventricular bundle are distinct anatomic structures with unique histological characteristics and innervation. *Circulation* **101**, 1049-59 (2000).

63. Barnet, V.A. *Cellular myocytes*. In: Iaizzo PA (ed) The handbook of cardiac anatomy, physiology, and devices, 2nd edn. Humana Press, Totowa NJ, 147-158 (2009)

64. Aschoff, L. Referat uber die Herzstorungen in ihren Beziehungen zu den Spezifischen Muskelsystem des Herzens. Verh Dtsch Pathol Ges 14:3–35 (1910).

65. Monckeberg, J.G. Beitrage zur normalen und pathologischen Anatomie des Herzens. Verh Dtsch Pathol Ges 14:64–71 (1910).

66. Atkinson, A. *et al.* Anatomical and molecular mapping of the left and right ventricular His-Purkinje conduction networks. *Journal of molecular and cellular cardiology* **51**, 689-701 (2011).

67. Matsuyama, T.-A. *et al.* Anatomic assessment of variations in myocardial approaches to the atrioventricular node. *Journal of cardiovascular electrophysiology* **23**, 398-403 (2012).

68. Monfredi, O., Dobrzynski, H., Mondal, T., Boyett, M.R. & Morris, G.M. The anatomy and physiology of the sinoatrial node--a contemporary review. *Pacing and clinical electrophysiology : PACE* **33**, 1392-406 (2010).

69. Anderson, K.R., Ho, S.Y. & Anderson, R.H. Location and vascular supply of sinus node in human heart. *British heart journal* **41**, 28-32 (1979).

70. Anderson, R.H., Yanni, J., Boyett, M.R., Chandler, N.J. & Dobrzynski, H. The anatomy of the cardiac conduction system. *Clinical anatomy (New York, N.Y.)* **22**, 99-113 (2009).

71. Li, J. *et al.* A detailed 3D model of the rabbit right atrium including the sinoatrial node, atrioventricular node, surrounding blood vessels and valves. *Computers in Cardiology, 2005* 603-606 (2005).

72. Dobrzynski, H. *et al.* Computer three-dimensional reconstruction of the sinoatrial node. *Circulation* **111**, 846-854 (2005).

73. Chandler, N.J. *et al.* Molecular architecture of the human sinus node: insights into the function of the cardiac pacemaker. *Circulation* **119**, 1562-75 (2009).

74. Kalman, J.M. *et al.* Radiofrequency catheter modification of sinus pacemaker function guided by intracardiac echocardiography. *Circulation* **92**, 3070-81 (1995).

75. Lee, R.J. *et al.* Radiofrequency catheter modification of the sinus node for "inappropriate" sinus tachycardia. *Circulation* **92**, 2919-28 (1995).

76. Garson, A.J., Bricker, J.T., Fisher D.J., Neish, S.R. eds. The science and practice of pediatric cardiology. Volume I. Baltimore, MD: Williams & Williams, 141-3, (1998).

77. Li, X-H. & Lu, F. *Catheter Ablation of Cardiac Arrhythmias.* In: Iaizzo PA (ed) The handbook of cardiac anatomy, physiology, and devices, 2nd edn. Humana Press, Totowa NJ, 411-442 (2009)

Clinical Assessment

Section Summary

Once an extensive knowledge of the fundamental anatomy of the four cardiac valves and the cardiac conduction system is established, one needs to understand how these features can be visualized clinically. Recent advances in the resolution of clinical imaging modalities, both spatially and temporally, have facilitated the diagnosis of valvular disease and greatly improved the success rate of surgical and transcatheter procedures. Echocardiography, Multi-slice Computed Tomography (MSCT) and Magnetic Resonance (MR) imaging have all become commonly used imaging modalities in cardiology. Additionally, significant advances in the ability to map the electrical activity of the heart have allowed for accurate analysis of the cardiac conduction system and the subsequent diagnosis of cardiac arrhythmias. This chapter will summarize the fundamentals of the three previously mentioned imaging modalities and discuss the current standard of excellence and the next generation of electrical mapping techniques. This will be followed by an investigation into the appropriate modality to use when sizing the aortic root for transcatheter aortic valve replacement (Tsang, 2012), and a review of the use of in vitro and in vivo imaging capabilities at the Visible Heart® laboratory (Bateman, 2011)

Michael G. Bateman MEng

Departments of Surgery and Biomedical Engineering, University of Minnesota, Minneapolis, MN, USA

2. Clinical Imaging of the heart

Common Clinically Used Cardiac Imaging Modalities

Echocardiography

Echocardiography uses the principle that sound waves travel at different speeds through materials with different acoustic densities, a property that varies with tissue density and elasticity, to non-invasively image organs within the body. Resolution of the images improves with increased frequency, but the wavelength is shortened in the process, which decreases the distance from the ultrasound transducer that can be imaged. As a result, adults are usually imaged using a 2-4 MHz transducer, while pediatric patients are imaged using a 7-12 MHz transducer[1].

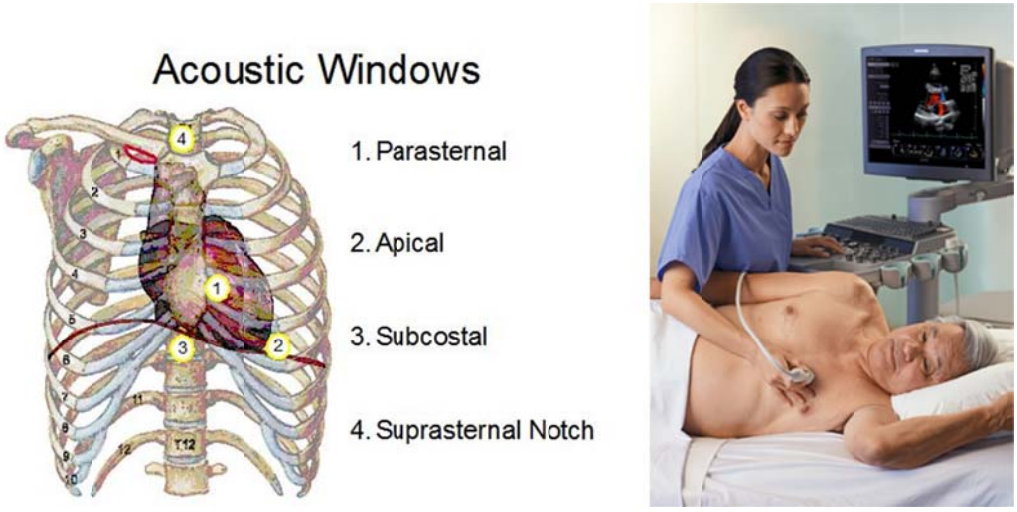

Figure 2.1: Transthoracic echocardiography obtains cardiac images by placing the transducer head in contact with the thorax at one of the following locations, or acoustic windows: parasternal, apical, subcostal, and the suprasternal notch.[1]

To date, transthoracic echocardiography (TTE) is the mainstay of cardiac diagnoses and monitoring in both adult and pediatric patients. Advances in two-dimensional imaging allow significant anatomic detail to be visualized, especially in smaller patients, and Doppler ultrasound allows direct visualization of altered flow patterns and noninvasive investigation of hemodynamics. TTE can be performed on a cooperative, awake patient, but the images are complicated by patient size, bone, soft tissue, and lung tissue interactions. As a result, the ultrasound beams from the transducer head must be aimed through acoustic windows in the thorax to image the heart. There are four typical acoustic windows; the parasternal, apical,

subcostal, and suprasternal notch figure (2.1). The parasternal window is typically used for 2 chamber, long-axis views and short axis views of the heart. The apical window is typically used for the standard 4 chamber, long-axis view. The subcostal window is particularly useful for patients with lung disease or recent open-heart surgery and provides good views of major vascular connections to the heart and the interatrial septum. Finally, the suprasternal window is valuable for aortic root imaging[2].

Transesophageal echocardiography (TEE) uses the same principles of 2D echocardiography as TTE and places the transducer posteriorly to the heart in the esophagus of an anesthetized patient. Although TEE is more invasive than TTE it has become routine when improved resolution and intraprocedural monitoring are required. Intracardiac echocardiography (ICE) provides better resolution than either TTE or TEE but is the most invasive of the three. The echocardiography transducer is placed into a vein and advanced through the superior vena cava into the right atrium. By placing the transducer directly into the heart, higher frequencies of sound waves can be used, creating excellent spatial resolution[2].

The future will see the continued development of intravascular ultrasound for diagnosis and the monitoring of interventional procedures and the growth of 3D echocardiography as an accepted imaging modality. Attempts to record and display cardiac ultrasound images in 3D format were first reported in the 1970s as investigators reconstructed a sequence of carefully recorded 2-dimensional (2D) echocardiograms into a 3D data set[3]. This methodology was limited by the need for offline data processing to create and display the 3D images. In the early 1990s, von Ramm and colleagues developed the first real-time 3D (RT3D) echocardiographic scanner, capable of acquiring volumetric data at frame rates sufficient to depict cardiac motion[4]. More recently, further improvements in design and engineering have led to the commercialization of RT3D echocardiography. This methodology has evolved quickly, and different versions of RT3D imaging are currently available on several platforms[5].

Magnetic Resonance Imaging

MR imaging uses the principle that in the presence of a strong magnetic field (0.5 – 3.0 Tesla (T) in clinical applications) atoms in the body are stimulated to emit radio waves. Eggen succinctly described that these radio waves are detected by an antenna placed around, or over, the body part of interest allowing an image of the body to be reconstructed[6]. Contrast (or difference in

brightness) in the MR image is primarily due to the varying inherent magnetic relaxation times within the tissue structure known as the longitudinal relaxation time (T1) and the transverse relaxation time (T2). These two time constants are dependent on the type, and structure, of atoms in the tissue of interest. By altering the timing and strength of the gradient fields during imaging, or through the use of contrast agents, differences in T1 and T2 values between differing tissues can be exploited to produce images that highlight a specific tissue of interest, due to the fact that the heart is continually moving. Cardiac MR scans are timed (or gated) to the patient's ECG such that a small portion of the image is captured per heartbeat, at the same time during the cardiac cycle. The result is a clear image of the heart without any distortion or blurring from cardiac motion[6].

Figure 2.2: Image of a 1.5T Siemens Avanto MRI (left) and a Siemens Somatom Sensation Spirit CT (right)

Computed Tomography

CT uses the same technology as fluoroscopic imaging and bases image acquisition on the principle of exposing the body of interest to an x-ray source and capturing the resulting remnant beam, determined by the material properties of the substance the beams pass through. The CT scanner is able to create three dimensional scans from this two dimensional imaging technique by rotating the emitting and receiving heads, or gantry, of the scanner around a given axis while acquiring multiple images. These images are then processed using a form of tomographic and multi planar reconstruction techniques to create a three dimensional image. With improved computing power continual cross sections, rather than individual images, could be processed as the gantry rotated. Known as helical CT scanning the technology has improved since its introduction in 1992 with faster gantry rotation, more powerful x-ray tubes, and improved interpolation algorithms[7]. This improved image processing power led to the development of

multi-slice CT (MSCT) and in 1998, mechanical spiral CT systems with simultaneous acquisition of four detector slices and a minimum rotation time of 500 ms were introduced that provided a substantial performance increase over the single- and dual-slice spiral CT systems that had been available until then. These multi-slice CT scanners can cover larger scan volumes with slice widths down to 1.0 mm and thus provide higher spatial resolution for improved visualization of small vessels and the complex anatomy[8]. Due to the speed of acquisition CT scanners do nor require gating and can instead record multiple phases of the cardiac cycle in a relatively short period of time

Cardiac Electrical Mapping

The Electrocardiogram

In 1902 Willem Einthoven reported the first electrocardiogram using a string galvanometer consisting of a massive electromagnet with a thin silver-coated string stretched across it. Electric currents that passed through the string would cause it to move from side to side in the magnetic field, these deflections string were then magnified and recorded on a moving photographic plate. The oscillations in the string provided information regarding the strength and direction of the electrical current[9].

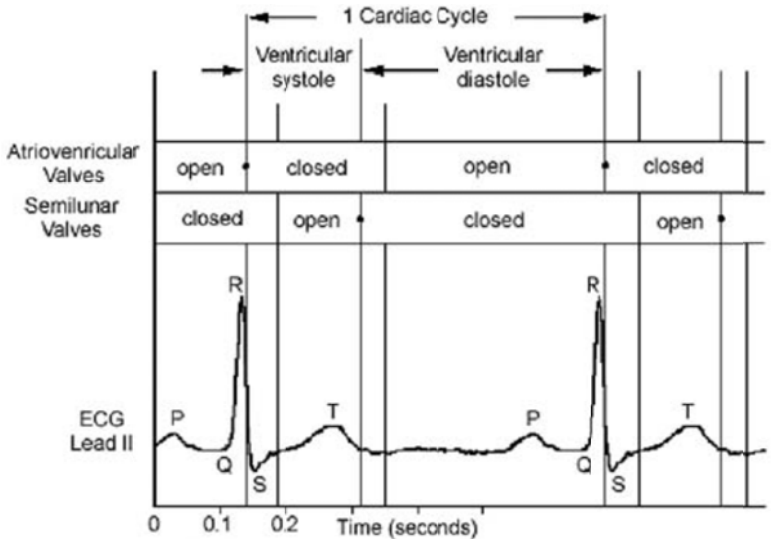

Figure 2.3. A typical Lead II ECG waveform is compared to the timing of atrioventricular and semilunar valve activity, along with which segments of the cardiac cycle the ventricles are in systole/ diastole. (Used with permission)

Today the recorded electrocardiogram (ECG), figure (2.3), is still the most common tool used to measure of how the electrical activity of the heart changes over time, as action potentials within

each myocyte propagate throughout the heart during each cardiac cycle. By utilizing the resultant electrical field present in the body, electrodes can be placed around the heart to measure potential differences as the heart depolarizes and repolarizes. Electrocardiography has progressed rapidly since it was first employed back in the early 1900s. New instruments that are smaller and more sophisticated as well as innovative analysis techniques are continually being developed[9].

Cardiac mapping

As the accuracy, quality and function of the technology available to record the potentials generated by the heart increased, so too did the understanding of the electrical properties of the cardiac muscle. With the development of small electrodes capable of detecting mV potentials Barker et al. set out to map the electrical propagation of the ECG across the surface of an exposed human heart in 1930[10]. But it wasn't until 1970 when Durer et al. performed multiple studies on human hearts from individuals who had been declared brain dead that the first true map was recorded. Measurements from as many as 870 intramural electrodes were simultaneously recorded and provided the first high-resolution insight into human cardiac activation, figure (2.4)[11].

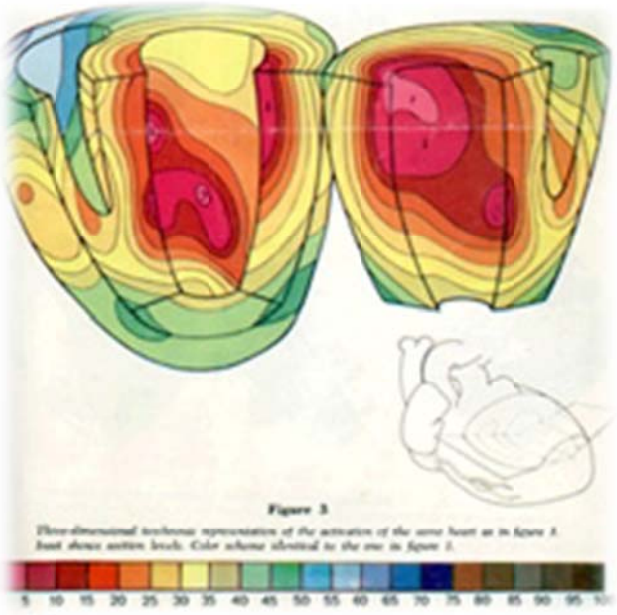

Figure 2.4 The intramural map of the cardiac activation sequence as recorded by Durer et al. (Used with permission)

Non-contact Mapping

The concept of non-contact mapping was first described by Taccardi in 1987 when he created a multi electrode array (MEA) catheter that was inserted into the ventricle of a canine model[12]. However, although it was possible for the group to record the electrical potentials generated by the myocardium they could not compensate for the signal decay that occurred across the blood volume between the voltage source and the electrodes. In 1992 Graydon Beatty and engineers at what soon became Endocardial Solutions Inc. (ESI) overcame this problem by utilizing improved computing power to run simultaneous laplacian equations to solve the inverse problem and therefore map the recorded signal back to the voltage source on the endocardial surface of the heart[13].

Now non-contact endocardial mapping of the heart is at the forefront of cardiac electrical imaging. Devices such as the EnSite® 3000 (St. Jude Medical, Inc., St. Paul, MN) are used frequently in hospital catheter laboratories across the country for the diagnosis and treatment of atrial and ventricular arrhythmias. Briefly, a multi-electrode array (MEA) catheter (St. Jude Medical, Inc., St. Paul, MN), see figure (2.5), is usually inserted into the heart via the vasculature. The balloon catheter is then inflated using a contrast media (allowing for visualization with fluoroscopy) before an EP catheter, termed a "roving" catheter, is introduced into the same chamber. This catheter is then used to create a geographical map of the internal anatomy of the chamber by localizing the distal electrode of the roving catheter to the MEA[14,15]. Once an anatomical map of the chamber has been produced the EnSite® system can record the electrical activity of the myocardium and then project this back onto the 3D geographical map. The system allows for over 3000 points of electrical data to be recorded every heart beat creating an electrical map with very high spatial and temporal resolution.

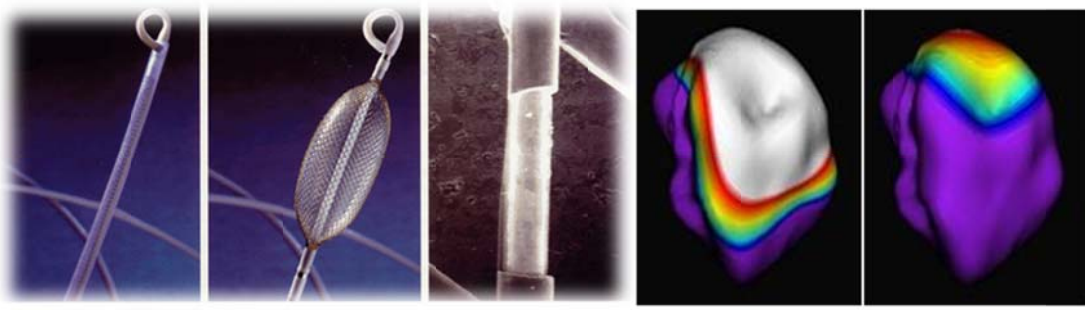

Figure 2.5: Image of EnSite® multielectrode array catheter. Image courtesy of St Jude Medical, Inc. (left) and an example map recorded in the Visible Heart® laboratory.

Non-invasive Cardiac Mapping

However, non-contact mapping is not without its faults; firstly it requires the insertion of a catheter into the cardiac chamber under fluoroscopic guidance and more significantly, can only provide an accurate map of the endocardial surface. This gives no indication of the depth of electrical activity potentially missing arrhythmias arising from deep within the myocardium. Additionally, modern ablation studies such as pulmonary vein ablation, demonstrated as an effective therapy for atrial fibrillation[16], requires careful control of the burn depth to avoid stenosis of the vessels themselves. As non-contact mapping systems do not give the operator any indication of the depth of therapy there has been extensive work in the development of trans-mural mapping techniques. A novell imaging technique that uses the analysis of thoracic electrocardiogram (ECG) recordings, a technique known as body surface potential mapping (BSPM), to determine the electrical activity of the heart has become an exciting and important new field of research[17].

Dr. He's research group at the University of Minnesota has been developing a non-invasive three dimensional (3D) electrocardiographic imaging system designed to supply information on trans-mural electrical activation without requiring any invasive surgery[17–20]. Coined 3D cardiac electrical imaging (3DCEI) the BSPMs are localized to a 3D heart model created using either magnetic resonance imaging (MRI) or computed tomography (CT). The system allows the user to pinpoint the origin of myocardial activation and image ventricular activation sequences and the distribution of transmembrane potentials, see figure (2.6).

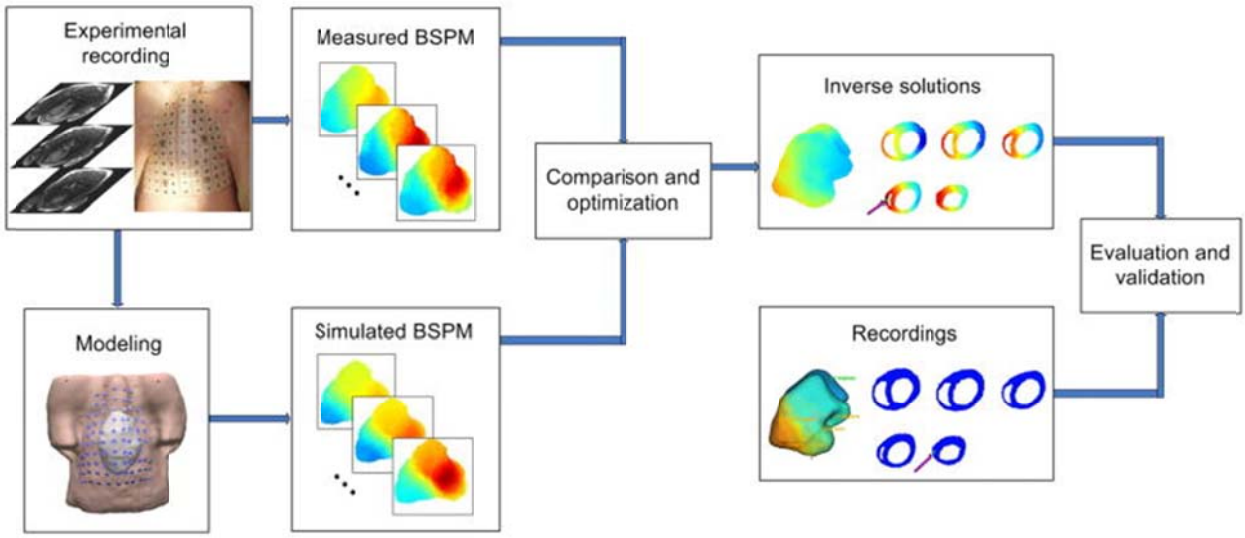

Figure 2.6: Schematic of the non-invasive 3D imaging approach in a swine model[17].

Recently, the 3DCEI technique has been validated using 3D intracardiac mapping in a rabbit model using trans-mural plunge electrodes to validate the trans-thoracic BSPM recordings[19]. Further work has been done to validate the system in an 80-90kg swine model whose cardiac size, heart-torso geometry and electrophysiological characteristics approximate that of an adult human[17].

Conclusion

Recent advances in the resolution of clinical imaging modalities, both spatially and temporally, have facilitated the diagnosis of valvular disease and greatly improved the success rate of surgical and transcatheter procedures. Echocardiography, Multi-slice Computed Tomography (MSCT) and Magnetic Resonance (MR) imaging have all become commonly used imaging modalities in cardiology. Additionally, significant advances in the ability to map the electrical activity of the heart have allowed for accurate analysis of the cardiac conduction system and the subsequent diagnosis of cardiac arrhythmias.

References

1. Quill, J.L. Atlas of Human Cardiac Anatomy. at **www.vhlab.umn.edu/atlas/echotutorial/echotutorial1.shtml**

2. Lohr, J.L. & Shanthi, S. *Introduction to Echocardiography*. In: Iaizzo PA (ed) The handbook of cardiac anatomy, physiology, and devices, 2nd edn. Humana Press, Totowa NJ, 319-330 (2009)

3. Dekker, D.L., Piziali, R.L. & Dong, E. A system for ultrasonically imaging the human heart in three dimensions. *Computers and biomedical research, an international journal* **7**, 544-53 (1974).

4. Sheikh, K., Smith, S.W., von Ramm, O. & Kisslo, J. Real-time, three-dimensional echocardiography: feasibility and initial use. *Echocardiography (Mount Kisco, N.Y.)* **8**, 119-25 (1991).

5. Hung, J. *et al.* 3D echocardiography: a review of the current status and future directions. *Journal of the American Society of Echocardiography : official publication of the American Society of Echocardiography* **20**, 213-33 (2007).

6. Eggen, M. Atlas of Human Cardiac Anatomy. at **www.vhlab.umn.edu/atlas/cmrtutorial/cmrtutorial1.shtml**

7. Kopp, A.F., Georg, C. & Claussen, C.D. [Multislice CT angiography of the upper abdomen. Stenosis of the superior mesenteric artery]. *RöFo : Fortschritte auf dem Gebiete der Röntgenstrahlen und der Nuklearmedizin* **172**, M1 (2000).

8. Kopp, A.F. *et al.* Multislice CT in cardiac and coronary angiography. *The British journal of radiology* **77 Spec No**, S87-97 (2004).

9. Dupre, A., Vieau, S. & Iaizzo, P.A. *Basic ECG theory, 12-lead Recordings and Their Interpretation*. In: Iaizzo PA (ed) The handbook of cardiac anatomy, physiology, and devices, 2nd edn. Humana Press, Totowa NJ, 257-270 (2009)

10. Barker, P., MacLeod, A. & Alexander, J. The excitory process observed in the exposed human heart. *American Heart Journal1* **5**, 720-742 (930).

11. Durrer, D. *et al.* Total excitation of the isolated human heart. *Circulation* **41**, 899-912 (1970).

12. Taccardi, B., Arisi, G., Macchi, E., Baruffi, S. & Spaggiari, S. A new intracavitary probe for detecting the site of origin of ectopic ventricular beats during one cardiac cycle. *Circulation* **75**, 272-81 (1987).

13. Kadish, A., Hauck, J., Pederson, B., Beatty, G. & Gornick, C. Mapping of atrial activation with a noncontact, multielectrode catheter in dogs. *Circulation* **99**, 1906-13 (1999).

14. Schmitt, H. *et al.* Diagnosis and ablation of focal right atrial tachycardia using a new high-resolution, non-contact mapping system. *The American Journal of Cardiology* **87**, 1017-21; A5 (2001).

15. Ihara, T. & Barr, R.C. Electrocardiographic inverse solution for ectopic origin of excitation in two-dimensional propagation model. *Medical and Biological Engineering and Computing* **32**, 41-50 (1994).

16. Natale, A. & Jalife, J. *Role of the Vagus in AF. In: Atrial Fibrillation, From Bench to Bedside*. *Contemporary Cardiology* **2**, 115-131 (Humana: 2008).

17. Liu, C. *et al.* Estimation of Global Ventricular Activation Sequences by Noninvasive Three-Dimensional Electrical Imaging: Validation Studies in a Swine Model During Pacing . *Journal of cardiovascular electrophysiology* (2007).doi:10.1111/j.1540-8167.2007.01066.x

18. He, B., Li, G. & Zhang, X. Noninvasive imaging of cardiac transmembrane potentials within three-dimensional myocardium by means of a realistic geometry anisotropic heart model. *IEEE Transactions on Biomedical Engineering* **50**, 1190-1202 (2003).

19. Zhang, X. *et al.* Noninvasive three-dimensional electrocardiographic imaging of ventricular activation sequence. *American Journal of Physiology- Heart and Circulatory Physiology* **289**, 2724-2732 (2005).

20. He, B., Liu, C. & Zhang, Y. Three-dimensional cardiac electrical imaging from intracavity recordings. *IEEE Transactions on Biomedical Engineering* **54**, 1454-1460 (2007).

3. Accuracy of Aortic Annuli Measurements Obtained From Three-Dimensional Echocardiography, Computed Tomography and Magnetic Resonance Imaging Using an In Vitro Model

Preface

The treatment of aortic stenosis in patients ineligible for surgical aortic valve replacement has progressed rapidly in recent times with ongoing clinical trials for the Edwards SAPIEN™ valve and the Medtronic CoreValve ReValving® leading the integration of this technology into common medical practice. Since transcatheter aortic valve replacement (TAVR) was first performed in 2002, more than 20,000 implantations have been completed to date(3,4). As with surgical aortic replacement acute conduction disturbances after TAVR, 29% of patients (Aktug, 2011), have been reported by physicians with some patients, 16% requiring permanent pacemaker implantation (Aktug, 2011). Additionally, the under sizing of a prosthesis for a given patient can lead to para-valvular leak or prosthesis migration, unacceptable procedural outcomes that are not associated with surgical repair. It is strongly believed that the possibility of under sizing a given prosthesis and the incidence of conduction abnormalities can be greatly reduced by accurately analyzing the dimensions of the aortic annulus.

To date, fluoroscopy and two-dimensional (2D) transesophageal echocardiography (TEE) have been primarily used to plan and guide TAVR procedures. However, real-time 3D echocardiography (RT3DE), multi-slice computed tomography (MSCT) and magnetic resonance imaging (MRI) are all able to provide 3D or multi-slice images of the aortic root. Accordingly, these imaging modalities have become more commonly used for TAVR procedure planning and execution. The motivation behind this investigation is to analyze the imaging capabilities of these three aforementioned imaging modalities by completing a series of measurements on perfusion fixed human heart specimens specifically prepared for this analysis. For this project I selected and prepared all the human heart specimens and was involved in data analysis, creation of figures and manuscript preparation.

Wendy Tsang MD[1], **Michael G. Bateman MEng**[2], Lynn Weinert BSc[1], Gian Pellegrini PhD[4], Victor Mor-Avi PhD[1], Lissa Sugeng MD, MPH[3], Hubert Yeung[4], Amit R. Patel MD[1], Alexander J. Hill PhD[4], Paul A. Iaizzo PhD[2], Roberto M. Lang MD[1]
[1]University of Chicago Medical Center, Chicago, IL, USA, [2]University of Minnesota, Minneapolis, MN, USA, [3]Yale University, New Haven, CT, USA, [4]Medtronic, Inc., Minneapolis, MN, USA

Published in the *Heart,* 2012 Aug;98(15):1146-52.

Summary

Objectives: To determine the accuracy of calcium-containing rings measurements imaged by 3D-echocardiography (3DE), multi-slice computed tomography (MSCT) and cardiac magnetic resonance (CMR) under ideal conditions against the true ring dimensions. To compare the accuracy of aortic annulus (AoA) measurements in ex-vivo human hearts using 3DE, MSCT and CMR. To determine the accuracy of AoA measurements in an in vivo human model.

Design: 3DE, MSCT and CMR imaging was performed on 30 calcium containing rings and 28 explanted human hearts. Additionally, 15 human subjects with clinical indication for MSCT underwent 3DE. Two experts in each modality measured the images.

Main outcome measures: Bias and intra-class correlation coefficient for accuracy of imaging measurements when compared to actual ring dimensions. Bias, intraclass correlation coefficient and variability were obtained when: 1) comparing explanted human heart AoA measurements from the two remaining imaging modalities to the most accurate one as determined from the ring measurements; and 2) in vivo human AoA measurements. Analysis was repeated on subgroups divided by aortic valve Agatston score.

Results: Against the known ring dimensions, CMR had the highest accuracy and lowest variability. MSCT measurements had high accuracy but wider variability and 3DE had the lowest accuracy with the largest variability. When 3DE and MSCT were compared to CMR, 3DE underestimated and MSCT overestimated AoA dimensions, but inter-measurement variability of 3DE and MSCT were similar. When divided by Agatston score, both 3DE and MSCT measurements were larger and showed greater variability with increasing calcium burden. The in vivo study showed that the correlation between 3DE and MSCT measurements was high, however, 3DE measurements were smaller than those measured with MSCT.

Conclusions: In the in vitro model, CMR measurements were the most accurate for assessing the actual dimensions suggesting that further investigations on its role in AoA measurement in TAVR are needed. However from the in vivo model, MSCT and 3DE are reasonable alternatives with the understanding that they can slightly over-and underestimate annular dimensions, respectively.

Introduction

Degenerative aortic stenosis is the most common valve disease in the United States[1, 2]. Traditionally, surgical aortic valve replacement was considered the 'gold standard' in treating this disease and improving prognosis. However, approximately 30% of patients with severe, symptomatic aortic stenosis are considered inoperable due to co-morbid conditions. Transcatheter aortic valve replacement (TAVR) is a new, less invasive treatment for aortic stenosis offered to this patient group. Since TAVR was first performed in 2002, more than 20,000 implantations have been completed to date[3, 4].

While TAVR is a less invasive procedure than surgical valve replacement, proper performance relies heavily on accurate quantification of the aortic annulus (AoA) dimensions. Without this information, difficulties may be encountered during prosthesis implantation due to incorrect sizing. To date, fluoroscopy and two-dimensional (2D) transthoracic and transesophageal echocardiography (TEE) have been primarily used to plan and guide TAVR procedures. However, these imaging modalities are limited in that they display three-dimensional (3D) structures in two dimensions. In contrast, real-time 3D echocardiography (3DE), multi-slice computed tomography (MSCT) and cardiac magnetic resonance (CMR) are all able to provide 3D or multi-slice images of the aortic root. Accordingly, these imaging modalities have become more commonly used for TAVR procedure planning and guidance. However, thorough comparative studies between these imaging modalities are scarce and/or the results often rely on modality correlations of measurements rather than accuracy against a true 'gold standard' [5-12].

To address this issue, we first employed an in vitro approach, in which we simulated calcified aortic valves by implanting constructed calcium rings in aortas or pulmonary arteries. We hypothesized that this model would be useful to determine the most accurate imaging modality for performing ring measurements in the presence of calcium under ideal imaging conditions. We also imaged exvivo human hearts fixed in gel to examine AoA dimension differences between imaging modalities. Having determined the most accurate imaging modality under ideal imaging conditions, we then imaged the AoA in patients to determine inter-modality differences.

The primary goals of this study were 1) to determine the accuracy of calcium-containing rings measurements imaged by 3DE, MSCT and CMR under ideal conditions against the true ring dimensions; 2) to compare the accuracy of AoA measurements in ex-vivo human hearts using

3DE, MSCT and CMR; and 3) to compare the accuracy of AoA measurements in living humans imaged using standard 3DE and MSCT protocols. In the second goal, the imaging modality that was found to be most accurate when compared to actual ring dimensions was used as the "gold-standard" for AoA dimension comparison.

Methods

In Vitro Studies

Calcium Rings: We used 30 specially constructed calcium rings that were precision-machined elliptical annuli of solid water phantom material (Gammex 457) and implanted into ex-vivo aortas. They ranged from 19-37 mm major outer diameters with eccentricity of 0.57 (i.e. major to minor outer diameter ratio of 1.22). The width and thickness of the annuli were held constant at 5-mm. Three channels (3-mm wide and 2-mm deep), arranged along the ellipse of the annuli, were filled with Calcium Hydroxyapatite [Ca10(PO4)6(OH)2] and held in place with cyanoacrylate (Loctite) and UV adhesives (Dymax, Figure 3.1A). The ring size tolerances from manufacturing were well below the imaging resolution of the utilized methodologies and thus should not be considered as a confounding factor in the image measurement variability. The manufactured rings were first measured when dry before implantation into the tissues, and then after explantation while still wet to ensure that the rings retained their measurement sizes. No differences in the sizes of the rings under either condition were noted.

Specimen Preparation: For AoA measurements, we imaged the aortas of 28 human cadaveric hearts with varying degrees of aortic valve calcification. The Research Ethics Boards of the University of Chicago and the University of Minnesota approved this study.

The fresh heart specimens were obtained from: 1) organ donors whose hearts were not deemed viable for transplantation and were donated for research (via LifeSource Upper Midwest Organ Procurement Organization); or 2) from bodies donated to the University of Minnesota's Anatomy Bequest Program. This study was reviewed and approved by these organizations prior to the completion of the imaging protocols. After excision, the fresh/un-fixed specimens were cleaned and perfusion-fixed in 10% buffered formalin, by attaching the cannulated great vessels to a system, which provided a pressure head of approximately 50 mmHg. This methodology fixes a given heart in end-diastole[13]. Subsequently, the hearts, saturated with formalin, were placed in 12"x7"x6" sealable polymer containers and submerged in 0.7% agar gel at

approximately 45°C. The hearts were then palpated to ensure that all possible air was ejected from the chambers and major vessels to reduce any air-tissue susceptibility artifacts, before being suspended in an anatomically correct position (Figure 3.1B). Once cooled to room temperature (~23 °C), all supports used to suspend the hearts were removed and any remaining air volume within the container was displaced with gel.

Image acquisition and formats: All in vitro imaging was performed on each heart within a 24-hour time frame using the same imaging methods for the rings and the fixed human hearts. Three-dimensional echocardiography was performed using an iE33 imaging system (Philips Healthcare, Andover, Mass.), equipped with a fully sampled matrix transthoracic echocardiography (TTE) transducer (S5-1). The top of the specimen-containing box was removed and the probe was placed on the gel surface. Slight pressure was applied to the gel when necessary to improve image quality, while minimizing disruption to the orientation of the specimen.

Initially, gain settings were optimized using a narrow-angled imaging mode, which allows acquisition of a 3DE pyramidal volume of approximately 30x60 degrees. Zoomed 3DE images of the entire ring were then acquired with frame rates ranging between 5 and 28 Hz (mean 17+5 Hz). Acquisition of 3D datasets was repeated three times to optimize image quality for analysis. All 3DE images were reviewed offline using commercial software (3DQ in QLAB, Philips) by a trained cardiologist. Three orthogonal views of the ring were used to extract a planar en-face view. This image, as well as a planar image of the AoA from each heart, was used for measurements (Figures 3.1F-H).

CMR was performed using a 3T system (Philips Healthcare, Best, Netherlands) with a SENSE head coil with 8 elements, which could fit around the box containing the gel-fixed heart. Spin-echo sequences were used to identify the ring or aorta. T1-weighted 3D ultrafast gradient echo images of the entire fabricated rings and aorta were acquired and exported in DICOM format to an independent workstation and reviewed by an experienced CMR reader using OsiriX software (v.3.8.1, Pixmeo Sarl, Switzerland). Images featuring a planar en face view of a given ring and one image of each heart's AoA were exported for measurements (Figures 3.1L-N).

MSCT scans were performed using a 256-slice Brilliance iCT (Philips Healthcare, Cleveland, Ohio) with prospective gating using a simulated ECG signal and with collimation 96 x 0.625 mm,

rotation time 270 ms, tube voltage 120kV and tube current 360 MA. The image slice thicknesses was 0.9 mm as was the reconstruction thicknesses. Datasets were then transferred to a remote workstation (Extended Brilliance Workspace, Philips) where an experienced CT reader reviewed the stacked images and exported two images for measurement: one image featuring a planar view of the ring, and one image featuring a planar view of a given AoA (Figures 3.1I-K). The AoA was defined as the plane at the point of leaflet insertion.

In Vitro Study Design: To determine the most accurate imaging modality against a true 'gold-standard' six independent observers, two experts for each modality (3DE, CMR and CT) performed measurements on the ring images in their respective imaging modality. To minimize the variability introduced with the selection of the imaging planes, the interpreters were provided with fixed images, which could not be manipulated. For each imaging modality, two orthogonal views used to ensure that true, centered, en-face views of the rings as well as the AoA were obtained. A schematic demonstrating the long- and short-axis measurements were provided as a guide for the interpreters (Figures 3.1C-E). For each imaging modality, four measurements were performed on each ring image: long- and short- axis measurements of the internal and external dimension of a given ring (Figures 3.1F, G, I, J, L, M).

Ring image quality was assessed using a three-grade scale, based on the visualization of the inner and outer ring edges: "0" if two or more inner or outer ring edges were poorly visualized; "1" if only one ring edge was poor visualized; and "2" if there were no visualization limitations. For the in vitro human heart images, AoA measurements from the remaining two imaging modalities were compared to the most accurate modality as determined from the first part of the study. Again, the same six independent observers performed measurements on the AoA images in their respective specialties. For each imaging modality a long- and short-axis measurement were obtained (Figure 3.1H, K, N).

To assess the impact of aortic valve calcification, the hearts were divided into three groups based on their aortic valve Agatston score. The Agatston score was calculated from the non-contrast CT images using OsiriX software with a detection threshold of 90 HU. Calcification was attributed to the aortic valve if it was clearly visible within the valve cusps. Supravalvular calcifications and calcification of the coronary arteries including the ostia were not included. The aortic valve Agaston score were used to divide the hearts into three groups: 1) no calcium with a

zero score; 2) mild-to-moderate calcium with a score between 1-500 HU; and 3) severe calcium with a score > 500 HU.

In Vivo Study

Image acquisition and formats: MSCT and 3DE used in the in vivo part of the study were performed within a 24-hour time frame on 16 patients (60+13 years, 6 males) referred for clinically indicated MSCT. Transthoracic 3DE images were acquired from an apical window using the iE33 imaging system (Philips, Andover, Massachusetts) with a matrix array transducer (X3-1). Initially, gain settings were optimized using a narrow-angled imaging mode, which allows acquisition of a 3DE pyramidal volume of approximately 30x60 degrees. Zoomed 3DE images from the left ventricular outflow tract to the ascending aorta were then acquired. Care was taken to ensure that the AoA was placed in the middle of the sector. Full-volume acquisition was performed using ECG gating over 4 consecutive cardiac cycles. Images were reviewed immediately to determine whether the aortic root was well visualized. Identical to the process described above, a single en-face view of the AoA was exported for measurement.

MSCT scans were performed using standard clinical protocols on a 16-slice multidetector scanner (Toshiba, Otawara, Japan). Nonionic iodinated contrast agent (Ultravist-370, Schering, Berlin, Germany) was injected into the antecubital vein (140 ml, 3.5 ml/s) and followed by a 50-ml saline bolus. Image acquisition was triggered by the appearance of contrast in the aortic root. Imaging parameters included 250 ms gantry rotation time with 5 mm per rotation, and tube voltage of 120 kV with currents of 300 mA. Scan data were then reconstructed at 0.5-mm slice thickness and 0.5-mm in-slice resolution using retrospective ECG-gating from early systole (0% of the RR interval) to late diastole (90% of the RR interval) at 10% steps. Beta-blockers were not given during the CT acquisition protocol.

In Vivo Study Design: AoA measurements from MSCT and 3DE were compared. Four independent observers performed measurements on the AoA images in their respective specialties. For each imaging modality, a long- and short-axis measurement was obtained.

Statistical Analysis

For the ring analysis, inner ring long- and short-axis measurements were grouped together and the same was done for the outer ring long- and short-axis measurements. For the in vitro AoA measurements, the long- and short-axis were grouped together. Bland-Altman analysis was used to compare measurements obtained with 3DE, MSCT and CMR to the actual ring dimensions and

between imaging modalities for the in vitro human AoA measurements. To estimate measurement errors between imaging modalities, intra-class correlation coefficients were calculated for comparisons between 3DE, MSCT and CMR measurements against actual ring dimensions. Intra-observer variability was not assessed, since the 3DE images could not be fixed for repeated measurements. The reproducibility of in vitro AoA measurements was evaluated using intra-class correlation and the coefficient of variation, calculated as the absolute difference between the corresponding pairs of measurements in percent of their mean. The Bland-Altman and intra-class correlation analyses were repeated for the three subgroups determined by the aortic valve Agatston score.

After performing MSCT and 3DE in living humans, the reproducibility of AoA measurements was evaluated using intra-class correlation and the coefficient of variation, calculated as the absolute difference between the corresponding pairs of measurements in percent of their mean. Comparison between the imaging modalities was performed with Bland-Altman analysis and intra-class correlation coefficient.

Results

Ring Analysis

Imaging of all 30 implanted rings was possible with MSCT, CMR and 3DE. For MSCT and CMR, image quality was graded “2” in all 30 rings. With 3DE, seventeen (57%) ring images received a score of “2”, four (13%) received a score of “1” and nine (30%) received a score of “0”. Poor visualization scores were due to acoustic shadowing caused by the calcified portions of the ring. When assessing the accuracy of the measurements obtained with 3DE, CMR and MSCT compared to the known ring dimensions, MSCT and CMR were found to be highly accurate with high correlation coefficients (Table 3.1) and near zero biases. However, the limits of agreement were slightly wider for MSCT compared to CMR. This pattern remained regardless of whether the inner or outer ring dimensions were measured. In contrast, 3DE had slightly lower correlation coefficients, and larger bias with wider limits of agreement (Table 3.1).

Table 3.1 Calcium ring analysis

	Accuracy		Inter-measurement	
	Outer Ring	Inner Ring	Outer Ring	Inner Ring
Intraclass Correlation Coefficient				
3DE	0.90	0.90	0.92	0.92
MSCT	0.97	0.98	0.98	0.97
CMR	0.97	0.99	0.95	0.98
Bias (lower, upper 95% limits of agreement), mm				
3DE	0.69 (-2.63, 4.00)	-1.01 (-3.93, 1.92)		
MSCT	0.06 (-1.86, 1.97)	0.36 (-1.08, 1.79)		
CMR	-0.11 (-1.93, 1.70)	0.18 (-0.94, 1.30)		

3DE=three-dimensional echocardiography, MSCT=multislice computed tomography, CMR=cardiac magnetic resonance

In Vitro Aortic Annulus Measurement Analysis

Imaging of the cadaveric AoA was feasible with MSCT, CMR and 3DE in all 28 hearts examined. Table 3.2 summarizes the baseline characteristics of the hearts measured. Given that CMR was determined in the ring experiment to have the highest accuracies and best reproducibility, this modality was used as the reference standard for subsequent comparisons of AoA measurements. When comparing AoA measurements derived from MSCT images against this reference standard, MSCT measurements were noted to slightly overestimate the AoA dimensions with relatively narrow limits of agreement (Table 3.2). In contrast, AoA measured from 3DE images resulted in a slight underestimation of annular dimensions with wider limits of agreement (Table 3.2).

When the inter-measurement reliability was examined, CMR had the highest intra-class correlation values with the narrowest percentage variability (Table 3.2). Repeated measurements showed that compared to CMR, 3DE and MSCT had lower correlation coefficients and wider variability. However, they had similar intra-class correlation values and percentage variability when compared to each other (Table 3.2).

When the AoA measurements were divided according to their aortic valve Agatston score, 3DE and MSCT intra-class correlation decreased with increasing valve calcification (Table 3.2). CMR had the highest ICC values across the groups. When the 3DE and MSCT measurements were compared to CMR, increasing valve calcium scores were associated with an increase in measured dimensions.

Table 3.2 In vitro human aortic annulus analysis

	Overall (n=28)	No Calcium (n=15)	Mild-Moderate Calcium (n=8)	Severe Calcium (n=5)
Baseline Characteristics				
Age, yr	59±18	50±17	62±10	78±15
Male gender, n	11	8	0	3
BMI, m sq.	28±7	28±8	28±5	29±9
Heart weight, g	443±165	399±88	469±107	531±165
Agatston Score, HU	2012±6920	0	72±59	11553±14061
Calcium Mass	335±1233	0	8.6±6.9	2060±2637
Calcium Volume	174+608	0	13.4±11.5	1060±1265
Intraclass correlation coefficient				
3DE	0.96	0.98	0.95	0.86
MSCT	0.94	0.92	0.80	0.28
CMR	0.98	0.98	0.99	0.96
Variability, %				
3DE	4.9±4.4	4.1±3.9	5.0±4.7	5.7±4.6
MSCT	5.3±3.9	4.2±3.5	5.6±3.0	3.9±4.0
CMR	3.2±2.6	3.2±2.6	2.5±2.6	4.2±2.7
Bias (lower, upper 95% limits of agreement), cm				
3DE	-0.13 (-0.67, 0.40)	-0.16 (-0.59, 0.26)	0.15 (-0.66, 0.36)	0.17 (-0.30, 0.64)
MSCT	0.13 (-0.22, 0.47)	0.12 (-0.25, 0.48)	0.17 (-0.28, 0.62)	0.23 (-0.15, 0.61)
CMR	*	*	*	*

*reference standard

3DE=three-dimensional echocardiography, MSCT=multi-slice computed tomography, CMR=cardiac magnetic resonance

In Vivo Aortic Annulus Measurement Analysis

Imaging of the AoA was feasible with MSCT and 3DE in all 15 human subjects (Figures 3.1O, P). 3DE resulted in smaller measurements compared to MSCT (Table 3.3). A high intra-class correlation was observed between 3DE and MSCT. When inter-measurement reliability was examined, MSCT had a higher intra-class correlation value than 3DE (Table 3.3). While the mean percentage variability was higher for MSCT compared to 3DE, 3DE had wider standard deviations.

Table 3.3 Human in vivo protocol

	3D Echocardiography	Computed Tomography
Inter-technique		
Intra-class correlation coefficient	0.87	*
Bias (lower, upper limits of agreement), cm	-0.10 (-0.52, 0.32)	*
Inter-measurement		
Intra-class correlation coefficient	0.85	0.97
Coefficient of variability, %	0.1±10.0	3.1±2.7

*reference standard

Discussion

TAVR is a recently developed technique that is offered as an alternative to surgical aortic valve replacement to patients with severe aortic stenosis considered to be high surgical risk[3, 9, 12, 14]. Accurate AoA measurement is critical for patient selection and successful valve implantation. Currently, 2D TTE and TEE have been the primary methods for determining AoA measurements for TAVR. Previous studies comparing these two imaging modalities have found that AoA measurements using TEE were typically larger than transthoracic measurements and the correlation with surgical/TAVR valve sizing was good but not excellent [7, 9, 15]. In comparison, studies using MSCT report that AoA areas were typically larger compared to 2D TTE, 2D TEE or 3D TEE[5, 8, 9, 11]. This again is in contrast to CMR where sagittal AoA measurements have been reported to have similar dimensions when compared to 2D TEE, whereas coronal AoA CMR measurements are significantly different[16, 17]. Some of the differences reported with 2D TTE/TEE can be attributed to the under appreciation of the elliptical AoA shape. However, the major limitation of these studies is that they lacked an absolute "gold standard" reference, such as throne achieved in this study by the use of phantom imaging to determine the true accuracy of each modality.

In the present study, we used a unique in vitro model stimulating a calcified aortic annulus to assess the true accuracy of 3DE, CMR and MSCT based measurements of a calcified aortic annulus. This in vitro model allows multiple sources of measurement variability to be controlled to help improve the understanding of the differences in accuracy and the factors involved in variability between imaging modalities.

With 3DE, poorer image quality, caused by shadowing of the calcium ring was noted in 57% of the ring images. Similar to clinical practice observations, imaging calcified aortic annuli or in our case fabricated calcium rings using CMR or MSCT did not result in artifacts, which can considerably affect measurement accuracy. In contrast, the poorer ring image quality caused by shadowing noted with 3DE resulted in lower accuracy, when compared to measurements obtained from MSCT or CMR images. Not only were measurements from MSCT and CMR more accurate, but they were also highly reproducible. Given that calcium ring measurements obtained with CMR displayed the highest accuracy and lowest variability this modality was chosen as the imaging reference standard for assessing AoA in this study.

When doing so, we found that 3DE measurements underestimated while MSCT overestimated AoA measurements. However, the intra-measurement variability for 3DE and MSCT were similar. These findings are consistent with published studies comparing 2D TTE, 2D TEE and MSCT AoA dimensions in TAVR planning[5, 9].

When we examined our results according to the amount of aortic valve calcification, we noted that AoA measurement variability on 3DE and MSCT but not CMR augmented with increasing amounts of calcium. When 3DE and MSCT AoA measurements were compared to CMR, as the magnitude of calcium increased, the measured dimensions increased as reflected by increasing positive biases. This suggests that the presence of significant amounts of calcium led observers to make larger measurements.

Having measured AoA from images obtained under ideal conditions, we sought to examine the performance of such measurements in vivo. Comparisons were performed between 3DE and MSCT, as these are the two modalities that are routinely used in the assessment of patients for TAVR. We found that there was good correlation between 3DE and MSCT measurements; however, 3DE measurements were slightly smaller than those obtained by MSCT and had wider variability.

It has previously been argued that MSCT AoA measurements are not equivalent to those from 2D TEE or 2D TTE because the imaging planes from which these measurements are obtained are more accurately identified on MSCT due to the ability to manipulate these images in 3D[18]. However, with appropriate acquisition protocols and new post-processing software available to manipulate CMR and 3DE images, accurate measuring planes can now be obtained with these two modalities. We have found in our in vitro model that CMR and 3DE have similar if not smaller AoA intra-measurement variability and can be performed without the radiation or iodine exposure required by MSCT imaging. Overall, the potential role of CMR in evaluating the aortic root and annulus in TAVR patients has been underappreciated. This study has demonstrated that for our in vitro model, even in the presence of calcium, CMR was the most accurate imaging modality with the highest level of reproducibility and should therefore be considered a reasonable option for AoA dimension assessments in TAVR patients.

Current clinical guidelines for the imaging-based assessment of the AoA in TAVR patients state that TEE is the preferred tool for the assessment of LV outflow tract morphology and aortic root

dimensions prior to device implantation[12]. As determined in our AoA sub study, transthoracic 3DE is a reasonable option along with MSCT to obtain AoA measurements. Of interest, a recent study found that using MSCT to determine AoA size would have changed TAVR strategy in 40-42% of patients because of the 1-2 millimeters greater size measurements obtained with MSCT compared to 2D TTE or TEE[9]. However, implantation based on 2D TEE measurements was successful in 33 of the 34 treated patients. When we examine these findings in the context of our results, MSCT is likely overestimating the true annular dimensions. Nevertheless, despite the underestimation of measurements obtained from echocardiography, ultimately there was no difference in outcomes, perhaps because the guidelines for determining aortic device size were developed using echocardiographic measurements[18].

Our in vitro model has the inherent limitation that it lacks cardiac pulsations or respiratory motion during image acquisition. These are usually the major sources of artifact in cardiac imaging that contribute to the variability encountered in measurements across imaging modalities. In planning this study, we sought to image the AoA phantom under ideal conditions in order to minimize the sources of variability and determine the highest possible accuracy of each imaging modality. Thus, while the 3DE and MSCT imaging protocols are similar to those used clinically, the CMR protocol used in our study is not feasible in a heart. Another limitation is the lack of contrast use on the MSCT images, which would be standard in clinical practice. This did not affect our results as MSCT had a near zero bias with excellent reproducibility. Lastly, while schematics of the rings were provided to the interpreters to define the long- and short-axis measurements, the interpreters may still not have identified the true center resulting in overestimation of the rings and AoA dimensions. In addition to this, greater variability in the AoA measurements could have been caused by heart anatomy distortion during fixation in the gel.

In summary, we found that for our in vitro model CMR was the most accurate method for assessing the implanted calcium ring phantoms. When CMR was used as the reference standard, MSCT and 3DE were found to be reasonable alternatives, particularly when recognizing that these modalities can slightly over- and underestimate annular dimensions, respectively. As well, increasing calcium burden leads to greater measurement variability and an absolute increase in measurements. From our in vivo model, agreement between MSCT and 3DE was good although 3DE had slightly smaller measurements and wider variability.

Disclosures

Dr. Tsang is funded through a CIHR research fellowship grant. This study was funded in part by a research grant from Medtronic, Minnesota, USA.

We would like to thank the organ donors and their families for their generous gifts of these specimens for research. We would also like to thank LifeSource for their support in recovering and transporting these specimens to the Visible Heart laboratory.

References

1. Roger VL, Go AS, Lloyd-Jones DM, et al. Heart Disease and Stroke Statistics--2011 Update: A Report From the American Heart Association. Circulation. 2011;123(4):e18-e209.

2. Nkomo VT, Gardin JM, Skelton TN, et al. Burden of valvular heart diseases: a population-based study. Lancet. 2006;368(9540):1005-11.

3. Cribier A, Eltchaninoff H, Bash A, et al. Percutaneous transcatheter implantation of an aortic valve prosthesis for calcific aortic stenosis: first human case description. Circulation. 2002;106(24):3006-8.

4. Buellesfeld L, Windecker S. Transcatheter aortic valve implantation: the evidence is catching up with reality. Eur Heart J. 2011;32(2):133-7.

5. Tops LF, Wood DA, Delgado V, et al. Noninvasive evaluation of the aortic root with multislice computed tomography implications for transcatheter aortic valve replacement. JACC Cardiovasc Imaging. 2008;1(3):321-30.

6. Schoenhagen P, Tuzcu EM, Kapadia SR, Desai MY, Svensson LG. Three-dimensional imaging of the aortic valve and aortic root with computed tomography: new standards in an era of transcatheter valve repair/implantation. Eur Heart J. 2009;30(17):2079-86.

7. Moss RR, Ivens E, Pasupati S, et al. Role of echocardiography in percutaneous aortic valve implantation. JACC Cardiovasc Imaging. 2008;1(1):15-24.

8. Kurra V, Kapadia SR, Tuzcu EM, et al. Pre-procedural imaging of aortic root orientation and dimensions: comparison between X-ray angiographic planar imaging and 3-dimensional multidetector row computed tomography. JACC Cardiovasc Interv. 2010;3(1):105-13.

9. Messika-Zeitoun D, Serfaty JM, Brochet E, et al. Multimodal assessment of the aortic annulus diameter: implications for transcatheter aortic valve implantation. J Am Coll Cardiol. 2010;55(3):186-94.

10. Burman ED, Keegan J, Kilner PJ. Aortic root measurement by cardiovascular magnetic resonance: specification of planes and lines of measurement and corresponding normal values. Circ Cardiovasc Imaging. 2008;1(2):104-13.

11. Ng AC, Delgado V, van der Kley F, et al. Comparison of aortic root dimensions and geometries before and after transcatheter aortic valve implantation by 2- and 3-dimensional transesophageal echocardiography and multislice computed tomography. Circ Cardiovasc Imaging. 2010;3(1):94-102.

12. Vahanian A, Alfieri O, Al-Attar N, et al. Transcatheter valve implantation for patients with aortic stenosis: a position statement from the European Association of Cardio-Thoracic Surgery (EACTS) and the European Society of Cardiology (ESC), in collaboration with the European Association of Percutaneous Cardiovascular Interventions (EAPCI). Eur Heart J. 2008;29(11):1463-70.

13. Anderson SE, Hill AJ, Iaizzo PA. Microanatomy of human left ventricular coronary veins. Anat Rec (Hoboken). 2009;292(1):23-8.

14. Descoutures F, Himbert D, Lepage L, et al. Contemporary surgical or percutaneous management of severe aortic stenosis in the elderly. Eur Heart J. 2008;29(11):1410-7.

15. Fan CM, Liu X, Panidis JP, et al. Prediction of Homograft Aortic Valve Size by Transthoracic and Transesophageal Two-Dimensional Echocardiography. Echocardiography. 1997;14(4):345-48.

16. Koos R, Altiok E, Mahnken AH, et al. Evaluation of aortic root for definition of prosthesis size by magnetic resonance imaging and cardiac computed tomography: Implications for transcatheter aortic valve implantation. Int J Cardiol. 2011.

17. Paelinck BP, Van Herck PL, Rodrigus I, et al. Comparison of Magnetic Resonance Imaging of Aortic Valve Stenosis and Aortic Root to Multimodality Imaging for Selection of Transcatheter Aortic Valve Implantation Candidates. Am J Cardiol. 2011.

18. Tuzcu EM, Kapadia SR, Schoenhagen P. Multimodality quantitative imaging of aortic root for transcatheter aortic valve implantation: more complex than it appears. J Am Coll Cardiol. 2010;55(3):195-7.

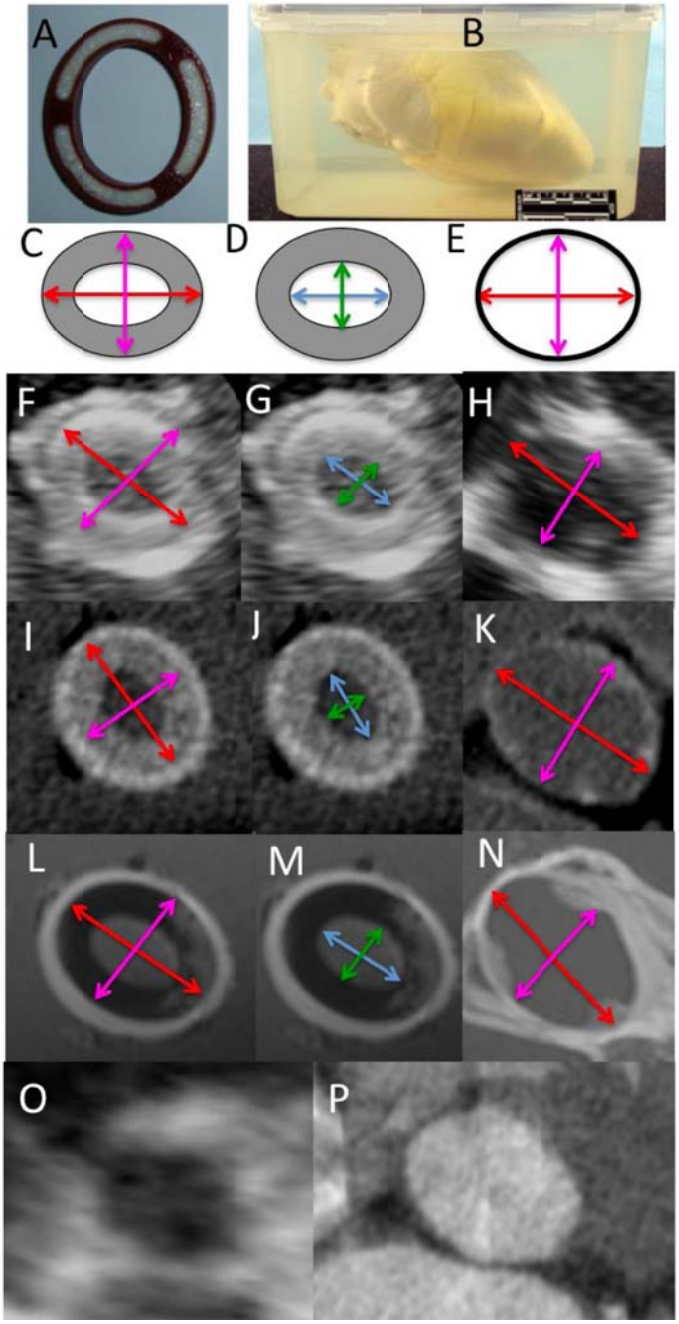

Figure 3.1: Image of a ring with calcium hydroxyapatite impregnated channels (A). Image of a perfusion fixed human heart preserved at end-diastole and contained in 10% formalin (B). Schematic of the outer ring measurements (C) in the long- (red arrows) and short-(pink arrows) axis and inner ring measurements (D) in the long- (blue arrows) and short- (green arrows) axis with three-dimensional echocardiography (F, G), multi-slice computed tomography (I, J), and cardiac magnetic resonance imaging (L, M). Schematic of aortic annulus long (red arrows) and short (pink arrows) axis measurements (E) with examples from 3D echocardiography (H), multi-slice computed tomography (K), and cardiac magnetic resonance imaging (N). Example from the human in vivo protocol of an aortic annulus imaged with transthoracic three-dimensional echocardiography (O) and multi-slice computed tomography (P)

4. Comparative imaging of cardiac structures and function for the optimization of transcatheter approaches for valvular and structural heart disease

Preface

The use of Visible Heart® methodologies when analyzing the performance of a novel device has allowed for critical examinations of device-tissue interactions specifically regarding the native anatomy. These research tools have provided product designers with a rapid method to critically assess device prototypes and allowed clinicians to directly visualize the deployment of new or problematic clinical systems. With the continued integration of transcatheter delivered valves into modern medicine the visualization and analysis of these systems in an in vitro setting provides a wealth of information to both the physician and engineer. Additionally, implantations of these devices will likely utilize simultaneous multiple imaging modalities (e.g., within a hybrid operating room), many of which can be replicated in the Visible Heart® laboratory. Continued use of each imaging technique in a laboratory setting will help provide insights to their advantages and faults in relation to their clinical usage.

The motivation behind this paper was to present a review of the capabilities of the Visible Heart® laboratory with respect to the imaging of both the anatomical environment into which these novel devices will be implanted and the procedures themselves. This resource has provided real time information regarding the interaction of the device, the delivery system and the physician with the heart and allowed for visual assessment of the functionality of the prosthesis post implantation. This review was written and edited by myself with assistance from Dr. Paul Iaizzo.

Michael G. Bateman MEng, Paul A. Iaizzo PhD

Departments of Surgery and Biomedical Engineering, University of Minnesota, Minneapolis, MN, USA

Published in the *International Journal of Cardiovascular Imaging,* 2011 Dec;27(8):1223-34.

Summary

The detailed assessment of cardiac anatomy using multiple imaging modalities is essential to understand the high degree of variations that exist in human hearts (i.e., with and without pathologies). Additionally, such information should provide one with important insights regarding which imaging modality will best provide the required visualization of device placement via a given transcatheter approach. We describe here a unique set of such studies performed on either preserved heart specimens or within reanimated large mammalian hearts, including human (using Visible Heart® methodologies). Such anatomical and device-tissue interface knowledge is critical for both design engineers and clinicians that seek to develop and/or employ less invasive cardiac repair approaches for patients with acquired or congenital structural heart defects.

Introduction

The pre- and post-evaluation of implantable cardiac devices requires innovative and critical testing in all phases of the design process. Over the past 13 years, our laboratory has utilized a number of research approaches to gain novel insights into the variability of human cardiac anatomies (normal or diseased) and the device-tissue interface. To do so, we have employed: 1) a large library of perfusion fixed human hearts (> 180); 2) an in vitro isolated heart model known as the Visible Heart®; and/or 3) multimodal imaging in various experimental settings. The use of such methodologies has allowed for novel examinations of device-tissue interactions as a means to evaluate transcatheter device placement and subsequent performance within human hearts of varying anatomies. More specifically, these research tools have provided novel insights for utilization in a number of different biomedical applications: 1) they give product designers a rapid method to critically assess device prototypes, thus expediting design decisions; 2) they allow clinicians to directly visualize the deployment of new or problematic clinical systems; and/or 3) they can be used to obtain educational images that are valuable to patients and students at all levels. It is clear that the future of cardiac devices will include beating heart procedures such as transcatheter delivered valves, and implantations will likely utilize simultaneous multiple imaging modalities (e.g., within a hybrid operating room). Each of these imaging modes helps to facilitate the proper positioning of cardiac devices during deployment, the refinement of device deployment procedures, and the eventual evaluation of resultant cardiac function within experimental and clinical settings. Continued use of each imaging

technique in a laboratory setting will help provide insights to their advantages and faults in relation to clinical usage.

Specifically, Visible Heart® methodologies allow for comparative functional imaging within an isolated working heart. Such visualization and the subsequent imaging have provided high resolution images of large mammalian hearts, including human hearts. As such, our laboratory has investigated the deployment of numerous types of transcatheter delivered valves and other devices under direct visualization with high resolution endoscopes and/or with simultaneous collection of fluoroscopic and echocardiographic images. Such valves or repair devices have been deployed into the aortic, mitral, or pulmonary positions of both the native anatomy and variously placed prostheses to simulate: 1) the potential range of beating heart ("off pump") procedures; and 2) the presence of anatomical abnormalities (e.g., calcification of the aortic valve).

General Methodologies

Perfusion Fixed Heart Specimens

An intricate understanding of cardiac anatomy remains one of the most important fundamentals in cardiovascular medicine and the cardiac device industry [1, 2]. Anatomical variations may have profound effects on both the performance and deployment of cardiac devices; thus a well-developed understanding of the relevant cardiovascular anatomies (in relation to both vascular approaches and within the heart itself) is critical at all levels of the device design and development process [3-5]. Our laboratory has the privilege to obtain fresh human heart specimens for educational and research purposes from: 1) organ donors whose hearts are not deemed viable for transplantation and are donated for research (via LifeSource, the Upper Midwest Organ Procurement Organization); and 2) bodies donated to the University of Minnesota's Anatomy Bequest Program. All study protocols requiring the use of these specimens were approved by the Institutional Review Board of the University of Minnesota. After excision, the fresh or unfixed specimens were subsequently cleaned and perfusion fixed in 10% buffered formalin by attaching the cannulated great vessels to a pressure head of approximately 50 mmHg. This technique, as described by Anderson et al. [5], fixes the hearts in an approximation of the end-diastolic state, providing a unique insight into the anatomical dimensions of a given specimen. Figure (4.1) demonstrates images that can be acquired from these specimens and shows some of the valve pathologies that can be visualized.

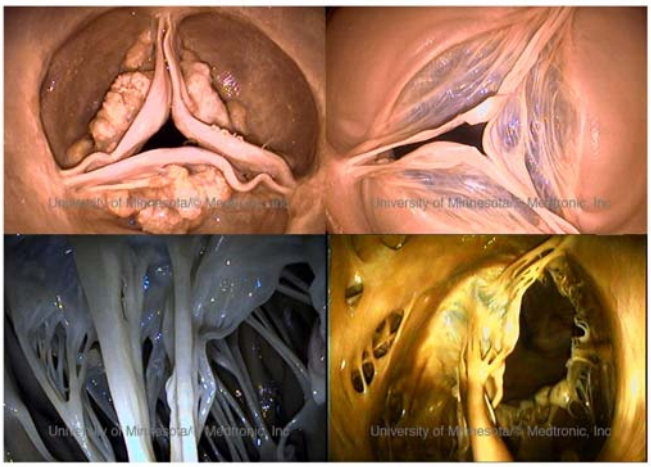

Figure 4.1. Images from perfusion fixed hearts in the Visible Heart® library: 1) image of a calcified aortic valve (upper left panel); 2) image of the pulmonary valve (upper right panel); 3) image of the subvalvular apparatus of the mitral valve (lower left panel); and 4) image of the tricuspid valve from the right ventricle (lower right panel). Modified from "The Atlas of Human Cardiac Anatomy" [30].

This unique library of more than 180 hearts to date provides researchers with an accurate insight into how potential transcatheter delivered valve technologies may interact with the surrounding cardiac anatomy. Studies have included investigations into the specific anatomy of the mitral valve leaflets [6], the relation of the aortic valve leaflets to the coronary ostia and the sinus of valsalva [7], and various anatomical studies of the sub-valvular apparatus of the mitral valve [8]. In addition to these anatomical investigations, such resources allow for the placement of prototype devices and the rapid comparison of how a device will interact with the surrounding cardiac anatomy in a variety of human specimens.

Comparative Static Imaging and 3D Modeling

With recent advances in cardiac imaging technology there has been extensive work in the analysis of the anatomical variation from patient to patient using clinically accepted modalities such as: 1) cardiac ultrasound (e.g., transthoracic, transesophageal, intracardiac, 2D, 3D, and/or 4D); 2) computed tomography (CT); 3) multi-slice computed tomography (MSCT); and 4) magnetic resonance imaging (MRI)(e.g., 1.5T, 3T, or greater)[9-12]. Within the Visible Heart® laboratory, we have been developing the library via the non-destructive imaging of each specimen using ultrasound, CT, and MRI. Preparation of the perfusion fixed hearts via suspension in a gel medium has allowed for a full complement of multimodal imaging to be performed on the hearts [13]. More specifically, high resolution image acquisition has allowed for detailed studies of the cardiac anatomy for a variety of cardiac pathologies, not possible with

current clinical imaging protocols. Such studies include the characterization of the position and size of the papillary muscle complexes within the left ventricle for dilated and hypertrophic cardiomyopathy specimens [14] and the analysis of fiber orientation of specimens in end-stage heart failure using diffusion tensor MRI (DTMRI)[15]. In addition, it has been possible to compare the ability of different imaging modalities to assess the anatomical characteristics of specific cardiac pathologies such as aortic stenosis, thus building on the work of other researchers [16].

Concurrently, these scans are being used to create a digital database of these specimens by the rendering of three dimensional computational models using software packages such as Mimics (Materialise, Leuven, Belgium). These computational models have paved the way for ongoing investigations into the use of three dimensional printing to create physical representations of the specimens for use as anatomical models for device design and educational purposes.

Features of the Visible Heart®

Our laboratory at the University of Minnesota has partnered with Medtronic, Inc. to develop the Visible Heart® methodologies which consist of a large mammalian isolated heart model that functions in either Langendorff [17], right-side working, or four-chamber working modes [18]. This isolated heart model involves the initial step of removing hearts from humans or animals using standard cardioplegia procedures [18, 19]. Once isolated, the hearts are reanimated and can eventually function with all four chambers working. Following reanimation, cardiac and systemic pressures and outputs are monitored and preloads and afterloads can be adjusted to simulate systemic vascular pathologies such as hypertension. Our laboratory routinely utilizes various imaging techniques (both endoscopes and fiberscopes) and has compared them to clinically available methods (e.g., fluoroscopy and echocardiography). This has provided very unique footage of normal and abnormal functional anatomy of both human and animal hearts, not only within a given chamber, but within vessels as well.

The isolated heart apparatus serves multiple roles, e.g., allowing operation in either Langendorff, right-side working, or four-chamber working modes. During the Langendorff mode, the left-side afterload is held constant with a coronary perfusion pressure of approximately 60 mmHg [18]. Thus, the flow through the coronaries is determined by dilation or constriction of the coronary arteries. Right-side working mode combines Langendorff retrograde aortic perfusion with antegrade, or physiologic, flow through the right atrium and

right ventricle (adjustable between ~3-5 L/min). During four-chamber working mode, the flow through the heart is normally determined by the intrinsic heart rate and contractility of the heart. The intrinsic heart rate can be modified by altering the temperature of the buffer or adding pharmacological agents. Although no model can perfectly mimic in vivo conditions, this apparatus allows for the re-creation of various cardiac states through control of preload and afterload pressures. We can also change the physical orientation of the heart to obtain clinically relevant medical images and/or to simulate the relative heart orientation during a planned clinical procedure.

When studying cardiac valves, it is important to understand that, while in four-chamber working mode, the aortic (left side) and pulmonary (right side) valves open during ventricular systole and close during ventricular diastole. Initially, there is a net movement of buffer into the ventricles through the open mitral (left side) and tricuspid (right side) valves during diastole due to the applied preloads. At this same time, the externally applied afterload in the aorta and pulmonary artery is greater than the pressure in the ventricles, effectively closing the aortic and pulmonic valves, respectively. As systole begins, the mitral and tricuspid valves close due to the pressure increase in the ventricles. Once the pressure in the left ventricle exceeds that of the aorta (the applied left heart afterload), the aortic valve opens and the buffer is ejected through the aortic valve. The same is true with the pulmonary valve as it opens when the pressure in the right ventricle exceeds that of the pulmonary artery (the applied right heart afterload). Typically, there are some micro-bubbles observed during ultrasonic imaging within the heart due to imperfect sealing of the preparation and/or inadvertent introduction of air, yet it is important to note that this does not prohibit imaging and may actually help one to visualize turbulent flow patterns. Furthermore, while in any of these modes, one may add a catecholamine and/or a bolus of calcium ions to upregulate hemodynamic functioning.

The Visible Heart® model has provided our scientists, engineers, and clinical collaborators with an innovative heart model to better understand how the dynamic forces and complex anatomic structures of the heart interact with a broad range of cardiac devices (e.g., pacing and defibrillation leads, pressure sensors, valves, and occluder devices). We are continually in the process of enhancing the overall utility of our system and methodologies, from improved mechanics to novel chemical additives to the buffer.

Employing Visible Heart® Methodologies to Develop Transcatheter Valve Technologies

Transcatheter valves and other such delivered devices have the potential to reduce operative morbidity, expand the indication for valve replacement or repair into non-surgical candidates, and treat patients who have been considered too high a risk for open heart surgery due to their current medical status. Currently, several human trials are ongoing, but the development of these devices remains limited by the inability to visualize the interaction of the devices with soft tissues of the heart. Recently, we have aggressively pursued the use of Visible Heart® methodologies as a viable tool for visualizing and evaluating the intracardiac performance of prototype and market released transcatheter valves in the pulmonary, aortic, and mitral positions [20, 21].

Use of the Visible Heart® in Transcatheter Valve Device Development

Additionally the Visible Heart® approach can be used to capture internal and external images of device implantations during near normal hemodynamic conditions (left ventricular systolic pressures of 70-90 mmHg). These images allow for evaluation of the delivery catheters, deployment balloons, stents, and tissue valves. Specifically, engineers and scientists are able to evaluate many aspects of transcatheter device design such as delivery catheters, deployed stent lengths, stent shapes, relative valve attachments, and/or interaction of these devices with native or conduit anatomies. For example, visualization of the delivery of a transcatheter pulmonic valve provided new insights into the design of valve leaflets in the pulmonary position to accommodate the low pressure gradients encountered in this location [20]. The implantation of transcatheter aortic valve replacements into the native aortic root of human hearts has highlighted the interaction of the stent with native leaflets and the mitral apparatus, thus illustrating the importance of precise stent sizing and positioning in order to avoid interaction with the anterior leaflet of the mitral valve and excessive pressure on the cardiac conduction system [21].

Modification of Normal Swine Heart Anatomies to Simulate Pathological States

The successful reanimation of human hearts using the Visible Heart® approach requires a level of cardiac health not always present in the available (donated) organs. Additionally, it is considered that the therapies for such pathologies cannot be adequately or ideally tested by using “healthy” swine hearts as a model. Consequently, to further the ability of the in vitro

model to test specific devices/prototypes, there has been ongoing work by our laboratory and collaborators to develop models specifically designed to simulate certain pathological states.

Alterations to the Right Ventricular Outflow Tract and the Pulmonary Valve

Recent advances in transcatheter delivered pulmonary valve technologies have also initiated the development of therapies for individuals with congenital defects and/or other specific patient populations. It is understood that valvular heart disease is a major cause of morbidity and mortality in patients who survive surgical correction for tetralogy of Fallot (TOF) [22], and the pathologies associated with TOF display a wide variation in the morphology of the right ventricular outflow tracts [23]. As such, planned therapies for these specialized pathologies need to adapt to a large variety of anatomical configurations, thus requiring extensive in vitro and in vivo testing before starting clinical studies. For example, here we describe the surgical adaptation of the swine model to approximate the right ventricular anatomy of such patients; a beating heart model of the relevant anatomy is created by compromising the pulmonary valve and dilating the outflow tract and annulus [24]. Once created in vivo, such models can be transferred to the Visible Heart® for in vitro analysis and visualization of the device-tissue interaction within this altered anatomy, see figure (4.6).

Mitral Valve Dysfunctions

To date, the Visible Heart® has also been used extensively in the development of percutaneous edge-to-edge mitral valve repair devices. In order to validate such techniques and to determine if mitral stenosis occurs after edge-to-edge repair, the swine model was surgically adapted by cutting a strut chordae under visual guidance in the P2 region of the posterior leaflet [25]. Such in vitro models have since been used to determine the effectiveness of percutaneous devices at capturing prolapsing leaflets and restoring valve function.

Aortic Valve Dysfunctions

With the intense interest in percutaneous aortic valve repair, there have been considerable advances in the design and development of transcatheter delivered prosthetic aortic valves. Our laboratory has been fortunate to utilize Visible Heart® methodologies to provide a beating heart model for the testing of such devices and their delivery systems. However, it should be noted that the testing of such devices in healthy swine anatomy does not always satisfactorily

approximate the environment and function of the devices' intended patient population. As such, our work in developing a model of severe aortic stenosis has been ongoing, with the specific aim of determining how large calcific deposits on the leaflets affect the deployment and function of such devices. To approximate severe stenosis of the aortic valve, we have: 1) directly adhered plastic models of calcifications to the leaflets to reduce leaflet motions; and 2) partially adhered the leaflet commissures to reduce the effective orifice areas of these valves [26]. To date this model has allowed for complete procedural testing of such devices, from balloon valvuloplasty to device deployment, and has provided useful insights into the potential interaction of deployed devices and the calcific deposits relative to the native anatomy.

Results

Swine Versus Human Anatomy

Although the swine model is used extensively for cardiac device testing due to similarities between human and swine relative cardiac anatomies, it must be noted that there are some variations in specific valve anatomies. Such inter-individual and inter-species variations have been extensively researched by Michaëlsson and Ho [27], and many other investigators have highlighted the impact of such work in medical device testing [18, 19, 28, 29]. More specifically, when testing aortic valve therapies in the swine model, it should be considered that there are inter-species differences in leaflet morphology and coronary ostia positioning, resulting in an increased likelihood of interaction between the two in swine [28]. Additionally, in swine: 1) the ascending aorta is typically shorter, i.e., the branch of the braciocephalic artery and the start of the aortic arch are closer to the aortic annulus; 2) there are only two primary arteries exiting the arch; and 3) there typically are no plaques present or calcific stiffening of the aorta [29]. Variations in the mitral and tricuspid valves can also occur, e.g., differences in the number of leaflets and the anatomy of the subvalvular apparatus. However, these variations are often attributed to inter-individual differences [27, 29]. Interestingly, the relationship between the various valves themselves and the cardiac conduction system is comparable between swine and human anatomies, and thus interaction between an aortic prosthesis, the mitral valve, and the conduction systems within the interventricular system can be quantified to a reasonable extent in the swine model [29].

Static Comparative Imaging

By embedding the hearts in agar gel our laboratory has been able to acquire images using a variety of clinical modalities such as echocardiography, CT, and MRI.

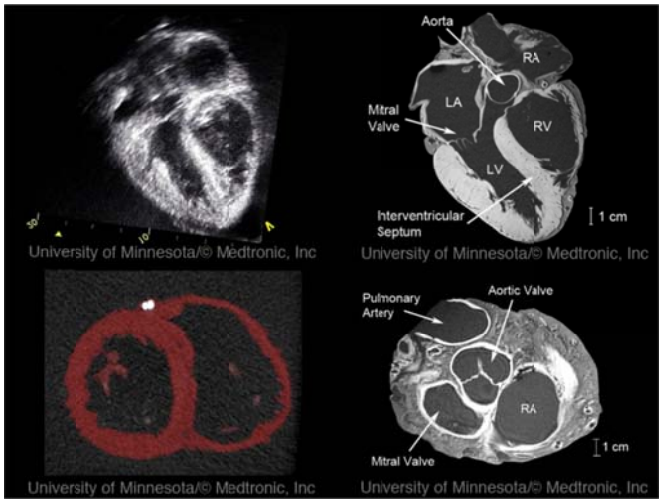

Figure 4.2. Images from perfusion fixed hearts from the Visible Heart® library: 1) a long axis four-chamber cardiac ultrasound view (upper left panel); 2); a long axis four-chamber MRI view (upper left panel); 3) a short axis CT view at the ventricular level showing calcium deposition in the anterior interventricular artery, the myocardium has been colored red in post processing to ease viewing (lower left panel); 4) a short axis MRI view at the valve level (lower right panel). Modified from Eggen et al. [13].

Several advantages of this approach include the following: 1) it reduces motion artifacts during imaging; 2) the relative orientations of the specimens are uniform for each imaging modality; and 3) the specimens have not been found to degrade. Shown in figure (4.2) are some of the results from these imaging studies showcasing the high resolution imaging capabilities.

Visualization of Functional Anatomies and Transcatheter Valve Implantations

Reanimation of human hearts using a clear blood substitute has allowed for the collection of unique footage of the functional human heart [18, 19]. More specifically, the laboratory has created a free access web site, "The Atlas of Human Cardiac Anatomy," in which we have placed such images for public educational use [30]. This site uniquely includes movie clips of functional cardiac anatomies, as well as comparative imaging using echo, fluoroscopy, and MRI. We plan to embellish the library by adding digital reconstructions on the web site in the near future. Examples of imaging capabilities within the human heart can be seen in Figure (4.3).

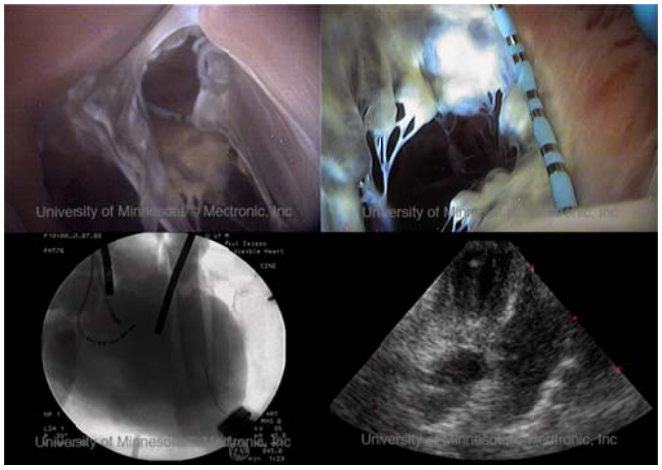

Figure 4.3. The tricuspid valve imaged using: 1) an endoscope placed within the right ventricle (upper left panel); 2) an endoscope placed within the right atrium (upper right panel); 3) fluoroscopy with an anterior-posterior orientation (lower left panel); and 4) ultrasound (lower right panel). Modified from "The Atlas of Human Cardiac Anatomy" [30].

In addition to video images of the functional anatomies, extensive footage of device implantations has been obtained utilizing Visible Heart® methodologies, including transcatheter delivered devices to the pulmonary and aortic positions as seen in Figures (4.4) and (4.5).

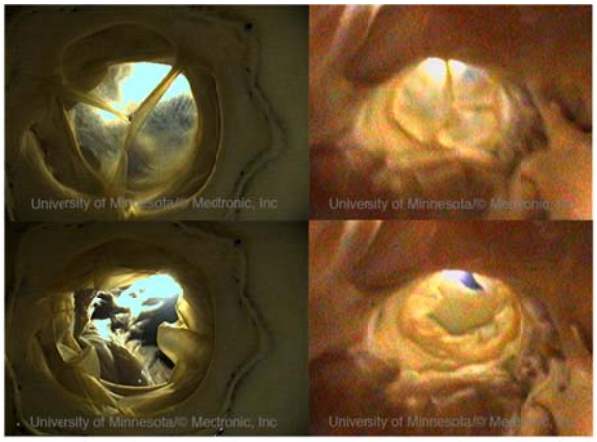

Figure 4.4. A transcatheter delivered pulmonary valve imaged from endoscopes placed within: 1) the pulmonary trunk during diastole (upper left panel); 2) the right ventricle during diastole (upper right panel); 3) the pulmonary trunk during systole (lower left panel); and 4) the right ventricle during systole (lower right panel). Modified from Quill et al. [20].

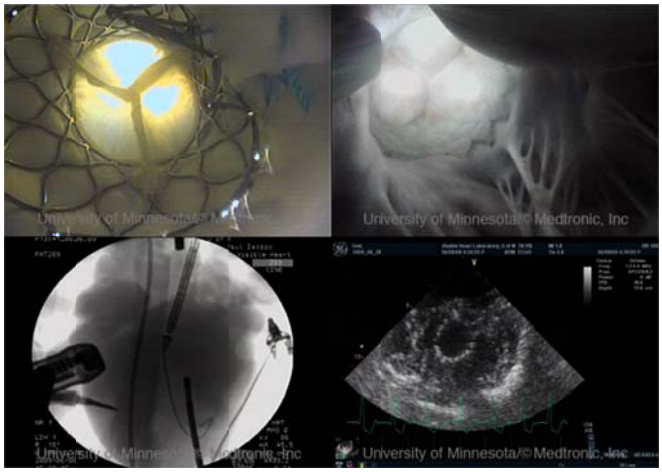

Figure 4.5. A transcatheter delivered aortic valve imaged using: 1) an endoscope placed within the ascending aorta (upper left panel); 2) an endoscope placed within the left ventricle (upper right panel); 3) fluoroscopy with an anterior-posterior orientation (lower left panel); and 4) ultrasound (lower right panel). Modified from Iaizzo et al. [21].

Models of Valvular Dysfunction

Figures (4.6-4.8) show examples of how the swine model has been surgically adapted to better represent the anatomy of human cardiac pathologies specific to valvular diseases. These images were taken employing the Visible Heart® approach and represent some of the in vitro models available to device designers.

Figure 4.6. An image showing the surgically created right ventricular outflow tract dilation of a swine heart; the remnants of the pulmonary valve can be seen in the foreground. Modified from Bateman et al. [24].

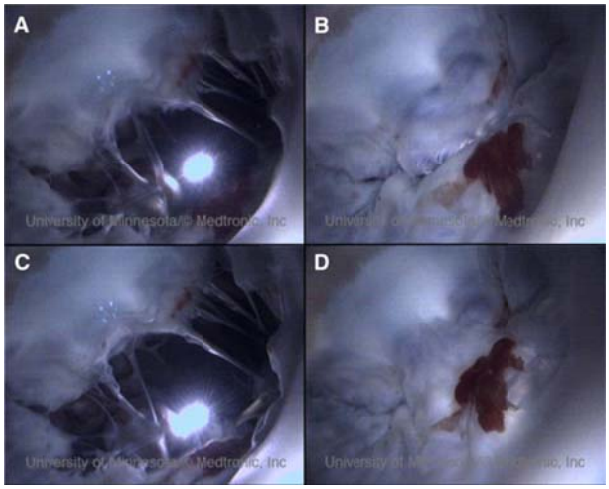

Figure 4.7. A mitral valve visualized during diastole (left) and systole (right) for the normal (top) and prolapsed state created by cutting a strut chordae of the P2 region (bottom). Modified from Quill et al. [25].

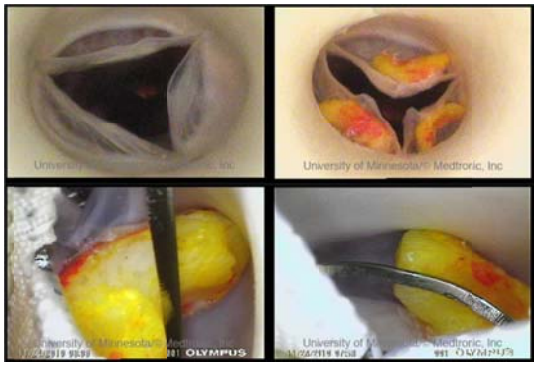

Figure 4.8. Images of an in vitro model of aortic stenosis: 1) an endoscope placed within the ascending aorta showing the native swine valve (upper left panel); 2) an endoscope placed within the ascending aorta showing the valve after the addition of calcifications (upper right panel); 3) an endoscope image of the non-coronary cusp after device implantation (lower left panel); and 4) an endoscope image of the left coronary cusp after device implantation (lower right panel). Modified from Bateman et al. [26].

Discussion

The complexity of intracardiac interventions has increased with the advent of transcatheter valve replacements and/or repairs. It is expected to further intensify as clinicians become more comfortable with these novel procedures of administering therapies and/or devices within the beating heart, and both clinicians and engineers continue to invent, design, and refine new product solutions. This is exemplified by the fact that in the field of transcatheter aortic valve implantation (TAVI) alone, two devices (CoreValve ReValving® system, Medtronic Inc., Minneapolis, MN and the Edwards SAPIENTM valve, Edwards Lifesciences, Irvine, CA) are

currently market released in Europe and enrolled in clinical trials in the United States, with up to 25 other new designs of TAVI devices currently under development [31]. These products approach and attempt to solve the challenges of TAVI by incorporating desirable features to improve the performance and efficacy of implantation (i.e., reducing complications and improving clinical outcomes). However, it is possible that attempts to improve these devices could lead to unexpected problems or compromise durability [32]. As such, it becomes more critical than ever for device developers to have a thorough understanding of: 1) the variations of cardiac valve anatomies that will occur in the patient populations they hope to treat; and 2) the results they obtain from in vitro and in vivo testing of potential therapies. These facts should be well known prior to presenting to regulatory bodies, such as the FDA, to gain approval for initial human clinical trials. It has been well documented that the premature enrollment of devices into poorly designed clinical trials can be detrimental to all involved, including prospective patients [33].

It should be noted that many of the newer transcatheter delivered technologies have presented clinicians with the opportunity to treat patient populations with even more complex cardiac valve pathologies, e.g., those previously inaccessible without open heart surgery. In doing so, there has been a rise in the "compassionate" (often off-label) use of such devices, making it even more critical to completely understand how a device performs when placed in alternate anatomical positions [34, 35]. It is also important to note that prior to such clinical use, these types of applications could be readily studied employing a variety of the experimental approaches we have discussed here, e.g., the implications of multiple prosthesis implantations (valve in valve) [36].

The Visible Heart® Laboratory

The Visible Heart® methodologies for valve visualization are intended to complement the work by others that employ other well-established in vivo or in vitro methods to test the reliability, durability, biocompatibility, or other parameters of newly developed transcatheter delivered valves or other devices [37-42]. Importantly, as clinicians push the current boundaries of transcatheter delivered therapies, multiple imaging modalities will be required to plan and guide these interventions. To date, all standardized imaging modalities utilized during intracardiac interventions exhibit some potential limitations, e.g., low temporal or spatial resolution, excessive exposure to ionizing radiation, and/or interference with the clinical operator's

freedom of movements. We believe that, in the near term, a combination of imaging modes will provide the information required to guide these complex interventions in the hybrid operating room. Hence, our laboratory may be providing "a glimpse into the future", by employing simultaneous or comparative imaging in an experimental setting. Here we have provided a small sampling of the direct visualization of transcatheter valve implantations that have been completed in our laboratory and the device testing that can be achieved using Visible Heart® methodologies.

Utilization of Visible Heart® methodologies has provided (and will continue to provide) unique visualization for a variety of cardiac device technologies and their delivery systems. Hence, we consider that the described anatomical preparations and in vitro models will aid both design engineers and physicians who hope to rapidly and effectively develop implant methodologies. Furthermore, as these novel therapies become clinically available and thus are implanted by more and more physicians, individuals will require continued education in the techniques required to navigate and deploy such devices. In response to this need, our laboratory has developed a free access web site, "The Atlas of Human Cardiac Anatomy," that can be utilized by cardiac device developers and clinical implanters to gain insights on variability in functional cardiac anatomies [30].

Nevertheless, our experimental setup is not without known limitations. For example, ischemic time prior to reanimation can compromise cardiac function, specifically contractility and pressure generation. The positioning of the heart on the apparatus may also affect the performance of these isolated hearts. Additionally, the lack of a pericardium may contribute to over-expansion of the atrial chambers, slightly different respective anatomical orientations of the great vessels and chambers, and/or differences in contractility compared to in vivo performance [43]. Finally, the use of a clear perfusate without an oxygen carrier may lead to low-level global ischemia and the development of tissue edema which will have an effect on the long-term viability of these reanimated hearts. Despite these limitations, this experimental approach can be considered as a model for acute heart failure.

In summary, the study of fixed and reanimated human hearts, using the various methodologies described here, provides novel insights into human cardiac anatomies. Additionally, one can better visualize anatomical alterations that occur with various pathologies and/or those that may occur following the deployment of devices in the heart. More specifically, the Visible

Heart® methodologies have provided a unique perspective of functional cardiac anatomy. By reanimating these hearts using a clear perfusate, we are able to visualize functional anatomy with endoscopes placed directly within various heart chambers and/or within the large diameter vessels of the heart. Using this generated database of images, one can easily identify the large degree of variability that exists in human valve and chamber anatomies (from both static and functional perspectives). We believe that such anatomic knowledge is critical for device designers and developers, as well as clinicians who utilize these less invasive cardiac repair approaches for patients with acquired or congenital structural heart defects. Furthermore, when direct visualization is simultaneously coupled with clinically employed imaging modalities, it provides further critical insights that can be used to more quickly and precisely advance such technologies. We consider that the utilization of both fixed specimens and Visible Heart® methodologies for device evaluation should be used in a complementary fashion with other techniques that utilize in vivo or in vitro methods to test the reliability, durability, biocompatibility, or other parameters of newly developed transcatheter devices. The continued testing of novel cardiac valve prostheses via in vitro and in vivo studies will provide scientists and engineers working in this field with the needed tools to drive the required research and development of the next generation of transcatheter delivered cardiac devices.

References

1. Anderson RH, Becker AE: The heart: Structure in health and disease. London, UK; New York, NY: Gower Medical Pub, 1992.

2. Weinhaus AJ, Roberts KP: Anatomy of the Human Heart. In: The Handbook of Cardiac Anatomy, Physiology, and Devices, Second Edition. Iaizzo PA (Ed.), Humana Press, Totowa NJ, USA, 59-85, 2009.

3. Loukas M, Sullivan A, Tubbs RS, Weinhaus AJ, DerDerian T, Hanna M: Chiari's network: review of the literature. Surgical and Radiologic Anatomy, 32: 895-901, 2010.

4. Maselli D, Guarracino F, Chiaramonti F, Mangia F, Borelli G, Minzioni G: Percutaneous Mitral Annuloplasty: An anatomic study of human coronary sinus and its relation with mitral valve annulus and coronary arteries. Circulation, 114: 377-380, 2006.

5. Anderson SE, Quill JL, Iaizzo PA: Venous valves within left ventricular coronary veins. Journal of Interventional Cardiac Electrophysiology, 23(2):95-9, 2008.

6. Quill JL, Hill AJ, Laske TG, Alfieri O, Iaizzo PA: Mitral leaflet anatomy revisited. Journal of Thoracic and Cardiovascular Surgery, 137(5):1077-81, 2009.

7. Quill JL, Geesling AG, Iaizzo PA: Transcatheter Aortic Valve Deployment: Interactions Between Native Leaflets and Coronary Ostia. Journal of Medical Devices, 3: 027530, 2009

8. Bateman MG, Russel C, Chan B, Hutton D, Iaizzo P: A detailed anatomical study of the papillary muscles and chordae tendineae of the left ventricle in perfusion fixed human hearts. In prep.

9. Ton-Nu T, Levine RA, Handschumacher MD, Dorer DJ, Yosefy C, Fan D, Hua L, Jiang L and Hung J: Geometric Determinants of Functional Tricuspid Regurgitation: Insights From 3-Dimensional Echocardiography. Circulation, 114:143-149, 2006.

10. Plass A, Valenta I, Gaemperli O, Kaufmann P, Alkadhi H, Zund G, Grünenfelder J, Genoni M: Assessment of coronary sinus anatomy between normal and insufficient mitral valves by multi-slice computertomography for mitral annuloplasty device implantation. European Journal of Cardio-thoracic Surgery, 33: 583-589, 2008.

11. Tops L, Wood D, Delgado V, Schuijf JD, Mayo JR, Pasupati S, Lamers FPL, van der Wall EE, Schalij MJ, Webb JG, Bax JJ: Noninvasive Evaluation of the Aortic Root With Multislice Computed Tomography, Journal of the American College of Cardiology, Imaging.1:321-330, 2008.

12. Salton CJ, Chuang ML, O'Donnell CJ, Kupka MJ, Larson MG, Kissinger KV, Edelman RR, Levy D, Manning WJ: Gender Differences and Normal Left Ventricular Anatomy in an Adult Population Free of Hypertension. Journal of the American College of Cardiology, 39: 1055-60, 2002

13. Eggen MD, Bateman MG, Iaizzo PA: Methods to Prepare Perfusion Fixed Cardiac Specimens for Multimodal Imaging: the Use of Formalin and Agar Gels. Submitted to the Journal of Medical Devices 2011.

14. Martel A, Bateman MG, Iaizzo H, Hjelle E, Iaizzo PA: Analysis of the Competence of Echocardiography at Determining Ventricular Cardiomyopathies. In Prep.

15. Eggen MD, Swingen CM, Iaizzo PA: Analysis of fiber orientation in normal and failing human hearts using diffusion tensor MRI, 2009 IEEE International Symposium on Biomedical Imaging: From Nano to Macro, 642-645, 2009.

16. Messika-Zeitoun D, Serfaty J-M, Brochet E, Ducrocq G, Lepage L, Detaint D, Hyafil F, Himbert D, Pasi N, Laissy J-P, Iung B, Vahanian A: Multimodal Assessment of the Aortic Annulus Diameter. Journal of the American College of Cardiology, 55:186-194, 2009.

17. O. Langendorff, "Untersuchungen am uberlebenden Saugenthierherzen [Investigations on the surviving mammalian heart]," Pflugers Arch., 61: 291-332, 1895.

18. E. Chinchoy, C.L. Soule, A.J. Houlton, et al., "Isolated four-chamber working swine heart model," Ann. Thorac. Surg., 5: 1607-1614, 2000.

19. A.J. Hill, T.G. Laske, J.A. Coles Jr., et al., “In vitro studies of human hearts,” Ann. Thorac. Surg., 79: 168-177, 2005.

20. J.L. Quill, T.G. Laske, A.J. Hill, P. Bonhoeffer, P.A. Iaizzo, “Direct visualization of a transcatheter pulmonary valve implantation within the Visible Heart®–A Glimpse into the Future,” Circulation, 116: e548, 2007.

21. Iaizzo PA, Hill AJ, Laske TG: Cardiac device testing enhanced by simultaneous imaging modalities: the Visible Heart®, fluoroscopy, and echocardiography. Expert Review of Medical Devices 5:51-8, 2008.

22. Wren, C. & O'Sullivan, J. Survival with congenital heart disease and need for follow up in adult life. Br. Med. J. 85: 438-443, 2001.

23. Schievano, S. et al. Variations in right ventricular outflow tract morphology following repair of congenital heart disease: Implications for percutaneous pulmonary valve implantation. J. Cardiovasc. Magn. Reson. 9: 687-695, 2007.

24. Bateman MG, Quill JL, Iaizzo PA, St. Louis JL: Induction of Right Ventricular Outflow Tract Dilation and Pulmonary Valve Insufficiency in a Porcine Model. In Prep.

25. Quill JL, Bateman MG, St. Louis JL, Iaizzo PA: Edge-to-edge repairs of P2 prolapsed mitral valves within isolated swine hearts. Journal of Heart Valve Disease (In press) 2010.

26. Bateman MG, Torrianni M, Menk A, Hill A, Iaizzo PA: Development of an Aortic Stenosis Swine Model using the Visible Heart®. In Prep.

27. Michaëlsson M, Ho SY: Congenital heart malformations in mammals: An illustrated text. London, UK; River Edge, NJ: Imperial College Press, 2000.

28. Sands MP, Rittenhouse EA, Mohri H et al.: An anatomical comparison of human, pig, calf, and sheep aortic valves. Annuals of Thoracic Surgery, 8: 407-14, 1969.

29. Hill A, Iaizzo PA: Comparative Cardiac Anatomy. In: The Handbook of Cardiac Anatomy, Physiology, and Devices, Second Edition. Iaizzo PA (Ed.), Humana Press, Totowa NJ, USA, 87-108, 2009.

30. http://www.vhlab.umn.edu/atlas/index.shtml

31. Bande M, Michev I, Sharp ASP, Chieffo A, Colombo A: Percutaneous Transcatheter Aortic Valve Implantation: Past Accomplishments, Present Achievements and Applications, Future Perspectives. [Review] Cardiology in Review, 18(3):111-124, 2010.

32. Webb J, Cribier A: Percutaneous transarterial aortic valve implantation: what do we know? Eur Heart J. 32 (2):140-147, 2011.

33. Kaul S, Diamond GA: Are Claims of Effectiveness of MitraClip Device Compared with Surgery for Severe Mitral Regurgitation Substantiated by the Evidence? A Critical Look at the EVEREST II Trial. Circulation, 122:A20910, 2010.

34. Roberts PA, Boudjemline Y, Celermajer D, Cheatham J, Eicken A, Ewert P, McElhinney D, Zahn E: Percutaneous Implantation of the Medtronic Melody Valve in the Tricuspid Position — A Multi-Institutional Multi-National Report. Circulation, 122:A16393, 2010.

35. Kalavrouziotis D, Doyle D; Rodés-Cabau J, Bagur R, DeLarochelliére R, Pibarot P, Dumont E: Transcatheter Aortic Valve Implantation in Patients With Severe Aortic Stenosis and Small Aortic Annulus. Circulation, 122:A19625, 2010.

36. Webb JG, Wood DA, Ye J et al.: Transcatheter Valve-in-Valve Implantation for Failed Bioprosthetic Heart Valves. Circulation,121:1848-1857, 2010.

37. Yoganthan, AP, Chandran KB, Sotiropoulos F. Flow in prosthetic heart valves: state-of-art and future directions. Ann. Biomed. Eng. 33(12): 1689-1694, 2005.

38. Gallegos RP, Nockel PJ, Rivard AL, Bianco RW. The current state of in-vivo pre-clinical animal models for heart valve evaluation. J. Heart Valve Dis. 14(3): 423-432, 2005.

39. Stachelek SJ, Alferiev I, Connolly JM, et al. Cholesterol-modified polyurethane valve cusps demonstrate blood outgrowth endothelial cell adhesion post-seeding in vitro and in vivo. Ann. Thorac. Surg. 81(1): 47-56, 2006.

40. Paniagua D, Induni E, Ortiz C, et al. Percutaneous heart valve in the chronic in vitro testing model. Circulation. 106: e51-e52, 2002.

41. Martin AJ, Christy JR. An in-vitro technique for assessment of thrombogenicity in mechanical prosthetic cardiac valves: evaluation with a range of valve types. J. Heart Valve Dis. 13(3): 509-520, 2004.

42. Bakhtiary F, Dzemail O, Steinseiffer U, et al. Opening and closing kinematics of fresh and calcified aortic valve prostheses: an in vitro study. J. Thorac. Cardiovas. Surg. 134(3): 657-662, 2007.

43. Richardson E, Hill AJ, Skadsnerg ND, Ujhelyi M, Xiao Y-F, Iaizzo PA. The pericardium. In: The Handbook of Cardiac Anatomy, Physiology, and Devices, Second Edition. Iaizzo PA (Ed.), Humana Press, Totowa NJ, USA, 125-136, 2009.

Models of Cardiac Valve Disease States

Section Summary

As discussed earlier in this document the successful reanimation of human hearts using the Visible Heart® methodologies requires a level of cardiac health not always present in the specimens that are donated to research. Additionally, it is considered that the therapies for such pathologies cannot be adequately or ideally tested by using “healthy” swine hearts as a model. Consequently, to further the ability of the in vitro model to test specific devices/prototypes, there has been ongoing work by our laboratory and collaborators to develop models specifically designed to simulate certain pathological states.

My work at the laboratory has concentrated on three specific models:

- The in-vitro creation of an aortic stenosis (AS) model in the beating swine heart.
- The in-vitro creation of a mitral prolapse model in the beating swine heart.
- The in-vivo creation of an insufficient pulmonary valve and dilated right ventricular outflow tract in a 20kg swine model

Each of the models will be described in depth in the following chapter and their potential use in the development of transcatheter delivered valve technologies will be discussed.

Michael G. Bateman MEng

Departments of Surgery and Biomedical Engineering, University of Minnesota, Minneapolis, MN, USA

5. Development of an Aortic Stenosis Swine Model using the Visible Heart®

Preface

The use of percutaneous technologies to deliver replacement aortic valves (TAVR) is fast becoming an accepted technique for treatment of severe aortic stenosis. This is exemplified by the fact that two devices (the CoreValve ReValving® system, Medtronic Inc., Minneapolis, MN and the Edwards SAPIEN™ valve, Edwards Lifesciences, Irvine, CA) are currently market released in Europe and enrolled in clinical trials in the United States, with up to 25 other new designs of TAVR devices currently under development (Bande, 2010). One of the predominant concerns with TAVR is the fact that in incidents of calcific stenosis, where heavy buildup of calcium deposition on the leaflet restricts their movement, the native leaflets are not removed. Instead they are pushed aside by the deployed device, often creating a non-uniform landing zone for the prosthesis. This uneven landing zone has been linked to potential para-valvular leak with the delivered prosthesis as the outer surface of the device fails to create a seal with the native anatomy.

Although the contribution of calcified native leaflets to para-valvular leak has been suspected for some time the ability to quantify this effect with in vitro investigations has been hampered by the static nature of traditional bench top models. We propose the use of Visible Heart® methodologies to create a dynamic, physiologically accurate model of the aortic anatomies of this patient population. To approximate severe stenosis of the aortic valve, we have experimentally reduced leaflet motion and partially fused the leaflet commissures to reduce the effective orifice areas of these valves. To date this model has provided useful insights into the potential interaction of deployed devices and the calcific deposits relative to the native anatomy. For this project I worked to integrate the stenosis model into the Visible Heart® set-up, completed data collection and analysis and am currently involved in the evolution of the model as new design and experimental needs are addressed.

Michael G. Bateman MEng[1], Mark W. Torrianni MS[2], Ana R. Menk BS[2], Alexander J. Hill PhD[2], Paul A. Iaizzo PhD[1]

[1]Departments of Surgery and Biomedical Engineering, University of Minnesota, Minneapolis, MN, USA
[2]Medtronic, Inc., Minneapolis, MN, USA

Introduction

With the intense interest in percutaneous aortic valve repair, there have been considerable advances in the design and development of transcatheter delivered prosthetic aortic valves[1]. Our laboratory has been fortunate to utilize Visible Heart® methodologies to provide a beating heart model for the testing of such devices and their delivery systems. As such, our work in developing a model of severe aortic stenosis has been ongoing, with the specific aim of determining how large calcific deposits on the leaflets affect the deployment and function of such devices. To date this model has allowed for complete procedural testing of such devices, from balloon valvuloplasty to device deployment, and has provided useful insights into the potential interaction of deployed devices and the calcific deposits relative to the native anatomy.

Calcific aortic stenosis (AS) is one of the most important diseases in older adults in the western world[2]. The gold standard to treat a symptomatic valve is through surgical replacement and in the past, balloon valvuloplasty (BAV) of the aortic valve was used as palliative treatment. The advent of transcatheter technology has led to the development of valved stents that can be placed using an antegrade or retrograde approach[3]. Most experience in this field has been gained using the Edwards SAPIEN™ and the CoreValve ReValving® system. Generally speaking, the prosthesis is positioned in the aortic root and, once deployed, crushes the calcified leaflets against the wall[4]. As such the level, position and hardness of the calcification on the leaflets greatly effects the deployment and function of the implanted valve.

Unlike the balloon deployed SAPIEN™ system the CoreValve® system relies on the expansion of a Nitinol frame to push the calcified leaflets aside and consequently is susceptible to irregular post implant function in the presence of asymmetric or excessive calcification[4]. The purpose of this model is to recreate the anatomy and morphology of a calcified aortic valve in the Visible Heart apparatus.

Methods

All Visible Heart® methodologies regarding in vivo swine studies and in vitro reanimation of large mammalian hearts as described by Chinchoy et al. are outlined in the paper "Edge-to-edge repairs of P2 prolapsed mitral valves in isolated swine hearts"[5,6], published later in this document.

Subsequent to recording the control data period Dobutamine (3 ml bolus, 500 µg/ml) and concentrated calcium (30 ml bolus, 100 mg/ml) were mixed with the buffer solution (~7.5 l) to optimize and maximize cardiac function. More specifically, following a 20-s waiting period to allow the drugs to take effect, each heart was switched from right-sided working mode into full four-chamber working (physiologic) mode. Hemodynamic signals were then stored and simultaneous video images recorded.

Following the collection of a normal data period the ascending aorta was cleaned and prepared for the procedure from the base of the aortic root to the braciocephalic branch. To minimise the amount of air that enters the coronary arteries the coronary sinus in the right atrium was blocked to hold a column of liquid in the coronary vasculature. Flow to the left artium and the aorta were then stopped before the heart was arrested and the ascending aorta was cut in the superior/inferior direction (axially to the vessel) creating a 2 inch incision through which the valve was accessed. Due to confidentiality agreements the detailed description of the creation of an accurate model of the calcific leaflets cannot be reported here. Briefly, plastic models of calcifications have been adhered to the leaflets to reduce leaflet motion and the leaflet commissures are partially adhered to reduce the effective orifice area. Once the procedure was complete the incision in the aorta was sutured shut before filling the left atrium, left ventricle and the aorta in succession. The afterload pressure on the aorta was then reapplied to pressurise the heart and the coronary sinus unblocked to restart flow to the coronary arteries. The heart was then allowed to rewarm and reperfuse with oxygenated Krebs-Henseleit buffer before administering calcium and dobutamine and defibrilating.

Data collection

Endoscopy: Endoscopic video images were obtained by employing 4 mm- and 6 mm-diameter endoscopes (IplexFX; Olympus Corporation, Tokyo, Japan), and images were obtained at 30 frames per second from both the ventricular and aortic sides of the aortic valve.

Hemodynamic: Hemodynamic monitoring of each reanimated heart was simultaneously conducted to assess the relative performance of the left atrium and ventricle. For this, Millar Mikro-Tip® pressure catheters (5 Fr, MPC 500; Millar, Houston, TX, USA) were placed in the ascending aorta, and in the left ventricle. Three-lead electrocardiographic (ECG) data (SpaceLabs, Redmond, WA, USA) and hemodynamic signals were acquired simultaneously using a data acquisition system (IOX; Emka, Paris, France).

Echocardiography: A long-axis echocardiographic view across the aortic valve was used to obtain aortic valve diameters and pulsed-wave Doppler images were used to measure the following parameters for the heart: heart rate, LVOT and aortic maximum and mean velocity and pressure gradient and velocity time interval.

Data analysis

Hemodynamic analyses: The following hemodynamic data were analyzed: left ventricular (LV) pressure, aortic pressure (Ao), and time derivatives of both (maximum dP/dt and maximum -dP/dt). Waveforms were plotted for each data period of the study, and the values then averaged over three consecutive beats. The time derivatives of ventricular pressure were considered as measures of relative contractility (maximum dP/dt) and relaxation (maximum -dP/dt) abilities.

Echocardiographic analysis: From the collected data the following parameters were calculated: LVOT area, aortic valve area (from both the velocity time intervals and from the maximum velocities) and the velocity ratio across the valve.

Results

Due to this being an experimental protocol the data has been displayed in two formats:

- Data showing the overall results from all 12 animals.
- A more in depth presentation of the data sets from three studies that were considered to be successful before data analysis.

Hemodynamic data

Table 5.1: Hemodynamic Data

	LVP [mmHg]		AoP [mmHg]		dP/dt LV [mmHg/s]		dP/dt Ao [mmHg/s]	
	Systole	**Diastole**	**Systole**	**Diastole**	**Systole**	**Diastole**	**Systole**	**Diastole**
Pre AS (11)	94 ± 20	10 ± 5	95 ± 19	31 ± 11	796 ± 149	-587 ± 163	752 ± 500	-407 ± 139
Post AS (12)	80 ± 18	23 ± 15	76 ± 17	25 ± 12	486 ± 191	-425 ± 178	512 ± 273	-380 ± 125
Difference	-12.87	12.32	-18.74	-5.82	-309.13	162.20	-239.26	26.65
% Diff.	-14.8	73.0	-22.0	-20.3	-48.2	-32.0	-37.9	-6.8

Table 5.2: Ratio of left ventricular pressure to aortic root pressure

LVP/AoP	Systole	Diastole
Pre AS (11)	0.99	0.44
Post AS (12)	1.09	0.96
Difference	0.10	0.52
% Diff.	9.5	74.0

Echocardiographic data

Table 5.3: In vivo vs. In vitro echocardiographic data

	Heart rate [bpm]	LVOT area [cm^3]	AV Vmax [m/s]	AVA by VTI [cm^3]	AVA by Vmax [cm^3]	Vmean ratio	Vmax ratio
In vivo (2)	105 ± 6	3.30 ± 1.50	1.07 ± 0.07	3.47 ± 1.85	2.60 ± 1.06	0.91	0.79
In vitro (2)	101 ± 40	2.99 ± 0.43	1.01 ± 0.13	3.41 ± 1.00	2.82 ± 0.93	1.00	0.93
Difference	-4.50	-0.31	-0.06	-0.06	0.22	0.09	0.14
% Diff.	-4.4	-9.8	-5.6	-1.8	8.1	8.9	15.7

Table 5.4: Echocardiographic data

	Heart rate [bpm]	LVOT area [cm^3]	AV Vmax [m/s]	AVA by VTI [cm^3]	AVA by Vmax [cm^3]	Vmean ratio	Vmax ratio
Pre AS (12)	95 ± 16	3.10 ± 0.50	1.03 ± 0.19	2.99 ± 0.70	3.06 ± 0.76	0.96	0.98
Post AS (11)	95 ± 14	2.92 ± 0.51	1.01 ± 0.13	3.17 ± 0.94	2.86 ± 0.46	1.00	0.99
Difference	0.40	-0.19	-0.02	0.18	-0.20	0.04	0.02
% Diff.	0.4	-6.4	-1.8	5.8	-6.9	4.5	1.8

Endoscopic data

Figure (5.1) shows images of a swine aortic valve both before and after completed procedure filmed from an endoscope placed within the ascending aorta showing the native swine valve during systole.

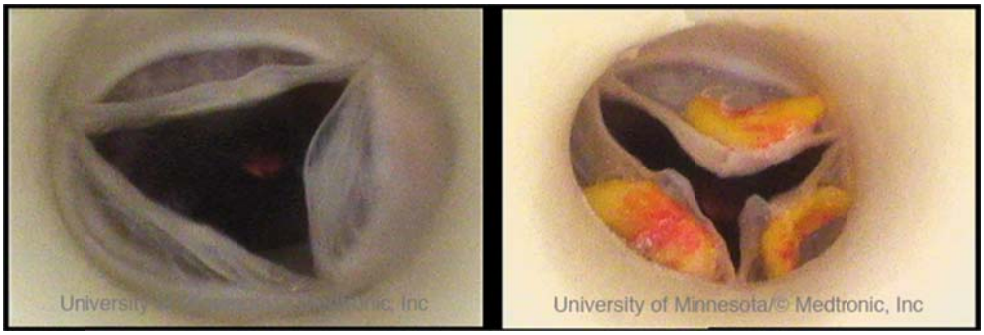

Figure 5.1: Images of the aortic valve from the Visible Heart apparatus

Detailed Data from Three Specific Studies

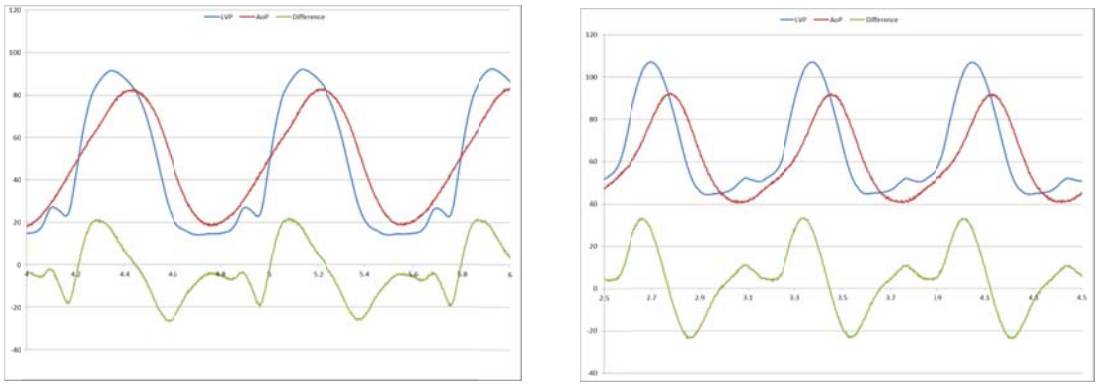

Figure 5.2: 3/1/2011 In vitro pressure traces from before (left) and after (right) creation of the AS model

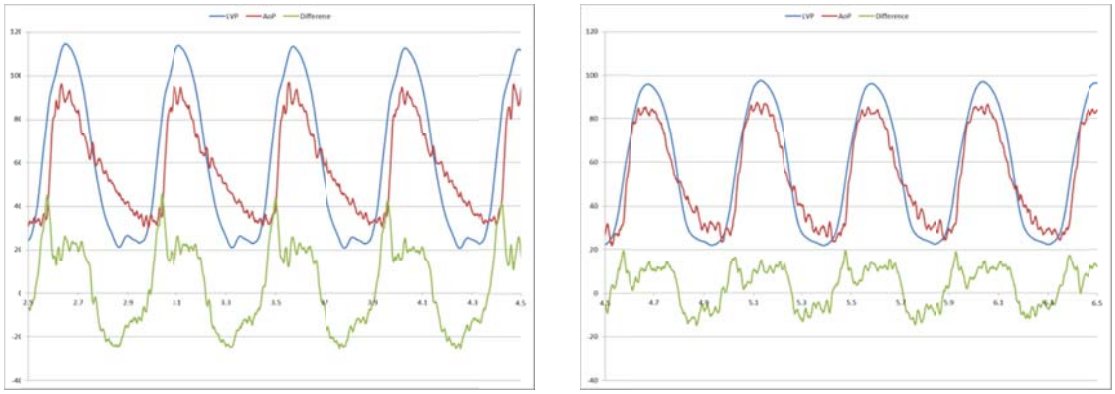

Figure 5.3: 6/23/11 In vitro pressure traces from before (left) and after (right) creation of the AS model

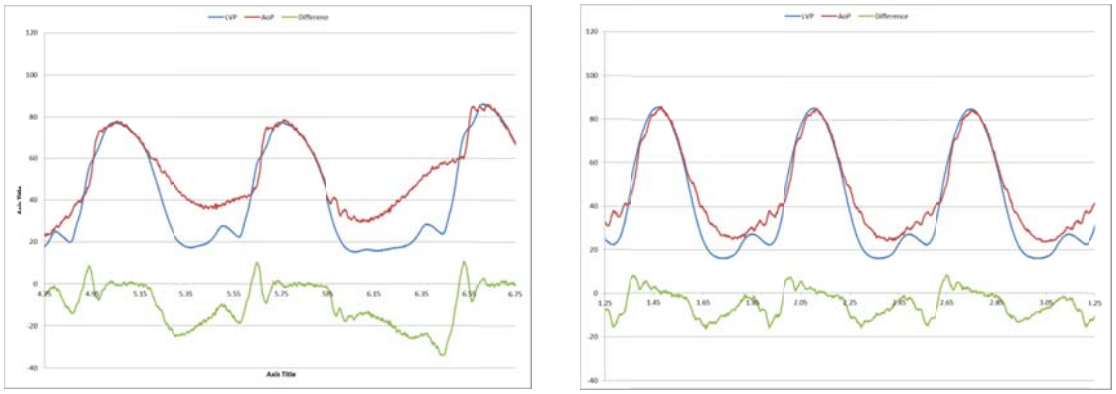

Figure 5.4: 7/19/11 In vitro pressure traces from before (left) and after (right) creation of the AS model

Table 5.5: Hemodynamic data

		3/1/2011		6/23/2011		7/19/2011	
		Pre AS	**Post AS**	**Pre AS**	**Post AS**	**Pre AS**	**Post AS**
LVP [mmHg]	**Systole**	92.47	114.32	118.44	102.92	87.38	86.30
	Diastole	13.49	35.79	20.56	19.09	13.57	16.13
AoP [mmHg]	**Systole**	83.18	94.09	96.42	92.55	86.67	86.10
	Diastole	9.34	33.28	28.47	23.24	18.72	21.59
LVP/AoP	**Systole**	1.11	1.22	1.23	1.11	1.01	1.00
	Diastole	1.44	1.08	0.72	0.82	0.72	0.75

Table 5.6: Echocardiographic data

	3/1/2011		6/23/2011		7/19/2011	
	Pre AS	**Post AS**	**Pre AS**	**Post AS**	**Pre AS**	**Post AS**
Heart rate [bpm]	78	87	129	116	72	92
LVOT area [cm^3]	2.73	2.13	2.69	2.84	3.30	3.14
AV Vmax [m/s]	1.05	0.91	1.10	n/a	0.92	1.19
AVA by VTI [cm^3]	2.46	2.29	2.70	n/a	4.12	4.32
AVA by Vmax [cm^3]	2.90	2.61	2.17	n/a	3.48	2.44
Vmean ratio	1.04	0.98	0.94	n/a	1.05	0.79
Vmax ratio	1.06	1.23	0.81	n/a	1.05	0.78

Table 5.7: Data summary of three "best" studies

	Pre AS	**Post AS**	**Difference**	**% Dif.**
LVP/AoP	1.12	1.11	-0.01	-0.6
AV Vmax [m/s]	1.02	1.05	0.03	2.6
AVA by Vmax [cm3]	2.85	2.53	-0.33	-12.1

Due to the low number of studies, n=2, we cannot complete a statistical analysis on these data, however, the correlation between echocardiographic measurements taken in vivo and in vitro is promising. There is an increase in the ratio between systolic left ventricular and aortic pressures of 9.5% (n=12). However, the ratio at diastole increased by 74.0%. The echocardiographic data pre and post AS does not exhibit any significant statistical findings. The three "best" studies yielded a 0.6% decrease in systolic pressure ratio, a 2.6% increase in velocity jet through the valve and a 12.1% decrease in effective orifice area.

Discussion

Although the video footage of the valves showed excellent results, confirming the creation of both inhibited leaflet motion and fused commissures, it was important to determine how the valve was function before and after the surgery. This was achieved by recording hemodynamic and echocardiographic data across the valve.

To successfully replicate the in vivo function of a stenotic valve we were looking for the following particular parameters to be met:

- An increase in the ratio between the left ventricular pressure and the aortic root pressure during systole
- An increase in aortic valve velocity
- A decrease in the effective orifice area of the valve

These characteristic changes are shown graphically in figures (5.5) and (5.6) representing the hemodynamic pressure waves and the Doppler echo traces respectively from humans with both healthy and stenotic aortic valves. In figure (5.5) it is important to note the distinct difference in the pressure traces above and below the valve defining the aortic kick, or the change in pressure as the valve closes. Also note the large change in the ratio between the peak left ventricular pressure and the peak aortic pressure in the healthy and stenotic valves. Figure (5.6) highlights how the velocity waveform increases in magnitude and decreases in width representing the characteristic jet that is caused by aortic stenosis.

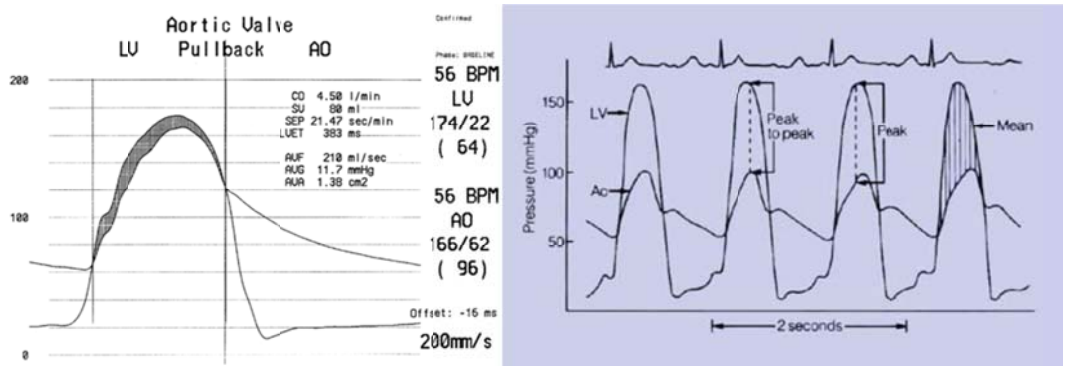

Figure 5.5: In vivo pressure traces from a healthy (left) and stenotic (right) aortic valve

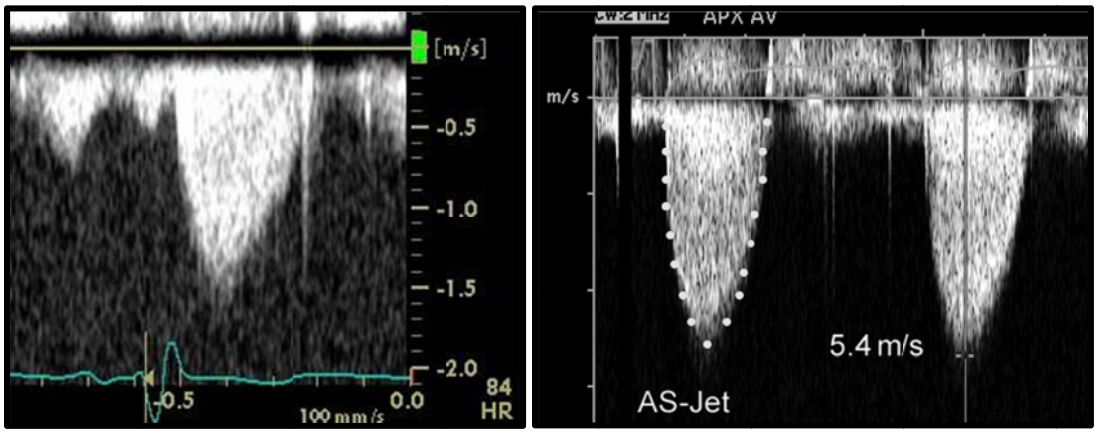

Figure 5.6: In vivo Doppler echocardiography traces from a healthy, Vmax 1.6ms, (left) and stenotic, Vmax 5.4ms, (right) aortic valve (Note the difference in scale in the y axis)

When considering the hemodynamic data as a whole it can be seen that the left ventricular and aortic pressures and the rate of pressure increase drop after the application of the stenosis model. This indicates a reduction in the effective function of the heart and will consequently affect absolute parameters measured via echocardiography, such as maximum flow velocity. The data shows an increase in the ratio of left ventricular pressure to aortic pressure from 0.99 to 1.09. Although this signifies an increase in stenosis this was not as significant an increase as expected. Interestingly, the data shows a dramatic increase in left ventricular diastolic pressure and a drop in aortic diastolic pressure indicating that the valve is not closing properly during systole and therefore allowing fluid back into the ventricle from the aorta.

When considering the overall echocardiographic data it can be seen that the data taken in vivo correlates well with the data taken before the stenosis model was applied proving that the Krebs-Henseleit buffer does not affect the readings. However, the data from before and after the application of the stenosis model do not show the changes in flow that we were expecting

to see. The data shows a 2% decrease in peak velocity and a minimal change in the calculated valve orifice area and the ratio of the flow velocity in the LVOT and the aorta. With absolute parameters such as the recording of the peak velocity this may be attributed to the loss of cardiac performance and interestingly when the peak velocity is normalized to the peak systolic left ventricular pressure, the maximum derivative of the pressure during systole and the peak velocity increase by 13% and 40% respectively. However this does not account for the relative measurements across the valve.

Although all echo exams were performed with the same probe placement to achieve the long axis view it is critical for all Doppler measurements to be made with the probe in line with the direction of flow. A possible explanation for this poor data correlation could be that the orientation may not have been consistent between measurements. Additionally, although the same amount of calcium and Dobutamine were added before each data collection period the short ischemic time during creation of the model will likely reduce the effectiveness of these agents and therefore change the pressure and flow properties of the left ventricle. Because of these discrepancies in the collected data and the expected results it was decided to analyze the three most recent studies more thoroughly. These three traces prove that despite model of aortic stenosis producing a good approximation of the disease with respect to leaflet movement and calcific mass, as shown by figure (5.1), we are not able to recreate the hemodynamic properties that would be associated with an aortic stenosis patient. Hence the current valve model cannot be deemed to accurately approximate the clinical pathology. The fundamental reason for this is the fact that we are loading the heart in an attempt to create a chronic disease in an acute setting. The resulting increased demand is not communicated to the heart as the isolated specimen has no autonomic connections and as such the left ventricle is unable to create the kind of pressure gradients seen across the valve in AS patients. Although cardiac performance can be adapted using catecholamines this may be a consistent limitation of the model.

Additionally, on many attempts the resulting low diastolic aortic pressures and increased left ventricular pressure indicate aortic valve regurgitation. This problem was often witnessed through the videoscopes as well and indicates that the fusion of the leaflet commissures needs to be carefully weighed against the possibility of causing valve regurgitation. As such the model clearly creates an excellent landscape to test novel aortic valve replacement technologies and

provide information on how a particular prosthesis interacts with the anatomy in a beating heart. However, as a test bed for function of a specific prosthesis it can be concluded that the pressures seen in this model do not satisfactorily mimic a stenotic aortic valve.

Model Improvements

In order to address the low diastolic pressure readings in the aorta during the normal data sets preliminary experiments were carried out in which the apparatus was adapted to alter the aortic afterload and hence to imitate a Windkessel aortic compliance chamber. The results can be seen in figure (5.7) and were able to achieve the following traces at two independent time points.

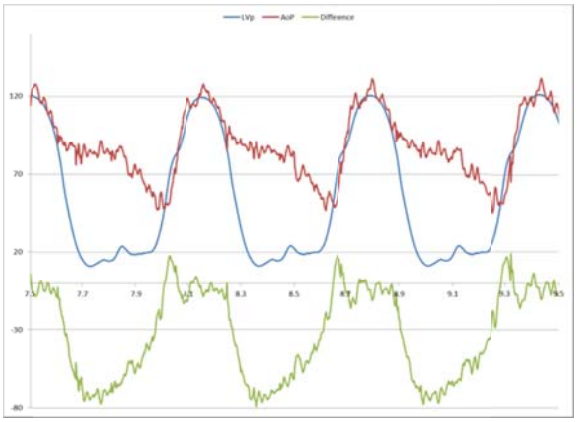

Figure 5.7: In vitro pressure traces with the apparatus adapted to simulate a Windkessel compliance chamber

These traces clearly show the aortic pressure trace representing the in vivo tracing for a healthy aortic valve as seen in figure (5.5). Adapting the apparatus in this way and experimenting with the catecholamine doses will improve the hemodynamic function of the model.

Conclusions

By introducing an aortic stenosis model to an isolated heart in the Visible Heart® apparatus we were able to visually create an approximation of a calcified stenotic aortic valve. This anatomical environment accurately estimates the valve anatomy of an aortic stenosis patient and proves that this dynamic model can be used to determine the ability of aortic valve replacement prostheses to perform in this complex geometry. However, investigations into the pressures and fluid flow through the valve have shown that the adapted valve model does not simulate the clinical valve pathology. Continued investigations into the improved control of the pressure gradients across the valve in order to better simulate fluid flow in the left ventricular outflow

tract and the aorta will help validate this model as a more complete test bed for aortic valve replacement therapies.

References

1. Bande, M., Michev, I., Sharp, A.S.P., Chieffo, A. & Colombo, A. Percutaneous transcatheter aortic valve implantation: past accomplishments, present achievements and applications, future perspectives. *Cardiology in review* **18**, 111-24 (2010)

2. Koos, R. *et al.* Quantification of aortic valve calcification using multislice spiral computed tomography: comparison with atomic absorption spectroscopy. *Investigative radiology* **41**, 485-9 (2006).

3. Bleiziffer, S. *et al.* Survival after transapical and transfemoral aortic valve implantation: talking about two different patient populations. *The Journal of thoracic and cardiovascular surgery* **138**, 1073-80 (2009).

4. Piazza, N. *et al.* Early and persistent intraventricular conduction abnormalities and requirements for pacemaking after percutaneous replacement of the aortic valve. *JACC Interventions* **1**, 310 (2008).

5. Chinchoy, E. *et al.* Isolated four-chamber working swine heart model. *The Annals of Thoracic Surgery* **70**, 1607-1614 (2000).

6. Quill, J.L., Bateman, M.G., St Louis, J.L. & Iaizzo, P.A. Edge-to-edge repairs of P2 prolapsed mitral valves in isolated swine hearts. *The Journal of heart valve disease* **20**, 5-12 (2011).

6. Edge-to-edge repairs of P2 prolapsed mitral valves in isolated swine hearts

Preface

Mitral valve dysfunction is classified according to a scale created by Carpentier based on the motion of the free edge of the leaflet relative to the plane of the annulus: type I, normal; type II, increased, as in mitral prolapse; type IIIA, restricted during systole and diastole, and type IIIB, restricted during systole. This paper reports on the acute assessment of edge-to-edge mitral valve repair and demonstrates the effectiveness of the procedure in correcting type II mitral regurgitation. Along with current products in clinical trial new devices and therapies, including percutaneous endovascular suture devices and percutaneous coronary sinus annuloplasty devices, that utilize the edge-to-edge repair technique are being developed.

By creating a model of type II mitral regurgitation using Visible Heart® methodologies, we were able to directly visualize the healthy, diseased and repaired mitral anatomy. Videoscopic, echocardiographic and hemodynamic assessments of both the heart function and the valve function were taken throughout the experiment and allowed for assessment of the valve to determine the effect of both the created prolapse and the edge-to-edge repair. For this project I assisted in the experimental design, set-up and data collection and was involved in the drafting of the manuscript.

Jason L. Quill PhD[1], **Michael G. Bateman MEng[2,3],** James L. St. Louis MD[2], Paul A. Iaizzo PhD[2,3]

[1]Medtronic, Inc., Minneapolis, MN, USA
Departments of [2]Surgery and [3]Biomedical Engineering, University of Minnesota, Minneapolis, MN, USA

Published in the *Journal of Heart Valve Disease,* 2011 Jan;20(1):5-12.

Summary

Background and aim of the study: The study aim was to determine if mitral stenosis occurred after edge-to-edge (E2E) repair of P2 mitral valve prolapse.

Methods: Six swine hearts were reanimated and videoscopes placed to view the mitral valve from the left atrium and left ventricle. Image analyses provided measures of the valve annulus area, orifice area, and regurgitant area. Hemodynamic data were collected (heart rates, left ventricular (LV) pressures, left atrial pressures, maximal LV dP/dt, and maximal LV -dP/dt) from three groups: (i) native functioning valve (Normal); (ii) mitral valve following excision of strut chordae from the P2 region (Prolapse); and (iii) following E2E repair.

Results: The mitral valve annulus areas were unaffected by the creation of prolapsed, or following repairs (Normal 10.50 ± 4.22 cm2; Prolapse 9.41 ± 3.70 cm2; E2E 9.66 ± 3.37 cm2; p <0.01), with similar decreases in annulus areas throughout the cardiac cycles, measured at 15 ± 3%. The orifice areas did not change with the creation of prolapses, but decreased following repairs (Normal 4.49 ± 2.70 cm2; Prolapse 4.13 ± 2.16 cm2; E2E 1.99 ± 1.19 cm2; p = 0.12). The regurgitant areas increased following induced prolapse, and returned to near-normal levels upon repair (Normal 0.20 ± 0.16 cm2; Prolapse 0.73 ± 0.35 cm2; E2E 0.12 ± 0.10 cm2; p <0.01). The max LV dP/dt measures did not decrease significantly, whereas max LV -dP/dt measures were decreased.

Conclusion: In this acute assessment of E2E repair of surgically induced mitral valve P2 prolapses, it was observed that a placed A2-P2 (Alfieri) stitch did not change the annulus area, but caused a significant decrease in the orifice area while successfully eliminating regurgitation, but without causing stenosis.

Introduction

Edge-to-edge (E2E) mitral valve repair (also known as the Alfieri stitch) is a surgical procedure in which the free edge of the anterior leaflet is sewn to the free edge of the posterior leaflet at the area of regurgitation, creating a double-orifice mitral valve (1-3). The main indications for this mitral repair procedure include bileaflet prolapse, anterior leaflet prolapse, commissural prolapse, and/or functional mitral regurgitation (4). This procedure has been shown also to be effective in a variety of clinical settings, with a low risk for creating mitral stenosis (5).

Due to the relative simplicity of the E2E approach, the ability to perform this procedure employing a percutaneous repair is being explored (6-8). In the Everest I trial for the MitraClip device (Evalve, Inc., Menlo Park, CA, USA), the majority of patients (14 of 24) presented with P2 prolapse prior to device implantation. Since posterior leaflet prolapse is conventionally repaired using quadrangular resection, the E2E technique mimicked by these devices should also be investigated for the repair of P2 prolapse, especially for mitral stenosis, which has been voiced as a concern regarding E2E repair (4).

In the present study, the repair of mitral valve P2 prolapses in isolated swine hearts with the E2E repair technique was investigated, where the orifice of the mitral valve could be directly visualized with Visible Heart® methodologies. More specifically, the use of an isolated heart preparation allowed for unique comparisons to be made between the valves while functioning normally, when regurgitant, and following repair. The specific aims were to: (i) determine the annulus areas, orifice areas, and regurgitant areas of mitral valves before and after the creation of P2 prolapse, and following E2E repair; and (ii) observe the pressure gradients across the valves to determine the relative degrees of mitral stenosis.

Materials and methods

Animals and surgical approach

The study protocol was reviewed and approved by the University of Minnesota Institutional Animal Care and Use Committee, and specifically designed to ensure the humane treatment of all animals, as indicated by the Guide for the Care and Use of Laboratory Animals. Six castrated, male swine were initially anesthetized via an intramuscular injection of telazol (7 mg/kg), after which intravenous access was gained through a superficial ear vein. Each animal was weighed, transported to the surgical table, and intubated, at which time isoflurane was administered as an anesthetic. When a surgical plane of anesthesia (>1.2 Minimum Alveolar Concentration) had been sustained, a medial sternotomy was performed. Subsequently, an aortic root cannula was sewn into the ascending aorta, heparin was administered, followed by the rapid administration (at ~150 mmHg via the aortic cannula) of a cold, high-potassium cardioplegia solution to depolarize the heart. Simultaneously, the chest cavity was filled with ice to sustain cooling, thereby lowering the metabolism of the cardiac cells. Once asystolic (flat-lined electrocardiographic recording), the heart was excised and prepared for reanimation.

Perfusion studies

Each isolated heart was reanimated using previously described Visible Heart methodologies (9). Briefly, the great vessels of the heart were cannulated and attached to the Visible Heart apparatus. Each heart was then warmed to body temperature, perfused with a Krebs-Henseleit buffer (9), and a native sinus rhythm elicited following defibrillatory shocks. Importantly, as the buffer utilized in these studies was clear, intracardiac imaging of the mitral valve was possible. Each heart was periodically switched between two modes of functional perfusion: right-sided working mode and full-working (physiologic) mode. Specifically, between data collection periods, the heart was placed in the right-sided working mode; this allowed the right side of the heart to perform normally, but there was no flow through the left side of the heart, such that the flow directed to the aortic valve had a sustained and slightly increased afterload. This increased afterload kept the aortic valve from opening, but allowed for continuous perfusion of the coronary system, thus minimizing global ischemia which would result from the lack of an oxygen carrier (e.g., red blood cells or artificial carrier) within the buffer solution. Prior to the data collection periods, the heart was switched into full-working (physiologic) mode, where there were physiologic preloads and afterloads so that all chambers and valves were functional.

Endoscopy

Endoscopic video images were obtained by employing 4 mm- and 6 mm-diameter endoscopes (IplexFX; Olympus Corporation, Tokyo, Japan), utilizing a right angle optical adaptor (AT120S/FF 120SF; Olympus Corporation) with a field of view of 120° and a focal range starting at 6 mm. Images were obtained at 30 frames per second from both the ventricular and atrial sides of the mitral valve. Specifically, the atrial camera was inserted via a camera port within a pulmonary vein, while the ventricular camera was inserted through a small puncture (also with a purse-string suture placed) directly into the left ventricular apex. The endoscopic video images were fed through the same video router as the echocardiography videos, and then synchronized for post-analyses.

Hemodynamic monitoring

Hemodynamic monitoring of each reanimated heart was simultaneously conducted to assess the relative performance of the left atrium and ventricle. For this, Millar Mikro-Tip® pressure catheters (5 Fr, MPC 500; Millar, Houston, TX, USA) were placed in the left atrium via a pulmonary vein access, and in the left ventricle via a trans-apical access. Three-lead

electrocardiographic (ECG) data (SpaceLabs, Redmond, WA, USA) and hemodynamic signals were acquired simultaneously using a data acquisition system (IOX; Emka, Paris, France).

Subsequent to the induction of a native sinus rhythm, the control (Normal) data period began. Dobutamine (3 ml bolus, 500 µg/ml) and concentrated calcium (30 ml bolus, 100 mg/ml) were mixed with the buffer solution (~7.5 l) to optimize and maximize cardiac function. More specifically, following a 20-s waiting period to allow the drugs to take effect, each heart was switched from right-sided working mode into full four-chamber working (physiologic) mode. Hemodynamic signals were then stored, and simultaneous video images recorded. It should be noted that the mitral valve was visualized directly from both the left atrium and the left ventricle throughout the data storage period. Simultaneously, during these data collection periods, a transthoracic echocardiography probe was used on the epicardial surface of the heart to obtain four-chamber apical views, followed by pulsed wave Doppler images of the mitral valve and two-dimensional (2D) color flow views (Acuson Cypress; Siemens Medical, Malvern, PA, USA). When the echocardiography data had been acquired the study period was ended, and the heart was switched into right-sided working mode. The buffer was replaced, as necessary, to minimize the amount of circulating dobutamine or high levels of calcium within the perfusion system.

Following the Normal data collection period, mitral regurgitation was created by cutting a strut chordae, under visual guidance, in the P2 region of the posterior leaflet. Specifically, a 5 mm ENDOPATH instrument with a 5DCS tip was inserted through the apex of the left ventricle (Ethicon Endo-Surgery, Inc., Cincinnati, OH, USA), with an endoscopic camera within the left ventricle being used to guide the tool location onto the chordae. When the endoscopy tool had been positioned appropriately, a chordae was cut and heart perfusion then switched into working mode to observe the resulting P2 prolapse. The endoscopic camera positioned within the left atrium was used to visualize the prolapsing region, in order to verify consistent areas of leaflet prolapse. Upon administration of dobutamine and extracellular calcium, data were obtained using previously described methodologies. In each heart, the P2 prolapse was then repaired using the E2E technique. With the heart in right-sided working mode, two perpendicular incisions were made on the superior aspect of the left atrium, thus creating a surgical window for repair by employing tissue spreaders. A surgical stitch was placed from the prolapsed P2 region on the posterior leaflet to the A2 region on the anterior leaflet, creating a

double-orifice valve. The tissue spreaders were removed, and the window surgically closed. Any air in the left atrium was aspirated using a syringe, after which the E2E data collection period was commenced, using the aforementioned protocols.

Hemodynamic analyses

The following hemodynamic data were analyzed: heart rate, left ventricular (LV) pressure, left atrial pressure, and time derivatives of ventricular pressure (maximum dP/dt and maximum -dP/dt). Waveforms were plotted for each data period of the study, and the values then averaged over three consecutive beats. The time derivatives of ventricular pressure were considered as measures of relative contractility (maximum dP/dt) and relaxation (maximum -dP/dt) abilities. As the hearts were in an ischemic environment, these parameters were used to assess the relative health of the hearts as the experiments progressed.

Endoscopic image analyses

Endoscopic images were analyzed over the course of one given cardiac cycle. More specifically, stored pulsed-wave Doppler waveforms were used to indicate several key frames for subsequent analyses. A 'start' image was defined when the mitral leaflets first opened, corresponding to the onset of forward flow in the echo waveforms. Three images were analyzed during diastole: (i) a frame corresponding to the leaflets fully opened (d1); (ii) a mid-fill time point (d2); and (iii) a frame just prior to the onset of leaflet closure (d3). When the filling phase ended, as noted on the pulsed-wave waveforms, a point was defined as the 'intercept'. The regurgitant waveform then began, corresponding to the systolic phases of the heart. The 'end' of regurgitation was then defined by both the pulsed-wave Doppler waveforms and direct visualization. The frames 's1', 's2', and 's3' were evenly divided between the intercept frame and the end frame. Once identified, these frames were imported into Photoshop 7.0.1 (Adobe Systems, Inc., San Jose, CA, USA) and the following dimensions calculated for each heart: annulus area; orifice area; regurgitant area; and anterior-posterior (A2-P2) diameter. The annulus area was identified by the change in color when tissue transitioned from leaflet tissue to muscle tissue. The orifice area was defined for the diastolic portion of the cardiac cycle (d1-d3) as the area within the annulus not occupied by leaflet tissue. The regurgitant area was defined for the systolic portion of the cardiac cycle (s1-s3) as the area within the annulus not occupied by leaflet tissue, or containing a prolapsed section of leaflet tissue. Dimensions were converted using both the anterior-posterior diameters obtained from endoscopic images and the mitral valve diameters from the four-chamber views of the heart, using echocardiography.

Echocardiographic analyses

Four-chamber echocardiographic views were used to obtain mitral valve diameters during diastole and systole. Pulsed-wave Doppler images were used to calculate the following parameters for each heart: mean velocity; mean gradient time; and velocity-time interval (VTI). The VTI was used to calculate the stroke volume of both forward and regurgitant flows, after which the stroke volume was used to calculate the regurgitant fraction for each heart. The orifice area for diastolic flows was calculated as the average of d1-d3 from the directly visualized areas, and the regurgitant flow during systole was determined using averages of s1-s3.

Statistical analysis

Analyses of variance (ANOVA) tests were performed using the aforementioned three groups: Normal, Prolapse, and E2E. All reported statistically significant differences were at $p < 0.05$ levels, and all values were reported as average ± SD, assuming a normal distribution. Although, for the reliable determination of the distribution, a greater sample size would have been required, the annulus area and normalized annulus area each showed a good correlation with a normal distribution ($R2 = 96.2\%$ and 92.6%, respectively).

Results

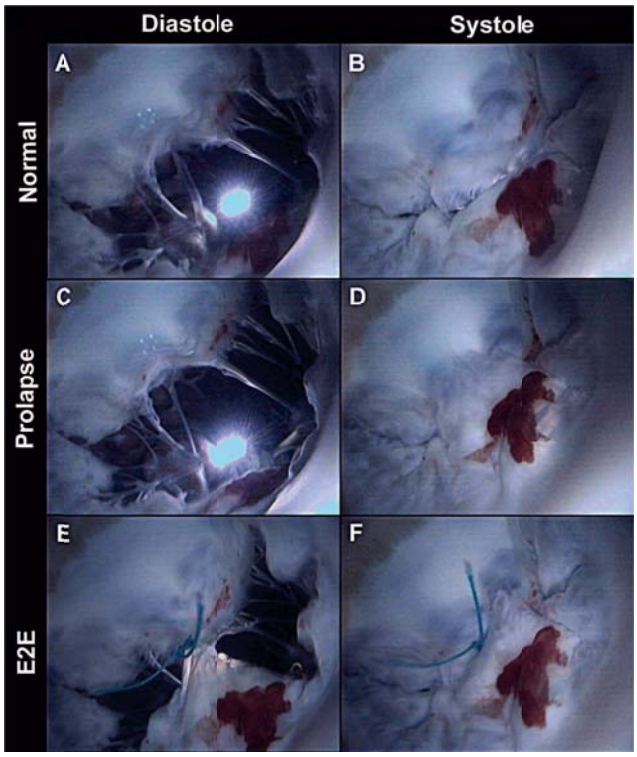

Figure 6.1: Mitral valve visualized during diastole (left) and systole (right) for the Normal (top), Prolapse (middle), and E2E(bottom) data periods. E2E: Edge-to-edge repair.

The hemodynamic data are summarized in Table 6.1 and further described below. The heart rates averaged 100 beats per minute across all experiments, and were consistent throughout the Normal, Prolapse, and E2E experimental phases. Likewise, atrial pressures were not statistically significant when the groups were compared (overall average of 17/10 mmHg). However, the left ventricles did elicit statistically significant decreases in LV systolic pressure and -dP/dt. Normal systolic pressures averaged 95 mmHg, then decreased to 79 mmHg during the Prolapse period, and decreased further to 54 mmHg in the E2E period. Similarly, -dP/dt values decreased in magnitude over the course of the experimental protocol (743, 608, and 402 mmHg/s for Normal, Prolapse, and E2E periods, respectively). The LV diastolic pressures and dP/dt values did not elicit significant changes, but both showed decreasing trends over the course of the experiments. The overall average LV diastolic pressure was 14 mmHg, and the overall average dP/dt value 804 mmHg/s.

Table 6.1: Hemodynamic Data

		Left Atrium		Left Ventricle			
	Heart Rate (bpm)	**Systole** (mmHg)	**Diastole** (mmHg)	**Systole** (mmHg)	**Diastole** (mmHg)	**max dp/dt** (mmHg/s)	**max -dp/dt** (mmHg/s)
Normal	106 ± 13	10 ± 7	18 ± 8	95 ± 16	17 ± 8	916 ± 244	-743 ± 200
Prolapse	100 ± 13	10 ± 10	18 ± 9	79 ± 14	18 ± 9	814 ± 274	-608 ± 289
E2E	96 ± 16	9 ± 6	14 ± 10	54 ± 9	8 ± 6	682 ± 374	-402 ± 121
P value	0.48	0.97	0.68	< 0.01*	0.11	0.43	0.045*

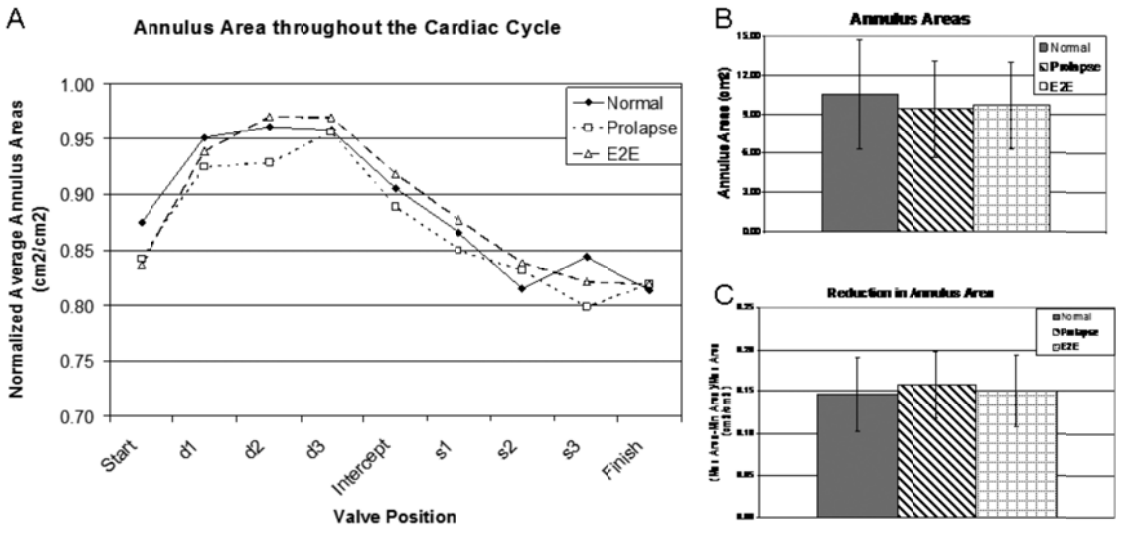

Figure 6.2: Annulus areas normalized against maximum annulus areas. with mean values plotted throughout the cardiac cycle (A). Note that average annulus areas (B) and average reduction in annulus areas (C) were preserved throughout the experiment. E2E: Edge-to-edge repair.

Annulus areas were tracked throughout the cardiac cycles, indicating average annulus areas and relative changes for the Normal, Prolapse, and E2E groups. Typical systolic and diastolic images are shown in Figure 6.1 for the Normal, Prolapse, and E2E groups, as seen from the left atrium. In general, the annulus areas increased during the opening of the mitral valves, with the maximum areas occurring during late diastole (d3), followed by decreasing areas with minimums occurring in late systole (s3). All three study phases followed this same general pattern (Figure 6.2A). The average annulus area between the three groups was 9.85 ± 2.67 cm2, with no statistical significance found throughout the study (Figure 6.2B). Finally, the average reduction in annulus area throughout the cardiac cycles was calculated, normalized against the maximum annulus area, and displayed graphically (Figure 6.2C). The overall average reduction in annulus area between the Normal, Prolapse, and E2E groups was 15 ± 3%.

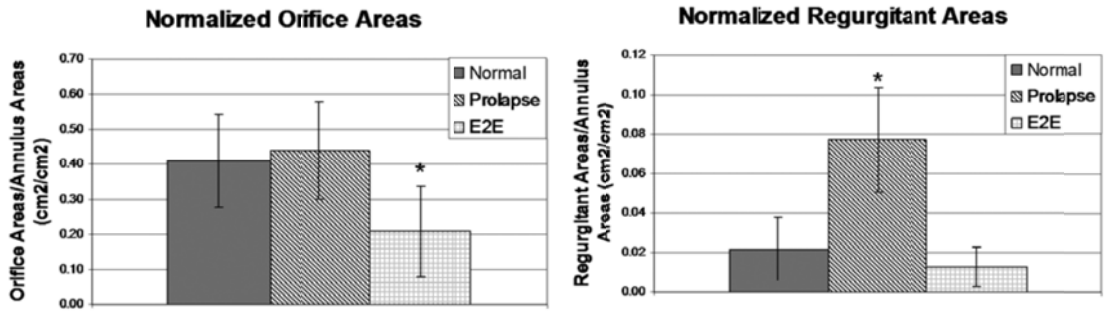

Figure 6.3: Orifice areas normalized against annulus areas. Note that the repaired valves (E2E group) had significantly lower orifice areas ($p < 0.05$). E2E: Edge-to-edge repair.

Figure 6.4: Regurgitant areas normalized against annulus areas. The repaired valves (E2E) had regurgitant areas that returned to Normal levels after the creation of P2 prolapses via cutting appropriate chordae. E2E: Edge-to-edge repair.

The mitral valve orifice area was defined as the area within the annulus that did not contain leaflets. When averaged over the diastolic phases of the cardiac cycle (d1-d3), the orifice areas for the Normal, Prolapse, and E2E groups were 4.49 ± 2.70, 4.13 ± 2.16, and 1.99 ± 1.19 cm2, respectively. Due to the somewhat high variability between valve sizes from heart to heart, the relative orifice areas were normalized against their corresponding annulus areas (Figure 6.3). Normalized values of orifice areas for Normal, Prolapse, and E2E groups were 41 ± 13%, 44 ± 14%, and 21 ± 13%, respectively (differences between groups: $p = 0.02$).

The regurgitant area was defined as the area within the annulus not occupied by leaflet tissue, and/or as the area containing a prolapsed section of leaflet tissue. These areas were averaged

over the duration of regurgitation during the systolic portions of the cardiac cycles (s1-s3). The regurgitant areas were increased from 0.20 ± 0.16 cm2 for the Normal group, and to 0.73 ± 0.35 cm2 for the Prolapse group, but were then decreased to 0.12 ± 0.10 cm2 for the E2E group. These values were normalized against their corresponding annulus areas (Figure 6.4). The normalized regurgitant areas for Normal, Prolapse, and E2E groups were 2 ± 2%, 8 ± 3%, and 1 ± 1%, respectively (differences between groups: p <0 .01).

The echocardiographic data were divided into forward flow and regurgitant flow measurements (Table 6.2). The measurements for forward flow that were found to be significantly affected were mean flow velocity (Normal 45 ± 12 cm/s; Prolapse 53 ± 12 cm/s; E2E 33 ± 8 cm/s) and peak velocity (Normal 72 ± 14 cm/s; Prolapse 77 ± 14 cm/s; E2E 55 ± 12 cm/s). The mean gradient time, VTI, and stroke volume were not significantly different. All measurements assessed for regurgitant flows were found to be significant, as might be expected when regurgitation is created and then repaired.

Table 6.2: Echocardiography measurements

Forward Flow Measurements	Normal	Prolapse	E2E	p value
mean velocity (cm/s)	45 ± 12	53 ± 12	33 ± 8	0.02*
mean gradient (mm Hg)	.98 ± .43	1.06 ± .4	.54 ± .25	0.06
time (ms)	186 ± 38	209 ± 73	197 ± 60	0.80
VTItotal	.08 ± .03	.09 ± .03	.06 ± .01	0.14
Peak Velocity (cm/s)	72 ± 14	77 ± 14	55 ± 12	0.03*
Peak Gradient (mmHg)	2.11 ± .86	2.29 ± .77	1.27 ± .49	0.06
CSAtotal (cm^2)	4.49 ± 2.7	4.13 ± 2.16	2.72 ± 2.21	0.41
SV total (cm^3)	35 ± 22	41 ± 28	18 ± 17	0.21
Regurgitation Measurements				
mean velocity (cm/s)	28 ± 7	29 ± 6	20 ± 3	0.03*
mean gradient (mm Hg)	.33 ± .14	.37 ± .13	.17 ± .04	0.02*
time (ms)	76 ± 18	132 ± 41	89 ± 38	0.03*
VTIregurge	.02 ± .01	.04 ± .02	.02 ± .01	0.04*
Peak Velocity (cm/s)	36 ± 7	41 ± 10	28 ± 5	0.03*
Peak Gradient (mmHg)	.54 ± .23	.72 ± .29	.33 ± .11	0.03*
CSA regurge (cm^2)	.2 ± .16	.73 ± .35	.25 ± .34	0.01*
SV regurge (cm^3)	.37 ± .25	3.11 ± 2.74	.52 ± .82	0.02*

The regurgitant fractions were analyzed based on VTIs derived from the echocardiography data, using the orifice and regurgitant areas determined from the endoscopic videos. The regurgitant fractions were then normalized against the maximum regurgitant fraction observed for each heart (Figure 6.5). The normalized regurgitant fraction for the Normal group was 10 ± 6%; this was increased to 57 ± 26% for the Prolapse group, but then returned to 13 ± 13% for the E2E

group (p <0.01). Trace regurgitations were observed in the endoscopic videos for three of the six repairs.

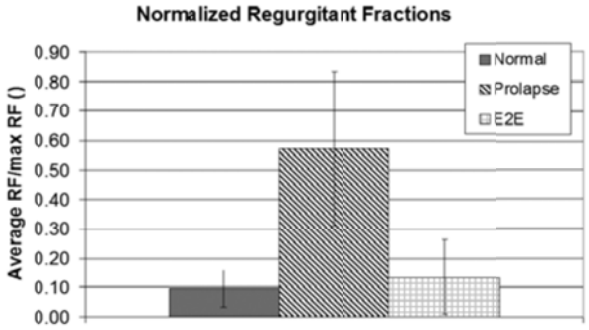

Figure 6.5: Regurgitant fractions normalized against maximum regurgitant fractions measured. Note that the repaired valves (E2E) had regurgitant fractions that returned to Normal levels after the creation of P2 prolapses. E2E: Edge-to-edge repair.

Discussion

The mitral valve annulus areas were found to be unaffected by the E2E technique in this isolated swine heart model. Qualitatively, annulus areas were found to follow the same pattern throughout the cardiac cycle, regardless of the study group, and were consistent with values reported previously (10,11). Neither the average annulus area nor the maximum change in annulus area were statistically significant between the Normal, Prolapse, and E2E experimental phases of this study. Overall, the maximum change in annulus areas was found to be 15 ± 3%, which is similar to sonomicrometry data obtained from both sheep (13 ± 13% change in annulus area (10)) and humans (reported change in annulus area of 18.2 ± 1.5% (12)).

In the present healthy swine hearts, the orifice areas were unaffected after P2 prolapses had been created, but were found to be significantly lower after the E2E repairs. It should be noted that Hasegawa et al. reported the orifice areas to be decreased by approximately 30% from normal mitral orifice areas after E2E repair in their isolated swine heart study (13). The numbers comparing Normal and E2E groups from the present study were higher than those reported by Hasegawa et al., although this discrepancy may have been caused in part by the decrease in overall cardiac function during the study.

Importantly, the regurgitant areas observed from the present E2E group did not differ significantly from the Normal group. Nevertheless, consistent P2 prolapses were created, and the E2E technique repaired the valve to Normal levels. Three of the six repairs showed small

areas of prolapse following repair; however, in all cases this was in the area of the prolapse prior to repair and directly adjacent to the repair stitch.

Study limitations

A primary limitation was that the buffer solution used in the isolated swine heart did not contain an oxygen carrier, but was super-saturated with oxygen to provide a maximal supply to the myocardium. Unfortunately, this resulted in the formation of microbubbles that were visible in the echocardiography views and which, in turn, decreased the effectiveness of color mapping to the point that the data could not be used. Although 2D echo images showed the micro-bubbles flowing through the heart, the images were of adequate quality for analysis. Likewise, the pulsed-wave Doppler images showed spectral broadening, but were still analyzed.

Echocardiography measurements were used to calibrate the diameter and area measurements. As the A-P diameter obtained from the four-chamber view echo image is longer than the actual A-P diameter, all annular sizes calculated in the present study were overestimated. However, by normalizing the measurements the calibration factor cancelled out and the normalized measurements remained accurate.

For regurgitant fraction analyses, raw values were not reported for two reasons. First, due to the altered hemodynamics of the in vitro set-up, the regurgitant fractions did not compare with clinically reported values for mitral valve prolapse. Second, it was difficult to analyze the pulsed-wave Doppler data, which typically resulted in artificially low VTI values for the regurgitant phase. Despite these limitations, however, it was considered valuable to compare the normalized values relative to regurgitant fractions during the various stages of the study.

Conclusion

To the best of present authors' knowledge, this is the first experimental study to directly visualize E2E repairs of a mitral valve following induced prolapse. It was noted that the creation of P2 prolapses by cutting appropriate chordae did not affect the valve orifice or annulus areas. Regurgitation was created in the Prolapse group, and effectively repaired using the E2E technique. The orifice areas of the mitral valve during diastole were decreased following E2E repairs relative to both the Normal and Prolapse phases by approximately 49% but, importantly, these decreases did not result in mitral stenoses. The results of the present study have provided novel insights and images relative to the repair of a prolapsed mitral valve by employing a

center-placed surgical stitch (E2E or Alfieri stitch). Although these results are both educational and clinically promising, additional studies should be conducted in models in which heart failure must be induced prior to repair.

The authors thank Mike Eggen, Eric Richardson, and Chris Rolfes for their participation in the data collection, Gary Williams for assistance with preparation of the images, and Monica Mahre for support related to manuscript submission. Funding for these studies was received from the Institute for Engineering in Medicine and the Department of Surgery, University of Minnesota; Medtronic, Inc. Jason Quill is currently an employee of Medtronic, Inc.

References

1. Nakanishi, K., Raman, J., Hata, M. & Buxton, B. Early outcome with the Alfieri mitral valve repair. J. Cardiol. 37, 263-266 (2001).

2. Alfieri, O. & Maisano, F. An effective technique to correct anterior mitral leaflet prolapse. J. Card. Surg. 14, 468-470 (1999).

3. Alfieri, O. et al. The double-orifice technique in mitral valve repair: a simple solution for complex problems. J. Thorac. Cardiovasc. Surg. 122, 674-681 (2001).

4. Alfieri, O., Maisano, F. & De Bonis, M. The edge-to-edge repair. Multimedia Manual of Cardio-thoracic Surgery 2005, 869 (2005).

5. Bhudia, S. K. et al. Edge-to-edge (Alfieri) mitral repair: results in diverse clinical settings. Ann. Thorac. Surg. 77, 1598-1606 (2004).

6. Alfieri, O. et al. “Edge-to-edge” repair for anterior mitral leaflet prolapse (Seminars in Thoracic and Cardiovascular Surgery Ser. 16, Elsevier, 2004).

7. Alfieri, O., Maisano, F. & Colombo, A. Percutaneous mitral valve repair procedures. European Journal of Cardio-thoracic Surgery 26, 36-38 (2004).

8. Alfieri, O. et al. Percutaneous mitral valve repair: an attractive perspective and an opportunity for teamwork. Ital. Heart J. 5, 723-726 (2004).

9. Chinchoy, E. et al. Isolated four-chamber working swine heart model. Ann. Thorac. Surg. 70, 1607-1614 (2000).

10. Timek, T. A. et al. Aorto-mitral annular dynamics. Ann. Thorac. Surg. 76, 1944-1950 (2003).

11. Komoda, T. et al. Mitral Annulus after Mitral Repair: Geometry and Dynamics. ASAIO Journal 48, 412 (2002).

12. De Simone, R. et al. A clinical study of annular geometry and dynamics in patients with ischemic mitral regurgitation: new insights into asymmetrical ring annuloplasty. European Journal of Cardio-Thoracic Surgery 29, 355-361 (2006).

13. Hasegawa, H. et al. Mitral valve motion after performing an edge-to-edge repair in an isolated swine heart. J. Thorac. Cardiovasc. Surg. 136, 590-596 (2008).

7. Induction of Right Ventricular Outflow Tract Dilation and Pulmonary Valve Insufficiency in a Porcine Model

Preface

As the technology driving transcatheter delivered valves advances, so too does the range of pathologies that can be treated. This has begun to include anatomically complex patients such as those that have undergone surgery to correct congenital heart defects. For example, it is understood that valvular heart disease is a major cause of morbidity and mortality in patients who survive surgical correction for tetralogy of Fallot (TOF), and the pathologies associated with TOF display a wide variation in the morphology of the right ventricular outflow tracts (RVOT). Current therapies for these patients are carefully selected based on imaging results and patient health. The Medtronic Melody® valve is the only FDA approved percutaneous device but is limited to specific sizes, often too small for this patient population. In response, physicians are pre-stenting the anatomy and using prostheses designed for the aortic position in what is known as 'off label' implantations.

As such, there is an inherent need for specialized devices that can adapt to a large variety of anatomical configurations, thus requiring extensive in vitro and in vivo testing before starting clinical studies. We describe here the surgical adaptation of the swine model to approximate the right ventricular anatomy of TOF patients; a beating heart model of the relevant anatomy is created by compromising the pulmonary valve (PV) and dilating the outflow tract and annulus. Once created in vivo, such models can either have prototype devices implanted to determine both acute performance and chronic adaptation, potentially providing information on how the device adapts to the growing patient. Additionally, the heart can be transferred to the Visible Heart® for in vitro analysis and visualization of the device-tissue interaction during implantation. For this project I worked closely with Dr. James St. Louis to develop the surgical procedure and wrote all IACUC proposals. Following this I assisted on all surgeries and imaging procedures, completed all data collection and analysis before collaborating with research animal resources on all post-operative care.

Michael G. Bateman MEng[1,2], Jason L. Quill PhD[3], James L. St. Louis MD[1], Paul A. Iaizzo PhD[1,2]

Departments of [1]Surgery and [2]Biomedical Engineering, University of Minnesota, Minneapolis, MN, USA
[3]Medtronic, Inc., Minneapolis, MN, USA

Introduction

The instance of pulmonary valve (PV) disease in adults is rare and usually coupled to systemic cardiac diseases such as pulmonary hypertension. However, in patients with complex congenital heart conditions it is often the principle reason for late stage complication[1]. In the United States approximately 36,000 babies are born with a heart defect each year, of which approximately 3,000 are diagnosed with tetralogy of Fallot (TOF)[2]. TOF typically includes four defects within the heart structures; a ventricular septal defect, narrowing of the pulmonary outflow tract, an aorta displaced over both ventricles, rather than exclusively from the left ventricle and a thickened muscular wall of the right ventricle, see figure (7.1).

Due to a significant reduction in the mortality rate during the surgical correction of complex congenital heart defects there has been a sharp increase in the number of these patients living to adulthood[3]. However, such surgical procedures often leave patients with pulmonary valve insufficiency (PI), aneurismal right ventricular outflow tracts (RVOTs) and valvular on conduit stenosis[4], see figure (7.2). In particular valvular heart disease is a major cause of morbidity and mortality in patients who survive surgical correction for tetralogy of Fallot leading to an increased focus on the need for a non-surgical means of correcting these specific pathologies[5].

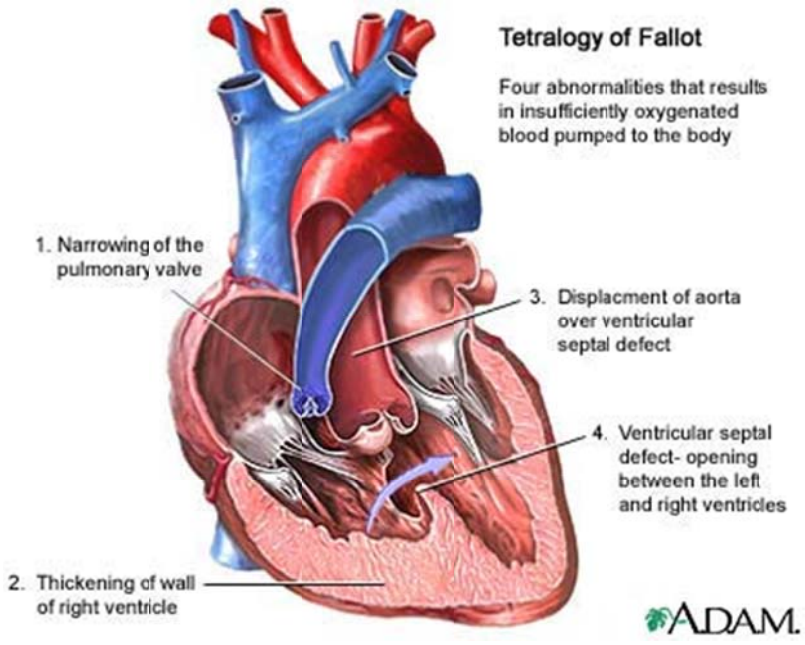

Figure 7.1. Diagram representing the 4 defects associated with tetralogy of Fallot, image courtesy of Medline Plus Medical Encyclopedia[6].

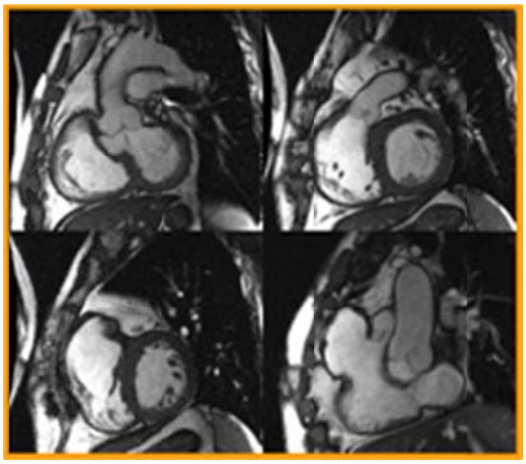

Figure 7.2. MRI displaying the dilated RVOT of a post-operative tetralogy of Fallot patient, image courtesy of the Children's Hospital of Wisconsin.

Transcatheter pulmonary valve implantation has proven to be an effective treatment for some TOF patients and the first implantation of a transcatheter pulmonary valve was reported by Bonhoeffer et al. in a 12-year-old patient with a regurgitant and stenotic prosthetic conduit in 2000[7]. Medtronic currently produces the Melody® valve (Medtronic, Inc., Minneapolis, MN) for clinical use in Europe and Canada. The valve is constructed from a valved bovine jugular vein sutured to a balloon expandable stent which can be delivered via the femoral or internal jugular veins. However, as a result of device design and the size of available valves the procedure is only available to patients with a specific anatomy at the implantation site (<22mm diameter). Patients with the pathologies associated with TOF display a wide variation in the morphology of their RVOTs often excluding them from Melody® valve implantation[2]. As such, some physicians experimenting with the implantation of prostheses designed for the aortic position, such as the Edwards SAPIEN™, both with and without prestenting[8-11]. These patients often present with right ventricular hypertrophy, brought on by the pulmonary regurgitation, and consequently can readily cope with the sturdier prosthesis. However, the prestenting and implant procedure is aggressive and designed for the more robust aortic anatomy and as such extra care must be taken to ensure the RVOT is not significantly damaged.

When considering the development of a novel therapy for these patients there have been two main approaches to date; modification of the device itself[12] and development of a supplemental device to work in concert with FDA approved devices such as the Melody® valve. These devices

will require extensive *in vitro* and *in vivo* testing before starting clinical studies. Zeltser et al. have created an animal model in piglets to evaluate the development of late-onset arrhythmias after tetralogy of Fallot repair[13]. However, to the best of the author's knowledge there has been no previous attempt to develop and animal model for the *in vivo* testing of novel transcatheter pulmonary valve replacement therapies for survivors of surgery for the correction of TOF.

Methodology

The study protocol was reviewed and approved by the University of Minnesota Institutional Animal Care and Use Committee, and specifically designed to ensure the humane treatment of all animals, as indicated by the Guide for the Care and Use of Laboratory Animals. 20-30kg castrated, male swine were initially anesthetized via an intramuscular injection of telazol (7 mg/kg), after which intravenous access was gained through a superficial ear vein. Each animal was weighed, transported to the surgical table, and intubated, at which time isoflurane was administered as an anesthetic until a surgical plane of anesthesia (>1.2 Minimum Alveolar Concentration) had been sustained.

Echocardiography imaging

Upon reaching a surgical plane of anesthesia, but prior to any surgical procedures, the animals were imaged using trans-thoracic echocardiography in order to assess cardiac function. In particular, pulmonary valve dimensions and flow through the PV and the RVOT was recorded to assess PV function.

Surgical procedure

Prior to any incisions, antibiotics (12-15mg/kg Cefazolin diluted in 5.0 ml sterile water) were administered intravenously over a 5 min. period. The initial surgery was performed under aseptic conditions with any and all incision sites properly disinfected prior to cutting and all equipment inserted or implanted into the animal being sterile. An arterial line was inserted to monitor systemic blood pressure and exhaled CO_2, ECG, heart rate and body temperature were constantly monitored to assess condition.

Access to the right ventricular outflow tract was gained through a lateral thoracotomy and the pulmonary artery was located via palpitation. The right ventricular out flow tract and main pulmonary artery were then elevated into the surgical field. An elliptical patch of HEMASHIELD® woven double velour fabric (Maquet, Germany) measuring approximately 10 mm at it largest width was sewn on to the surface of the main pulmonary artery and extending across the

pulmonary annulus and continuing inferiorly along the right ventricular out flow tract using 4-0 prolene suture (Ethicon Inc., Sommerville, NJ) and an incision was made along the length of the graft. A period of inflow occlusion was created by restricting flow through the inferior and superior vena cava. Working through the cut made in the patch the main pulmonary artery was incised longitudinally with the incision being carried across the pulmonary annulus and the three leaflets of the pulmonary valve being excised. Working in continuity with the pulmonary artery incision, an incision was made into the anterior wall of the right ventricular outflow tract was completed. The cut made in the patch was then closed with a running 4-0 prolene suture to achieve hemostatsis.

Following stabilization, a 15 Fr chest tube (Axiom Medical Inc., Torrance, CA) was then placed into the chest via separate incisions and secured in place with absorbable 4-0 vicryl suture (Ethicon Inc., Sommerville, NJ). The chest retractor was then removed and the thoracotomy closed over an expanded left lung with 0-0 absorbable vicryl sutures (Ethicon Inc., Sommerville, NJ). Before the animal was recovered cardiac function was assessed via echocardiography to validate the induced PI and analyze the acute change in right ventricular function. The animals were then allowed to recover and were closely monitored for three weeks before imaging and assessment.

At three weeks the animals were anesthetized as previously described and imaged using trans-thoracic echocardiography in order to assess cardiac function. Once the heart had been imaged *in vivo* and hemodynamic data and electrical data had been recorded the animals were prepped for surgery as described above. If the heart had not remodeled or there had been no creation of PI the animal was euthanized with high potassium solution (2-4 mEq/kg) delivered intravenously whilst still under profound levels of anesthesia. After euthanasia the heart was excised for analysis and assessment of the changes in the cardiac anatomy as described previously by Chinchoy et al. and perfusion fixed in formalin as described by Anderson et al.[14,15]

Device Implantation (Pending successful creation of the animal model)

Before device implantation heparin (350 IU/kg) will be administered as an anticoagulation agent. The pulmonary valve replacement system will be implanted either via a trans-venous or trans-apical approach.

Trans-venous approach: A cut-down will be performed to access either the femoral vein or a jugular vein depending on the specific anatomy of the animal. A guidewire is advanced through the heart and into the pulmonary artery system through the right atrium and right ventricle. The valve delivery system will then be advanced over the guidewire and the valve implanted into the altered RVOT

Trans-apical approach: Access to the right ventricular apex will be achieved via a lateral thoracotomy. A right anterio-lateral thoracotomy will be made and the chest will be entered via the fifth or sixth inter-costal space (determined via palpitation and image analysis). A rib retractor will be placed and the lung retracted posteriorly. The pericardium will be incised longitudinally following which the right ventricular apex will be prepped with a purse string and then accessed via an arterial needle puncture followed by the introduction of a standard sheath. A guidewire is advanced into the pulmonary arterial system through the right ventricle. As before the valve delivery system will then be advanced over the guidewire and the valve implanted into the altered RVOT.

Upon completion of the device implantation the animal will be recovered, cardiac function will be assessed via echocardiography to validate the device deployment and analyze the acute change in right ventricular function. The animals will then be allowed to recover and will be closely monitored for two weeks before imaging and study termination.

Postsurgical follow up and study termination

At two weeks post surgery the animals will be anesthetized as previously described and imaged using trans-thoracic echocardiography in order to assess cardiac function. Once the heart had been imaged *in vivo* and hemodynamic data and electrical data had been recorded the animals were prepped for surgery as described above. The animals will then be euthanized with high potassium solution (2-4 mEq/kg) delivered intravenously whilst still under profound levels of anesthesia. After euthanasia the heart will be excised for analysis of the device implantation as described previously by Chinchoy et al. and perfusion fixed in formalin as described by Anderson et al.[14,15]

Results

After the attempted surgery on 10 animals including 4 investigational acute studies we have successful taken 3 animals to term. The two most recent surgeries (March/April 2011), although

successful have not yielded either the PV insufficiency or the RVOT dilation that we would expect to see considering the damage caused. However, by altering the administration of fluids and drugs we have improved the surgical outcomes, i.e. the recovery chances of the animal.

Table 7.1: Summary of studies

Surgeries attempted:	**10**
Acute/Investigational:	4
Successful surgeries:	3
Animals surviving to term:	3

Summary of successful surgeries:

Animal #10: 03/24/11, 17.8kg male swine, surgery successful. Amioderone and lactated ringers used, no dobutamine needed. First attempt at suturing the PV leaflet to the PA wall. Animal showed PV prolapse and slight regurgitation during echo work ups, performed at approximately 7 days, see figures (7.3) and (7.4).

Term date: 04/28/2011, 46.5kg. Upon termination heart was once again enlarged but upon reanimation PV seemed to function better than expected and RVOT dilation was predominantly below (proximal) to the PV annulus.

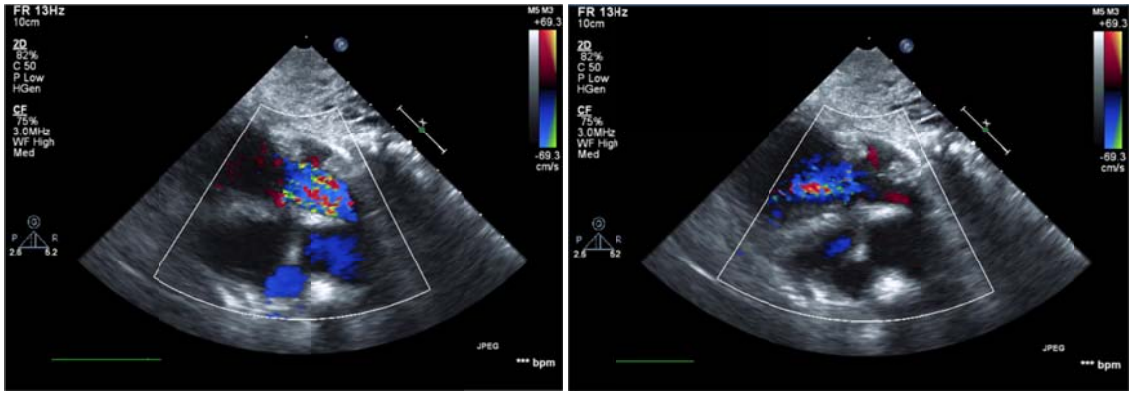

Figure 7.3: Echo of pulmonary valve at one week showing significant regurgitation, systole on left and diastole on the right.

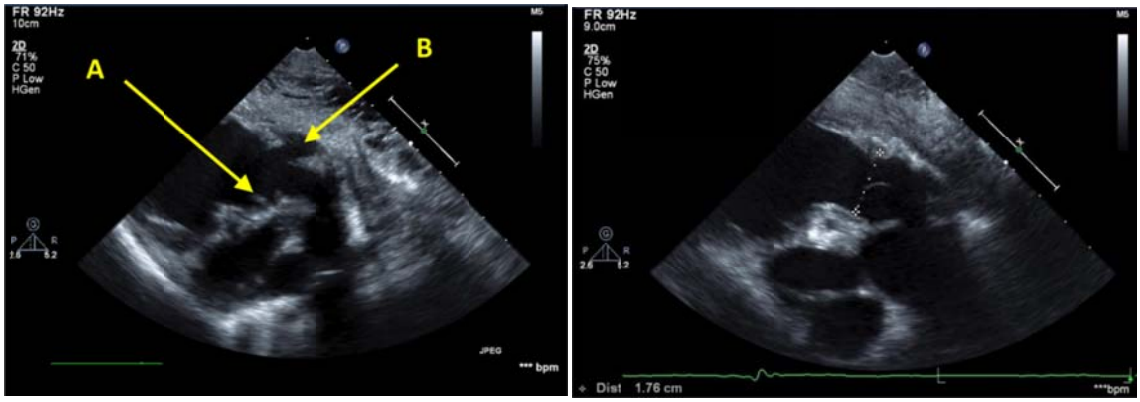

Figure 7.4: Echo from two patients: Patient 10 (left) shows the pulmonary valve at one week showing significant leaflet flail (A) and a large recess distal to the valve (B). Patient 9 (right) at 13 days showing an enlarged pulmonary annulus at 17.6mm from ~10mm pre surgery.

Animal #9: 02/10/11, 25.4kg male swine, surgery successful. Amioderone used, animal perfused with lactated ringers in place of blood and dobutamine used to elevate HR rather than epinephrine. Animal showed significant RVOT dilation during echo work up, performed at approximately 13 days, see figure (7.4).

Term date: 03/01/2011, 35.2kg

Upon termination heart seemed to be significantly enlarged, however the RVOT did not appear overly dilated. Upon post-mortem inspection the heart had a large abscess between the epicardial surface and the pericardium.

Animal #1: 04/09/09, 26.4kg male swine, successful surgery.Normal ECG, slightly bradycardic with low BP on recovery. No echo work up was completed due to animal health.

Term date: 04/28/09, 39.6kg

Upon termination of the first animal we found no evidence of PI. However, the animal showed a significant dilation of the right ventricle and in particular a two-fold increase in the diameter of the RVOT.

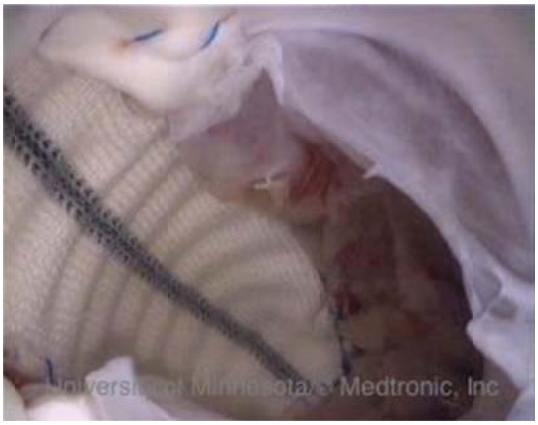

Figure (7.5). An image showing the surgically created right ventricular outflow tract dilation of one of the acute studies reanimated on the Visible Heart® apparatus; the remnants of the pulmonary valve can be seen in the foreground.

Discussion

Although a 50% survival rate is well below the accepted success rate for this study the majority of morbidities were due to unforeseen errors that have since been corrected. Of the three successful surgeries all three animals made it to term indicating that survival of the surgery is the major hurdle in this study. However, the two most recent surgeries have not yielded either the PI or the RVOT dilation that we would expect to see considering the damage caused during surgery. This has been particularly surprising given the results of imaging two weeks post-surgery showing signs of pulmonary leaflet flail and valve regurgitation. However, the apparent ability of the right heart to function with moderate pulmonary regurgitation means that a review of the surgical technique will be needed to develop a true model of the clinical disease state. With a repeatable study established we can adapt the valve procedure in the following way:

- Ensure the patch is positioned over the valve annulus and dilates both the pulmonary artery and the high RVOT.
- Immobilize the PV leaflets to ensure valve regurgitation

By developing a successful experimental technique for this procedure we will be able to repeatedly create an animal model with highly abnormal RVOT anatomy. By implanting an experimental device into a 20kg swine one will be able to see how the device adapts to the rapid growth of the animal after recovery hence providing a unique insight as to the potential performance of the device when implanted into pediatric patients. It is understood that the

successful model is not without limitations: lack of a repaired ventricular septal defect or a truly hypertrophic right ventricle will result in a more efficient heart with a higher cardiac output. However, the accurate recreation of the anatomical landscape of the landing zone for such a device in the targeted patient population will be a valuable test bed to design engineers.

Conclusions

By administering amioderone pre-surgery and perfusing the animals with lactated ringers rather than blood we have improved the surgical outcomes, i.e. the recovery chances of the animal. The two most recent surgeries, although successful have not yielded either the PV insufficiency or the RVOT dilation that we would expect to see considering the damage caused. Therefore before continuing, a review of the surgical technique is recommended to improve the outcome of the procedures and successfully create a suitable animal model.

References

1. Coats, L. & Bonhoeffer, P. New percutaneous treatments for valve disease. *British medical journal* **93**, 639-644 (2007).

2. Tetralogy of Fallot - Diagnosis and Treatment Options at Mayo Clinic. **www.mayoclinic.com/health/tetralogy-of-fallot/**

3. Schievano, S. *et al.* Variations in right ventricular outflow tract morphology following repair of congenital heart disease: Implications for percutaneous pulmonary valve implantation. *Journal of Cardiovascular Magnetic Resonance* **9**, 687-695 (2007).

4. Coats, L. *et al.* The potential impact of percutaneous pulmonary valve stent implantation on right ventricular outflow tract re-intervention. *European Journal of Cardio-thoracic Surgery* **27**, 536-543 (2005).

5. Wren, C. & O'Sullivan, J.J. Survival with congenital heart disease and need for follow up in adult life. *British medical journal* **85**, 438-443 (2001).

6. MedlinePlus Medical Encyclopedia: Tetralogy of Fallot. **www.nlm.nih.gov/medlineplus/ency/imagepages/18088.htm**

7. Bonhoeffer, P. *et al.* Percutaneous replacement of pulmonary valve in a right-ventricle to pulmonary-artery prosthetic conduit with valve dysfunction. *The Lancet* **356**, 1403-1405 (2000).

8. Bertels, R.A., Blom, N.A. & Schalij, M.J. Edwards SAPIEN transcatheter heart valve in native pulmonary valve position. *Heart (British Cardiac Society)* **96**, 661 (2010).

9. Ewert, P., Horlick, E. & Berger, F. First implantation of the CE-marked transcatheter Sapien pulmonic valve in Europe. *Clinical research in cardiology : official journal of the German Cardiac Society* **100**, 85-7 (2011).

10. Fiszer, R., Szkutnik, M., Hijazi, Z.M. & Białkowski, J. [Transcatheter implantation of Edwards-SAPIEN THV valve in pulmonary position]. *Kardiologia polska* **69**, 749-50 (2011).

11. MacDonald, S.T., Carminati, M. & Butera, G. Percutaneous implantation of an Edwards SAPIEN valve in a failing pulmonary bioprosthesis in palliated tetralogy of Fallot. *European heart journal* **32**, 1534 (2011).

12. Boudjemline, Y., Agnoletti, G., Bonnet, D., Sidi, D. & Bonhoeffer, P. Percutaneous pulmonary valve replacement in a large right ventricular outflow tract: An experimental study. *Journal of the American College of Cardiology* **43**, 1082-1087 (2004).

13. Zeltser, I. *et al.* The roles of chronic pressure and volume overload states in induction of arrhythmias: An animal model of physiologic sequelae after repair of tetralogy of Fallot. *The Journal of thoracic and cardiovascular surgery* **130**, 1542-1548 (2005).

14. Anderson, S.E., Quill, J.L. & Iaizzo, P.A. Venous valves within left ventricular coronary veins. *Journal of Interventional Cardiac Electrophysiology* **23**, 95-99 (2008).

15. Chinchoy, E. *et al.* Isolated four-chamber working swine heart model. *The Annals of Thoracic Surgery* **70**, 1607-1614 (2000).

Electrical Mapping of the Cardiac Conduction System

Section Summary

Electrical mapping of the heart has been an established field of electrophysiology since the first recorded electrocardiogram by Einthoven in 1902. Multi electrode mapping in the late twentieth century by Durrer et al. has led to the development of real time non-contact mapping systems that are regularly used in cardiac electrophysiology laboratories for the diagnosis and treatment of atrial and ventricular arrhythmias.

Due to the increased awareness of the effect of transcatheter delivered devices on the conduction system we have initiated a collaboration with Drs. Boyett and Dobrzynski at the University of Manchester to document the electrical activity and the three dimensional anatomical detailing of the human cardiac conduction system. This study requires both the receipt of a suitable specimen and the validation of the methodology to ensure successful mapping of a human heart in the Visible Heart® apparatus. As such, we have conducted several validation studies where swine hearts were mapped in vivo and in vitro and the resulting maps compared. In addition to in vitro non-contact mapping studies we have been developing an invasive mapping system to map trans-mural electrical propagation patterns, potentially allowing for the detection of conduction abnormalities deep within the myocardium. Working with Dr. He's team we have developed an invasive quadripolar electrode array that can be used to electrically map the heart.

The conduction system already plays an important role in the design and development of transcatheter delivered aortic valves. By developing tools that allow for the accurate real time assessment of the electrical activation of the heart in vitro and improving the understanding of the cardiac conduction system the lab can better assess the effect of device implantation on the hearts electrical pathways.

Michael G. Bateman MEng

Departments of Surgery and Biomedical Engineering, University of Minnesota, Minneapolis, MN, USA

8. Mapping the Electrical Activation of a Human Heart in vitro using Non-contact Mapping in the Visible Heart® Apparatus

Preface

The incidence of acute conduction abnormalities has been associated with aortic valve replacement for many years with current papers reporting a need for permanent pacemaker implantation in 3-8% of patients undergoing surgical replacement. This number is increased to 16-18% when considering patients that undergo transcatheter aortic valve repair (TAVR). In order to investigate this further the University of Minnesota and the University of Manchester are building a collaboration to both electrically and anatomically map the specifics of the human cardiac conduction system.

To ensure that an electrical map of a reanimated human heart taken in vitro was accurate the non-contact mapping system needed to be validated in the Visible Heart® apparatus. As such, we have conducted several validation studies where swine hearts were mapped in vivo and in vitro and the resulting maps compared. Presented here is the methodology for these studies, the results from one animal as a proof of concept and the proposed methodology for the final investigation. For this project I worked to adapt the non-contact mapping system for use in the Visible Heart® apparatus and completed data collection and analysis.

Michael G. Bateman MEng, Paul A. Iaizzo PhD

Departments of Surgery and Biomedical Engineering, University of Minnesota, Minneapolis, MN, USA

Introduction

As described previously the cardiac conduction system consists of a series of specialized heart cells that control the sequence of excitation and rate of contraction of the remaining myocardium. The development of sophisticated transcatheter delivered cardiac therapies and surgical techniques has led to a continued need for a more detailed understanding of the cardiac conduction system. In particular the high septum of the left ventricular outflow tract has become an area of significant interest. Piazza et al. report an incidence of acute left bundle branch block of up to 55% after TAVR implantation and postulated that the close anatomical relationship between the aortic valve and the branching AV bundle of the conduction system may explain the increase: "There exists the possibility of the aortic prosthesis overlapping the left bundle branch [after implantation] and potentially crushing it."[1]. More recently Aktug et al. completed an investigation using both the Medtronic CoreValve® and the Edwards SAPIEN™ and reported the following:

- Acute conduction disturbances after surgical aortic valve replacement have been reported in between 15% and 33% of patients[2,3]
    - Permanent pacemaker required in 3-8% of patients[4-6]
- Improved preoperative sizing and implantation protocols (specifically regarding implantation depth) have reduced acute conduction disturbances in TAVR patients to 29% of patients[4]
    - Permanent pacemaker required in 16%-18% of patients[7,8]

Although there is a high instance of fragility within the conduction system of the patient population undergoing TAVR procedures there remains a distinct need to understand the anatomy of the electrical conduction system between the AV node and the bundle of His.

Methods

All Visible Heart® methodologies regarding in vivo swine studies and in vitro reanimation and fixation of large mammalian hearts as described by Chinchoy et al., Hill et al. and Anderson et al. have been outlined previously[9–11].

Non-contact mapping

The concept and fundamental methodology behind non-contact mapping has been described previously in this thesis. The specific methodologies for this study are as follows:

Once the animal or explanted heart is stabilized the multi-electrode array (MEA) catheter (St. Jude Medical, Inc., St. Paul, MN) was inserted into the right atrium via the right jugular vein and the superior vena cava. The balloon catheter was then inflated using a 50/50 mixture of saline and contrast media, fully expanding the MEA in the chamber before the MEA catheter is connected to the EnSite® 3000 non-contact mapping system and validated. This process is visualized in figure (8.1). A quadripolar EP catheter (Model MC 6022-7 Fr, 110cm, Medtronic, Inc., Minneapolis, MN), was then used to map the endocardial geometry of the right atrium[12,13]. Once an anatomical map of the right atrium has been produced the EnSite® system was used to map the propagation of the cardiac electrical signal from the SA node through to the AV node, see figures (8.2) and (8.3).

Creation of a 3-D anatomical model

This technique has been described in detail by Li and Dobrzynski[14–16]. Briefly, the heart will be scanned using a high resolution MRI (3T or higher) to create a short axis stack of the SA, AV node and the His-Purkinje system. These images are then imported into the workspace of MATLAB and stacked to produce a 3D array with anisotropic elements. The anatomical features of the heart containing the electrical conduction system will then be cut into sections to be stained with Masson's Trichrome, or immunoenzyme labeled for SA node specific markers; middle (160/165-kDa) neurofilament (NF-M) and 90-pS conductance connexin isoform (Cx43). The process of staining the sections will allow the researchers to differentiate between electrically active myocardial cells and contractile myocardial cells and therefore build a 3D model of the conduction system.

Validation of the Non-contact Mapping Technique

To validate the in vitro mapping methodology the right atrium of an 80kg swine was electrically mapped in vivo before the heart was explanted to the Visible Heart® apparatus and the map repeated.

Results

Mapping of a Human Heart

Due to the unpredictability of when the laboratory receives a specimen from LifeSource that can be reanimated we have not been able to complete this aspect of the study.

Validation of the Non-contact Mapping Technique

Figures (8.1-8.3) show the MEA within the right atrium of a reanimated swine heart and the resulting maps indicating the earliest activation point of the right atrium, the sinoatrial node, and the latest activation point of the right atrium, the pathway into the atrioventricular node.

Figure 8.1. Videoscopic (left) and fluoroscopic (right) images of the MEA in the right atrium of a reanimated swine heart on the Visible Heart® apparatus.

Discussion

It can be seen from the figures (8.2) and (8.3) that the ability of the non-contact mapping system to locate the earliest activation point does not seem to be compromised by the environment within the visible heart apparatus. However, the anatomical map onto which the electrical map is projected is not consistent. There are a number of factors that may have caused this inconsistency: 1) the fact that the heart had been explanted and is no longer under the same physiological conditions as before, i.e. a smaller right atrial preload reduces the size of the chamber, see figure (8.1), and 2) the introduction of large amounts of noise to the system. Whilst mapping in the animal the connections from the MEA balloon to the roving catheter and the ECG cables are all through the highly conductive tissue of the body and blood. When the heart is excised these connections run through pathways of electrode gel and Krebs-Henseleit buffer.

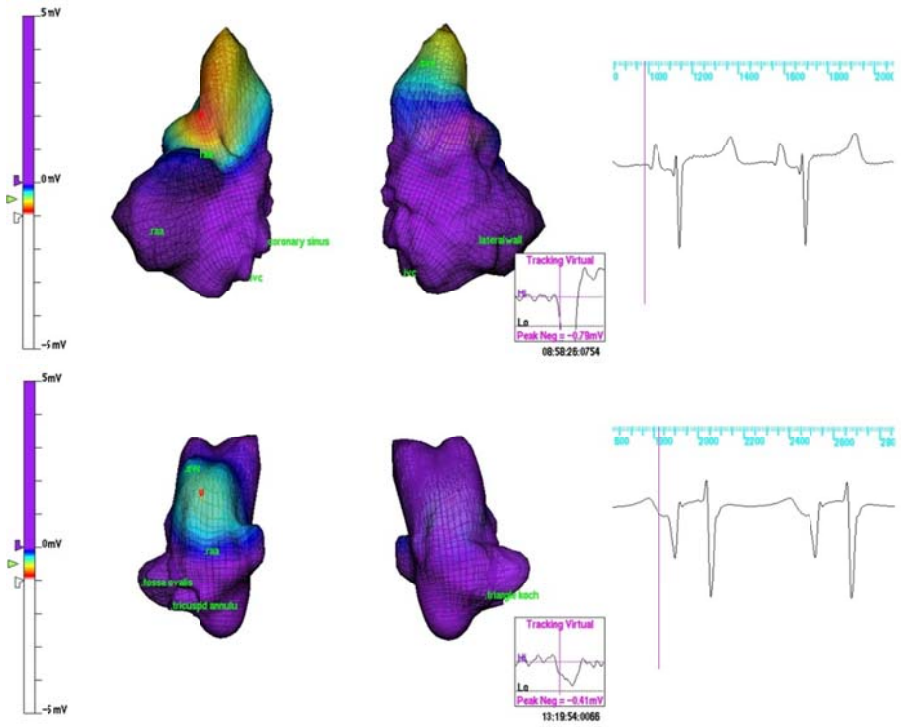

Figure 8.2. Activation of the sinoatrial node both in vivo (above) and in vitro (below)

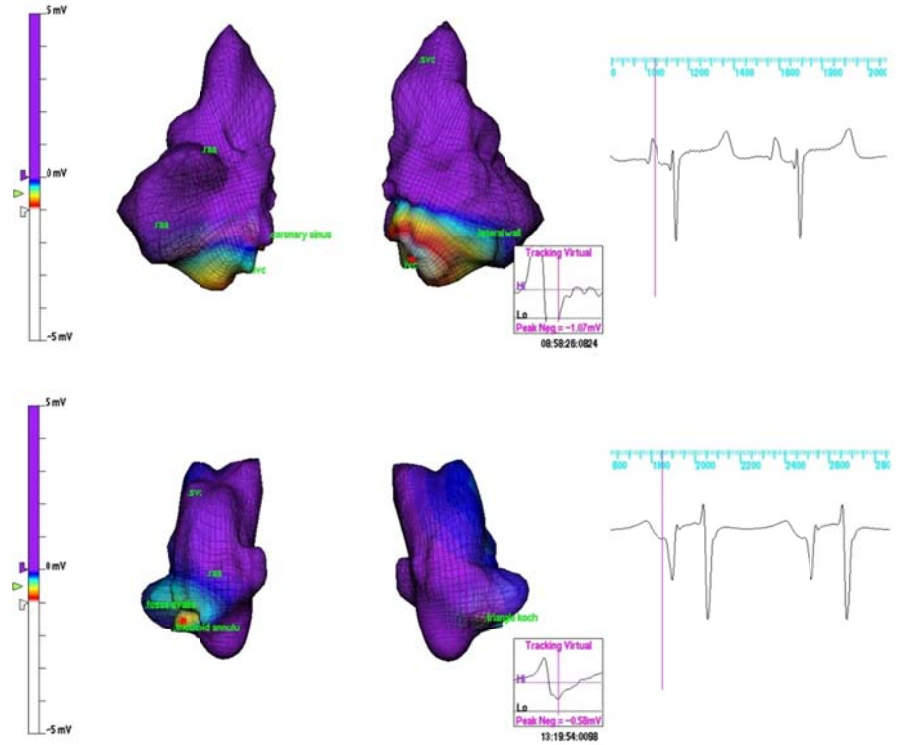

Figure 8.3. End of the atrial activation sequence as the signal passes into the atrioventricular node both in vivo (above) and in vitro (below)

The addition of multiple heavy duty electronic machines such as blood pumps, videoscopic cameras and monitors creates a large amount of background noise that is particularly difficult to shield against.

However, the right atrium of a human heart is anatomically larger than that of the swine model. This fact coupled with specifically working to shield the heart from the surrounding noise will dramatically improve the quality of the anatomical map created by the non-contact mapping system. This in turn will improve the electrical map and the read voltages will be 'projected' to the correct anatomy.

Conclusion

The pilot studies completed here show that the non-contact mapping system can be adapted to record electrical maps of the heart in reanimated hearts on the Visible Heart® apparatus. With careful technique and improvement of electrical shielding an accurate endocardial activation map of the right atrium can be collected from a human specimen. This heart will then be fixed and shipped to our collaborators to create a 3D anatomical model of the conduction system to compare to the endocardial electrical map of the right atrium shedding light on how the electrical activation relates to the anatomical position of the SA node and the AV node.

Additionally, the validation of the use of the non-contact mapping system in the Visible Heart® apparatus has opened the door for the simultaneous imaging and electrical mapping of the heart during device implantation. Ultimately, a better understanding of the cardiac conduction system will provide engineers developing the next generation of transcatheter implanted aortic valves with the knowledge to ensure that stent design helps to reduce the instance of acute post-procedural conduction complications.

References

1. Piazza, N. *et al.* Early and persistent intraventricular conduction abnormalities and requirements for pacemaking after percutaneous replacement of the aortic valve. *JACC Interventions* **1**, 310 (2008).

2. Thomas, J.L. *et al.* Prognostic significance of the development of left bundle conduction defects following aortic valve replacement. *The Journal of thoracic and cardiovascular surgery* **84**, 382-6 (1982).

3. El-Khally, Z. *et al.* Prognostic significance of newly acquired bundle branch block after aortic valve replacement. *The American journal of cardiology* **94**, 1008-11 (2004).

4. Limongelli, G. *et al.* Risk factors for pacemaker implantation following aortic valve replacement: a single centre experience. *Heart (British Cardiac Society)* **89**, 901-4 (2003).

5. Koplan, B.A., Stevenson, W.G., Epstein, L.M., Aranki, S.F. & Maisel, W.H. Development and validation of a simple risk score to predict the need for permanent pacing after cardiac valve surgery. *Journal of the American College of Cardiology* **41**, 795-801 (2003).

6. Dawkins, S. *et al.* Permanent pacemaker implantation after isolated aortic valve replacement: incidence, indications, and predictors. *The Annals of thoracic surgery* **85**, 108-12 (2008).

7. Aktug, O. *et al.* Incidence and predictors of left bundle branch block after transcatheter aortic valve implantation. *International journal of cardiology* (2011).doi:10.1016/j.ijcard.2011.03.004

8. Tchetche, D. *et al.* Thirty-day outcome and vascular complications after transarterial aortic valve implantation using both Edwards Sapien and Medtronic CoreValve bioprostheses in a mixed population. *EuroIntervention : journal of EuroPCR in collaboration with the Working Group on Interventional Cardiology of the European Society of Cardiology* **5**, 659-65 (2010).

9. Chinchoy, E. *et al.* Isolated four-chamber working swine heart model. *The Annals of Thoracic Surgery* **70**, 1607-1614 (2000).

10. Hill, A.J. *et al.* In vitro studies of human hearts. *The Annals of Thoracic Surgery* **79**, 168-177 (2005).

11. Anderson, S.E., Quill, J.L. & Iaizzo, P.A. Venous valves within left ventricular coronary veins. *Journal of Interventional Cardiac Electrophysiology* **23**, 95-99 (2008).

12. Ihara, T. & Barr, R.C. Electrocardiographic inverse solution for ectopic origin of excitation in two-dimensional propagation model. *Medical and Biological Engineering and Computing* **32**, 41-50 (1994).

13. Schmitt, H. *et al.* Diagnosis and ablation of focal right atrial tachycardia using a new high-resolution, non-contact mapping system. *The American Journal of Cardiology* **87**, 1017-21; A5 (2001).

14. Li, J. *et al.* Development of 3-D anatomically-detailed mathematical models of the sinoatrial and atrioventricular nodes. *Computers in Cardiology, 2004* 89-92 (2004).

15. Li, J. *et al.* A detailed 3D model of the rabbit right atrium including the sinoatrial node, atrioventricular node, surrounding blood vessels and valves. *Computers in Cardiology, 2005* 603-606 (2005).

16. Dobrzynski, H. *et al.* Computer three-dimensional reconstruction of the sinoatrial node. *Circulation* **111**, 846-854 (2005).

9. Development of a Trans-mural Electrode system for Measuring Intra-cardiac Electrical Activity

Preface

With established devices such as the EnSite® 3000 (St. Jude Medical, Inc., St. Paul, MN) non-contact mapping is considered the gold standard in current mapping techniques. However, the system requires the insertion of a catheter based multi-electrode array (MEA) into the cardiac chamber under fluoroscopic guidance and can only provide an accurate map of the endocardial surface giving no indication of the depth of electrical activity. With the introduction of non-invasive electrical imaging techniques known as body surface potential mapping systems there is increased interest in the trans-mural propagation of the myocardial electrical activity.

We present here the development of a series of electrodes that are constrained by three specific criteria:

- The distal pole of the electrodes has to be referenced to the endocardial surface (to allow for comparison to an endocardial mapping system).
- The electrodes will have to be securely fixed and perform within the hostile environment of the closed chest.
- The delivery system will need to be as efficient and minimally invasive as possible.

Working with Dr. He's team we have developed an invasive quadripolar electrode array that can be used to electrically map the heart. For this project I worked with John Uphoff on the conception, design and build of the device, conducted preliminary studies on the Visible Heart® apparatus and collaborated with Dr. He's team to record the in vivo signals from 32 electrodes simultaneously with a non-contact mapping system and a novel trans thoracic mapping system.

Michael G. Bateman MEng[1,2], John S. Uphoff[3], Bin He PhD[2], Paul A. Iaizzo PhD[1,2]

Departments of [1]Surgery, [2]Biomedical Engineering and Biochemistry, Molecular Biology and Biophysics[3], University of Minnesota, Minneapolis, MN, USA

Introduction

Non-contact endocardial mapping of the heart is at the forefront of cardiac electrical imaging. Devices such as the EnSite® 3000 (St. Jude Medical, Inc., St. Paul, MN) are used frequently in hospital catheter laboratories across the country for the diagnosis and treatment of atrial and ventricular arrhythmias. However, these systems are not without their faults; firstly they require the insertion of a catheter based multi-electrode array (MEA) into the cardiac chamber under fluoroscopic guidance and more significantly they can only provide an accurate map of the endocardial surface giving no indication of the depth of electrical activity. Therefore, although localization of arrhythmias on the endocardial surface can be achieved, arrhythmias arising from deep within the myocardium may be missed. This limitation is also a concern during catheter ablation. Ablation around the pulmonary veins has been demonstrated as an effective therapy for atrial fibrillation[1], however, aggressive ablation in this area can lead to stenosis of the vessels. As non-contact mapping systems do not give the operator any indication of the depth of therapy there has been extensive work in the development of trans-mural mapping techniques. Consequently, the non-invasive electrical imaging techniques of arrhythmic activities by the analysis of thoracic electrocardiogram (ECG) recordings, a technique known as body surface potential mapping (BSPM), has become an exciting and important new field of research[2]. In order to validate such systems the Visible Heart® laboratory is working to develop an invasive electrode designed to measure the propagation of the activation sequence across the myocardium.

Background

There have been various attempts at creating accurate trans-mural electrodes over the years;

Kramer et al. and Pogwizd et al. developed a mapping system for recording premature ventricular contractions and ventricular tachycardia in canine and feline hearts[3,4]. Electrodes were constructed using a design first documented by Kasell et al. whereby 50μm tungsten wires were insulated and then contained within a 21-guage straight needle and fixed with epoxy[5]. All electrode poles were spaced in pairs at 500μm and then distributed evenly along the needle. Kramer et al. successfully implanted 50 electrodes in the canine heart with no significant alteration in hemodynamic parameters when assessed up to 60 minutes after electrode insertion proving the durability of the myocardium in response to the insertion of multiple needles.

Moore et al. improved on the previously described technique using 75μm insulated silver wire contained within a 20 gauge needle, as used by Hooks et al. in their electrode array[6,7]. This manufacture technique resulted in extremely accurate electrode spacing and improved signal conductivity.

Dosdall et al. and Caldwell et al. completed plunge electrode studies using a design based on the work of Rogers et al. Briefly, 50μm silver wires are threaded through the wall of modified heat-shrink tubing lined with fiberglass spaced at 1mm intervals. The tubing was then shrunk around the wires and finally epoxy was injected into the tubing and cured with the needle clamped to maintain a linear form[8–10].

Other groups have chosen to adapt existing products. Laske et al. successfully evaluated the myocardial activation sequences for pacing the His bundle using modified deep brain stimulation leads (Model 3387, Medtronic, Inc., Minneapolis, MN)[11].

Methods

All Visible Heart® methodologies regarding in vivo swine studies and in vitro reanimation and fixation of large mammalian hearts as described by Chinchoy et al. and Anderson et al. have been outlined previously[12,13].

Design Criteria

In the present study the design of the electrodes has to take three specific criteria into consideration that excluded the use of the previously described electrode designs:

- The distal pole of the electrodes has to be referenced to the endocardial surface (to allow for comparison to an endocardial mapping system) rather than the traditional technique of referencing the electrode to the epicardial surface.
- Although the electrodes will be placed with the heart exposed via a medial sternotomy the chest will have to be re-approximated again to use the 3DCEI system. Hence the electrodes will have to be securely fixed and perform within the hostile environment of the closed chest.
- It has been noted that during cardiac intervention swine are particularly sensitive to cardiac arrhythmias[14]. Thus the delivery system will need to be as efficient and minimally invasive as possible.

Electrode Design and Fabrication

In order to adhere to these specific design criteria we designed a basic trans-mural quadripolar electrode as follows. The authors have previously presented work on an electrode design based around high resistance silver wire. The following describes the development and prototyping of an improved electrode design based on Nitinol, stainless steel hypotube, polyamide tubing and ultra-fine insulated stainless wire and PTFE heat shrink tubing.

1. The electrode rings are constructed (courtesy of LSA, MN) by laser welding a 12” length of 0.002” stainless steel nylon coated wire to a precut length of 0.05” OD, 0.0405” ID 304 stainless steel hypotube. See figure (9.1)
2. The arms are constructed by baking 0.005” Nitinol wire tied tightly around a 0.5” OD spherical aluminum jig with a center hole so that the Nitinol forms and holds a C shape when cooled.
3. Four rings are then threaded onto a 0.5” length of 0.04” OD thin walled orange polyamide tubing.
4. A second 0.5” length of 0.03” OD thin walled orange polyamide tubing is then threaded down the center of the first pushing the nylon coated stainless steel wire to the side between the polyamide tubing.
5. Three Nitinol C arms and one straight 4” length of Nitinol are then threaded through the center of the assembly and arranged so that the three arms sit at 120° from each other.
6. The proximal end of the assembly is threaded through a 10” length of 0.05” OD thin walled blue polyamide tubing everything but the electrode itself and the proximal end of the four stainless steel wires are showing.
7. The electrodes are then set in place using high viscosity UV curing adhesive to position and hold the C arms and the four electrode rings.
8. Finally, the four stainless wires are soldered to a standard telephone jack so that they can quickly and easily be attached to the breakout box.

The final assembly can be seen in figure (9.1). Once assembled each electrode ring is tested to ensure that it is isolated from the three other rings thereby limiting the amount of signal interference across the channels.

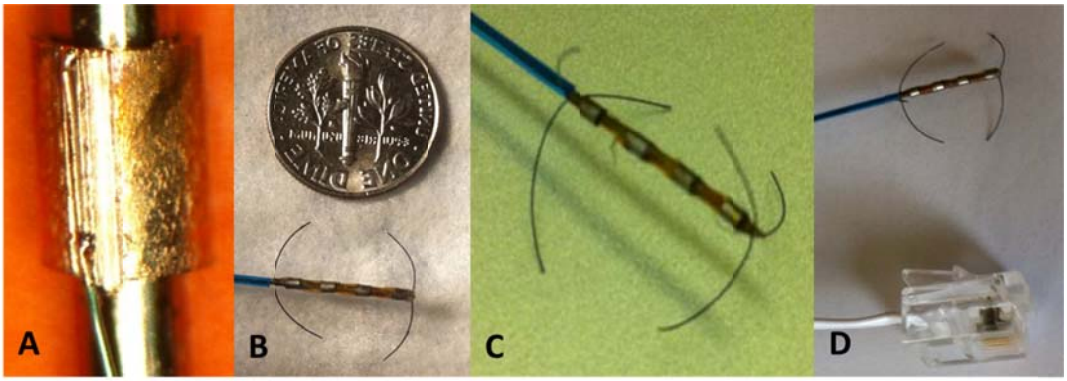

Figure 9.1. The laser welded electrode ring (A) and the finished assembly (B-D). The standard telephone jack for connection to the breakout box can be seen in D.

Figure 9.2. Photograph of the bespoke breakout box constructed to create a quick and easy interface with the recording equipment.

The electrodes were designed to be connected to two bespoke breakout boxes, see figure (9.2), which were in turn connected to the recording equipment via male to male 68 pin SCSI-3 cables (supplied by GovConnection, Merrimack, NH).

Figure 9.3. Footage from inside the ventricle showing the distal tip of the electrode.

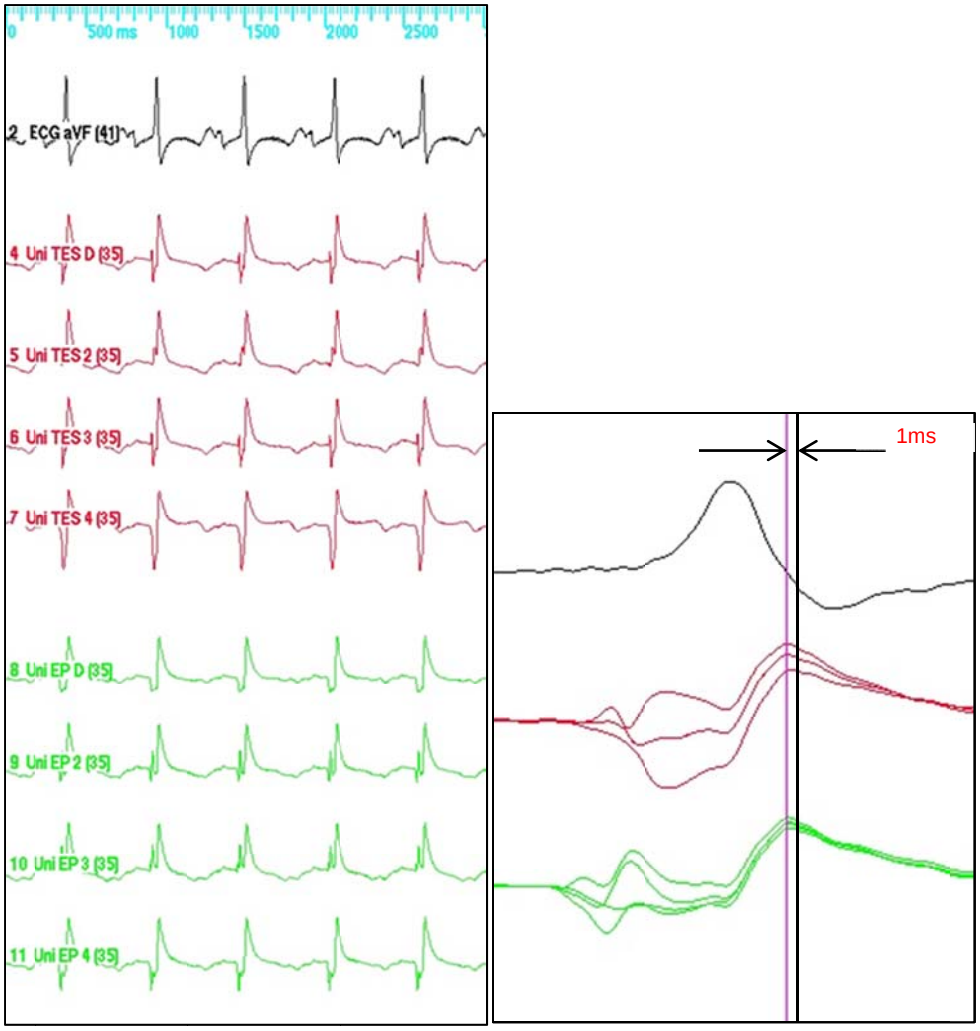

Figure 9.4. (left)Traces from two electrodes in left ventricle of a swine heart reanimated in the Visible Heart® Apparatus. The ECG can be seen in black at the top with two electrodes, one in red and one green, from the distal electrode at the top and the proximal at the bottom

Figure 9.5. (right) Closer analysis of signals *in vitro* shows good signal magnitude and minimal noise with variability between the four poles of the electrode showing isolation of these signals. The QRS of the ECG is at the top in black with the four signals from two electrodes superimposed on top of one another below. Note, one of the red signals was corrupt due to the proximal electrode being out of the myocardium.

Results

Electrode placement was achieved by inserting the delivery needle into the left ventricular myocardium and advancing the electrode until the Nitinol arms unfolded against the endocardial surface. The needle was then withdrawn in a proximal direction over the electrode allowing the epicardial arms to snap into place fixing the electrode in position. The delivery needle was then withdrawn until a safe distance from the heart. A slight force was then applied

to the electrode to ensure a secure positioning. Figure (9.3) displays the arms of the transmural electrode gripping the endocardial surface and holding the distal electrode in place. From these preliminary experiments we were able to obtain excellent signals to a temporal resolution of 5ms, shown in figure (9.4) and (9.5).

Discussion

The work presented here highlights the development of a reusable system for measuring the electrical activation across the myocardium. We have since manufactured 32 individual quadripolar electrodes and completed an in situ experiment recording 128 channels simultaneously. The data from this study is still being analyzed in collaboration with Dr. He's group.

The goal of this investigation was to develop a system that can be used for in situ and in vitro studies to provide quick analysis of the global activation of the heart with much more accuracy than the ECG. The resulting product, although exhibiting a poor spatial resolution across the myocardium due to the limited number of channels that can be recorded shows a good temporal resolution. The next steps in this project are to improve the manufacturing process to create electrodes with improved spacing and deliverability. Additionally, provision of a more user friendly and flexible interface allowing the system to be attached to different recording devices, will dramatically improve the usability of the system.

Conclusions

We have successfully completed the prototyping, development and experimental validation of a Nitinol wire based quadripolar electrode designed for the recording of trans-mural electrocardiograms. The preliminary results suggest that the design has potential to provide a secure and repeatable way of delivering a quadripolar electrode into the myocardium. This system will provide valuable information during the testing of cardiac therapies in the Visible Heart® laboratory.

References

1. Natale, A. & Jalife, J. *Role of the Vagus in AF. In: Atrial Fibrillation, From Bench to Bedside*. *Contemporary Cardiology* **2**, 115-131 (Humana: 2008).

2. Liu, C. *et al.* Estimation of Global Ventricular Activation Sequences by Noninvasive Three-Dimensional Electrical Imaging: Validation Studies in a Swine Model During Pacing .

Journal of cardiovascular electrophysiology (2007).doi:10.1111/j.1540-8167.2007.01066.x

3. Kramer, J.B., Saffitz, J.E., Witkowski, F.X. & Corr, P.B. Intramural reentry as a mechanism of ventricular tachycardia during evolving canine myocardial infarction . *Circulation research* **56**, 736-754 (1985).

4. Pogwizd, S.M. & Corr, P.B. Reentrant and nonreentrant mechanisms contribute to arrhythmogenesis during early myocardial ischemia: results using three-dimensional mapping . *Circulation research* **61**, 352-371 (1987).

5. Kasell, J. & Gallagher, J.J. Construction of a multipolar needle electrode for activation study of the heart . *The American Journal of Physiology* **233**, H312-7 (1977).

6. Moore, K.B., Kimball, T. & Steadman, B. Silver-silver chloride plunge electrode needles and chloriding monitor . *IEEE transactions on bio-medical engineering* **37**, 532-535 (1990).

7. Hooks, D.A. & Trew, M.L. Construction and Validation of a Plunge Electrode Array for Three-Dimensional Determination of Conductivity in the Heart . *IEEE transactions on bio-medical engineering* **55**, 626-635 (2008).

8. Dosdall, D. *et al.* Transmural and endocardial Purkinje activation in pigs before local myocardial activation after defibrillation shocks. *Heart Rhythm* **4**, 758-765 (2007).

9. Caldwell, B.J. *et al.* Intramural measurement of transmembrane potential in the isolated pig heart: validation of a novel technique . *Journal of cardiovascular electrophysiology* **16**, 1001-1010 (2005).

10. Rogers, J.M., Melnick, S.B. & Huang, J. Fiberglass needle electrodes for transmural cardiac mapping . *IEEE transactions on bio-medical engineering* **49**, 1639-1641 (2002).

11. Laske, T.G., Skadsberg, N.D., Hill, A.J., Klein, G.J. & Iaizzo, P.A. Excitation of the intrinsic conduction system through his and interventricular septal pacing . *Pacing and clinical electrophysiology : PACE* **29**, 397-405 (2006).

12. Chinchoy, E. *et al.* Isolated four-chamber working swine heart model. *The Annals of Thoracic Surgery* **70**, 1607-1614 (2000).

13. Anderson, S.E., Quill, J.L. & Iaizzo, P.A. Venous valves within left ventricular coronary veins. *Journal of Interventional Cardiac Electrophysiology* **23**, 95-99 (2008).

14. Hughes, H.C. Swine in cardiovascular research . *Laboratory animal science* **36**, 348-350 (1986).

Thesis Summary

As the fields of cardiac surgery and cardiology continue to rapidly develop and expand, innovative and revolutionary devices and therapies are continually introduced and developed. For these novel devices to succeed in a complex and competitive market their design and development must first evolve from a strong fundamental knowledge of both cardiac anatomy and electrophysiology. In particular, the distinct need for improved valvular heart repair therapies and technologies that are available to a greater portion of the patient population has driven the development of transcatheter delivered valve therapies. Today, with transcatheter aortic valve repair (TAVR) establishing itself as an accepted technique for treatment of severe aortic stenosis in patients that cannot undergo surgery, it is important to thoroughly understand all potential effects of these therapies on any given type of patient.

The chapters of this thesis describe the work I have completed in the Visible Heart® laboratory, which have allowed me to build solid foundations of both cardiac anatomy and electrophysiology, which I then applied to different imaging and mapping modalities. The dynamic nature of the Visible Heart® methodologies and results which one can obtain from such are continually evolving entities: specifically, they allowed me to develop and utilize novel in vitro and in vivo models of valve disease specifically designed to test of new therapies. The majority of my research has focused on the intellectual needs to develop and test TAVR; ranging from the assessment of imaging modalities for accurate patient sizing to the development of techniques to determine the performance and effect of novel devices on the heart. When considering TAVR as a treatment for aortic stenosis, it is widely accepted that the current market released treatments, although an exceptional option for those patients who cannot undergo surgery, do not currently compare to the outcomes currently obtained with surgical valve replacement. The two main reasons for this include: 1) the increased incident of acute left bundle branch block, and 2) the fact that the native leaflets are not removed leaving a highly irregular “landing zone” in patients with heavily calcified aortas. As such, pre-procedural imaging is critical to the success of these procedures, both from the standpoint of choosing the correct prosthesis size and to better define the anatomy into which the device is to be implanted. This in turn dramatically reduces the incidences of conduction anomalies due to prosthesis misplacements and/or facilitates in determining the best way to limit para-valvular leaks post implantation.

However, as transcatheter procedures becomes more common and are eventually adopted by interventional cardiac facilities from smaller hospitals, the high costs of such thorough imaging will drive the need for a TAVR prosthesis that is both easier to implant (under echocardiographic guidance for example) and limits these post-procedural concerns. The development of such devices will be significantly enhanced with the use of dynamic in vitro testing systems, such as the Visible Heart® that allows for the creation of bespoke anatomies. In addition to this, an in vitro approach allows the investigator to visualize how the heart reacts, both physically and electrically, to the implanted device, thus providing critical information to the design team before embarking on expensive and time consuming pre-clinical large animal studies. Within this thesis the concept of creating an experimental model of the clinical pathology has been applied in several cases: e.g., the creations of a regurgitant mitral valve or an insufficient pulmonary valve, like those in tetralogy of Fallot (TOF) patients. Both pathologies have an inherent need for a competent transcatheter delivered device, specifically due to the high risk nature of the patients precluding them from surgical procedures.

I have completed several studies designed to improve the laboratories ability to assess the electrophysiological effects of a particular therapy. More specifically, the validation of the use of the non-contact mapping system in the Visible Heart® apparatus has opened the door for the simultaneous imaging and electrical mapping of the heart during device implantation. In addition, the development of an invasive mapping system to determine trans-mural electrical propagation patterns has allowed us to collaborate with other researchers at the University on the development of state of the art electrical mapping technologies.

When considering the research topics covered in this thesis it is clear that much work could be done in this area and as we look to the future of the clinical treatment of valve disease new challenges will surface. Soon, hybrid operating rooms within catheterization laboratories will give physicians the ability to simultaneously image with fluoroscopy, echocardiography and trans-thoracic mapping technologies whilst implanting replacement valve technologies with integrated pacing systems. From both the physician's and the patient's perspective it is critical that these devices are generated from a thorough understanding of the underlying pathology to ensure the highest performance of these therapies in man. As such, a better understanding of the interactions of novel transcatheter devices and their delivery systems with human cardiac anatomies and their associated conduction systems are critical for the advancement of these

medical devices. I believe that my research and the ongoing projects that have been initiated in our laboratory are truly translational and as such will help to bridge the gaps between the physicians and device engineers.

My experience in the Visible Heart® laboratory has taught me so much more than the work presented in this thesis. The collaborative atmosphere fostered by Dr. Iaizzo has taught me the value of asking questions and more importantly, listening to the answers. My opportunity to have worked with key opinion leaders both from the medical field and from industry has provided insight into the medical device industry rarely available through academia alone. Additionally, my involvement in outreach programs such as lab tours, lecture opportunities through University courses and conferences, and my continued involvement in the Atlas of Cardiac Anatomy has allowed me the opportunity to give back and educate others. I have been first author on four chapters on cardiac anatomy and device testing, co-authored four papers in peer reviewed journals, with several more articles in submission, and presented material at a number of conferences. It is with this foundation that I will pursue a career innovating and developing the next generation of cardiac therapies to treat those with severe valvular pathologies.

Bibliography

Aktug, O. et al. Incidence and predictors of left bundle branch block after transcatheter aortic valve implantation. Int. J. Card. Mar 30 epub (2011).

Alfieri, O. & Maisano, F. An effective technique to correct anterior mitral leaflet prolapse. J. Card. Surg. 14, 468-470 (1999).

Alfieri, O. et al. The double-orifice technique in mitral valve repair: a simple solution for complex problems. J. Thorac. Cardiovasc. Surg. 122, 674-681 (2001).

Alfieri, O. et al. “Edge-to-edge” repair for anterior mitral leaflet prolapse (Seminars in Thoracic and Cardiovascular Surgery Ser. 16, Elsevier, 2004).

Alfieri, O., Maisano, F. & Colombo, A. Percutaneous mitral valve repair procedures. European Journal of Cardio-thoracic Surgery 26, 36-38 (2004).

Alfieri, O. et al. Percutaneous mitral valve repair: an attractive perspective and an opportunity for teamwork. Ital. Heart J. 5, 723-726 (2004).

Alfieri, O., Maisano, F. & De Bonis, M. The edge-to-edge repair. Multimedia Manual of Cardio-thoracic Surgery 2005, 869 (2005).

Anderson, K.R., Ho, S.Y. & Anderson, R.H. Location and vascular supply of sinus node in human heart. British heart journal 41, 28-32 (1979).

Anderson, R.H., Devine, W. a., Ho, S.Y., Smith, A. & McKay, R. The myth of the aortic annulus: The anatomy of the subaortic outflow tract☆. The Annals of Thoracic Surgery 52, 640-646 (1991).

Anderson RH, Becker AE: The heart: Structure in health and disease. London, UK; New York, NY: Gower Medical Pub, 1992.

Anderson, R.H., Razavi, R. & Taylor, A.M. Cardiac anatomy revisited. Journal of anatomy 205, 159-77 (2004).

Anderson, R.H., Yanni, J., Boyett, M.R., Chandler, N.J. & Dobrzynski, H. The anatomy of the cardiac conduction system. Clinical anatomy (New York, N.Y.) 22, 99-113 (2009).

Anderson SE, Quill JL, Iaizzo PA: Venous valves within left ventricular coronary veins. Journal of Interventional Cardiac Electrophysiology, 23(2):95-9, 2008.

Anderson SE, Hill AJ, Iaizzo PA. Microanatomy of human left ventricular coronary veins. Anat Rec (Hoboken). 2009;292(1):23-8.

Asante-Korang A, O’Leary PW, Anderson RH (2006) Anatomy and echocardiography of the normal and abnormal mitral valve. Cardiol Young 16(Suppl 3):27-34

Aschoff, L. Referat uber die Herzstorungen in ihren Beziehungen zu den Spezifischen Muskelsystem des Herzens. Verh Dtsch Pathol Ges 14:3–35 (1910).

Athanasiou, T. et al. Preservation of the mitral valve apparatus: evidence synthesis and critical reappraisal of surgical techniques Eur. J. Cardiothoracic. Surg. 33, 391-401 (2008)

Atkinson, A. et al. Anatomical and molecular mapping of the left and right ventricular His-Purkinje conduction networks. Journal of molecular and cellular cardiology 51, 689-701 (2011).

Atlas of Human Cardiac Anatomy. www.vhlab.umn.edu/atlas

Bande M, Michev I, Sharp ASP, Chieffo A, Colombo A: Percutaneous Transcatheter Aortic Valve Implantation: Past Accomplishments, Present Achievements and Applications, Future Perspectives. [Review] Cardiology in Review, 18(3):111-124, 2010.

Bakhtiary F, Dzemail O, Steinseiffer U, et al. Opening and closing kinematics of fresh and calcified aortic valve prostheses: an in vitro study. J. Thorac. Cardiovas. Surg. 134(3): 657-662, 2007.

Barker, P., MacLeod, A. & Alexander, J. The excitory process observed in the exposed human heart. American Heart Journal1 5, 720-742 (930).

Barker, T.A. & Wilson, I.C. Surgical anatomy of the mitral and tricuspid valve. In: Bonser RS, Pagano D, Haverich A (eds) Mitral Valve Surgery. Springer-Verlag London Limited, 3-19 (2011).

Barnet, V.A. Cellular myocytes. In: Iaizzo PA (ed) The handbook of cardiac anatomy, physiology, and devices, 2nd edn. Humana Press, Totowa NJ, 147-158 (2009).

Becker, A.E. & De Wit, A.P. Mitral valve apparatus. A spectrum of normality relevant to mitral valve prolapse. British heart journal 42, 680-9 (1979).

Berdajs, D., Lajos, P., Turina, M.I. A new classification of the mitral papillary muscle. Medical Science Monitor. 11(1), BR18-21 (2005)

Bertels, R.A., Blom, N.A. & Schalij, M.J. Edwards SAPIEN transcatheter heart valve in native pulmonary valve position. Heart (British Cardiac Society) 96, 661 (2010).

Bhudia, S. K. et al. Edge-to-edge (Alfieri) mitral repair: results in diverse clinical settings. Ann. Thorac. Surg. 77, 1598-1606 (2004).

Bleiziffer, S. et al. Survival after transapical and transfemoral aortic valve implantation: talking about two different patient populations. The Journal of thoracic and cardiovascular surgery 138, 1073-80 (2009).

Bonhoeffer, P. et al. Percutaneous replacement of pulmonary valve in a right-ventricle to pulmonary-artery prosthetic conduit with valve dysfunction. The Lancet 356, 1403-1405 (2000).

Boudjemline, Y., Agnoletti, G., Bonnet, D., Sidi, D. & Bonhoeffer, P. Percutaneous pulmonary valve replacement in a large right ventricular outflow tract: An experimental study. Journal of the American College of Cardiology 43, 1082-1087 (2004).

Brewer, R.J., Deck, J.D., Capati, B. & Nolan, S.P. The dynamic aortic root. Its role in aortic valve function. The Journal of thoracic and cardiovascular surgery 72, 413-7 (1976).

Buellesfeld L, Windecker S. Transcatheter aortic valve implantation: the evidence is catching up with reality. Eur Heart J. 2011;32(2):133-7.

Burman ED, Keegan J, Kilner PJ. Aortic root measurement by cardiovascular magnetic resonance: specification of planes and lines of measurement and corresponding normal values. Circ Cardiovasc Imaging. 2008;1(2):104-13.

Caldwell, B.J. et al. Intramural measurement of transmembrane potential in the isolated pig heart: validation of a novel technique . Journal of cardiovascular electrophysiology 16, 1001-1010 (2005).

Capps, S.B., Elkins, R.C. & Fronk, D.M. Body surface area as a predictor of aortic and pulmonary valve diameter. The Journal of thoracic and cardiovascular surgery 119, 975-82 (2000).

Cavalcanti, J.S., de Melo, N.C.V. & de Vasconcelos, R.S. Morphometric and topographic study of coronary ostia. Arquivos brasileiros de cardiologia 81, 359-62, 355-8 (2003).

Carpentier, A. Cardiac valve surgery--the “French correction” . The Journal of thoracic and cardiovascular surgery 86, 323-337 (1983).

Chandler, N.J. et al. Molecular architecture of the human sinus node: insights into the function of the cardiac pacemaker. Circulation 119, 1562-75 (2009).

Chinchoy, E. et al. Isolated four-chamber working swine heart model. The Annals of Thoracic Surgery 70, 1607-1614 (2000).

Choure, A.J. et al. In vivo analysis of the anatomical relationship of coronary sinus to mitral annulus and left circumflex coronary artery using cardiac multidetector computed tomography: implications for percutaneous coronary sinus mitral annuloplasty. Journal of the American College of Cardiology 48, 1938-45 (2006).

Coats, L. et al. The potential impact of percutaneous pulmonary valve stent implantation on right ventricular outflow tract re-intervention. European Journal of Cardio-thoracic Surgery 27, 536-543 (2005).

Coats, L. & Bonhoeffer, P. New percutaneous treatments for valve disease. British medical journal 93, 639-644 (2007).

Congiu, S. et al. Mitral insufficiency with a double-orifice mitral valve in an adult patient. The Journal of thoracic and cardiovascular surgery 134, 250-1 (2007).

Cook, a C. & Anderson, R.H. Attitudinally correct nomenclature. Heart (British Cardiac Society) 87, 503-6 (2002).

Cribier A, Eltchaninoff H, Bash A, et al. Percutaneous transcatheter implantation of an aortic valve prosthesis for calcific aortic stenosis: first human case description. Circulation. 2002;106(24):3006-8.

Dawkins, S. et al. Permanent pacemaker implantation after isolated aortic valve replacement: incidence, indications, and predictors. The Annals of thoracic surgery 85, 108-12 (2008).

De Simone, R. et al. A clinical study of annular geometry and dynamics in patients with ischemic mitral regurgitation: new insights into asymmetrical ring annuloplasty. European Journal of Cardio-Thoracic Surgery 29, 355-361 (2006).

Dekker, D.L., Piziali, R.L. & Dong, E. A system for ultrasonically imaging the human heart in three dimensions. Computers and biomedical research, an international journal 7, 544-53 (1974).

Delgado, V. et al. Assessment of mitral valve anatomy and geometry with multislice computed tomography. JACC. Cardiovascular imaging 2, 556-65 (2009).

Deng, X. et al. A rare case of Gerbode defect associated with double orifice mitral valve. The Thoracic and cardiovascular surgeon 58, 372-4 (2010).

Descoutures F, Himbert D, Lepage L, et al. Contemporary surgical or percutaneous management of severe aortic stenosis in the elderly. Eur Heart J. 2008;29(11):1410-7.

DiDio, L.J., Rodrigues, H. & Baptista, C.A. The papillary muscles of the left ventricle and the cardiac segments Surg. Radiol. Anat. 12, 281-285 (1990)

Dobrzynski, H. et al. Computer three-dimensional reconstruction of the sinoatrial node. Circulation 111, 846-854 (2005).

Dosdall, D. et al. Transmural and endocardial Purkinje activation in pigs before local myocardial activation after defibrillation shocks. Heart Rhythm 4, 758-765 (2007).

Dupre, A., Vieau, S. & Iaizzo, P.A. Basic ECG theory, 12-lead Recordings and Their Interpretation. In: Iaizzo PA (ed) The handbook of cardiac anatomy, physiology, and devices, 2nd edn. Humana Press, Totowa NJ, 257-270 (2009).

Durrer, D. et al. Total excitation of the isolated human heart. Circulation 41, 899-912 (1970).

Eggen MD, Swingen CM, Iaizzo PA: Analysis of fiber orientation in normal and failing human hearts using diffusion tensor MRI, 2009 IEEE International Symposium on Biomedical Imaging: From Nano to Macro, 642-645, 2009.

Eggen, M., Bateman, M. & Iaizzo, P.A. Methods to Prepare Perfusion Fixed Cardiac Specimens for Multimodal Imaging: The Use of Formalin and Agar Gels. Journal of Medical Devices 5, 027539-1 (2011).

Eggen, M. Atlas of Human Cardiac Anatomy. at www.vhlab.umn.edu/atlas/cmrtutorial/cmrtutorial1.shtml

Elfenbein, B. & Paplanus, S.H. Duplication of the mitral and tricuspid valves. Archives of pathology 85, 675-80 (1968).

El-Khally, Z. et al. Prognostic significance of newly acquired bundle branch block after aortic valve replacement. The American journal of cardiology 94, 1008-11 (2004).

Erdemli, O. et al. A Double-Orifice Atrioventricular Valve Case: Intraoperative Transesophageal Echocardiography in Diagnosis and Treatment. Anesth. Analg. 97, 650-653 (2003).

Ewert, P., Horlick, E. & Berger, F. First implantation of the CE-marked transcatheter Sapien pulmonic valve in Europe. Clinical research in cardiology : official journal of the German Cardiac Society 100, 85-7 (2011).

Fan CM, Liu X, Panidis JP, et al. Prediction of Homograft Aortic Valve Size by Transthoracic and Transesophageal Two-Dimensional Echocardiography. Echocardiography. 1997;14(4):345-48.

Fenoglio, J.J., Tuan-Duc-Pham, Wit, A.L., Bassett, A.L. & Wagner, B.M. Canine mitral complex. Ultrastructure and electromechanical properties. Circulation research 31, 417-30 (1972).

Fiszer, R., Szkutnik, M., Hijazi, Z.M. & Białkowski, J. [Transcatheter implantation of Edwards-SAPIEN THV valve in pulmonary position]. Kardiologia polska 69, 749-50 (2011).

Filip, D.A., Radu, A. & Simionescu, M. Interstitial cells of the heart valves possess characteristics similar to smooth muscle cells. Circulation research 59, 310-20 (1986).

Gallegos RP, Nockel PJ, Rivard AL, Bianco RW. The current state of in-vivo pre-clinical animal models for heart valve evaluation. J. Heart Valve Dis. 14(3): 423-432, 2005.

Gams, E. et al. Importance of the mitral apparatus for left ventricular function: an experimental approach . European journal of cardio-thoracic surgery : official journal of the European Association for Cardio-thoracic Surgery 6 Suppl 1, S17-23; discussion S24 (1992).

Gams, E. et al. Importance of the left ventricular subvalvular apparatus for cardiac performance . The Journal of heart valve disease 2, 642-645 (1993).

Garson, A.J., Bricker, J.T., Fisher D.J., Neish, S.R. eds. The science and practice of pediatric cardiology. Volume I. Baltimore, MD: Williams & Williams, 141-3, (1998).

Goicolea, F.J. et al. Double mitral orifice associated with a bicuspid aortic valve detected using bidimensional echocardiography. Revista española de cardiología 42, 65-7 (1989).

Greenfield, W. Double Mitral valve. Translactions of the Pathological Society of London 27, 128-9 (1876).

Gross, L. & Kugel, M.A. Topographic Anatomy and Histology of the Valves in the Human Heart. The American journal of pathology 7, 445-474.7 (1931).

Hasegawa, H. et al. Mitral valve motion after performing an edge-to-edge repair in an isolated swine heart. J. Thorac. Cardiovasc. Surg. 136, 590-596 (2008).

He, B., Li, G. & Zhang, X. Noninvasive imaging of cardiac transmembrane potentials within three-dimensional myocardium by means of a realistic geometry anisotropic heart model. IEEE Transactions on Biomedical Engineering 50, 1190-1202 (2003).

He, B., Liu, C. & Zhang, Y. Three-dimensional cardiac electrical imaging from intracavity recordings. IEEE Transactions on Biomedical Engineering 54, 1454-1460 (2007).

Heyse, A.M. et al. Mitral insufficiency with congenital double-orifice mitral valve in an elderly patient. European journal of echocardiography: the journal of the Working Group on Echocardiography of the European Society of Cardiology 4, 334-5 (2003).

Hill, A.J. et al. In vitro studies of human hearts. The Annals of Thoracic Surgery 79, 168-177 (2005).

Hill, A.J. Attitudinally Correct Cardiac Anatomy. In: Iaizzo PA (ed) The handbook of cardiac anatomy, physiology, and devices, 2nd edn. Humana Press, Totowa NJ, 15-22 (2009).

Hill A, Iaizzo PA: Comparative Cardiac Anatomy. In: The Handbook of Cardiac Anatomy, Physiology, and Devices, Second Edition. Iaizzo PA (Ed.), Humana Press, Totowa NJ, USA, 87-108, 2009.

Hooks, D.A. & Trew, M.L. Construction and Validation of a Plunge Electrode Array for Three-Dimensional Determination of Conductivity in the Heart . IEEE transactions on bio-medical engineering 55, 626-635 (2008).

Hughes, H.C. Swine in cardiovascular research . Laboratory animal science 36, 348-350 (1986).

Hung, J. et al. 3D echocardiography: a review of the current status and future directions. Journal of the American Society of Echocardiography : official publication of the American Society of Echocardiography 20, 213-33 (2007).

Iaizzo PA, Hill AJ, Laske TG: Cardiac device testing enhanced by simultaneous imaging modalities: the Visible Heart®, fluoroscopy, and echocardiography. Expert Review of Medical Devices 5:51-8, 2008.

Icardo, J.M. & Colvee, E. Atrioventricular valves of the mouse: II. Light and transmission electron microscopy. The Anatomical record 241, 391-400 (1995).

Icardo, J.M. & Colvee, E. Atrioventricular valves of the mouse: III. Collagenous skeleton and myotendinous junction. The Anatomical record 243, 367-75 (1995).

Ihara, T. & Barr, R.C. Electrocardiographic inverse solution for ectopic origin of excitation in two-dimensional propagation model. Medical and Biological Engineering and Computing 32, 41-50 (1994).

Itoh, A. et al. Active stiffening of mitral valve leaflets in the beating heart. American journal of physiology. Heart and circulatory physiology 296, H1766-73 (2009).

Kadish, A., Hauck, J., Pederson, B., Beatty, G. & Gornick, C. Mapping of atrial activation with a noncontact, multielectrode catheter in dogs. Circulation 99, 1906-13 (1999).

Kalavrouziotis D, Doyle D; Rodés-Cabau J, Bagur R, DeLarochelliére R, Pibarot P, Dumont E: Transcatheter Aortic Valve Implantation in Patients With Severe Aortic Stenosis and Small Aortic Annulus. Circulation, 122:A19625, 2010.

Kalman, J.M. et al. Radiofrequency catheter modification of sinus pacemaker function guided by intracardiac echocardiography. Circulation 92, 3070-81 (1995).

Karas, S. et al. Well-functioning double-orifice mitral valve in a young adult. Journal of clinical ultrasound: JCU 31, 170-3

Kasell, J. & Gallagher, J.J. Construction of a multipolar needle electrode for activation study of the heart . The American Journal of Physiology 233, H312-7 (1977).

Kaul S, Diamond GA: Are Claims of Effectiveness of MitraClip Device Compared with Surgery for Severe Mitral Regurgitation Substantiated by the Evidence? A Critical Look at the EVEREST II Trial. Circulation, 122:A20910, 2010.

Keith, A. & Flack, M. The form and nature of the muscular connections between the primary divisions of the vertebrate heart. Journal of Anatomy and Physiology 41, 172 (1907).

Kim, S.-J., Shin, E.-S. & Lee, S.-G. Congenital double-orifice mitral valve with mitral regurgitation due to flail leaflet in an elderly patient. The Korean journal of internal medicine 20, 251-4 (2005).

Komoda, T. et al. Mitral Annulus after Mitral Repair: Geometry and Dynamics. ASAIO Journal 48, 412 (2002).

Koos, R. et al. Quantification of aortic valve calcification using multislice spiral computed tomography: comparison with atomic absorption spectroscopy. Investigative radiology 41, 485-9 (2006).

Koos R, Altiok E, Mahnken AH, et al. Evaluation of aortic root for definition of prosthesis size by magnetic resonance imaging and cardiac computed tomography: Implications for transcatheter aortic valve implantation. Int J Cardiol. 2011.

Koplan, B.A., Stevenson, W.G., Epstein, L.M., Aranki, S.F. & Maisel, W.H. Development and validation of a simple risk score to predict the need for permanent pacing after cardiac valve surgery. Journal of the American College of Cardiology 41, 795-801 (2003).

Kopp, A.F., Georg, C. & Claussen, C.D. [Multislice CT angiography of the upper abdomen. Stenosis of the superior mesenteric artery]. RöFo : Fortschritte auf dem Gebiete der Röntgenstrahlen und der Nuklearmedizin 172, M1 (2000).

Kopp, A.F. et al. Multislice CT in cardiac and coronary angiography. The British journal of radiology 77 Spec No, S87-97 (2004).

Kramer, J.B., Saffitz, J.E., Witkowski, F.X. & Corr, P.B. Intramural reentry as a mechanism of ventricular tachycardia during evolving canine myocardial infarction . Circulation research 56, 736-754 (1985).

Kron, J., Standerfer, R.J. & Starr, A. Severe mitral regurgitation in a woman with a double orifice mitral valve. British heart journal 55, 109-11 (1986).

Kumar, N., Kumar, M. & Duran, C.M. A revised terminology for recording surgical findings of the mitral valve . The Journal of heart valve disease 4, 70-77 (1995).

Kunzelman, K.S., Cochran, R.P., Verrier, E.D. & Eberhart, R.C. Anatomic basis for mitral valve modelling. The Journal of heart valve disease 3, 491-6 (1994).

Kunzelman, K.S., Grande, K.J., David, T.E., Cochran, R.P. & Verrier, E.D. Aortic root and valve relationships. Impact on surgical repair. The Journal of thoracic and cardiovascular surgery 107, 162-70 (1994).

Kurra V, Kapadia SR, Tuzcu EM, et al. Pre-procedural imaging of aortic root orientation and dimensions: comparison between X-ray angiographic planar imaging and 3-dimensional multidetector row computed tomography. JACC Cardiovasc Interv. 2010;3(1):105-13.

Kwan, J. et al. 3D geometry of a normal tricuspid annulus during systole: a comparison study with the mitral annulus using real-time 3D echocardiography. European journal of echocardiography : the journal of the Working Group on Echocardiography of the European Society of Cardiology 8, 375-83 (2007).

Lam, J.H., Ranganathan, N., Wigle, E.D. & Silver, M.D. Morphology of the human mitral valve. I. Chordae tendineae: a new classification. Circulation 41, 449-58 (1970).

Langendorff, O "Untersuchungen am uberlebenden Saugenthierherzen [Investigations on the surviving mammalian heart]," Pflugers Arch., 61: 291-332, 1895.

Laske, T.G., Skadsberg, N.D., Hill, A.J., Klein, G.J. & Iaizzo, P.A. Excitation of the intrinsic conduction system through his and interventricular septal pacing . Pacing and clinical electrophysiology : PACE 29, 397-405 (2006).

Laske, T.G., Shrivastav, M. & Iaizzo, P.A. The Cardiac Conduction System. In: Iaizzo PA (ed) The handbook of cardiac anatomy, physiology, and devices, 2nd edn. Humana Press, Totowa NJ, 159-176 (2009).

Lee, D.I. et al. Double-orifice mitral valve. Clinical cardiology 22, 425 (1999).

Lee, R.J. et al. Radiofrequency catheter modification of the sinus node for "inappropriate" sinus tachycardia. Circulation 92, 2919-28 (1995).

Li, J. et al. Development of 3-D anatomically-detailed mathematical models of the sinoatrial and atrioventricular nodes. Computers in Cardiology, 2004 89-92 (2004).

Li, J. et al. A detailed 3D model of the rabbit right atrium including the sinoatrial node, atrioventricular node, surrounding blood vessels and valves. Computers in Cardiology, 2005 603-606 (2005).

Li, X-H. & Lu, F. Catheter Ablation of Cardiac Arrhythmias. In: Iaizzo PA (ed) The handbook of cardiac anatomy, physiology, and devices, 2nd edn. Humana Press, Totowa NJ, 411-442 (2009).

Limongelli, G. et al. Risk factors for pacemaker implantation following aortic valve replacement: a single centre experience. Heart (British Cardiac Society) 89, 901-4 (2003).

Linka, A.Z., Fatio, R. & Jost, C.A. Double orifice mitral valve. Heart British Cardiac Society 84, 244 (2000).

Liu, C. et al. Estimation of Global Ventricular Activation Sequences by Noninvasive Three-Dimensional Electrical Imaging: Validation Studies in a Swine Model During Pacing . Journal of cardiovascular electrophysiology (2007).

Lohr, J.L. & Shanthi, S. Introduction to Echocardiography. In: Iaizzo PA (ed) The handbook of cardiac anatomy, physiology, and devices, 2nd edn. Humana Press, Totowa NJ, 319-330 (2009).

Loukas M, Tubbs RS, Louis Jr. RG, Apaydin N et al. An endoscopic and anatomical approach to the septal papillary muscle of the conus. Surg. Radiol. Anat. 31:701–706,2009.

Loukas M, Sullivan A, Tubbs RS, Weinhaus AJ, DerDerian T, Hanna M: Chiari's network: review of the literature. Surgical and Radiologic Anatomy, 32: 895-901, 2010.

Luschka H. Die Anatomie des Menschen, Vol. 1, Part 2. H. Laupp, Tubingen. 1863.

MacDonald, S.T., Carminati, M. & Butera, G. Percutaneous implantation of an Edwards SAPIEN valve in a failing pulmonary bioprosthesis in palliated tetralogy of Fallot. European heart journal 32, 1534 (2011).

Marron, K. et al. Innervation of human atrioventricular and arterial valves. Circulation 94, 368-75 (1996).

Martin AJ, Christy JR. An in-vitro technique for assessment of thrombogenicity in mechanical prosthetic cardiac valves: evaluation with a range of valve types. J. Heart Valve Dis. 13(3): 509-520, 2004.

Martinez, R.M., O'Leary, P.W. & Anderson, R.H. Anatomy and echocardiography of the normal and abnormal tricuspid valve. Cardiology in the Young 16, 4 (2006).

Maselli D, Guarracino F, Chiaramonti F, Mangia F, Borelli G, Minzioni G: Percutaneous Mitral Annuloplasty: An anatomic study of human coronary sinus and its relation with mitral valve annulus and coronary arteries. Circulation, 114: 377-380, 2006.

Matsuyama, T.-A. et al. Anatomic assessment of variations in myocardial approaches to the atrioventricular node. Journal of cardiovascular electrophysiology 23, 398-403 (2012).

Messika-Zeitoun D, Serfaty J-M, Brochet E, Ducrocq G, Lepage L, Detaint D, Hyafil F, Himbert D, Pasi N, Laissy J-P, Iung B, Vahanian A: Multimodal Assessment of the Aortic Annulus Diameter. Journal of the American College of Cardiology, 55:186-194, 2009.

Messika-Zeitoun D, Serfaty JM, Brochet E, et al. Multimodal assessment of the aortic annulus diameter: implications for transcatheter aortic valve implantation. J Am Coll Cardiol. 2010;55(3):186-94.

Michaëlsson M, Ho SY: Congenital heart malformations in mammals: An illustrated text. London, UK; River Edge, NJ: Imperial College Press, 2000.

Middelhof, C.J.F.M. & Becker A.E. Ventricular septal geometry: a spectrum with clinical relevance. In: Wenink ACG et al. (eds) The ventricular septum of the heart. Martinus Nijhoff Publishers, The Hague, Netherlands (1981)

Misfeld, M. & Sievers, H.-H. Heart valve macro- and microstructure. Philosophical transactions of the Royal Society of London. Series B, Biological sciences 362, 1421-36 (2007).Netter, F. Atlas of human anatomy. Saunders, Philadelphia PA, USA: (2006).

Monckeberg, J.G. Beitrage zur normalen und pathologischen Anatomie des Herzens. Verh Dtsch Pathol Ges 14:64–71 (1910).

Monfredi, O., Dobrzynski, H., Mondal, T., Boyett, M.R. & Morris, G.M. The anatomy and physiology of the sinoatrial node--a contemporary review. Pacing and clinical electrophysiology : PACE 33, 1392-406 (2010).

Moore, K.B., Kimball, T. & Steadman, B. Silver-silver chloride plunge electrode needles and chloriding monitor . IEEE transactions on bio-medical engineering 37, 532-535 (1990).

Moss RR, Ivens E, Pasupati S, et al. Role of echocardiography in percutaneous aortic valve implantation. JACC Cardiovasc Imaging. 2008;1(1):15-24.

Muriago, M., Sheppard, M.N., Ho, S.Y. & Anderson, R.H. Location of the coronary arterial orifices in the normal heart. Clinical anatomy (New York, N.Y.) 10, 297-302 (1997).

Nakanishi, K., Raman, J., Hata, M. & Buxton, B. Early outcome with the Alfieri mitral valve repair. J. Cardiol. 37, 263-266 (2001).

Natale, A. & Jalife, J. Role of the Vagus in AF. In: Atrial Fibrillation, From Bench to Bedside. Contemporary Cardiology 2, 115-131 (Humana: 2008).

Ng AC, Delgado V, van der Kley F, et al. Comparison of aortic root dimensions and geometries before and after transcatheter aortic valve implantation by 2- and 3-dimensional transesophageal echocardiography and multislice computed tomography. Circ Cardiovasc Imaging. 2010;3(1):94-102.

Nkomo VT, Gardin JM, Skelton TN, et al. Burden of valvular heart diseases: a population-based study. Lancet. 2006;368(9540):1005-11.

Paelinck BP, Van Herck PL, Rodrigus I, et al. Comparison of Magnetic Resonance Imaging of Aortic Valve Stenosis and Aortic Root to Multimodality Imaging for Selection of Transcatheter Aortic Valve Implantation Candidates. Am J Cardiol. 2011.

Perloff, J.K. & Roberts, W.C. The mitral apparatus. Functional anatomy of mitral regurgitation. Circulation 46, 227-39 (1972).

Paniagua D, Induni E, Ortiz C, et al. Percutaneous heart valve in the chronic in vitro testing model. Circulation. 106: e51-e52, 2002.

Piazza, N. et al. Early and persistent intraventricular conduction abnormalities and requirements for pacemaking after percutaneous replacement of the aortic valve. JACC Interventions 1, 310 (2008).

Piazza, N. et al. Anatomy of the aortic valvar complex and its implications for transcatheter implantation of the aortic valve. Circulation. Cardiovascular interventions 1, 74-81 (2008).

Plass A, Valenta I, Gaemperli O, Kaufmann P, Alkadhi H, Zund G, Grünenfelder J, Genoni M: Assessment of coronary sinus anatomy between normal and insufficient mitral valves by multi-slice computertomography for mitral annuloplasty device implantation. European Journal of Cardio-thoracic Surgery, 33: 583-589, 2008.

Pogwizd, S.M. & Corr, P.B. Reentrant and nonreentrant mechanisms contribute to arrhythmogenesis during early myocardial ischemia: results using three-dimensional mapping . Circulation research 61, 352-371 (1987).

Quill JL, Laske TG, Hill AJ, Bonhoeffer P, Iaizzo PA, "Direct visualization of a transcatheter pulmonary valve implantation within the Visible Heart®–A Glimpse into the Future," Circulation, 116: e548, 2007.

Quill JL, Hill AJ, Laske TG, Alfieri O, Iaizzo PA: Mitral leaflet anatomy revisited. Journal of Thoracic and Cardiovascular Surgery, 137(5):1077-81, 2009.

Quill JL, Geesling AG, Iaizzo PA: Transcatheter Aortic Valve Deployment: Interactions Between Native Leaflets and Coronary Ostia. Journal of Medical Devices, 3: 027530, 2009.

Quill, J.L., Bateman, M.G., St Louis, J.L. & Iaizzo, P.A. Edge-to-edge repairs of P2 prolapsed mitral valves in isolated swine hearts. The Journal of heart valve disease 20, 5-12 (2011).

Quill, J.L. Atlas of Human Cardiac Anatomy. at www.vhlab.umn.edu/atlas/echotutorial/echotutorial1.shtml

Racker, D.K. & Kadish, A.H. Proximal atrioventricular bundle, atrioventricular node, and distal atrioventricular bundle are distinct anatomic structures with unique histological characteristics and innervation. Circulation 101, 1049-59 (2000).

Reid, K. The anatomy of the sinus of Valsalva. Thorax 25, 79-85 (1970).

Restivo A, Smith A, Wilkinson JL, Anderson RH. The medial papillary complex and its related septomarginal trabeculation. A normal anatomical study on human hearts. J.Anat. 163: 231-242, 1989.

Richardson E, Hill AJ, Skadsberg ND, Ujhelyi M, Xiao Y-F, Iaizzo PA. The pericardium. In: The Handbook of Cardiac Anatomy, Physiology, and Devices, Second Edition. Iaizzo PA (Ed.), Humana Press, Totowa NJ, USA, 125-136, 2009.

Ritchie, J., Warnock, J.N. & Yoganathan, A.P. Structural characterization of the chordae tendineae in native porcine mitral valves. The Annals of thoracic surgery 80, 189-97 (2005).

Ritchie, J., Jimenez, J., He, Z., Sacks, M.S. & Yoganathan, A.P. The material properties of the native porcine mitral valve chordae tendineae: an in vitro investigation. Journal of biomechanics 39, 1129-35 (2006).

Roberts PA, Boudjemline Y, Celermajer D, Cheatham J, Eicken A, Ewert P, McElhinney D, Zahn E: Percutaneous Implantation of the Medtronic Melody Valve in the Tricuspid Position — A Multi-Institutional Multi-National Report. Circulation, 122:A16393, 2010.

Rogers, J.M., Melnick, S.B. & Huang, J. Fiberglass needle electrodes for transmural cardiac mapping . IEEE transactions on bio-medical engineering 49, 1639-1641 (2002).

Roger VL, Go AS, Lloyd-Jones DM, et al. Heart Disease and Stroke Statistics--2011 Update: A Report From the American Heart Association. Circulation. 2011;123(4):e18-e209.

Salton CJ, Chuang ML, O'Donnell CJ, Kupka MJ, Larson MG, Kissinger KV, Edelman RR, Levy D, Manning WJ: Gender Differences and Normal Left Ventricular Anatomy in an Adult Population Free of Hypertension. Journal of the American College of Cardiology, 39: 1055-60, 2002.

Sands MP, Rittenhouse EA, Mohri H et al.: An anatomical comparison of human, pig, calf, and sheep aortic valves. Annuals of Thoracic Surgery, 8: 407-14, 1969.

Sasaoka, T., Ohguri, H., Makita, Y., Kurokawa, S. & Izumi, T. Double-orifice mitral valve in an elderly patient with tetralogy of Fallot. Japanese Heart Journal 37, 503-507 (1996).

Seccombe, J.F., Cahill, D.R. & Edwards, W.D. Quantitative MorpholoBy of the Normal Human Tricuspid Valve: Autopsy Study of 24 Cases. In Situ 212, 203-212 (1993).

Schievano, S. et al. Variations in right ventricular outflow tract morphology following repair of congenital heart disease: Implications for percutaneous pulmonary valve implantation. J. Cardiovasc. Magn. Reson. 9: 687-695, 2007.

Schmitt, H. et al. Diagnosis and ablation of focal right atrial tachycardia using a new high-resolution, non-contact mapping system. The American Journal of Cardiology 87, 1017-21; A5 (2001).

Schoenhagen P, Tuzcu EM, Kapadia SR, Desai MY, Svensson LG. Three-dimensional imaging of the aortic valve and aortic root with computed tomography: new standards in an era of transcatheter valve repair/implantation. Eur Heart J. 2009;30(17):2079-86.

Schultz, C.J. et al. Three dimensional evaluation of the aortic annulus using multislice computer tomography: are manufacturer's guidelines for sizing for percutaneous aortic valve replacement helpful? European heart journal 31, 849-56 (2010).

Séguéla, P.-E., Dulac, Y. & Acar, P. Double-orifice mitral valve assessed by two- and three-dimensional echocardiography in a newborn. Archives of cardiovascular diseases 104, 361-362 (2011).

Sharma, S., Loya, Y.S. & Daxini, B.V. Coarctation of aorta with unusual association of diverticulum of the left ventricle and double orifice mitral valve. International Journal of Cardiology 30, 113-115 (1991).

Sheikh, K., Smith, S.W., von Ramm, O. & Kisslo, J. Real-time, three-dimensional echocardiography: feasibility and initial use. Echocardiography (Mount Kisco, N.Y.) 8, 119-25 (1991).

Silver, M.D., Lam, J.H., Ranganathan, N. & Wigle, E.D. Morphology of the human tricuspid valve. Circulation 43, 333-48 (1971).

Sonne, C. et al. Age and body surface area dependency of mitral valve and papillary apparatus parameters: assessment by real-time three-dimensional echocardiography. European journal of echocardiography : the journal of the Working Group on Echocardiography of the European Society of Cardiology 10, 287-94 (2009).

Stachelek SJ, Alferiev I, Connolly JM, et al. Cholesterol-modified polyurethane valve cusps demonstrate blood outgrowth endothelial cell adhesion post-seeding in vitro and in vivo. Ann. Thorac. Surg. 81(1): 47-56, 2006.

Swanson, M. & Clark, R.E. Dimensions and geometric relationships of the human aortic valve as a function of pressure. Circulation research 35, 871-82 (1974).

Taccardi, B., Arisi, G., Macchi, E., Baruffi, S. & Spaggiari, S. A new intracavitary probe for detecting the site of origin of ectopic ventricular beats during one cardiac cycle. Circulation 75, 272-81 (1987).

Tawara, S. Das reizleitungssystem de saugetierherzens: eine anatomichhisologische studie uber das atrioventricularbundel und die Purkinjeschen faden. Verlag von Gustav Fischer, Jena, Germany. (1906).

Tchetche, D. et al. Thirty-day outcome and vascular complications after transarterial aortic valve implantation using both Edwards Sapien and Medtronic CoreValve bioprostheses in a mixed population. EuroIntervention : journal of EuroPCR in collaboration with the Working Group on Interventional Cardiology of the European Society of Cardiology 5, 659-65 (2010).

Thomas, J.L. et al. Prognostic significance of the development of left bundle conduction defects following aortic valve replacement. The Journal of thoracic and cardiovascular surgery 84, 382-6 (1982).

Thubrikar, M., Piepgrass, W.C., Shaner, T.W. & Nolan, S.P. The design of the normal aortic valve. The American journal of physiology 241, H795-801 (1981).

Timek, T. A. et al. Aorto-mitral annular dynamics. Ann. Thorac. Surg. 76, 1944-1950 (2003).

Ton-Nu T, Levine RA, Handschumacher MD, Dorer DJ, Yosefy C, Fan D, Hua L, Jiang L and Hung J: Geometric Determinants of Functional Tricuspid Regurgitation: Insights From 3-Dimensional Echocardiography. Circulation, 114:143-149, 2006.

Tops L, Wood D, Delgado V et al. Noninvasive Evaluation of the Aortic Root With Multislice Computed Tomography, Journal of the American College of Cardiology, Imaging.1:321-330, 2008.

Trowitzsch, E., Bano-Rodrigo, A., Burger, B.M., Colan, S.D. & Sanders, S.P. Two-dimensional echocardiographic findings in double orifice mitral valve. Journal of the American College of Cardiology 6, 383-387 (1985).

Tsakiris, A.G., Mair, D.D., Seki, S., Titus, J.L. & Wood, E.H. Motion of the tricuspid valve annulus in anesthetized intact dogs. Circulation research 36, 43-8 (1975).

Turner, K. & Navaratnam, V. The positions of coronary arterial ostia. Clinical anatomy (New York, N.Y.) 9, 376-80 (1996).

Tuzcu EM, Kapadia SR, Schoenhagen P. Multimodality quantitative imaging of aortic root for transcatheter aortic valve implantation: more complex than it appears. J Am Coll Cardiol. 2010;55(3):195-7.

Vahanian A, Alfieri O, Al-Attar N, et al. Transcatheter valve implantation for patients with aortic stenosis: a position statement from the European Association of Cardio-Thoracic Surgery (EACTS) and the European Society of Cardiology (ESC), in collaboration with the European Association of Percutaneous Cardiovascular Interventions (EAPCI). Eur Heart J. 2008;29(11):1463-70.

van Buuren, F., Faber, L. & Bogunovic, N. Double orifice mitral valve with normal function: an echocardiography and MRI study of a rare finding. European heart journal 32, 137 (2011).

van der Bel-Kahn, J., Duren, D.R. & Becker, A.E. Isolated mitral valve prolapse: chordal architecture as an anatomic basis in older patients. Journal of the American College of Cardiology 5, 1335-40 (1985).

Veronesi, F. et al. A study of functional anatomy of aortic-mitral valve coupling using 3D matrix transesophageal echocardiography. Circulation. Cardiovascular imaging 2, 24-31 (2009).

Victor, S. & Nayak, V.M. The tricuspid valve is bicuspid. The Journal of heart valve disease 3, 27-36 (1994).

Vollebergh, F.E. & Becker, A.E. Minor congenital variations of cusp size in tricuspid aortic valves. Possible link with isolated aortic stenosis. British heart journal 39, 1006-11 (1977).

Webb JG, Wood DA, Ye J et al.: Transcatheter Valve-in-Valve Implantation for Failed Bioprosthetic Heart Valves. Circulation,121:1848-1857, 2010.

Webb J, Cribier A: Percutaneous transarterial aortic valve implantation: what do we know? Eur Heart J. 32 (2):140-147, 2011.

Weinhaus AJ, Roberts KP: Anatomy of the Human Heart. In: The Handbook of Cardiac Anatomy, Physiology, and Devices, Second Edition. Iaizzo PA (Ed.), Humana Press, Totowa NJ, USA, 59-85, 2009.

Wenink, A.C. The medial papillary complex. British heart journal 39, 1012-8 (1977).

Westaby, S., Karp, R.B., Blackstone, E.H. & Bishop, S.P. Adult human valve dimensions and their surgical significance. The American journal of cardiology 53, 552-6 (1984).

Westendorp, I.C.D., de Bruin-Bon, H. a C.M. & Hrudova, J. Double orifice mitral valve; a coincidental finding. European journal of echocardiography: the journal of the Working Group on Echocardiography of the European Society of Cardiology 7, 463-4 (2006).

Wren, C. & O'Sullivan, J. Survival with congenital heart disease and need for follow up in adult life. Br. Med. J. 85: 438-443, 2001.

Wilcox, B., Cook, A. & Anderson, R.H. Surgical anatomy of the valves of the heart. In: Wilcox BR, Cook AC, Anderson RH (eds) Surgical anatomy of the heart. Cambridge University Press, Cambridge, UK 45-82 (2005).

Wójcik, A., Klisiewicz, A., Szymański, P., Różański, J. & Hoffman, P. Double-orifice mitral valve - echocardiographic findings. Kardiologia polska 69, 139-43 (2011).

Yacoub, M. Anatomy of the mitral valve chordae and cusps. (1976).

Yoganthan, AP, Chandran KB, Sotiropoulos F. Flow in prosthetic heart valves: state-of-art and future directions. Ann. Biomed. Eng. 33(12): 1689-1694, 2005.

Yurdakul, Y. et al. Congenital double-orifice mitral valve. Report of a case with valve replacement. Japanese heart journal 21, 545-50 (1980).

Zalzstein, E., Hamilton, R., Zucker, N., Levitas, A. & Gross, G.J. Presentation, natural history, and outcome in children and adolescents with double orifice mitral valve. The American Journal of Cardiology 93, 1067-1069 (2004).

Zeltser, I. et al. The roles of chronic pressure and volume overload states in induction of arrhythmias: An animal model of physiologic sequelae after repair of tetralogy of Fallot. The Journal of thoracic and cardiovascular surgery 130, 1542-1548 (2005).

Zhang, X. et al. Noninvasive three-dimensional electrocardiographic imaging of ventricular activation sequence. American Journal of Physiology- Heart and Circulatory Physiology 289, 2724-2732 (2005).

Zhu, D., Chen, A. & Zhao, Q. Surgical repair for isolated congenital double-orifice mitral valve. European journal of cardio-thoracic surgery: official journal of the European Association for Cardio-thoracic Surgery 39, 268-70 (2011).

Appendicies

A1. Case study: Anatomical and functional report of a Double Orifice Mitral Valve

Michael G. Bateman MEng[1], Stephen A. Howard BA[1], Lesa Nord BA[1], Alexander J. Hill PhD[2], Robert H. Anderson MD FCRPath[3], Paul A. Iaizzo PhD[1]

[1]Departments of Surgery and Biomedical Engineering, University of Minnesota, Minneapolis, MN, USA
[2]Medtronic, Inc., Minneapolis, MN, USA
[3]The Institute of Child Health, UCL, London, UK

Summary

Background: First described by Greenfield in 1876, the double orifice mitral valve (DOMV) is a rare congenital malformation that commonly presents with other malformations. In a very few isolated cases the abnormality presents as an isolated incident in asymptomatic adults. We present here a heart recovered from a 45 year-old male with no known past medical history of cardiac problems with a naturally occurring bridge between the aortic and mural leaflets.

Methods: Using Visible Heart methodologies the recovered heart was reanimated and stabilized before recording hemodynamics and imaging the mitral valve from above and below. The specimen was then formalin fixed under pressure before being imaged and finally dissected to investigate the double orifice valve.

Results: Pre surgical echocardiographic and hemodynamic data showed no evidence of any left ventricular (LV) anomalies often associated with DOMVs and trivial mitral valve regurgitation. Upon reanimation the heart performed well, HR 82bpm, LV pressure 95/12 mmHg and contraction 629.6mmHg/s, with no evidence of valve disfunction. A post fixation pathological work up indicated no cardiac abnormalities.

Discussion: The data reported here indicates that the presence of a DOMV has had a negligible effect on the cardiac health of a patient. This may have interesting clinical implications regarding the perception of edge to edge repairs of patients with moderate to severe mitral regurgitation. Nevertheless one must consider that the patient described here grew into adulthood with the DOMV and did not have the feature surgically induced later in life.

Background

The left atrioventricular valve, or mitral valve as it is commonly known, has aortic (or anterior) and mural (or posterior) leaflets; each hinged from an annulus, and restrained by two papillary muscle complexes with their tendinous cords. In a healthy valve the two leaflets are separated along their full lengths of coaptation so that, during diastole, a single orifice is formed between the left atrium (LA) and left ventricle (LV). As defined by Carpentier, in 1976, the mitral valve consists of two opposing leaflets— a posterior leaflet with three scallops, an anterior leaflet with one scallop and regions of each leaflet described with alphanumerically assigned regions (Figure 1)[1].

We present here a human specimen with a naturally occurring bridge between the two leaflets at the midpoint of the valve, the A2-P2 region, thus creating a double orifice within the native valve.

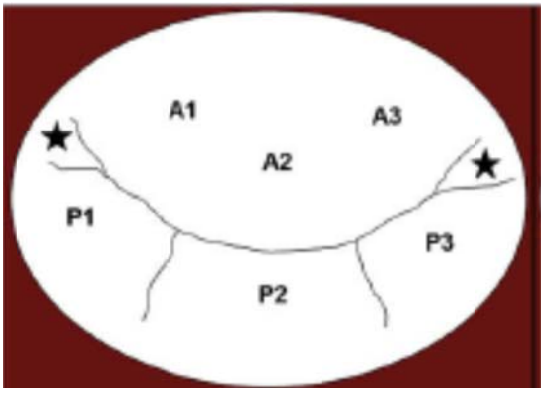

Figure A.1: Carpentier's nomenclature of the mitral valve is diagrammed. The anterior leaflet has one scallop and is divided into three regions (A1-A3). The posterior leaflet is divided into three scallops, each with its own region (P1-P3).

Greenfield was the first to describe a double orifice mitral valve (DOMV) in 1876[2] and approximately 200 cases of this congenital malformation have been reported since[3]. Initially, instances were discovered during post-mortem examinations or in organs explanted during transplant procedures; however the development and increased use of cardiac ultrasound examinations in the late 20th century has led to more clinical reports of such malformations. Yet instances are still rare with Wojcik et al. finding only nine cases in ultrasound exams from close to 80,000 patients referred to hospital with echocardiograms performed between 1993 and 2006[3]. It is believed that the bridge is caused by abnormal development of the mitral valve from the primary fold and the primitive left ventricle during the delamination process[4,5]. This malformation has been further classified by Trowitzsch et al. defining three different types[6]:

1. Complete bridge type: Two separate complete orifices are visible from the leaflet edges all the way through the body of the leaflet. Both the orifices are circular, almost equal in size, and appear like a pair of spectacles.
2. Incomplete bridge type: A connection is seen between the anterior and posterior leaflets only at the leaflet edges. At the mid-basal level, the mitral valve appears normal.
3. Hole type: A single orifice is present at the leaflet level. An additional smaller orifice is visible in one of the two commissures oriented roughly at a right angle to the main orifice.

The DOMV commonly presents with another congenital malformation, such as: an atrioventricular septal defect, aortic coarctation, a ventricular septal defect, an interrupted aortic arch, a subaortic stenosis, an atrial septal defect, a bicuspid aortic valve or a patent arterial duct[3,7–13]. It should also be noted that a DOMV can occasionally coexist with more complex cardiac malformations such as tetralogy of Fallot or Shone syndrome[14,15]. The abnormality can present as an isolated incident and if detected early can be corrected surgically[16]. In adults, isolated cases have been reported in patients admitted for chest pain, shortness of breath, or heart murmurs[17–23] and are usually only reported as asymptomatic in younger adults[22]. Patients over 40 yrs often present with additional symptoms such as severe

valvular dysfunctions, pulmonary hypertension and/or cardiomegaly[17–19,23]. The present authors found only two reported cases of DOMV in elderly asymptomatic patients: one 42 year old described by Lee et al.[20] and the other a 75 year old reported by Kim et al.[21].

Case Study Information

A 45 year-old male, BMI 30.4, was hospitalized with severe thoracic trauma and a large intracranial hemorrhage. Once stabilized in the hospital the patient maintained an average BP and HR of 130/68 mmHg and 105 bpm respectively. Phenylephrine administration was required to treat hypovolemic shock and maintain adequate blood pressures.

Before organ removal heart tones were found to be normal and systemic perfusion was adequate. An echocardiographic evaluation of cardiovascular function was performed and concluded that cardiac rhythm was regular and wall motions appeared normal. The left ventricular ejection fraction was estimated at 65%, wall thickness was reported at 8mm and the aortic root measured 31mm in diameter. Dimensions of all cardiac chambers were described as normal. No stenosis of any valve or regurgitation of the semi lunar valves were reported. Yet, trivial mitral valve and mild tricuspid valve regurgitations were noted. The individual had no known past medical history of cardiac problems.

Methods

Upon receiving the heart from LifeSource (Organ Procurement Organization, St. Paul, MN), the specimen was visually inspected and weighed before being prepared for reanimation using Visible Heart methodologies[24]. Briefly, while still in cardioplegia the great vessels of the heart were cannulated and the heart was perfused and re-warmed with a modified Krebs Heinseleight buffer. The heart was then defibrillated and allowed to function autonomously in sinus rhythm while basic hemodynamic data was recorded. With the heart beating in a four chamber working mode the valve was simultaneously imaged using both a 4mm and a 6mm diameter endoscope (Olympus Corporation, Tokyo, Japan), which were advanced into the LA via the right superior pulmonary vein, and the LV via an apical incision[25]. Once the data and video footage had been recorded the specimen was removed from the apparatus and perfusion fixed in 10% buffered formalin by attaching the cannulated great vessels to a pressure head of approximately 50 mmHg. This technique, as was first described by Anderson et al., fixes the heart in an approximation of the end-diastolic state, see figure (A.5)[26]. At this point internal footage of the fixed heart was recorded using 4mm and 6mm diameter endoscopes (Olympus Corporation, Tokyo, Japan)[27].

Subsequently, the heart (saturated with formalin) was suspended in agar gel and imaged with MRI as described by Eggen et al.[28] CMR imaging was performed using a 3D, T1-weighted, gradient-echo scan sequence in a 3 Tesla scanner (Trio; Siemens Medical Systems, US), to create high resolution short- and long-axis image stacks of the fixed specimen.

After imaging, the heart were removed from the agar gel and dissected as follows:

1. Both atria were removed to expose the cardiac skeleton. The apex was then carefully removed allowing visualization of the sub-valvular apparatus of the mitral valve.
2. An incision was then made up the free wall of the left ventricle avoiding the subvalvular apparatus.
3. The papillary muscles were then dissected off the walls of the left ventricle.
4. Subsequently, the tissue surrounding the annulus was dissected away to isolate the valve and subvalvular apparatus.

During the dissection the heart was further inspected to determine the relative health of the specimen.

Results

Images and data from reanimated heart

This heart's wet weight on arrival was 446g. A still image of the heart on the apparatus can be seen in figure (A.2) and functional images of the DOMV were reported by Howard et al. and selected stills are shown in figure (A.3) (unpublished data). At the time the footage was taken, approximately 1 hour after the heart was defibrillated, the heart rate was 82bpm. The baseline pressures across the mitral valve were 12mmHg in the LV and 15mmHg in the LA during diastole and 95mmHg in the LV and 13mmHg in the LA during systole, figure (A.4). The LV pressure derivatives were +629.6mmHg/s on myocardial contraction and -513.4mmHg/s on myocardial relaxation, see table (A.1). The LV wall thickness taken at the papillary level from a long axis echocardiographic shot was 13.5mm. This increase in LV wall thickness is due to the ionic and oncotic levels of the modified Krebs Henseleight buffer only approximating those of blood and therefore creating a gradient between the tissue and the fluid.

	HR [bpm]	LVSP [mmHg]	LVEDP [mmHg]	+dLVP/dt [mmHg/s]	-dLVP/dt [mmHg/s]
Previously Reanimated Human Hearts (N=11)	90.3 ± 16.3	42.7 ± 19.9	14.9 ± 5.9	382.7 ± 159.7	-333.7 ± 156.5
DOMV	82	95.0	13.0	629.6	-513.4

Table A.1. Hemodynamic data when compared to previously reanimated hearts[24].

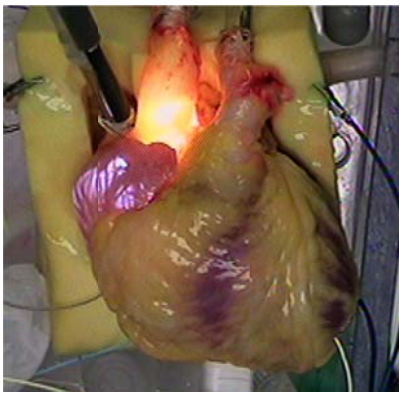

Figure A.2: Still shot of the reanimated heart on the apparatus in an approximation of the anterior posterior aspect. Light from the endoscopes can be seen in the right atrium and the ascending aorta. Video footage of the functioning valve can be found in the supplementary data.

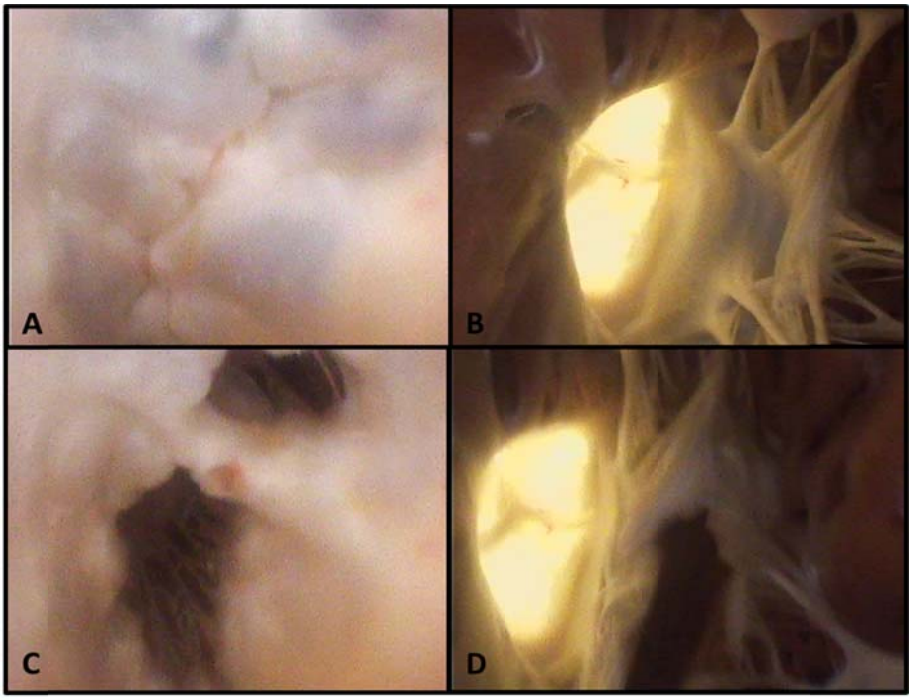

Figure A.3: Shown here is a series of four screenshots of a human mitral valve in both systole (A&B) and diastole (C&D) from the left atrium (A&C) and the left ventricle (B&D). These images clearly show the fibrous connection between the mural (postero-inferior) and aortic (antero-superior) leaflets in the central (second) region.

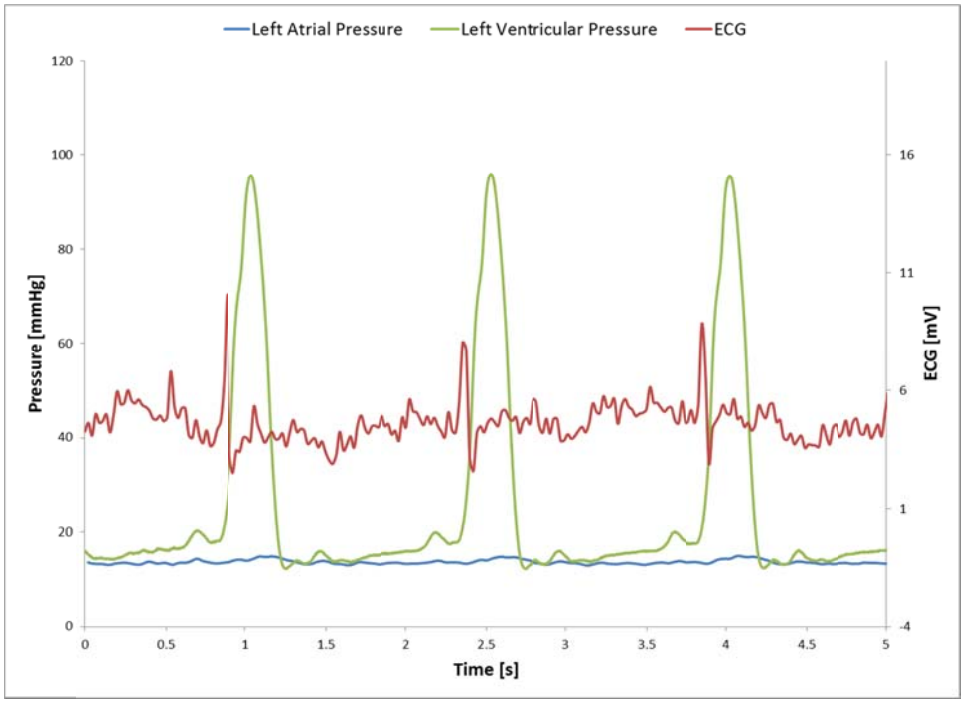

Figure A.4: Left ventricular pressure, green, and left atrial pressure, blue, over time. ECG, red, is superimposed on an alternate y axis scale.

Cardiac walls

Upon inspection of the ventricles there were no septal defects or abnormalities in the trabeculation or chamber walls. The left and right ventricle had volumes of approximately 35cm^3 and 140cm^3 respectively with wall thicknesses measured at the papillary levels of 19.7mm and 8.4mm, respectively: this somewhat excessive thickness was in part due to fluid absorption during the reanimation process. The appendages of both atria were unremarkable and no visual abnormalities of the atrial walls were recorded. The atrial septum showed a distinct valve of foramen that was fully closed/sealed. No other congenital wall defects were observed upon examination.

Cardiac vasculature

The cardiac vasculature showed no evidence of any occlusions or abnormal branching in either the venous or arterial systems. Very slight calcific depositions were found lining the right coronary artery approximately 4 cm from the ostium and the left coronary artery at the bifurcation of the left anterior descending and the circumflex.

Cardiac valves, see Figure (A.5)

The pulmonary valve exhibits three distinct leaflets and had an average annular diameter of 27.0 mm, with no signs of stiffening or fibrosis. The aortic valve annulus had a major diameter of 29.5 mm and a minor diameter of 19.5mm and also showed no calcification on either the leaflets or the annulus: the valve displays a typical tri-leaflet orientation with little to no fibrosis of the left and right coronary leaflets. The non coronary leaflet shows a fibrotic ridge running from the annulus to the leaflet node; although this may be the initiation of leaflet calcification it was not deemed severe enough to affect leaflet movement. The sinus and ascending aorta showed no signs of calcification.

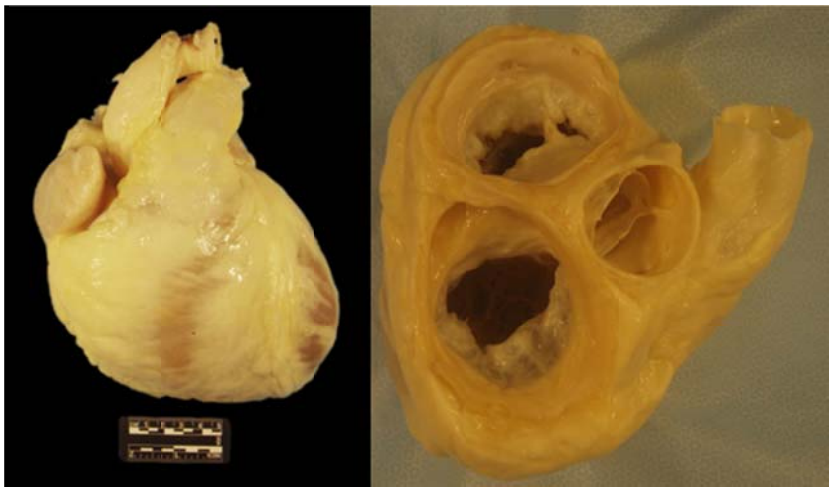

Figure A.5: Left) Anterior shot of the heart after fixation. Right) Shot of the mitral, aortic and tricuspid valves.

The tricuspid valve was found to be normal, showing only minor fibrosis of the anterosuperior and septal leaflets. All three leaflets were distinct and showed no signs of commisuural fusions.

The tricuspid annulus measured 41.9 mm by 41.2 mm. The subvalvular apparatus of the valve was considered as unremarkable: the chordal attachments of the antero-superior and inferior valves were shared by the anterior and posterior papillary complexes. Numerous fibrous conduction bands were observed between the two complexes and the surrounding endocardial surface. The smaller septal complex supported the lesser regions of the septal and antero-superior leaflets at the commissure.

The Double Orifice Mitral Valve, see Figure (A.6)

The mitral valve was found to exhibit slight calcifications on the ventricular side of the aortic leaflet and negligible calcifications on the ventricular side of the mural leaflet. The aortic leaflet displayed no visible clefts whereas the mural leaflet possessed two large clefts near the fibrous connection: one toward the superior commissure and one large cleft toward the inferior commissure, thus presenting three distinct scallops. The mitral annulus measured 40.3mm by 26.7mm. The sub-valvular apparatus was observed to be made up of two distinct papillary complexes. The superoposterior papillary (often described as antero-lateral) complex, was formed of one muscle with three distinct heads and six chordal attachments to both leaflets at the superior commissure. This superoposterior complex supported the entire connection with two large fibrous chordal connections. The rest of the valve appeared to be supported by the larger inferoanterior muscle complex (often described as posteromedial) formed again of one muscle with three distinct heads. However, the chordal attachments of this complex were more numerous with twelve counted, all being more densely fenestrated.

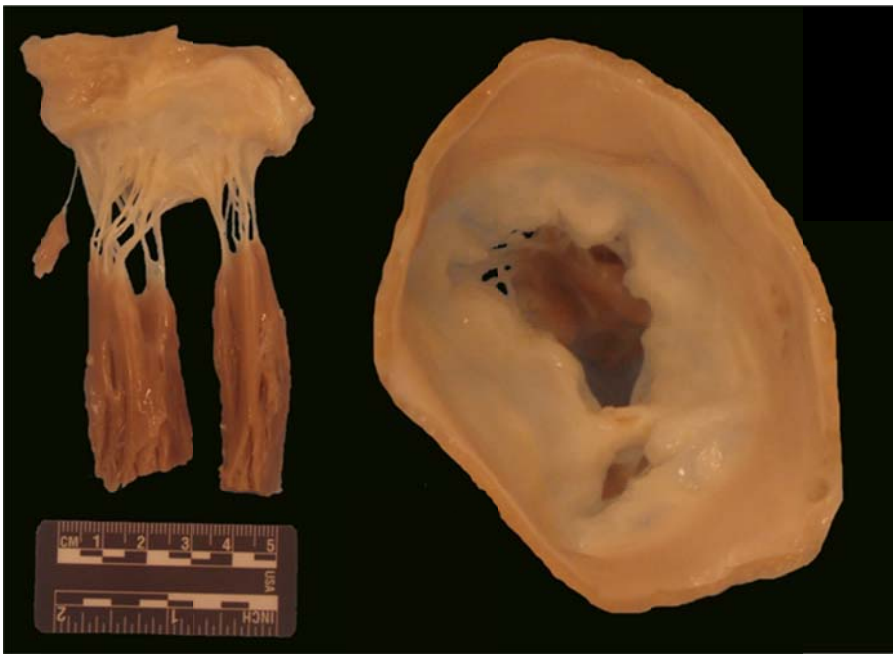

Figure A.6: Images of the dissected mitral valve showing: a) the subvalvular apparatus of the valve and b) the valve from the left atrium highlighting the fibrous connection between the valve leaflets.

The fibrous connection of the mitral valve observed here could best be defined as an incomplete bridge which was situated toward the superior commissure of the center scallops of the two

leaflets. This formation resulted in a smaller superior (anterolateral) orifice, of approximately 25 mm^2, and a larger inferior (posteromedial) orifice, approximately of 148 mm^2.

MRI and subsequent image analyses

MRI images taken with a voxel size of 0.44mm x 0.44mm x 1.60mm were imported into Mimics 14.2 (Materialise, Leuven, Belgium) and used to create a three dimensional model of this individual's mitral valve and its associated sub-valvular apparatus, see figure (A.7)[27].

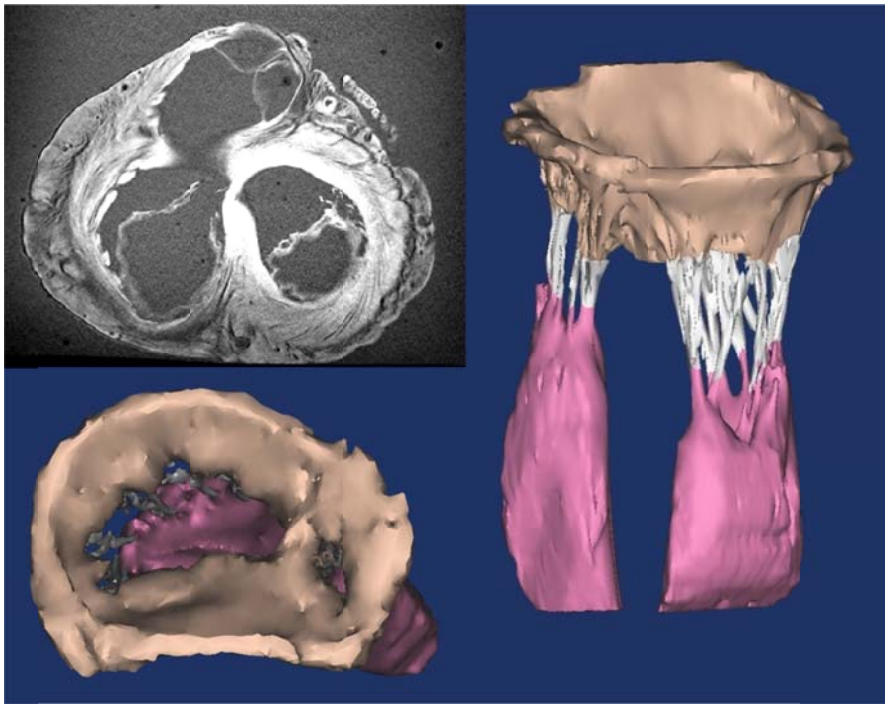

Figure A.7: a) Short axis MR image taken at the level of the mitral valve. Mimics reconstruction of the DOMV viewed from above (b) and from the side (c).

Discussion

DOMV is a rare congenital abnormality that usually presents coexisting with other congential malformations[3]. The majority of these isolated cases are reported for patients presenting with other cardiac or circulatory symptoms. We considered here that for this reason, clinical reports of a DOMV in a patient over the age of 40 years old would be even rarer. However, it should be noted that typically patients with asymptomatic DOMVs exhibit no cardiac functional abnormalities and thus rarely undergo the appropriate examinations to diagnose such a bridge thus significantly reducing the incidence of asymptomatic DOMV patients.

The post-mortem examination of a heart recovered from a 45 year old male, whose cause of death and previous medical history showed no evidence of a congenital malformation, presents a unique case. The DOMV or fibrous bridge was not recognized until the heart was reanimated within our laboratory: the condition of the heart during preparation gave no indication of cardiomegaly or any other sign of left ventricular hypertrophy or dilation often associated with dysfunctional mitral valves. The echocardiographic exam performed just prior to organ removal/recovery, made no mention of any valve stenosis and only noted a trivial mitral

regurgitation. Once reanimated the heart performed well when compared to other specimens, see table A.1.

To further confirm this aforementioned hypothesis, a pathological work up of the heart was performed, concentrating on the anatomical health of the valves, the left ventricle and determining the existence of any other congenital abnormalities. Our findings of this examination indicated that this individual's heart was in good health and apart from the DOMV exhibited no cardiac abnormalities. It should be noted that this examination was somewhat hindered by the swelling of the heart during the prior reanimation process. However, unpublished data from the lab and information from echocardiographic exams appear to confirm that this altered anatomy was the result of tissue fluid retention during the reanimation process and not due to any pre-existing cardiovascular conditions of the patient. Finally, the MR imaging of this perfusion fixed heart specimen, has allowed for the construction of a complete model of the specimen as a potential educational tool[27].

The results presented here may have interesting clinical implications regarding the perception of edge to edge repairs of patients with moderate to severe mitral regurgitation. For example, the Alfieri stitch has been used to surgically repair mitral leaflet prolapse[29] and concerns have been raised regarding the function of a dual orifice valve in relation to a single orifice valve. Yet, Quill et al. showed in a number of in-vitro swine studies that this type of procedure did not cause mitral stenosis in otherwise healthy valves[30]. Nevertheless one must consider that the patient described here grew into adulthood with the DOMV and did not have the feature surgically induced later in life.

Conclusions

The footage and data of a rarely reported congenital malformation of the mitral valve presented in this paper indicates that in this isolated instance of a double orifice mitral valve had a negligible effect on the cardiac health of a patient. The 45 year old individual presented with a healthy and anatomically unremarkable heart indicating that the fibrous connection between the opposing mitral leaflets did not result in a dysfunctional valve.

References

1. Carpentier, A. Cardiac valve surgery--the "French correction" . *The Journal of thoracic and cardiovascular surgery* **86**, 323-337 (1983).

2. Greenfield, W. Double Mitral valve. *Translactions of the Pathological Society of London* **27**, 128-9 (1876).

3. Wójcik, A., Klisiewicz, A., Szymański, P., Różański, J. & Hoffman, P. Double-orifice mitral valve - echocardiographic findings. *Kardiologia polska* **69**, 139-43 (2011).

4. Elfenbein, B. & Paplanus, S.H. Duplication of the mitral and tricuspid valves. *Archives of pathology* **85**, 675-80 (1968).

5. Erdemli, O. *et al.* A Double-Orifice Atrioventricular Valve Case: Intraoperative Transesophageal Echocardiography in Diagnosis and Treatment. *Anesth. Analg.* **97**, 650-653 (2003).

6. Trowitzsch, E., Bano-Rodrigo, A., Burger, B.M., Colan, S.D. & Sanders, S.P. Two-dimensional echocardiographic findings in double orifice mitral valve. *Journal of the American College of Cardiology* **6**, 383-387 (1985).

7. Zalzstein, E., Hamilton, R., Zucker, N., Levitas, A. & Gross, G.J. Presentation, natural history, and outcome in children and adolescents with double orifice mitral valve. *The American Journal of Cardiology* **93**, 1067-1069 (2004).

8. Westendorp, I.C.D., de Bruin-Bon, H. a C.M. & Hrudova, J. Double orifice mitral valve; a coincidental finding. *European journal of echocardiography: the journal of the Working Group on Echocardiography of the European Society of Cardiology* **7**, 463-4 (2006).

9. Sharma, S., Loya, Y.S. & Daxini, B.V. Coarctation of aorta with unusual association of diverticulum of the left ventricle and double orifice mitral valve. *International Journal of Cardiology* **30**, 113-115 (1991).

10. Séguéla, P.-E., Dulac, Y. & Acar, P. Double-orifice mitral valve assessed by two- and three-dimensional echocardiography in a newborn. *Archives of cardiovascular diseases* **104**, 361-362 (2011).

11. Deng, X. *et al.* A rare case of Gerbode defect associated with double orifice mitral valve. *The Thoracic and cardiovascular surgeon* **58**, 372-4 (2010).

12. van Buuren, F., Faber, L. & Bogunovic, N. Double orifice mitral valve with normal function: an echocardiography and MRI study of a rare finding. *European heart journal* **32**, 137 (2011).

13. Goicolea, F.J. *et al.* Double mitral orifice associated with a bicuspid aortic valve detected using bidimensional echocardiography. *Revista española de cardiología* **42**, 65-7 (1989).

14. Sasaoka, T., Ohguri, H., Makita, Y., Kurokawa, S. & Izumi, T. Double-orifice mitral valve in an elderly patient with tetralogy of Fallot. *Japanese Heart Journal* **37**, 503-507 (1996).

15. Linka, A.Z., Fatio, R. & Jost, C.A. Double orifice mitral valve. *Heart British Cardiac Society* **84**, 244 (2000).

16. Yurdakul, Y. *et al.* Congenital double-orifice mitral valve. Report of a case with valve replacement. *Japanese heart journal* **21**, 545-50 (1980).

17. Congiu, S. *et al.* Mitral insufficiency with a double-orifice mitral valve in an adult patient. *The Journal of thoracic and cardiovascular surgery* **134**, 250-1 (2007).

18. Heyse, A.M. *et al.* Mitral insufficiency with congenital double-orifice mitral valve in an elderly patient. *European journal of echocardiography: the journal of the Working Group on Echocardiography of the European Society of Cardiology* **4**, 334-5 (2003).

19. Kron, J., Standerfer, R.J. & Starr, A. Severe mitral regurgitation in a woman with a double orifice mitral valve. *British heart journal* **55**, 109-11 (1986).

20. Lee, D.I. *et al.* Double-orifice mitral valve. *Clinical cardiology* **22**, 425 (1999).

21. Kim, S.-J., Shin, E.-S. & Lee, S.-G. Congenital double-orifice mitral valve with mitral regurgitation due to flail leaflet in an elderly patient. *The Korean journal of internal medicine* **20**, 251-4 (2005).

22. Karas, S. *et al.* Well-functioning double-orifice mitral valve in a young adult. *Journal of clinical ultrasound: JCU* **31**, 170-3

23. Zhu, D., Chen, A. & Zhao, Q. Surgical repair for isolated congenital double-orifice mitral valve. *European journal of cardio-thoracic surgery: official journal of the European Association for Cardio-thoracic Surgery* **39**, 268-70 (2011).

24. Hill, A.J. *et al.* In vitro studies of human hearts. *The Annals of Thoracic Surgery* **79**, 168-177 (2005).

25. Chinchoy, E. *et al.* Isolated four-chamber working swine heart model. *The Annals of Thoracic Surgery* **70**, 1607-1614 (2000).

26. Anderson, S.E., Quill, J.L. & Iaizzo, P.A. Venous valves within left ventricular coronary veins. *Journal of Interventional Cardiac Electrophysiology* **23**, 95-99 (2008).

27. Atlas of Human Cardiac Anatomy. **http://www.vhlab.umn.edu/atlas**

28. Eggen, M., Bateman, M. & Iaizzo, P.A. Methods to Prepare Perfusion Fixed Cardiac Specimens for Multimodal Imaging: The Use of Formalin and Agar Gels. *Journal of Medical Devices* **5**, 027539-1 (2011).

29. Alfieri, O. *et al.* The double-orifice technique in mitral valve repair: a simple solution for complex problems. *The Journal of thoracic and cardiovascular surgery* **122**, 674-681 (2001).

30. Quill, J.L., Bateman, M.G., St Louis, J.L. & Iaizzo, P.A. Edge-to-edge repairs of P2 prolapsed mitral valves in isolated swine hearts. *The Journal of heart valve disease* **20**, 5-12 (2011).

A2. Anatomy posters

A detailed anatomical study of the papillary muscles and chordae tendineae of the left ventricle in perfusion fixed human hearts

Michael G. Bateman MEng, Cori E. Russel BS, Brian Y. Chan BS, Devon E. Hutton BA and Paul A. Iaizzo PhD

Departments of Surgery and Biomedical Engineering University of Minnesota, Minneapolis, MN, USA

Videoscopic images of unique septal and medial papillary muscle complexes recorded from reanimated human hearts

Michael G. Bateman MEng, Paul A. Iaizzo PhD

Departments of Surgery and Biomedical Engineering University of Minnesota, Minneapolis, MN, USA

A detailed anatomical study of the papillary muscles and chordae tendineae of the left ventricle in perfusion fixed human hearts

Michael G. Bateman, M.Eng[1,2], Cori E. Russell, B.Sc, Brian Y. Chan, B.Sc, Devon E. Hutton, B.A, Paul A. Iaizzo, PhD[1,2,3]
Departments of Biomedical Engineering[1], Surgery[2], and Physiology[3],
University of Minnesota, Minneapolis, MN 55455

Background

Classical cardiac anatomical terminology describes the existence of two papillary muscles in the left ventricle (LV): the anterolateral and the posteromedial[1]. However, it is well known by surgeons that an individual's heart can exhibit a large variation in the shape, size, and location of papillary muscles and that cardiac pathologies can greatly alter their characteristics. With the development of transcatheter devices designed for left-sided delivery and minimally invasive mitral valve repair procedures there is a need for a more detailed analyses of these anatomical variations.

The general anatomy features of the LV papillary muscles was recently revisited by Berdajs et al., where an initial attempt was made to classify papillary muscles based on anatomical type; however, no measurements of length or location in relation to the septum were taken[2]. In addition, hearts were not studied in a uniform end diastolic state. Similarly, DiDio et al. documented the positioning of the papillary muscles relative to the arterial perfusion of the ventricle, but did not relate these findings to the muscle's type, function or interaction with the mitral valve[3]. Further, many other studies have focused on the right ventricular papillary muscles or the LV chordae, without detailed analysis of the papillary muscles relative to their anatomies or positioning.

Objectives

To date, we have observed only a fraction of hearts in our Visible Heart® laboratory's library (>150 human hearts) that elicit the "classically defined papillary anatomies" and believe that a novel, but appropriate, terminology can and should be developed which will greatly benefit planned mitral valve surgeries and/or the design and development of left-sided trans-catheter delivered systems and devices. Therefore, the goals of this present project were to use the large anatomical resources of our library to create a detailed anatomical map of the relative position of the papillary muscles in the left ventricle and to create a classification system for the variations in their anatomical shapes.

Methodology

Fifty one perfusion fixed human hearts were employed for this study due to the unique attributes of their preservation, whereby 10% formalin was continuously pumped into the great vessels so as to permanently fix each heart in an end-diastolic state[4].

The hearts were then embedded in 7% agar gel and high resolution short- and long-axis image stacks were acquired using a 3D, T1-weighted, gradient-echo scan sequence in a 3 Tesla scanner (Trio; Siemens Medical Systems, US), see Figure 1.

The DICOM files were then analyzed using OsiriX Imaging Software (OsiriX Foundation. Switzerland) to determine the positions and sizes of each papillary muscle complex relative to the septal wall, then measure LV volumes and myocardial wall thicknesses and assign a complex type, see results.

The relative papillary complex type was verified using endoscopic video footage, (IplexFX, Olympus Corporation, Tokyo, Japan), e.g., see Figure 4.

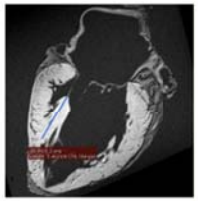

Figure 1: Example slice from a two chamber long axis stack with length measurements.

Acknowledgements

The authors would like to thank Mike Eggen PhD, Maria LaNasa and Kiley Schmidt for their assistances in this project.

We would like to thank the heart donors and their families for their generous gifts of these hearts which made this research possible and also LifeSource (St. Paul, MN) for their help with the organ recoveries and their continued support.

Results and Discussion

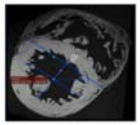

Figure 2: Short axis OsiriX screenshot.

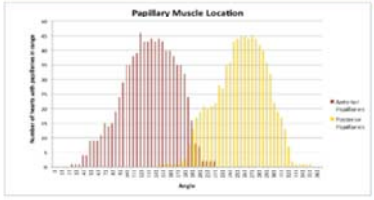

Figure 3: Angular distribution of anterior and posterior papillary muscle complexes.

Angle measurements were taken as shown in Figure 2. The midpoint of the septal wall of each heart served as the zero degrees landmark and subsequent angles were measured in a counterclockwise rotation around the LV. Analyses of the relative papillary muscle complex locations within the LV displayed two peaks of muscle density relating to the traditionally defined anterior and posterior positions, see Figure 3.

This approach may also allow for better monitoring of the progression of chamber remodeling that may occur with heart failure. In many cases cardiac remodeling results in the gradual repositioning of the papillary muscles such that changes in papillary muscle location, in addition to other traditional markers, could serve as an indicator of disease states and identify progression along a continuum of left ventricular heart failure.

Type I: Single | Type II: Multiple | Type III: Staggered | Type IV: Bifurcated

Figure 4: Endoscopic images displaying the four types of papillary muscle.

Through the analyses of both the acquired high resolution MR scans and endoscopic images we have been able to group the papillary muscle complexes into four distinct types: single, multiple, staggered and bifurcated.

Within the hearts presented here the papillary muscle morphology was predominantly Type I in both the anterior (30%) and posterior (50%) regions of these hearts, see Figure 5.

Additionally, the papillary muscle morphology has been subcategorized to define each papillary head and the relative chordae attachment within the complex (data not published here).

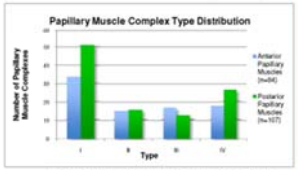

Figure 5: Number of papillary muscles within each type.

Results and Discussion

To define the relative disease state of each heart a volume:wall thickness ratio was determined by comparing the cube root of the LV volume to the myocardial wall thickness at the papillary level. The results indicate grouping of the hearts into three distinct ranges that define the of characteristics of three disease or non-pathological states: left ventricular hypertrophy (LVH) hearts shared a ratio < 3.5; normal hearts fell between 3.5 - 5.5; and dilated cardiomyopathy (DCM) hearts > 5.5. See Figure 6.

This information is currently being used to determine how the distributions of papillary muscles varies depending on the relative defined disease states.

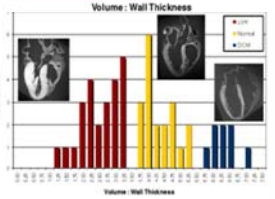

Figure 6: Ratio of ³√volume:myocardial wall thickness and assigned pathology.

Limitations

The current methodology does not allow each papillary muscle complex to be imaged perfectly in the native anatomical plane. This inability to standardize the configuration of images to the same reference plane may have introduced some imprecision when comparing measurements between specimens. To correct for this, we are currently working on inputting the DICOM files into a 3D modeling software such as Mimics® (Materialise, Leuven, Belgium) and analyzing specific complex lengths and volumes in three dimensions.

For the data set presented in this poster multiple users were responsible for analyzing mutually exclusive sets of data, potentially introducing inter-operator variability in collected measurements. Thus, data analyses is ongoing and we are ensuring that each image set will be analyzed by two or more operators so as to eliminate such potential errors.

Conclusions and Future Work

The work presented in this poster represents the preliminary stages of a research project designed to create detailed anatomical maps of the relative positions of the papillary muscles within the left ventricle of a large sample of uniquely preserved human hearts. Additionally, we hope to create a classification system for the high degree of observed variations in these specimens' anatomical shapes and positions. We describe that the LV papillary muscles are far more diverse in nature than the traditionally defined: i.e. one anterior and one posterior complex. This variability can be further confounded by the presence of disease. Further, we suggest that by better defining the types and the positions of these complexes, one could create a simplified anatomical mapping system of their relative distributions. Such information could then better provide a needed understanding of the impacts of device placements: e.g. positioning pacing leads relative to papillary locations which may lead to improved papillary muscle synchrony and decreased mitral regurgitation in response to pacing. We are currently working to utilize the MR images to better define the total endocardial surface areas.

Importantly, continued efforts are required to anatomically analyze the muscles found at each location for the largest sample size of hearts possible and to describe the distribution of chordae and their respective connections to their mitral valves. This detailed anatomical information will be applicable to surgeons investigating mitral chordae repair and/or biomedical engineers developing artificial chordae and chordae attachment devices.

References

1. Athanasiou, T. *et al.* Preservation of the mitral valve apparatus: evidence synthesis and critical reappraisal of surgical techniques *Eur. J. Cardiothoracic. Surg.* 33, 391-401 (2008)
2. Berdajs, D., Lajos, P., Turina, M.I. A new classification of the mitral papillary muscle. *Medical Science Monitor.* 11(1), BR18-21 (2005)
3. DiDio, L.J., Rodrigues, H. & Baptista, C.A. The papillary muscles of the left ventricle and the cardiac segments *Surg. Radiol. Anat.* 12, 281-285 (1990)
4. Anderson, S.E., Quill, J.L. & Iaizzo, P.A. Venous valves within left ventricular coronary veins. Journal of Interventional Cardiac Electrophysiology 23, 95-99 (2008)

Program #:

Videoscopic images of unique septal and medial papillary muscle complexes recorded from reanimated human hearts

Michael G. Bateman, M.Eng[1,2], Paul A. Iaizzo, PhD[1,2,3]

Departments of Biomedical Engineering[1], Surgery[2], and Physiology[3], University of Minnesota, Minneapolis, MN 55455

Abstract: The continued rapid development of right-sided cardiac transcatheter therapies has led to an increase in the application of such technologies; thus there is a renewed interest as to the nuances of the anatomies within the right heart chambers. The use of Visible Heart® methodologies in over forty reanimated human hearts (deemed not viable for transplant) has allowed us to capture unique footage of the internal anatomy of the right ventricle. Presented here is a selection of images of unique tricuspid septal and medial papillary complexes recorded from within the right ventricle displaying the wide variety of morphologies and anatomies of the valve apparatus. Such varied and complex anatomies could potentially alter, or be altered by the delivery of right-sided transcatheter therapies: e.g., increasing the possibility of damage to the functional anatomy of sub-valvular apparatus. We consider here that such images can be employed as educational tools for both clinicians and device designers to better understand the dynamic internal anatomies of the human heart.

Background

Advances in cardiac catheterization laboratory procedures have resulted in a marked increase in the number of right sided transcatheter therapies being conducted. These can include prosthetic pulmonary valve and ventricular pacing lead implantations. Coupled with the continuous development of novel devices and therapies this has led to an increased interest in the functional anatomy of the tricuspid sub-valvular apparatus. The tricuspid valve, as reported by Anderson et al., possesses inferior, septal and antero-superior leaflets and displays extensive chordal attachments to the ventricular septum through markedly eccentric papillary muscles [1]. The attachment of the tricuspid valve to the septal region of the right ventricle has been described by many anatomists; including Luschka [2], Wenink [3], Anderson [4], Seccombe [5] and Loukas [6]. The attachment is generally considered to consist of two complexes: septal and medial. The septal papillary complex can consist of a collection of small muscles in close proximity and usually attaches to both the septal and antero-superior leaflets. In addition, chordae may extend from the septal wall itself without a distinguishable papillary muscle head [7]. The medial complex lies superior and distinct from the septal complex and, as with the septal complex, consists of a collection of muscles and chordal attachments to both the septal and antero-superior leaflets [3].

Objectives

As evidenced by their generic anatomical definitions these muscle complexes can exhibit markedly different features from patient to patient. The Visible Heart® apparatus allows us to present unique footage of the variation in the septal and medial papillary complexes by comparing the functional anatomy of over forty human hearts. Presented here is a selection of unique anatomies recorded using Visible Heart® methodologies.

Methodology

Using St. Thomas cardioplegia and standard transplant surgery procedures, human hearts deemed not viable for transplant are explanted to an isolated heart apparatus. The hearts are cleaned of excess tissue and the great vessels cannulated before being connected to the Visible Heart® apparatus and perfused with warm modified Krebs-Henseleit buffer and defibrillated[8]. Following reanimation, cardiac outputs and systemic pressures are monitored and 4mm and 6mm diameter endoscopes (Olympus Corporation, Tokyo, Japan) are advanced into the heart chambers allowing for visualization of the internal structures. To visualize the functioning tricuspid valve the hearts operate in a four-chamber working mode, whereby fluid flows through both sides of the heart.

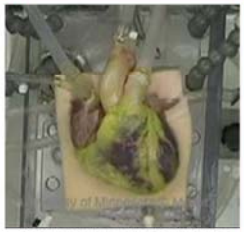

Fig 1: Isolated human heart set up in the Visible Heart® apparatus

Images

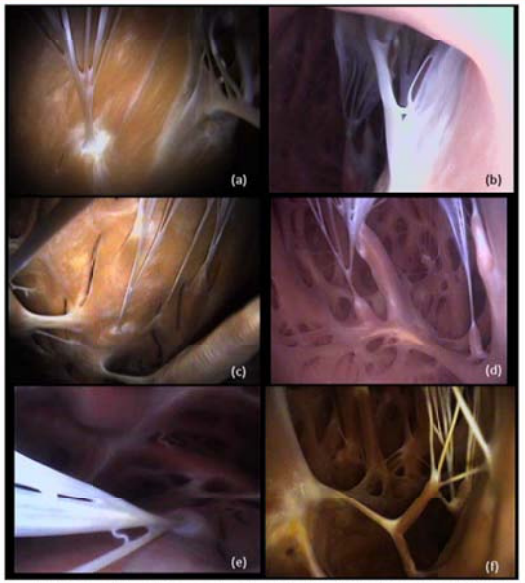

Figure 1: (a) Two medial papillary complexes branching from high on the septal wall, HH015. (b) Medial papillary complex displaying a fenestrated, or fan, chordae, HH191. (c) Four septal papillary complexes branching from the septal wall with no discernible muscle heads, HH015. (d) A small septal papillary muscle complex with extremely fine chordae attaching to the septal leaflet with a medial papillary complex above, HH146 (e) A heart displaying a sturdy medial complex connecting to the septal leaflet, HH171 (f) An anomalous septal papillary complex with many tendinous attachments to neighboring structures, HH134.

Discussion

Fenestrated chordae tendinae (figures 1a (to the right of the image) and 1b) and extremely fine chordal attachments (figures 1c and 1d (to the right of the image)) exhibit a fine web of tendinous structures that could potentially prove problematic when attempting the delivery of apical pacing leads through the sub-valvular apparatus of the tricuspid valve.

Figures 1a, 1b, 1c and 1e display septal and medial complexes with chordae tendinae that project from the wall of the chamber with little to no discernible papillary muscle heads. Such anatomies can create problems during the delivery of transcatheter pulmonary valve therapies. Without the presence of papillary muscle heads the delivery system can potentially interact directly with the chordae increasing the possibility of chordal rupture.

Figures 1d and 1e highlight the anatomical differences between septal and medial papillary complexes. In figure 1d the chordae to the right of the image attach to a small septal papillary muscle head branching form the trabeculation near the base of the interventricular septum and a large medial papillary muscle complex branching from the septal wall. The anterior papillary muscle complex, consisting of two distinct muscle heads, can be seen in the center of the image.

Figure 1f exhibits a truly anomalous structure whereby tendinous structures project from the papillary muscle to neighboring papillary complexes, back to the septal wall, to other chordae in addition to connections to the valve itself. Of particular interest is the interaction of the septal and medial papillary muscle complexes in which both display chordal attachments to each other as well as to the valve leaflets.

Figure 2 below shows three instances of potential device-chordae interactions from footage taken in the Visible Heart® apparatus: 2a shows an RVA pacing lead (5076 Medtronic, Inc.), 2b shows an passive fixation lead (4074 Medtronic, Inc.) and 2c shows the Melody® pulmonary valve replacement delivery system (Melody® Medtronic, Inc.).

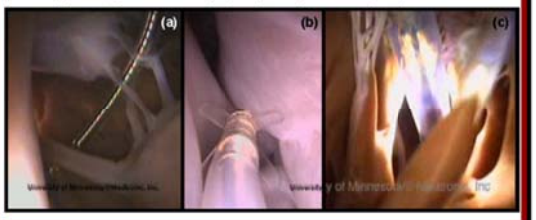

Conclusions

These images demonstrate the potential difficulties that a clinician may encounter while maneuvering a lead or transcatheter device through the tricuspid valve to approach the right ventricle from the venous vasculature via the right atrium. Damage to such structures could potentially lead to tricuspid insufficiency and the consequent pathologies associated with such a disorder. Therefore, these images act as an educational tool for clinicians and device designers in the understanding of the internal anatomy of the heart to ensure that all potential anatomical variations are accounted for when undertaking catheter based procedures in the right ventricle. In addition to the still images that can be seen here functional video footage of these specimens can be seen on the Atlas of Human Cardiac Anatomy [9].

www.vhlab.umn.edu/atlas is accessible using the 2D barcode to the left

Acknowledgements

We would like to thank the heart donors and their families for their generous gifts of these hearts which made this research possible and also LifeSource (St. Paul, MN) for their help with the organ recoveries and their continued support.

References

1. Anderson RH, Razavi R, Taylor AM. Cardiac Anatomy Revisited. J. Anat. 205: 159–177, 2004.
2. Luschka H. Die Anatomie des Menschen, Vol. 1, Part 2. H. Laupp, Tubingen. 1863.
3. Wenink AC. The medial papillary complex. Br Heart J. 39: 1012-1018, 1977.
4. Restivo A, Smith A, Wilkinson JL, Anderson RH. The medial papillary complex and its related septomarginal trabeculation. A normal anatomical study on human hearts. J. Anat. 163: 231-242, 1989.
5. Seccombe JF, Cahill DR, Edwards WD. Quantitative Morphology of the Normal Human Tricuspid Valve: Autopsy Study of 24 Cases. Clinical Anat. 6:203-212, 1993.
6. Loukas M, Tubbs RS, Louis Jr. RG, Apaydin N et al. An endoscopic and anatomical approach to the septal papillary muscle of the conus. Surg. Radiol. Anat. 31:701–706, 2009.
7. Weinhaus AJ, Roberts KP: Anatomy of the Human Heart. In: The Handbook of Cardiac Anatomy, Physiology, and Devices, Second Edition. Iaizzo PA (Ed.), Humana Press, Totowa NJ, USA, 59-85, 2009.
8. Hill AJ, Laske TG, Coles Jr. JA, Sigg DC et al. In vitro studies of human hearts. Ann Thorac Surg. 2005;79(1):168-177.
9. www.vhlab.umn.edu/atlas

Book chapter: Cardiac Devices and Testing

Michael G. Bateman MEng[1], Stephen A. Howard BA[1], Christopher Rolfes BS[1], Timothy Laske PhD[2] and Paul A. Iaizzo PhD[1]

[1]Departments of Surgery and Biomedical Engineering University of Minnesota, Minneapolis, MN, USA
[2]Medtronic, Inc., Minneapolis, MN, USA

Summary

From the earliest reported cardiac surgeries in the late 19th century the exponential improvements in surgical techniques and operating times has opened the door for the development of novel cardiac devices. The design and development of cardiac devices in the 21st century is driven by the innovation and resources of an industry forecast to be worth $266 billion by 2012. This market growth is symbolized by the many patent applications submitted each year create novel devices or embellish existing products.

The chapter seeks to provide a brief description of the history of cardiac surgery, the evolution of cardiac devices and a glimpse into the future of the industry as a background to the design process. The fundamental principles involved with the design and development of cardiac devices are laid out: from an explanation of the many stages involved with device design and the biological factors and material properties that engineers must consider when prototyping and testing devices through to the steps taken by a medical device company to successfully deliver their product to market. Additionally, the chapter includes examples of market available cardiac devices and illustrates the novel devices and therapies currently in development.

As the fields of cardiac surgery and cardiology continue to rapidly develop and expand the cardiac device industry, this will in turn provide innovative and revolutionary devices and therapies. Although many devices are conceived from a need within the operating room or cardiac catheterization laboratory, their designs and developments often leads to novel procedures and techniques that continue to improve the treatment for the cardiac pathologies. There is little doubt that these innovative improvements will extend and enhance the overall qualities of the lives of patients worldwide.